University of Liège
Faculty of Medicine
GIGA-Cancer

Laboratory of Connective Tissue Biology
Dr Alain Colige

Antagonistic roles of ADAMTS2 in cancer progression: inhibiting primary tumor growth while being essential for metastatic spread

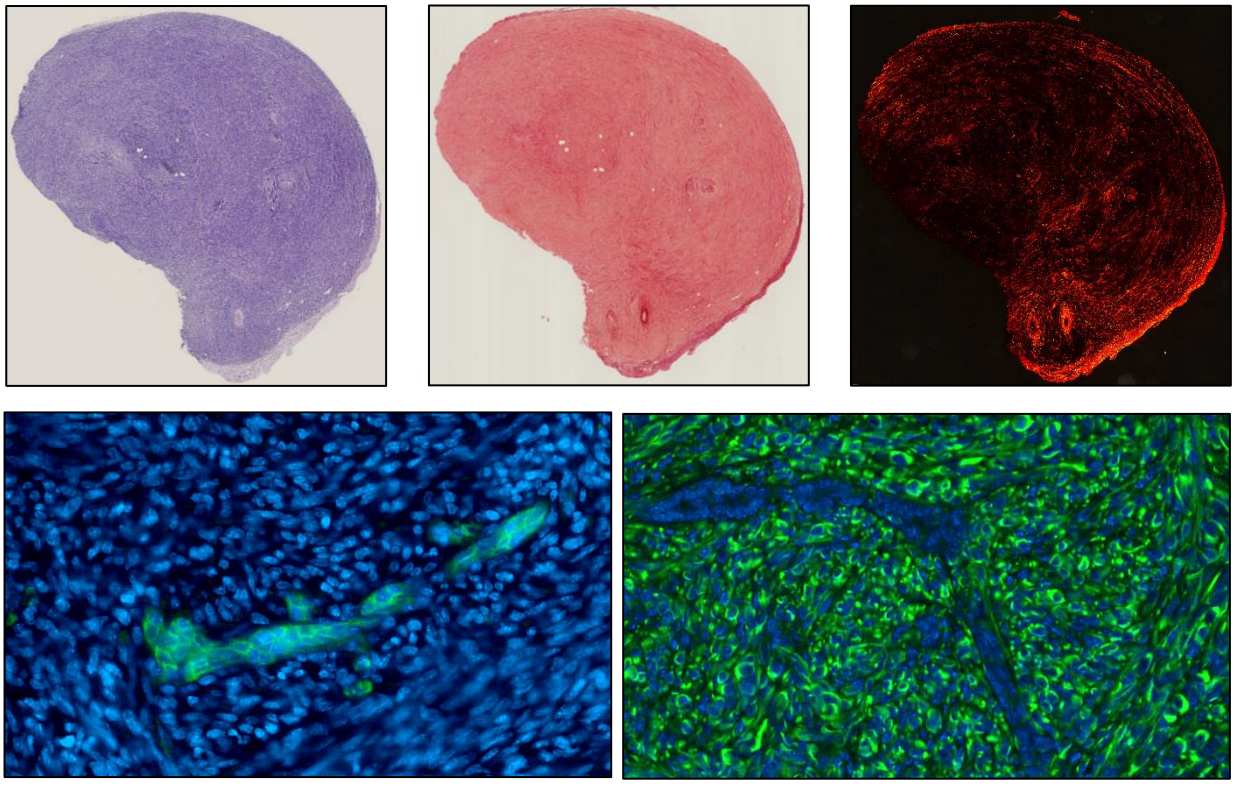

JOANNES Loïc

Thesis submitted in partial fulfillment of the requirements for the degree of PhD in biomedical and pharmaceutical sciences

Academic year 2023/4-2024/5

Acknowledgment

In this section, I would like to bring to the fore people that directly or indirectly took part in the completion of this work. Some were actively involved in the realization of the wide range of experiments this project brought me to, others gave me key insights in experiments that were much obscure to me while some help me to keep every day at the lab more exciting than the previous one.

First of all, I would like to thank Alain Colige for the opportunity he gave me to work with him. He has been an inspiration and a scientific model that drove most of my improvements in reasoning, brainstorming and overall as a scientist. I am very glad that I performed my thesis in his lab.

Laura Dupont was for sure the most important person involved in the success of this project. Through her experience and reliability, she took care of every *in vivo* models which are at the heart of ADAMTS2 study. It was a pleasure to collaborate with her along these years.

Esther Arpigny joined us at the lab later on but quickly became the sunlight of the LCTB. Always listening and having a laugh, she became the most important person for me during the end of this thesis and I can't thank her enough for our daily talk and her guidance from her unmatched social intelligence.

Mudrika Tripathi was really something. So much energy in this small body, we had a hard time getting along at the start but ultimately became good friend. Always a pleasure to chitchat in her office.

I want also to mention the rest of the LCTB: Christophe Deroanne, Julie Cremer and Nancy Garbacki always ready to give a hand or to share their insights.

Throughout this project, I collaborated with other labs without which the most challenging experiments would not have been possible. I had the precious help of Michael Herfs's lab and especially Pascale Hubert, Marie Ancion and Margaux Luyckx for flow cytometry design and analysis on tumors. Thomas Marichal's lab for single cell RNA sequencing analysis done by Joan Abinet and flow cytometry analysis on lungs done with the help of Wen Peng.

Table of content

Abbreviations list

ADAM	a disintegrin and metalloproteinase
ADAMTS	a disintegrin and metalloproteinase with thrombospondin motifs
ADAMTSL	a disintegrin and metalloproteinase with thrombospondin motifs like
ADCC	antibody-dependent cellular cytotoxicity
ADCP	antibody-dependent cellular phagocytosis
apCAF	antigen presenting CAF
ARG1	arginase 1
BMDM	bone marrow-derived macrophage
BMP	bone morphogenetic protein
CAF	cancer-associated fibroblast
CAR	chimeric antigenic receptor
CCBE1	collagen and calcium binding EGF domain 1
CDC	complement-dependent cytotoxicity
CDCC	complement-dependent cellular cytotoxicity
COMP	cartilage oligomeric matrix protein
CTL	cytotoxic lymphocyte
CUB	complement C1r/C1s, Uegf, Bmp1
DAMP	damage-associated molecular pattern
DC	dendritic cell
DKK	dickkopf-related protein 3
DLL	delta-like
EC	endothelial cell
ECM	extracellular matrix
EMT	epithelial to mesenchymal transition
FACIT	fibril associated collagen with interrupted triple helix
FGF	fibroblast growth factor
GAG	glycosaminoglycan
GITR	glucocorticoid-induced TNF receptor
HKLLS	Hennekam lymphangiectasia–lymphedema syndrome
HPG-ALD	hyperbranched polyglycerol-aldehyde
iCAF	inflammatory CAF
IHC	immunohistochemistry
IL	interleukin
INOS	inducible nitric oxide synthase
iTRAQ	isobaric tag for relative and absolute quantitation
KLK	kallikrein related peptidase
KO	knockout
LOX	lysyl oxidase

LOXL	lysyl oxidase like
LTBP	latent TGFβ binding protein
MARCO	macrophage receptor with collagenous structure
MDSC	myeloid derived suppressor cell
MMP	matrix metalloproteinase
MMTV-PyMT	mouse mammary tumor virus-polyoma middle tumor-antigen
MS	mass spectrometry
MT-MMP	membrane-type MMP
N-TAILS	terminal amine isotopic labeling of substrates
NK	natural killer
OS	overall survival
PBMC	peripheral blood mononuclear cell
PD-1	programmed cell death protein 1
PDGF	platelet-derived growth factor
PDL1	programmed cell death protein-ligand 1
PLAC	protease and lacunin
PSA	prostate specific antigen
SLRP	small leucine rich proteoglycan
TAM	tumor-associated macrophages
TCR	T cell receptor
TGFβ1	transforming growth factor beta 1
TGFβR	transforming growth factor beta receptor
TIMP	tissue inhibitor of metalloproteinases
TME	tumor micro-environment
TRAIL	tumor-necrosis-factor related apoptosis inducing ligand
TS2-KO	ADAMTS2 knockout
TSP	thrombospondin
TSR1	thrombospondin type 1 repeat
UEGF	urinary epidermal growth factor
VEGF	vascular endothelial growth factor
VEGFR	vascular endothelial growth factor receptor
vWF	Von Willebrand factor
WT	wild type
αSMA	alpha smooth muscle actin

Introduction

I. Connective tissue

Connective tissue is one of the four main structures in our body, along with epithelia, muscles and nerve tissue. It provides mechanical stability and structural support for various tissues and organs. It also provides a structure for the exchange of nutrients and metabolites between cells, and with the circulatory system, via blood and lymphatic vessels. In addition, it enables intercellular communications, energy storage, inflammatory and immune responses, and the storage and release of growth factors and chemokines. Its composition and mechanical properties are also crucial to tissue physiology and the regulation of the residing cells, notably via modulation of their migration, survival, proliferation and differentiation.

Connective tissues contain several cell types of different embryonic origins:

- Fibroblastic cells (fibrocytes, osteocytes, chondrocytes ...) are responsible for the formation, remodeling and homeostasis of the extracellular matrices (ECM) which are characteristic of connective tissues (see below);
- Endothelial cells form the inner layer of blood and lymphatic vessels;
- Adipocytes produce fat for energy storage and thermal insulation;
- Mast cells trigger inflammation by releasing heparin and histamine, and regulate blood coagulation during wound healing;
- Macrophages are involved in the elimination of foreign bodies or damaged cells. They can also fuse and differentiate into osteoclasts;
- Extensions of neuronal and Schwann cells form nerve fibers.

I.A. The extracellular matrix

The composition and structure of the ECM vary according to the specific functions and needs of each tissue. Most often, its main scaffold consists in collagen structures to which macromolecules such as proteoglycans and glycoproteins are associated.

Collagens, especially fibrillar collagens, are central to this work and will be described in greater details, while the other components of the ECM will be mentioned only briefly.

I.A.1. Collagens

Collagens are the most abundant proteins in the extracellular matrix. They are involved in the maintenance of its structure and mechanical resistance. Collagens are also involved in cell adhesion, migration, haptotaxis and survival. Those processes are the keystones of tissue growth, differentiation and healing, but also participate in most pathological processes.

Collagens are composed of three polypeptides, called alpha chains, which associate to form at least one triple helical domain. These collagen trimers can be either homotrimeric (three identical alpha chains) or heterotrimeric (alpha chains expressed by two or three different genes). The sequence of alpha chains is conserved between species and is characterized by the repetition of a G-X-Y triplet, where G is glycine, and X and Y are often proline (Pro) or hydroxyproline (Hyp), respectively. Because of its small size, glycine is the only residue capable of occupying a central position in a triple helix. The pattern of one glycine every three amino acids is therefore required to the formation of the triple helix. Proline and hydroxyproline residues stabilize the triple helix through the formation of hydrogen bridges and electrostatic interactions involving lysine and aspartate residues (Figure 1)[1].

Figure 1: Triple helical structure of collagens. A polypeptide composed of repeats of the G-X-Y triplet forms a left-hand helix called the α chain. Three α chains combine to form a right-hand triple helix, with glycine residues (Gly) at the center of the triple helix, while residues in position X (often a Pro) and Y (often a Hyp) are located at the periphery.

To this day, 43 individual collagen genes have been identified in the human genome, allowing the formation of 28 different types of collagens (annotated from I to XXVIII based on their chronological discovery)[2].

It must be mentioned also that such "triple helical domain" is not exclusive to collagens as it can be found in other secreted or membrane proteins (C1q complement protein, adiponectin, ficoline, acetylcholinesterase and macrophage receptor with collagenous structure (MARCO)).

Collagens are divided in 8 main families:

- Fibrillar collagens (Types I, II, III, V, XI, XXIV et XXVII)
- Fibril associated collagens with interrupted Triple Helix (FACIT) (Types IX, XII, XIV, XVI, XIX, XX, XXI et XXII)
- Type IV collagen family (Type IV)
- Collagens forming hexagonal networks (Types VIII and X)
- Forming beaded filaments (Types VI, XXVIII)
- Forming anchoring fibrils (Type VII)
- Transmembrane collagens (Types XIII, XVII, XXIII and XXV)
- Multiplexin collagens (Types XV and XVIII)

In this work, a focus will be made on fibrillar collagens, especially type I collagen.

I.A.1.a. Fibrillar collagens

Fibrillar collagens are the most abundant collagens among vertebrates. Collagen fibrils vary in diameter from 15 to 500 nm, and even more in some tissues. Fibrils combine to form long fiber bundles in the ECM, where they contribute to the mechanical properties of skin, bone, cartilage, vessels and tendons. They are most abundant in skin, bone, cartilage, blood vessels and tendons.

Fibrillogenesis (formation of collagen fibrils) is a complex biological process involving multiple intra- and extra-cellular steps (Figure 2). α-chains are synthesized as precursors (pre-procollagens) containing a signal peptide and extensions (amino and carboxy-terminal propeptides) on either side of the central collagen domain. During translation, nascent polypeptides are enzymatically modified via hydroxylation of proline and lysine residues by prolyl-3 and -4 hydroxylases and lysyl hydroxylase, respectively. In addition, a galactosyl residue alone or followed by a glucosyl is enzymatically transferred to the hydroxyl group of hydroxylysine. Concurrently, three pro-alpha chains then spontaneously assemble in a process triggered by the formation of disulfide bridges in the carboxy-terminal propeptide, allowing the formation of the triple helical structure, starting from the carboxy-terminal propeptide and moving towards the aminopropeptide like a zipper. Mature collagen molecules are then secreted into the extracellular environment. During[3,4] and/or after secretion, amino- and carboxy-propeptides are cleaved by, respectively, aminoprocollagen peptidases (a disintegrin and metalloproteinase with thrombospondin motifs **(**ADAMTS) 2, 3 or 14) and carboxyprocollagen peptidases (mainly bone morphogenetic protein 1 (BMP1)), leaving two short free non-helical sequences, the telopeptides, on either side of the triple helix (Figure 3)[5].

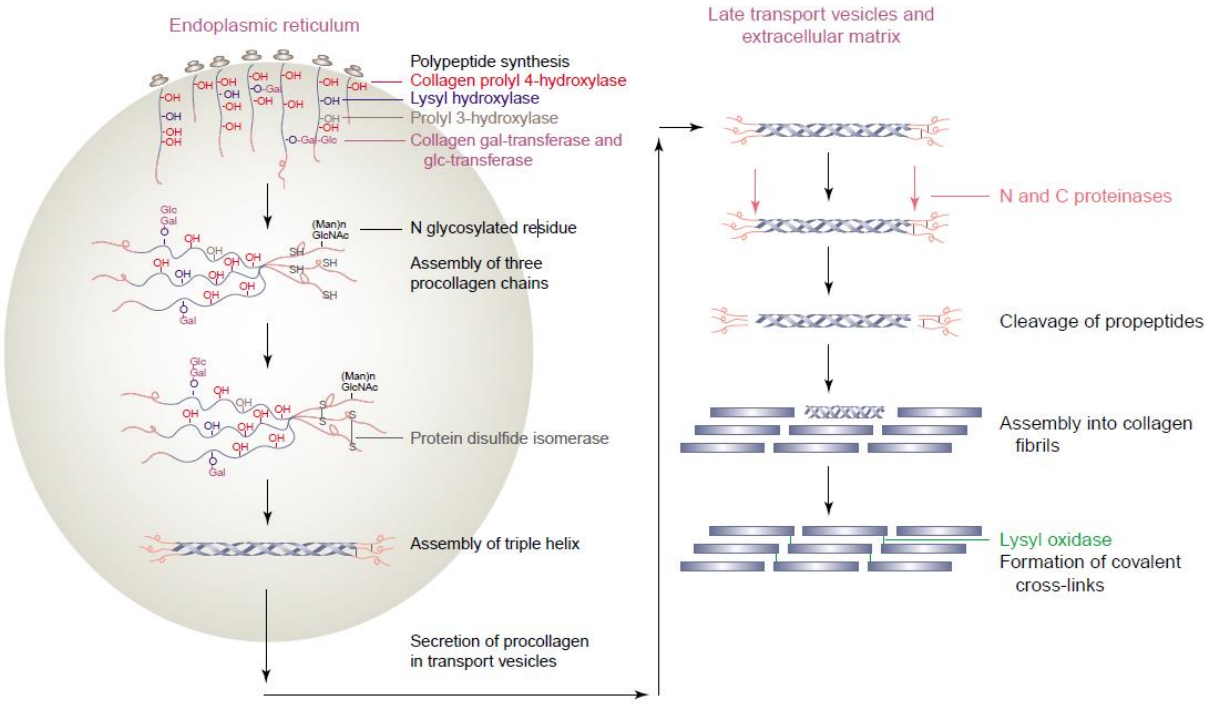

Figure 2: Fibrillogenesis of fibrillar collagens and supramolecular assemblies. After the pre-procollagen chains have been translated by ribosomes and secreted into the endoplasmic reticulum, the peptide signal is cleaved, releasing the α-procollagen chains. Hydroxylation of the proline and lysine residues then occurs, with some hydroxylysines being later glycosylated. The modified monomeric alpha chains assemble starting at their C-terminus to form the triple helix. Procollagen molecules are then secreted. During or after secretion, the amino- and carboxy-propeptides are excised by procollagen proteinases, leading to spontaneous assembly of the trimeric molecules into fibrils. These structures are then consolidated by the formation of covalent bonds initiated by the oxidation of some lysine and hydroxylysine residues into reactive aldehyde derivatives[6].

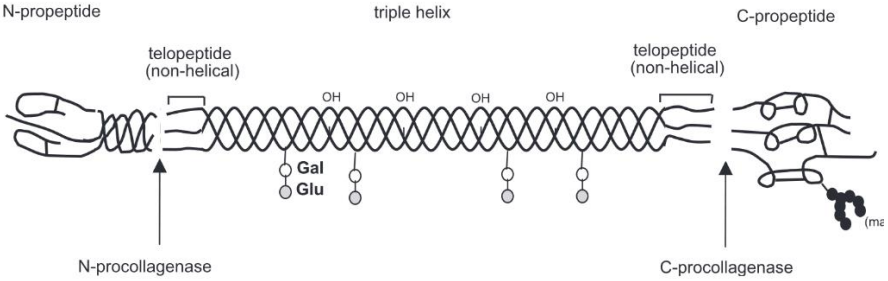

	COL1A1			COL1A2		
	N-propeptide	**Mature alpha chain**	**C-propeptide**	**N-propeptide**	**Mature alpha chain**	**C-propeptide**
Human	a.a. 23-161 (14 kDa)	a.a. 162-1218 (95 kDa)	a.a. 1219-1464 (28 kDa)	a.a. 23-79 (6 kDa)	a.a. 80-1119 (94 kDa)	a.a. 1120-1366 (28 kDa)
Mouse	a.a. 23-151 (13 kDa)	a.a. 152-1207 (95 kDa)	a.a. 1208-1453 (25 kDa)	a.a. 23-85 (6 kDa)	a.a. 86-1125 (94 kDa)	a.a. 1126-1372 (28 kDa)

Figure 3: Molecular structure of fibrillar procollagens and location of propeptides for type I collagen. After assembly of the triple helical procollagen, the amino- and carboxy-terminal propeptides are cleaved by aminoprocollagen proteinases (ADAMTS2, 3 or 14) and carboxyprocollagen proteinase (mainly BMP1). Only two short non-helical sequences, the telopeptides, are conserved on either side of the mature triple helix[7]. The size (in a.a.) and expected molecular weight (excluding post-translational modifications) are reported for the propeptides and mature chains of human and mouse COL1A1 and COL1A2.

Propeptide cleavage reduces the solubility of collagen trimers, which then spontaneously associate to form fibrils and fibers. These macromolecules are then stabilized by intra- and intermolecular covalent bonds catalyzed by lysyl oxidase. Complexes formed by two (or three) cross-linked alpha chains are known as beta (or gamma) chains. Their relative abundances increase with age due to the accumulation of covalent bounds resulting from lysyl oxidase and transglutaminase activity[8] and through chemical reactions involving "advanced glycation end products"[9].

Seven types of fibrillar collagens have been reported (types I, II, III, V, XI, XXIV and XXVII) which are formed by the assembly of 12 different alpha chains.

Type I collagen is the most abundant protein in the human body. It represents 90% of the organic matter in bones and is dominant in the dermis, tendons, ligaments and cornea. It is also found in all interstitial connective tissues except cartilages and vitreous humor. Type I collagen is a heterotrimer made out of two alpha 1 chains and one alpha 2 chain. It forms fibrils in association with type III collagen (in skin and blood vessels) and/or type V collagen (in tendon, bone, skin and cornea). Proteoglycans and FACIT collagens can also interact with type I collagen-containing fibers, regulating their formation and refining their rheological properties. In tendons and fascia, type I collagen provides mechanical strength through the formation of a parallel structure of compacted fibers stabilized by cross-links, while in the skin, its more "wavy" organization provides a degree of elasticity in addition to resistance to tearing. In bone, its association with hydroxyapatite determines biomechanical properties in terms of load, tensile strength and torsional rigidity.

Type II collagen is a homotrimer of COL2A1. It is found in the hyaline cartilage, the vitreous humor, the notochord and the pulposus nucleus of intervertebral discs. In cartilage, it is found in fibers in association with type XI and IX collagens. Compared to type I collagen, type II collagen displays more hydroxylysines and glycation residues which increase its capacity to interact with proteoglycans.

Type III collagen is a homotrimer of COL3A1. It is found in tissues containing type I collagen except in bones. It is particularly abundant in elastic tissues like blood vessels, the digestive tube, uterus and skin.

Type V collagen is present in only minor amounts within heterotypic type I collagen fibrils. However, it appears to play a critical role in collagen fibrillogenesis as it controls the initiation of collagen fibril assembly and regulates their diameter. It forms heterotypic fibrils with type I and type III collagens and can be found in bone, cornea, muscle, liver lung and placenta.

I.A.2. Elastic fibers and elastin

Elastic fibers are extracellular components that confer elasticity and resilience to tissues and organs such as large blood vessels, lungs and skin. Their formation first requires the formation of fibrillin-rich microfibrils in close association with fibronectin fibers, which then serve as primary scaffolds. Elastin is the main constituent of elastic fibers, accounting for 90% of its content. It is secreted, stabilized by crosslinking resulting from the activity of lysyl oxidase (and related enzymes) and associates with microfibrils to form elastic fibers.

I.A.3. Glycoproteins

Glycosylation (covalent bonding of carbohydrate molecules to a protein core) is one of the main post-translational modifications of proteins, thereby modifying their properties and functions. It affects, for example, ECM proteins (such as collagens), enzymes (such as ADAMTS2, 3 and 14), hormones (such as erythropoietin), cytokines (such as osteopontin) and immunoglobulins. N-glycosylation takes place on an asparagine (N) residue in an N-X-S/T sequence (where X represents any amino acid except proline). These carbohydrate chains are generally quite short, but can be highly branched. Carbohydrate chains can also be added to the hydroxyl group (O-glycosylation) of serine, threonine or hydroxylysine residues.

I.A.4. Proteoglycans

A proteoglycan consists of a protein core bearing variable numbers of glycosaminoglycan (GAG) chains covalently bonded to serine residues. GAGs are made up of a linear repetition of disaccharide units bearing negatively charged sulfate and carboxyl groups. They can be of the "chondroitin sulfate", "keratan sulfate", "dermatan sulfate" and "heparan sulfate" types, depending on the nature of the disaccharide unit. The biological functions of proteoglycans are multiple and variable. This complexity results both from the nature of the core protein and from the wide range of mechanisms modifying their structure. As for glycoproteins, they serve as intermediate binding site for ECM constituent and can serve for storage and presentation of growth factors to their receptors. Proteoglycans can be separated in three main groups based on their ECM and sub-cellular localization. The only known intracellular proteoglycan is serglycine. Extracellular proteoglycans include small leucine-rich proteoglycan (SLRP) and hyaluronan-bound proteoglycan (Hyalectans) like aggrecan and versican. Membrane bound proteoglycans are syndecans and glypicans (Figure 4).

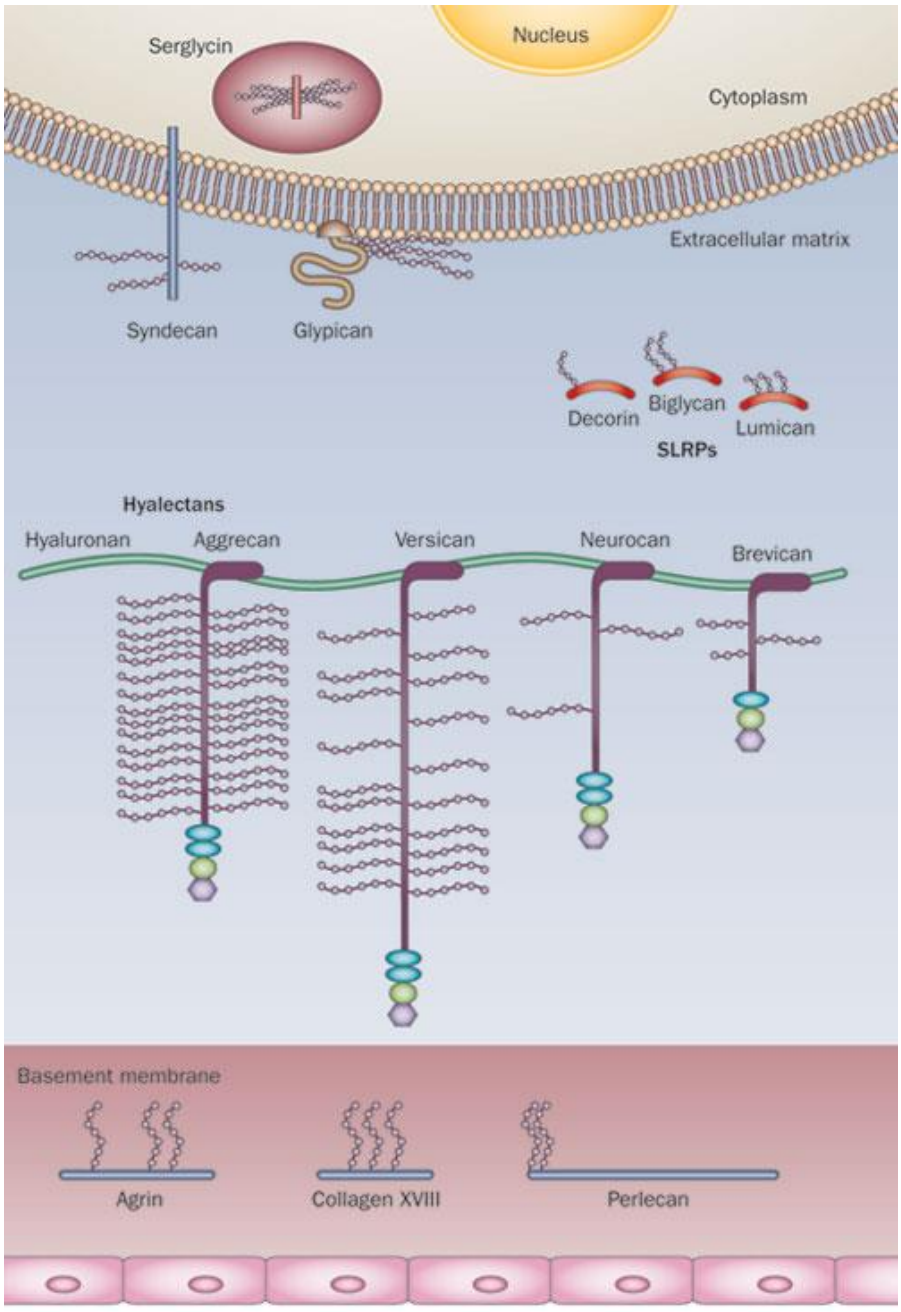

Figure 4: Proteoglycan classes based on localization. The only intracellular proteoglycan known to date is serglycine. Extracellular proteoglycans include hyalectans (aggrecan, versican, neurocan and brevican), which associate with hyaluronic acid in the ECM, and SLRPs (decorin, biglycan, lumican ...). Basement membrane proteoglycans include, perlecan, agrin and collagen XVIII. Finally, cell-associated proteoglycans include syndecans, which are transmembrane, and glypicans, which are anchored into the plasma membrane[10].

I.B. Cells in connective tissue

Connective tissues contain several cell types of different embryonic origins. They have different functions and may be resident or circulating. These cells include:

- Fibroblastic cells (fibroblasts, osteocytes, chondrocytes …) are responsible for the formation, remodeling and homeostasis of the ECM components (collagens, elastin, proteoglycans …);
- Adipocytes are specialized mesenchymal cells with the ability to produce and store fat for energy storage and thermal insulation;
- Endothelial cells form the inner layer of the blood and lymphatic vessels. Besides their primary role in blood or lymph sequestration, they are also involved in immune cell intravasation and extravasation, and in signaling during inflammation;
- Neurons residing (nucleus) in the spinal cord spread their axon in most tissue of the body where they provide innervation. They are surrounded in peripheral tissues by Schwann cells that from a myelin sheath around the axons and allow action potential to travel meter long neurons;
- Resident immune cells are mainly present in the infection prone organs that are in close contact with the environment such as lungs, intestine, liver and skin. Each tissue has specialized resident immune cells such as Kupffer cells in the liver sinusoids, the alveolar and interstitial macrophages in the lung and the Langerhans dendritic cells in the skin. Other specialized immune cells residing in the ECM are osteoclasts in bone, megakaryocytes in bone marrow, macrophages in adipose tissue, astrocytes in brain, lymphocytes in lymphoid organs and in the intestinal villi.

I.C. Cell-ECM interactions

Cell adhesion, migration, proliferation and differentiation are constantly regulated by signals from the environment. Cells are able to receive these signals via a variety of specific receptors that can bind membrane-associated molecules of adjacent cells (cell-cell interactions), secreted molecules (growth factors, cytokines) and components of the ECM (cell-ECM interactions).

Integrins are the main family of receptors responsible for adhesion between cells and their environment. They are heterodimers of non-covalently associated α and β subunits. In vertebrates, 18 α-subunits and 8 β-subunits can assemble into 24 different receptors. In general, an integrin can bind several ligands with different affinities. Conversely, an ECM protein, such as fibronectin, can be recognized by several integrins on identical or different sequences, forming a complex network of potential interactions. Each subunit has a large extracellular domain, a

transmembrane sequence and usually a short intracellular domain. Binding of the extracellular domain to the ECM is triggered by a specific amino acid sequence such as the RGD triplet for fibronectin or the GFOGER sequence for collagens (O for hydroxyproline). Intracellular domains allow indirect binding to the actin cytoskeleton via a complex of structural proteins and kinases, forming focal adhesions[11].

In contrast to resident cells, some cells interact with the ECM only moderately or only occasionally under specific circumstances. For example, mesenchymal stem cells circulating in the blood can infiltrate tissues to repair damaged tissue. The ECM serves as a support for migration[12], but also as a polarization signal for stem cells to differentiate into the appropriate cell type[13].

Migrating immune cells undergo different types of interactions as they leave blood vessels towards their final destination, guided by gradients of chemotactic signals. They first attach themselves to adhesion molecules expressed on the apical surface of endothelial cells. After extravasation from blood vessels, they interact with the ECM, which serves as a mechanical support for their migration[14] and participates to their activation/polarization[15].

II. Proteolytic enzymes

Proteases are proteins with a catalytic site capable of cleaving peptide bonds. They are involved in a plethora of physiological and pathological phenomena, from nutrient digestion to blood coagulation and wound healing. They are classified into several groups based on their amino acid residues (serine, threonine, cysteine, aspartate, glutamate) or the metal ion present in the catalytic site.

Most metalloproteases in the metzincin family play roles in connective tissue homeostasis. They share a conserved HExxHxxGxxH/D zinc-binding sequence in their catalytic site and a conserved Met-turn domain, essential for the three-dimensional conformation of the catalytic domain. Metzincins can be subdivided into serralysines (prokaryotic enzymes exclusively), matrixins, astacins and adamalysins (Figure 5).

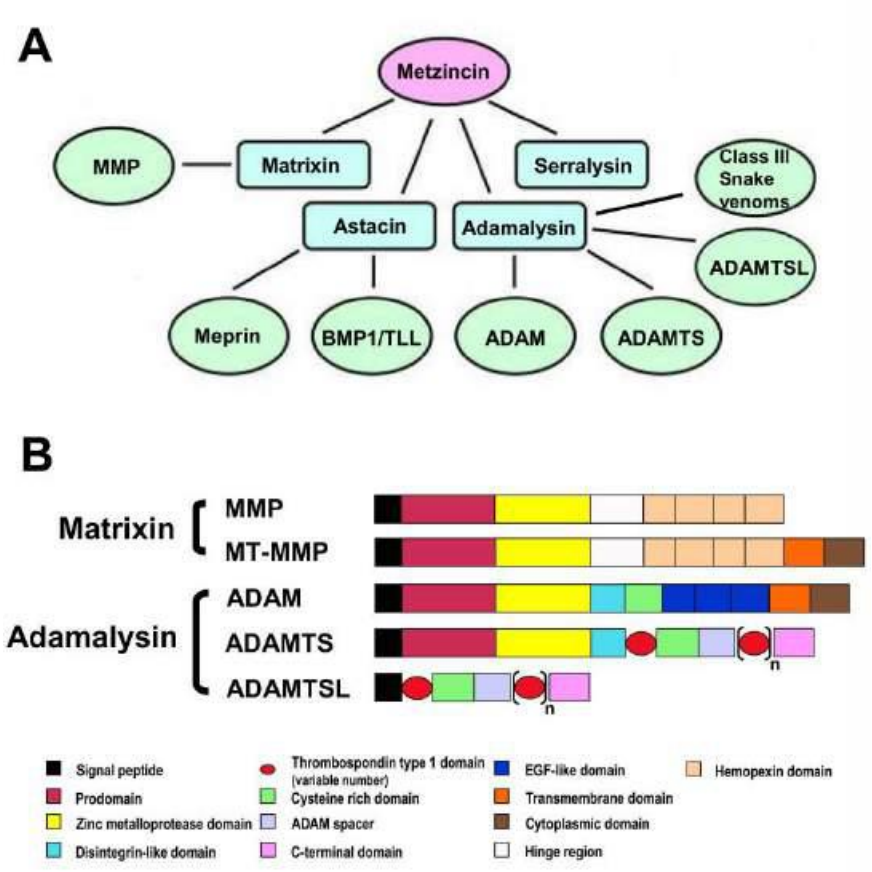

Figure 5: The metzincin family and general structure of matrixins and adamalysins. **(A)** Schematic representation of metzincin family subgroups. **(B)** Each MMP, ADAM and ADAMTS begins with a signal peptide, followed by a prodomain and a zinc metalloprotease domain. Most MMPs have a C-terminal hemopexin region. Four of the six membrane-type MMPs (MT-MMPs) and all the ADAMs have a transmembrane domain and an intracytoplasmic domain. ADAMs and ADAMTSs are characterized by the presence of a disintegrin domain and a cysteine-rich domain. ADAMTS also possess variable numbers (from 1 to 15) of type I thrombospondin repeats, a

spacer domain, and, for most of them, a specific C-terminal domain. ADAMTSL are homologous to ADAMTS but possess neither a prodomain nor a catalytic domain, making them ECM macromolecules rather than enzymes[16].

II.A. Matrixins

Matrixins are commonly known as matrix metalloproteases (MMPs). Twenty-three MMPs have been identified in human, 17 being secreted in the extracellular space and 6 being attached to the cell membrane. They were initially thought to regulate the ECM accumulation by degrading its protein components. But it became rapidly clear that they are involved in a plethora of additional processes such as the proteolytic activation or inhibition of factors like cytokines and chemokines. They are therefore central in physio-pathological situations like wound healing, angiogenesis, arthritis or cancer. Furthermore, MMP-mediated ECM degradation revealed to be more than just a destruction process as cleavage of ECM proteins can generate bioactive peptides called matrikines[17]. Such matrikines can originate from elastin[17], collagens[18], aggrecan, fibronectin, laminins, tenascin, syndecan[19] or thrombospondin[20], among others. They are reported to be involved in chemotaxis and inflammation[17], regulation of migration by interaction with integrins, and endothelial cell apoptosis[18,20].

II.B. Astacins

Astacins are involved in development, morphogenesis, matrix assembly, tissue differentiation and metabolism through a variety of functions such as digestive degradation of polypeptides, extracellular protein processing or activation of growth factors. Within this family, BMP1 and its related enzymes play key roles in ECM regulation by cleavage of the C-propeptide of type I and III procollagens, and of the N- and C-propeptides of type V procollagens. They are also involved in lysyl oxidase proteolytic activation (and thus in both collagen maturation and collagen/elastin fiber stabilization[21]), in transforming growth factor beta 1 (TGFβ1) activation (release) and SLRPs maturation[22].

II.C. ADAMs

A disintegrin and metalloprotease (ADAM) are metzincins possessing a transmembrane domain. This family contains 25 different proteins in human which all share a similar structure. ADAMs have an extracellular domain with a typical metzincin catalytic site and a disintegrin domain, a transmembrane domain and a cytoplasmic tail. They have a broad range of physiological roles like fertilization through the spermatozoid fixation and fusion to the oocyte or shedding of ectodomain of other membrane-bound proteins. For example, ADAM17 can cleave (and activate or inactivate) cytokines and growth factors, growth factor receptors and cell

adhesion factors, among many others[23,24]. As MMPs, they are therefore involved in many physio-pathological processes, including inflammation, cancer progression and neurological disorders.

II.D. ADAMTS

ADAMTS is another family of extracellular metalloproteases structurally similar to ADAMs, but without any transmembrane domain. To date, 19 ADAMTS have been described (numbered from 1 to 20, ADAMTS11 and ADAMTS5 being the same protein). The two first identified members of the ADAMTS family were ADAMTS1 and ADAMTS2 which have been described in 1997 by a Japanese team[25] and our laboratory[26], respectively. ADAMTS are present in both mammals and invertebrates like *Caenorhabditis elegans* and *Ciona intestinalis*. The maturation process of ADAMTS and the functional characterization of their domains have been thoroughly studied in our laboratory, especially for ADAMTS2 which will be taken as reference in this introduction.

After the signal peptide, ADAMTS can be considered to be organized into two main regions: the proteolytic domain, comprising the prodomain as well as the catalytic and disintegrin domains, and the ancillary domain forming the C-terminal part of the enzyme. Although lacking enzymatic activity, this last domain is important as it is involved in interactions with substrates, potential co-activators and the ECM.

II.D.1. Structure

Pro-domain/Pro-peptide: The signal peptide is followed by a propeptide which preserves enzymatic latency for most members of the ADAMTS family (Figure 6). Activation of these enzymes is mediated by the cleavage of a specific consensus sequence between the prodomain and the catalytic domain by enzymes of the proprotein convertase family, such as furin,

Metalloprotease domain: The catalytic site within the metalloproteinase domain is formed by the “HExxHxxGxxH” consensus sequence which is common to all metzincins. The three histidines shape the catalytic domain to interact with a zinc ion which is required for the catalytic activity. This structure is facilitated by a conserved glycine residue which tolerates a very tight hairpin loop and, therefore, allows the correct positioning of the three histidines. As for all MMPs and ADAMs, the zinc binding site is followed at short distance (13 to 19 amino acids) by a conserved methionine residue, crucial for the correct conformation of the catalytic site. One or two calcium ions also participate to the 3D structure and are necessary for proper activity[27].

Disintegrin domain: The catalytic domain is followed by a conserved domain called "disintegrin domain" (Figure 6). It is closely related to the one present in ADAMs but with a different pattern of cysteine residues localization. To date, the ability of the ADAMTS disintegrin domain to bind to integrins has never been demonstrated experimentally.

Thrombospondin I motifs: Following the disintegrin domain, all ADAMTS have a "thrombospondin type 1 repeat" domain (TSR1) (Figure 6). Such TSR1 domain is also found in various other ECM proteins, where they are involved in heparin interaction, TGFβ1 activation, cellular adhesion and angiogenesis inhibition. Except for ADAMTS4, all ADAMTSs contain 1 to 14 additional TSR1 repeats closer to the C-terminal extremity of the protein. Unlike the central TSR1 domain, these C-terminal TSR1 domains are less similar to the TSR1 present in other proteins and ADAMTSs. This suggests that these domains significantly contribute to the functional specificity of each ADAMTS.

Cystein rich domain: The central TSR1 domain is followed by a cysteine-rich domain that is very similar between ADAMTS (Figure 6). In ADAMTS2 and 13, this domain also contains an RGD sequence that could potentially bind to integrins.

Spacer domain: This domain lacks any specific signature or 3D structure. Its sequence is less conserved between the different ADAMTSs and no specific function has been assigned to it so far.

Additional domains: The most C-terminal part of ADAMTSs is highly variable and allows their sub-classification in 4 sub-families (Figure 6):

- ADAMTS9 and ADAMTS20 each possess a "gon-1 domain", gon-1 being an Adamts found in *C. elegans* where it is involved in gonad development.
- The protease and lacunin (PLAC) domain is found in ADAMTS2, 3, 6, 7, 12, 14, 16, 17, 18 and 19. This domain of around 40 a.a. is mainly characterized by the presence of six highly conserved cysteines. It is often associated with other domains, such as the thrombospondin type I repeat (as in ADAMTS) and the Kunitz proteinase inhibitor domain.
- The CUB domain (Complement C1r/C1s, Urinary epidermal growth factor (UEGF), BMP1) is only found in ADAMTS13.
- The mucine domain is only found in ADAMTS7 and ADAMTS12, between the third and fourth of their 7 TSR1 C-terminal domains. It is rich in serines, prolines and threonines residues, and is therefore likely to be highly glycosylated. This domain also contains attachment sites for one or more chains of chondroitin sulfate, identifying ADAMTS7 and 12 as being also proteoglycans[28].

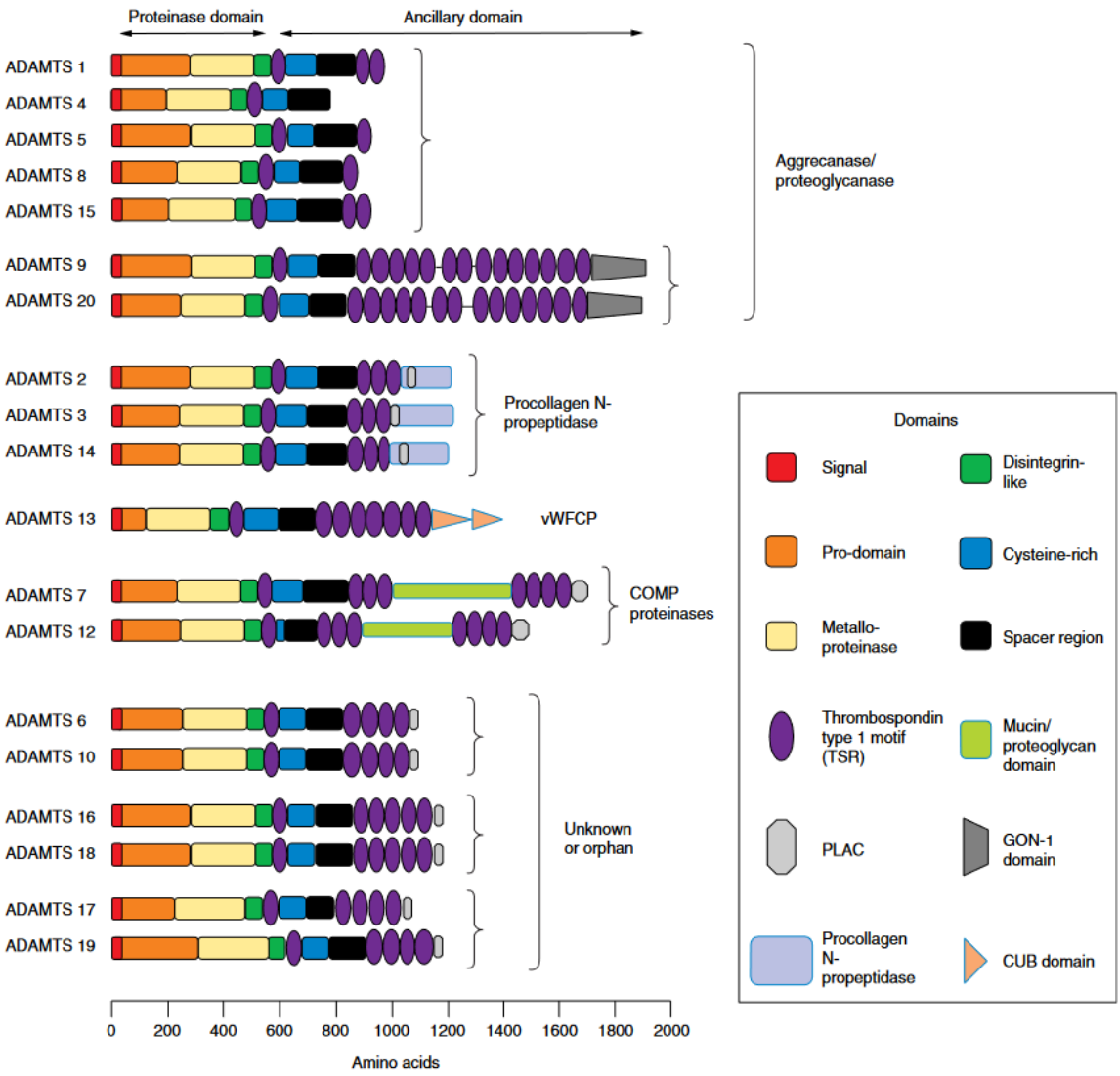

Figure 6: Phylogenetic organization and structure of the ADAMTS family. In addition to a signal peptide, all ADAMTSs have an identical organization of their N-terminal protease domain, which comprises the prodomain, the catalytic domain characteristic of metalloproteases, a disintegrin-like domain, a TSR1, a cysteine-rich domain and a spacer domain. ADAMTSs can be characterized and subdivided on the basis of their specific activities and substrates, which depends in particular on the variable organization of their C-terminal auxiliary domain. This comprises at least one TSR1 (except for ADAMTS4) and possibly other domains. Proteoglycanases (or aggrecanases) are a subgroup of ADAMTSs capable of cleaving proteoglycans and aggrecan in particular. Another group of ADAMTSs, characterized by the presence of a mucin domain, includes ADAMTS7 and 12. This particular domain gives them the status of proteoglycan. Data suggest that these two ADAMTS are capable of cleaving COMP. To date, ADAMTS13 is the only ADAMTS known to cleave von Willebrand factor. ADAMTS2, 3 and 14 share an identical organization with high sequence homology. They are characterized by the presence of 3 TSRs in their C-terminal region, an aminoprocollagen proteinase domain and a PLAC domain. These are the only ADAMTSs known to have aminoprocollagen proteinase activity[29].

II.D.2. Post-translational modifications and enzymatic activity regulations

All ADAMTSs (with the exception of ADAMTS13) are secreted as zymogen, their activity being repressed by the interaction of the N-propeptide with the catalytic domain. Their activation therefore requires N-propeptide cleavage, a process mediated by pro-protein convertases at a specific consensus sequence separating the pro-domain from the metalloproteinase domain.

Additionally, proteolytic cleavages of the ancillary C-terminal domain of some ADAMTSs (ADAMTS2, 4 and 13) have been shown to increase their proteolytic activity, a mechanism probably linked to conformational changes or substrate recognition[30]. Both autocatalytic processing and cleavage by other proteases have been reported.

To date, only a limited number of natural inhibitors have been described for ADAMTS, like the tissue inhibitor of metalloprotease 3 (TIMP3) or the broad-spectrum inhibitor alpha-macroglobulin. Other mechanisms of inhibition are expected to result from domain competition/domain masking by proteins with a similar structure. For example, papilin (an ADAMTSL member) has been shown to competitively inhibit ADAMTS2 activity *in vitro* likely due to the structural similarity between the two proteins[31]. Similar mechanisms has been hypothesized for the other ADAMTSL, but never experimentally confirmed[32].

Despite their high structural similarities, a wide range of specific functions have been reported for the different ADAMTS. Beyond the differences in their expression pattern, it is considered that the nature and composition of their C-terminal domains are key determinants for their specificity. In this manuscript, only the most studied ADAMTS (ADAMTS1, 4, 5, 13), as well as ADAMTS2, 3, 7, 12 and 14, which are directly related to projects of our laboratory, will be further described.

II.D.3. ADAMTS1, 4 and 5

ADAMTS1,4 and 5 are classified as "aggrecanases" due to their ability to cleave aggrecan. Many other substrates have been described such as other proteoglycans (versican, brevican, SRLPs, syndecan, decorin, biglycan), fibromodulin or cartilage oligomeric matrix protein (COMP).

ADAMTS1 was first associated with inflammation[33], organogenesis[34] and inhibition of angiogenesis, notably by preventing the vascular endothelial growth factor (VEGF) from interacting with its receptor[35] and by degrading angiogenic factors[36]. ADAMTS1 has also been described as an important factor in the tumorigenic process[37,38]. It is also able to inhibit lymphatic sprouting *in vitro* by interfering with the VEGFR3-VEGFC signaling[39]. Finally, our laboratory showed that ADAMTS1 is also involved the TGFβ2 pathway and participates in the control of versican accumulation in myxomatous valves in human[40].

Aggrecan degradation is one of the first signs of cartilage degeneration[41]. ADAMTS4 and ADAMTS5 have a very similar structure, have been linked to osteoarthritis and display

aggrecanase activity *in vitro*. However, while ADAMTS5 knockout mice are efficiently protected from osteoarthritis, ADAMTS4 knockout mice are not. ADAMTS4 also differs from ADAMTS5 as it is overexpressed in an inflammatory context while ADAMTS5 is constitutively expressed[42]. Inhibitors for aggrecanases are being investigated as treatment for osteoarthritis (ADAMTS inhibitors will be further described in the discussion).

II.D.4. ADAMTS13

ADAMTS13 is the only member of the ADAMTS family with a C-terminal end formed by CUB domains. It processes polymers of von Willebrand factors (vWF), a large plasma glycoprotein, to generate multimers of optimal size for proper blood coagulation. A mutation in ADAMTS13 results in thrombotic thrombocytopenic purpura, an autosomal recessive disease characterized by extensive microvascular thrombosis.

II.D.5. ADAMTS7 and 12

ADAMTS7 and 12 are unique enzymes within the ADAMTS family due to the presence of a highly glycosylated mucin-like domain containing glycosaminoglycan attachment sites, explaining why these two ADAMTS can also be considered as proteoglycans[28]. Both ADAMTS7 and ADAMTS12 are able to cleave COMP[43,44] which has been associated with cartilage degradation and osteoarthritis[45–48]. ADAMTS12 was also shown to negatively regulate the differentiation of chondrocytes[49].

ADAMTS7 is overexpressed in response to inflammation[47] and is considered as pro-atherogenic. In humans, polymorphisms that reduce ADAMTS7 secretion and activity are associated with a reduction in coronary heart disease. In mouse models, mutation of the ADAMTS7 catalytic site[50] and immunization against ADAMTS7[51] both reduce atherosclerosis.

ADAMTS12 is expressed in mesenchymal cells such as fibroblasts, adipocytes, chondrocytes or stellate cells. Several studies also indicate that ADAMTS12 plays a role in inflammatory processes. In asthma models, exacerbated inflammation was identified in the lungs of ADAMTS12 knockout mice sensitized to ovalbumin or house dust mites[52]. Similar results were observed in colons subjected to chronic exposure to dextran sulfate sodium[53]. There is strong evidence suggesting that the absence of ADAMTS12 potentiates the immunological inflammation response in pathological state. Another peculiar observation is that the combined absence of ADAMTS7 and ADAMTS12 (in ADAMTS7/ADAMTS12 double knockout mice) leads to heterotopic ossification[54]. Several publications also indicate a role for ADAMTS12 in cancer progression. Although these data were sometimes confusing, with studies indicating that it has either pro- or anti-cancer properties, depending on the type of cancer[55,56,57]. The mechanisms involved have not been fully elucidated neither, although regulation of inflammation and angiogenesis may be involved[58,59]. The antitumor properties of ADAMTS12 may also be linked to the enzyme's ability to bind fibulin-2 via its mucin domain[60,61].

II.D.6. ADAMTS2,3 and 14

II.D.6.a. Discovery and initial characterizations

Within the ADAMTS family, ADAMTS 2, 3 and 14 form the "aminoprocollagen peptidase" subgroup. They have identical domain composition and high sequence similarity. They were cloned and characterized in our laboratory and are the subject of this doctoral thesis. They will therefore be described in greater details.

ADAMTS2

The first description of an enzyme possessing "aminoprocollagen peptidase" activity resulted from the pioneering work of Lapière *et al* in studies aimed at identifying the cause of dermatosparaxis in cattle, a hereditary disease characterized by extreme fragility of the skin, a defect resulting from the accumulation of type I collagen still retaining its aminopropeptide end[62]. But it wasn't until the 1990s that the enzyme responsible for this activity was cloned and fully characterized in our laboratory, and named ADAMTS2 according to current nomenclature[63,26]. On the basis of this information, mutations affecting ADAMTS2 activity were found to be the cause of bovine dermatosparaxis, but also of the dermatosparaxis type of Ehlers-Danlos syndrome, a human hereditary disease with the same characteristics as animal dermatosparaxis[64,65]. A dozen of other patients with different types of mutations were later identified by us and other[66–73].

In 2001, an ADAMTS2 knockout (TS2-KO) mouse model was developed[74]. These mice show extreme skin fragility, as previously observed in dermatosparactic animals and human patients. In addition, they also enabled a more complete characterization of all the potential defects resulting from the absence of ADAMTS2 activity. ADAMTS2 knockout neonates are normal, and pups develop normally for up to 2 weeks. Collagen fibrils are normal and the skin is not particularly fragile. However, at one month of age, abnormal processing of type I collagen and skin fragility are clearly visible. An another striking phenotype of these mice is the azoospermia of male mice causing sterility. The underlying mechanism of male mouse infertility, which is probably unrelated to collagen biology, has never been identified. TS2-KO mice were reported to have an abnormally thin lung parenchyma, through a mechanism that is neither associated with inflammatory cells infiltration nor elastin, collagen or basement membrane alterations[75]. Analysis of collagen content in TS2-KO mice also demonstrated that type III and type V procollagens are additional substrates of ADAMTS2. More surprisingly, it showed also that a significant proportion (around 30%) of type I collagen was fully processed in the skin of TS2-KO mice, with proportions even higher in other tissues such as tendon, cornea or bone[76]. This clearly suggested that at least one additional enzyme also exhibits aminoprocollagen peptidase activity, an observation that has largely contributed to the identification of ADAMTS3 and ADAMTS14 as additional aminoprocollagen peptidases[77].

ADAMTS3

The ADAMTS3 cDNA sequence has first been reported in 1997 as a gene product of unknown function (KIAA0366)[78] and defined as an ADAMTS closely after[79]. The aminoprocollagen peptidase activity of the ADAMTS3 was only identified later by its capacity to process type I and type II procollagens, similarly to ADAMTS2[80,75].

As with ADAMTS2, an ADAMTS3 knockout mouse model was developed. However, no offspring were obtained due to embryonic lethality caused by altered placental vessels and massive generalized edema in the embryo resulting from lack of lymphatic network formation. The common underlying cause has been identified. It is not related to the aminoprocollagen peptidase activity of ADAMTS3 but to its ability to cleave pro-VEGFC into fully active VEGFC capable of interacting with and stimulating VEGFR3, a receptor critically involved in the regulation of lymphatic endothelial cells[81]. Based on these data, it was later found for the first time that hypomorphic mutations in ADAMTS3 in human patients result in distinctive facial features and cause primary lymphedema, an inherited disease now known as Hennekam lymphangiectasia-lymphedema syndrome-3[82]. Additionally, it was found that ADAMTS3 is also able to cleave and inactivate reelin in the brain, suggesting that ADAMTS3 inhibition may be an effective treatment for neuropsychiatric and neurodegenerative disorders[83]. It is worth noting that ADAMTS2 was later identified as being also able to cleave reelin[84].

ADAMTS14

ADAMTS14 has been identified by two research groups[77,85]. Our laboratory has shown that its expression largely overlaps with ADAMTS2 and that it possesses only very limited aminoprocollagen peptidase activity, despite its structural similarity to ADAMTS2 and ADAMTS3. ADAMTS14 knockout mice have been generated, but do not show any significant phenotype, except some resistance to weight-gain under obesogenic conditions[86]. To test whether ADAMTS14 expression might be responsible for the mature type I collagen still present in TS2-KO mice, mice deficient in both ADAMTS2 and ADAMTS14 were generated. Collagen maturation was not further impaired in double KO mice, demonstrating that the main function of ADAMTS14 *in vivo* is unlikely to be related to collagen processing. Unexpectedly, mice lacking both ADAMTS2 and ADAMTS14 developed skin lesions reminiscent of human atopic dermatitis, with root cause being related to pathological activation of immune cells[87]. This suggested a hitherto unknown involvement of these two enzymes in the regulation of the immune system, at least at the skin level.

II.D.6.b. ADAMTS2: regulation of expression and potential association to pathological states

Among the aminoprocollagen peptidases, ADAMTS2 has been the most extensively characterized. As it represents also the main focus of the present study, this chapter will concentrate primarily on the mechanisms regulating its expression and activity, with potential or proven relationships with several acquired diseases or pathological conditions.

Initial experiments have shown that ADAMTS2 expression is strongly correlated with that of fibrillar collagens, in line with its identified aminoprocollagen peptidase activity. As examples, ADAMTS2 mRNA expression is stimulated *in vitro* by pro-fibrotic factors such as TGFβ1[88]. It is also highly expressed in connective tissues during embryogenesis, and in pathological situations such as fibrodysplasia[89], cardiac hypertrophy induced by pressure overload[90] and liver fibrosis[91] and cirrhosis[92,93].

In human, multiple variants or single nucleotide polymorphisms of ADAMTS2 have been linked to pathologies such as premature rupture of the gestational sac[94], myopia[95], central corneal thickness[96], brain aneurysms[97] and pediatric stroke[98]. Finally, ADAMTS2 mRNA expression in the anterior cingulate correlates with the tau and amyloid load which are markers of neurodegenerative diseases[99]

Alcohol consumption increases ADAMTS2 mRNA expression in the muscle[100], while endoplasmic reticulum stress and glucose deprivation tend to decrease its expression in chondrocyte and dermal fibroblasts[101]. Gonadotropin releasing hormone[102], radiotherapy of the salivary gland[103] and hypoxia[104] all result in an increased expression of ADAMTS2. Expression of ADAMTS2 in peripheral blood mononuclear cells (PBMCs) is 10-fold higher for patient with schizophrenia as compared to controls[105]. Anti-psychotic drugs decrease ADAMTS2 expression with correlations to response to treatment[106]. The regulatory pathway has been identified and involved the dopaminergic signaling of the D1 dopamine receptor, and the activation of cAMP/CREB and MAPK/ERK signaling[105].

II.D.6.c. ADAMTS2 and the immune system

The first observation of a potential link between ADAMTS2 and the immune system results from a study showing a strong induction of ADAMTS2 expression in monocytes and macrophages treated with glucocorticoids[107]. It was later shown that macrophages recruited from the circulation can also express ADAMTS2[108]. Finally, more recent publications confirmed that ADAMTS2 is one of the most overexpressed gene in response to glucocorticoids especially in monocytes and macrophages[109,110]. It was also reported that ADAMTS2 expression in blood leukocytes can be predictive of the preterm birth in pregnant patient[111], although this correlation may result from the fact that women at risk of preterm birth receive glucocorticoid treatment as part of a therapeutic regimen against preterm birth.

Both schizophrenia (see above) and the response to glucocorticoids could be intertwined as it is known that cortisol level in schizophrenia patient is elevated which may increase ADAMTS2 expression in PBMC in those patients[112].

In other types of experimental approaches, cultured osteosarcoma cells have been shown to overexpress ADAMTS2 after treatment with IL-6[113] and IL-1α[114]. In the same line, intestinal villus inflammation from a celiac disease mouse model shows also increased ADAMTS2 expression[115]. The aminoprocollagen proteinases have also been linked to pathological processes associated with inflammation. As examples, upregulations of ADAMTS2 and 14 expression have been described

in the cartilage of patients with osteoarthritis[116] as well as in the meniscus of rat and mice in models of early osteoarthritis[117,118].

II.D.6.d. ADAMTS2: functions beyond procollagen processing

As reported above, the first discovered function of ADAMTS2 has been the cleavage of the aminopropeptide of fibrillar collagens. The first compelling evidence that ADAMTS2 plays roles other than procollagen processing was provided by our laboratory. Recombinant ADAMTS2 was shown to reduce endothelial cell proliferation and induce detachment from the substrate, leading to their apoptosis. Dephosphorylation of ERK1/2 and myosin light chain is probably involved in these ADAMTS2-mediated morphological alterations. These effects were not observed in mesenchymal cells, demonstrating the specificity of these regulations. Nucleolin, a nuclear protein also present on the cell surface, was identified as a receptor for ADAMTS2, which could mediate its antiangiogenic properties[119].

Other investigations were carried out in our laboratory as an effort to provide a more comprehensive overview of ADAMTS2 substrates. These studies were based on the use of a specific proteomic approach requiring the labeling of N-terminal amine of proteins (NH2-Terminal Amine Labeling of Substrates: N-TAILS) using iTRAQ markers (isobaric Tag for Relative and Absolute Quantification). They allowed the discovery of new substrates of ADAMTS2 and its role in TGFβ signaling[120].

II.E. Determination of protease substrates with Terminal Amine Isotopic Labeling of Substrates

iTRAQ is an isotopic and isobaric tag. It is made up of three parts (Figure 7, A): a functional group that reacts specifically with primary amines; a reporter group, whose mass varies from 114.1 to 117.1 Da and enables identification of the tagged peptide via tandem mass spectrometry; and a "balance" group whose mass varies inversely to that of the reporter in order to maintain an identical total mass of 145 Da to the tag, regardless of that of the reporter[121]. The mass variations of the reporters and the balance groups are due to the presence of certain isotopes ^{13}C, ^{15}N and ^{18}O (Figure 7, B). The iTRAQ reagent therefore does not increase the peptide complexity of samples from multiple proteomes, as it does not differentially modify peptide mass. Therefore, identical peptides labeled with different iTRAQ markers cannot be distinguishable in the first dimension of mass spectrometry, since they are detected with their intrinsic mass increased by 145 Da, regardless of the sample from which they originate. It is only in the second MS/MS dimension, after fragmentation of the peptides and iTRAQ markers, that identifications can be made. The relative abundance of each of the reporter ions therefore enables to determine directly, for each peptide, what proportion is derived from each of the experimental conditions, while the peptide fragmentation products enables to identify their sequence and protein origin (Figure 7, C).

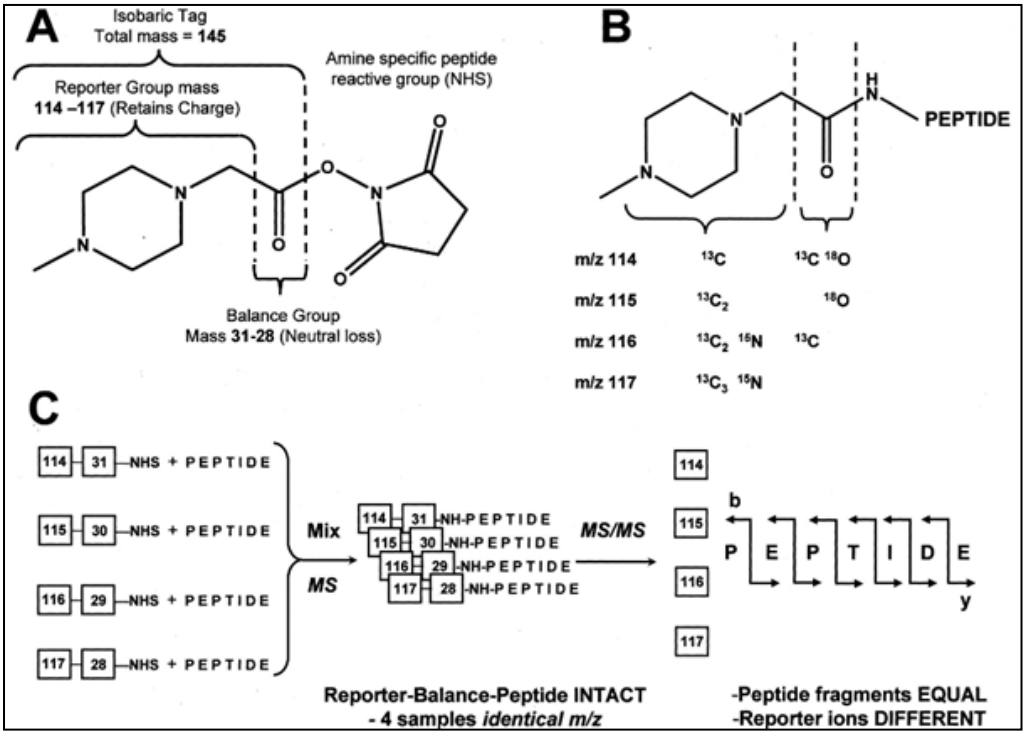

Figure 7: Schematic representation of the iTRAQ tags and their MS/MS fragmentation. (A) Representation of the isobaric tag composed of the reporter group which allows sample identification and the balancer group that compensates for the mass variation of the reporter group. (B) Composition of the different ITRAQ tags in carbon (C), oxygene (O) and nitrogen (N). (C) Schematic representation of the MS/MS strategy. First, the samples are individually labeled with a different ITRAQ tag. Next, samples are pooled and tag peptides are selected based on the m/z ratio. The same peptide tagged with different ITRAQ tags has the same mass and thus the same m/z ratio. In the fragmentation (MS/MS), the reporter is release which allow the identification of the sample of origin.

Developed in 2010, iTRAQ-TAILS (Terminal Amine Isotopic Labeling of Substrates) is a high-throughput relative quantification technic based on tandem mass spectrometry (MS/MS) analyses. This technic aims to highlight a difference in the relative abundance of N-terminal peptides present in samples containing or not a studied protease[122–124]. Any peptide whose relative abundance is modified suggests that the protein from which it is derived is a substrate for the protease under study.

During the iTRAQ-TAILS procedure, the samples to be analyzed, either containing or not the protease of interest, are harvested, reduced and alkylated to avoid the formation of polypeptide complexes. The "free" amines (present at the N-termini and on the side chains of the lysines) are then specifically labelled, and thus blocked, by specific iTRAQ isobaric markers (one for each of the conditions compared). It is worth mentioning that N-terminal peptides can be either neo-N-termini newly generated by the protease under study, or mature N-terminal peptides corresponding to the N-terminus of the labeled mature protein. The samples are then mixed in equal proportions and digested by a specific endopeptidase (usually trypsin), resulting in the formation of two types

of small peptides: N-terminal peptides whose primary amine is blocked by iTRAQ, and newly generated internal peptides with a free N-terminal primary amine. N-terminal peptides are then specifically enriched by negative selection using a specific polymer HPG-ALD (hyperbranched polyglycerol-aldehyde), which reacts with free primary amines to form covalent bonds. This polymer will therefore only retain tryptic peptides, since the initially free N-terminal ends have been labeled and blocked by iTRAQ. Samples enriched in peptides of interest are then analyzed by MS/MS. An abundance ratio is calculated for each peptide identified, reflecting the relative abundance of that peptide in the condition with protease compared to the negative control (Figure 8). A ratio of around 1 indicates a similar overall abundance of the peptide in the conditions with and without the studied protease. This is the case for mature N-terminal peptides or for peptides resulting from proteolysis independent of the protease under study. A "protease/control" ratio >1 indicates that the protein from which it is derived could be a substrate for the protease of interest. Furthermore, the N-terminus of the identified peptide marks the potential cleavage site. Finally, a "protease/control" ratio < 1 means that the peptide of interest disappears in the presence of the protease. This may be the result of cleavage by the protease within the peptide, providing an indirect sign of enzymatic activity. In theory, any peptide with a ratio >1 or < 1 should have a corresponding peptide of the same protein with an inverse ratio. Although this is sometimes the case, MS/MS analyses rarely allow their simultaneous detection, due to the limitations (size, ionization, masking by other more abundant peptides, etc.) inherent in the technique (Figure 9).

iTRAQ-TAILS has enabled the identification of numerous substrates of different enzymes including several MMPs[124,125] and cathepsins[126] *in vitro*, and also on biological fluids *in vivo*[127]. Our laboratory was the first to implement and adapt this approach to the study of ADAMTS *in vitro* as a way to provide a more comprehensive characterization of their repertoire of substrates and functions. ADAMTS2, 3 and 14 were evaluated in parallel using *in vitro* models[120]. The N-TAILS analyses unambiguously identified the already known cleavage sites in procollagen I, III and V, confirming the specificity and reliability of the experimental approach. Amongst the newly identified substrates, many are involved in the TGFβ signaling pathway (LTBP1, DKK3 and TGFβRIII) showing that the three enzymes can modulate cell phenotype and connective tissue homeostasis though mechanisms independent of their aminoprocollagen peptidase activity. Lysyl oxidase (LOX) and Lysyl Oxidase-Like 1 (LOX-L1), two enzymes participating in the modification and stabilization of collagen fibrils, were also identified as potential substrates. These cleavages were validated later using complementary approaches and were shown to modulate the activity of both LOX and LOX-L1[21], which confirmed the relevance of the N-TAILS experimental approach to identify “novel” functions of ADAMTS enzymes.

Based on these positive results, the Laboratory of Connective Tissues Biology decided to go one step further, in terms of relevance and complexity, by analyzing mouse skin samples to search for substrates of ADAMTS2 and 14 in *in vivo* samples[128]. As I was partly involved in that study, it will be described in detail in the "Results" section of this manuscript.

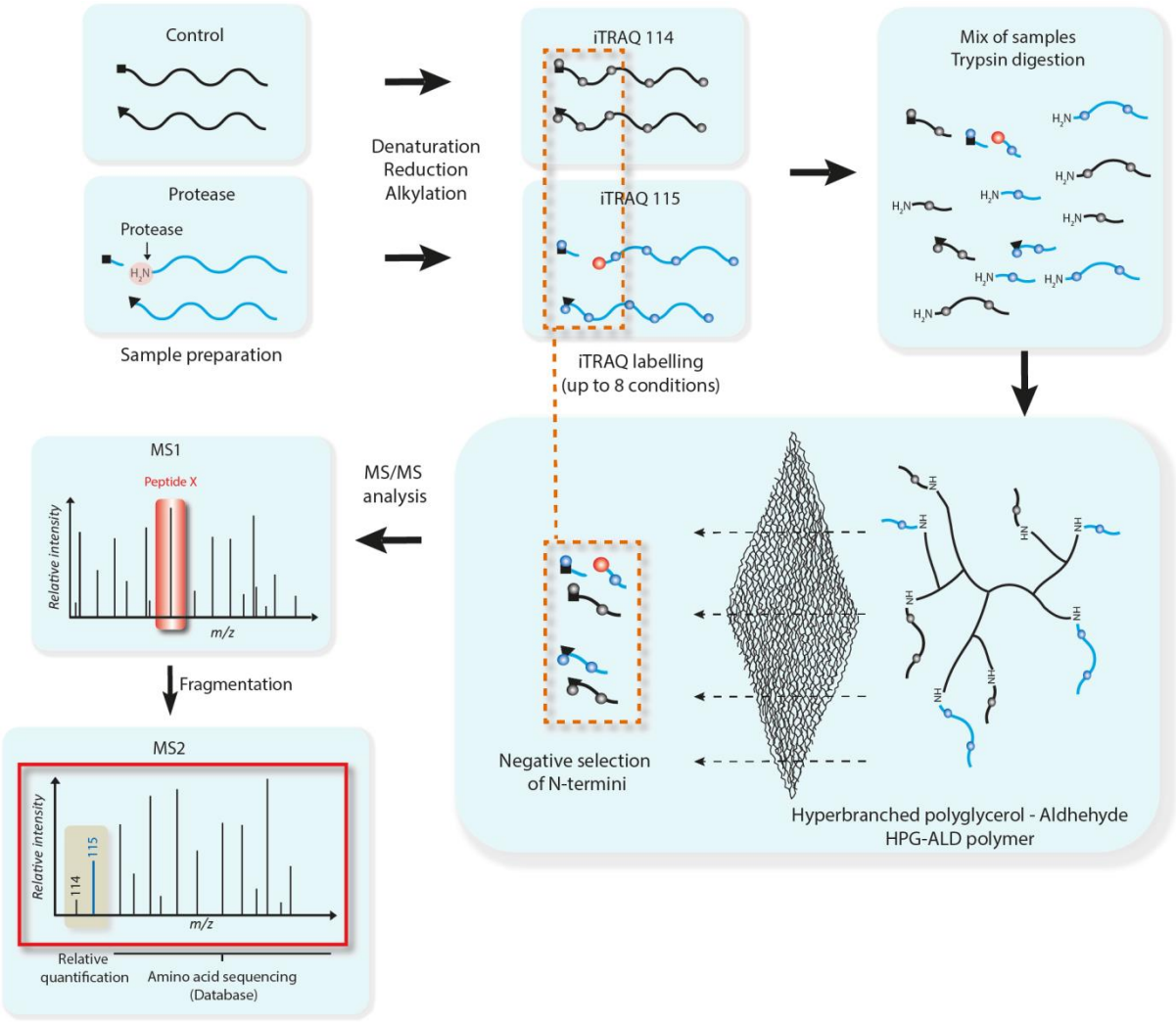

Figure 8: Schematic representation of the iTRAQ-TAILS experimental protocol. Proteins from control and protease-treated samples undergo denaturation, reduction and alkylation. Both conditions are then labeled with a specific iTRAQ tag here (ITRAQ 114 for control and ITRAQ 115 for the protease sample) that reacts with primary amines located on the lysine side chain and at the free N-terminal ends already present or generated by the protease. After labeling, samples were mixed in equivalent proportions and digested with trypsin. The samples are then mixed with the HPG-ALD polymer which reacts with the primary amines, retaining the peptides generated by trypsin, but not the N-termini (labeled by iTRAQ), and are therefore negatively selected. This sample enriched in N-terminally labeled peptides is finally analyzed by MS/MS, enabling both identification and relative quantification of the labeled peptides.

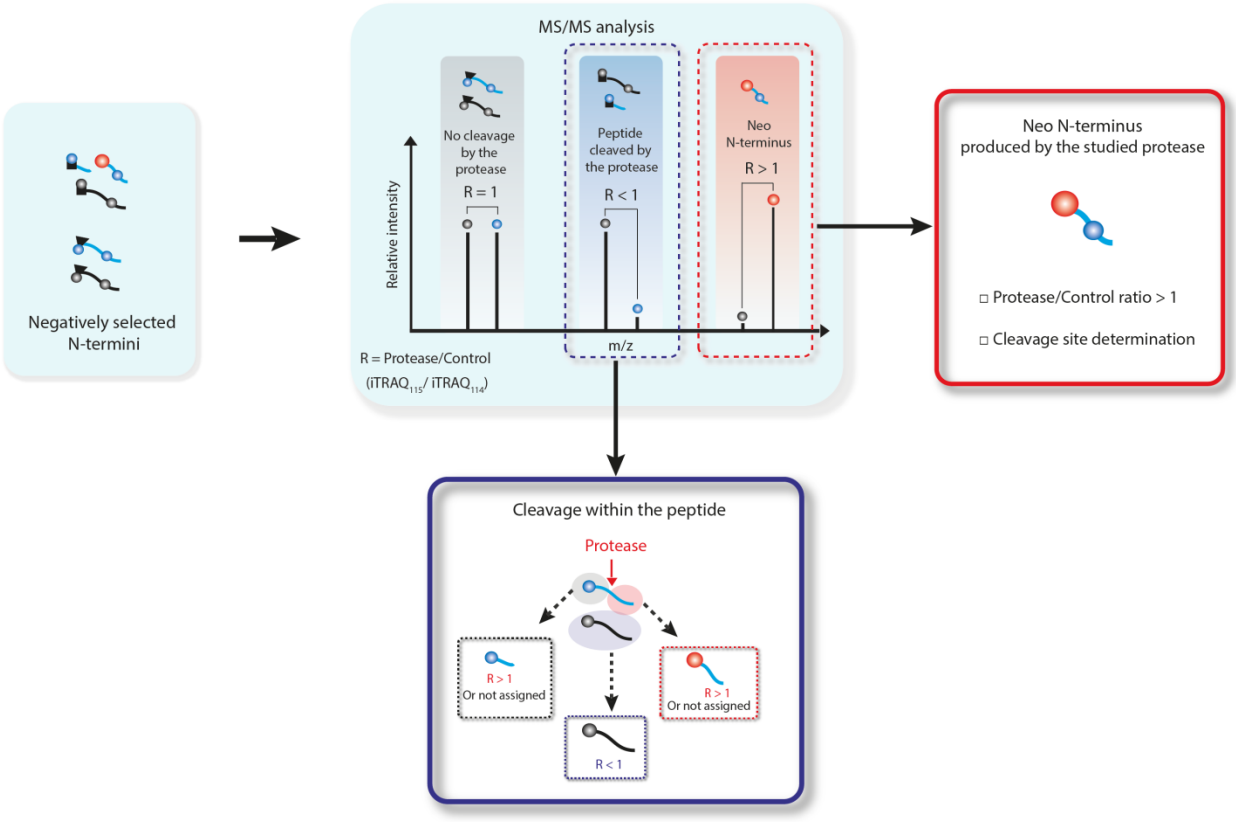

Figure 9: Schematic representation of the semi-quantitative process of ITRAQ label peptide analysis between a control and protease condition. MS/MS analysis of the N-terminal peptides resulting from iTRAQ-TAILS sample preparation results in the determination of the relative abundance, in the presence and absence of the protease studied, of each peptide identified. A ratio close to 1 means that there is no effect of the protease on the identified protein. A "protease/control" ratio significantly greater than 1 suggests that the identified peptide is probably generated by the protease. In this case, the N-terminus of the peptide marks the cleavage site. A ratio of less than 1 can be explained by cleavage within the identified peptide by the protease, but also by distant cleavage leading to more complete degradation of the substrate by other proteases. In this case, precise identification of the cleavage site is impossible. Theoretically, any peptide with a ratio less than 1 should correspond to two peptides with a ratio greater than 1, resulting from the genesis of both peptides by cleavage of the initial protein. In practice, this is rarely the case, due to intrinsic limitations of the technique (adequate peptide size, iTRAQ labeling, insufficient resolution, etc.).

III. The vascular system

The development of the vascular system is one of the first events in organogenesis. Tissues and organs depend on it for the supply of nutrients and oxygen, and for the removal of metabolites. Vasculogenesis refers to the differentiation of endothelial precursor cells (angioblasts) into endothelial cells (ECs) and the de novo formation of a primitive vascular network. Angiogenesis is the process of growing new capillaries from pre-existing blood vessels, through various mechanisms, principally sprouting and intussusception (Figure 10)[129].

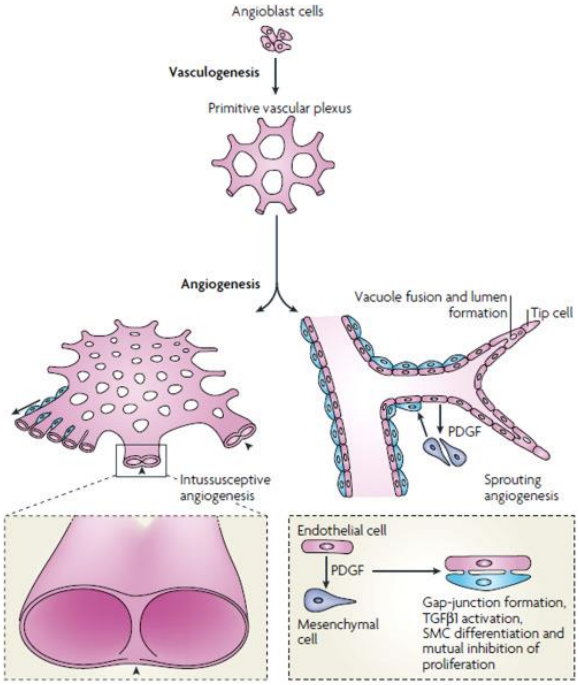

Figure 10: Vasculogenesis and Angiogenesis. The differentiation of angioblasts, or endothelial precursor cells, from mesoderm and the formation of primitive vascular plexus from angioblasts are the two distinct steps during the onset of vascularization that together constitute vasculogenesis. Angiogenesis refers to the growth of new capillaries from preexisting blood vessels either via sprouting or intussusception[129].

III.A. Angiogenesis

Angiogenesis takes place during defined physiological processes, such as embryonic implantation, wound healing, the ovarian cycle and the hair cycle. Multiple mechanisms of angiogenesis have been described, of which cell sprouting is one of the most common.

Endothelial cells form the inner layer of blood vessels. They lie on a specialized ECM (basement membrane) providing mechanical support and physical separation with the surrounding tissue. The basement membrane consists of a scaffold of collagen type IV interconnected to a

laminin network through heparan sulphate proteoglycans, such as perlecan, and small glycoproteins, such as nidogens.

An angiogenic process can be triggered by a wide range of stimuli, including hypoxia, inflammation or mechanical factors such as shear stress. For vascular budding, the initial step of angiogenesis involves dilation of the vascular network and nitric oxide-induced vascular permeability, resulting in extravasation of plasma proteins forming a temporary platform for the migration of endothelial cells. This migration requires the prior destabilization of mature vessels by the detachment of smooth muscle cells, via angiopoietin 2, and the degradation of basal lamina molecules by several proteases, including MMPs. A few endothelial cells from destabilized capillaries initiate the formation of new vessels. These "tip cells" migrate and guide the growth of the bud, being followed by proliferating endothelial cells (named stalk-cells). During this process the integrity of the growing vessel and its perfusion are conserved. The bud migration is mainly regulated by a dialogue between the VEGF-VEGFR2 and Notch-DLL4 signaling. When tip cells reach another bud or an existing capillary, they lose their mobile phenotype and establish strong junctions with newly contacted endothelial cells. The formation of the vascular lumen may occur during the growth of the endothelial bud or after connection with the newly contacted vessel. The lateral distribution of adhesion molecules and the acquisition of apico-basal polarity initiate the formation of the lumen. The generation of the new vessel and the flow of blood reduce hypoxia, the local expression of VEGF and endothelial cell proliferation. Endothelial cells secrete platelet-derived growth factor B (PDGF-B), which induces the recruitment of pericytes and vascular smooth muscle cells smooth muscle cells. Pericytes then establish direct contact with capillary endothelial cells of capillaries and immature vessels, while the smooth muscle cells covering arteries and veins are separated from endothelial cells by a continuous basal lamina[129,130].

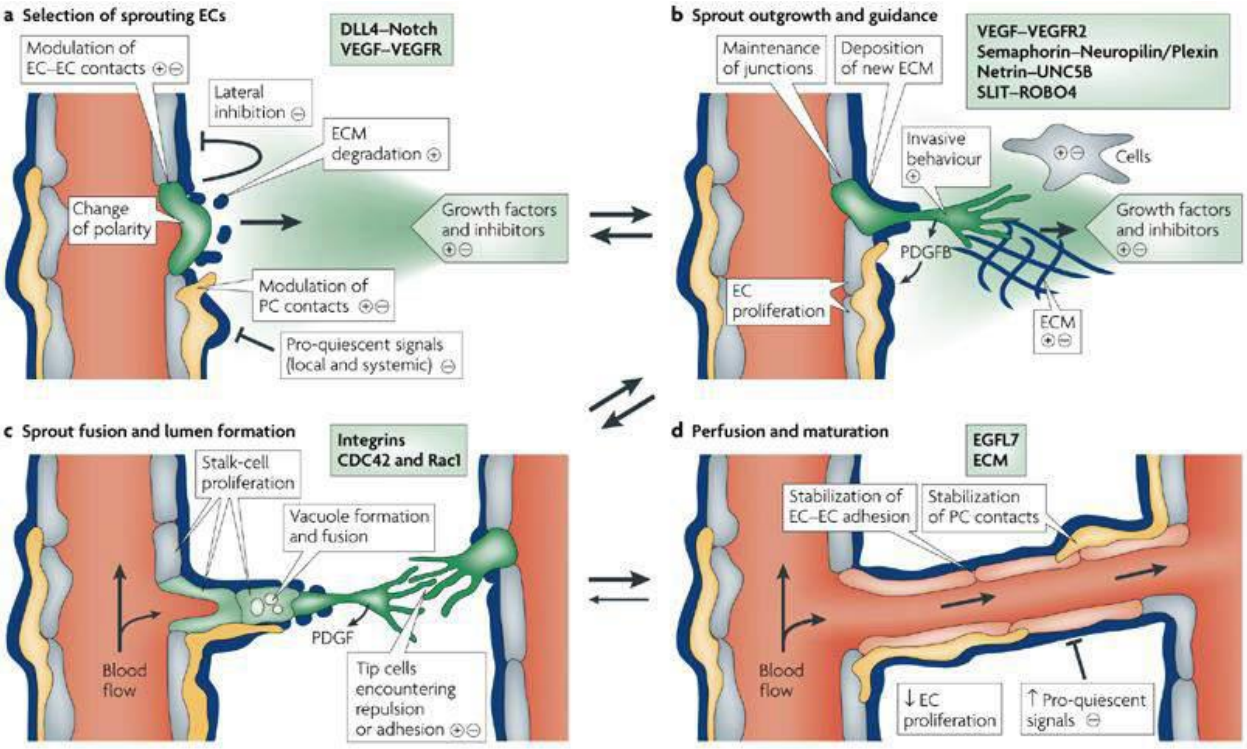

Figure 11: Angiogenic sprouting. (a) Angiogenic sprouting is controlled by the balance of pro (+) and anti (-) angiogenic signals. When angiogenesis is induced, some endothelial cells (green) respond to the pro-angiogenic signal. The sprouting process consists of several stages: loss of an apico-basal polarity, induction of motility and invasion, modulation of contacts with adjacent cells and degradation of the surrounding extracellular matrix. **(b)** The growing bud of cells is guided by a gradient of growth factors. Other processes may include attractive (+) or repulsive (-) signals from the matrix and cells present surrounding tissue. The secretion of PDGF budding endothelial cells promotes the recruitment of pericytes to the vessels being formed to help maintain EC-EC junctions and prevent vascular permeability. **(c)** Adhesive and repulsive interactions also occur when cells interact to allow fusion of the adjacent bud with a vessel. **(d)** The fusion process at the EC-EC interface establishes a continuous lumen. Blood flow supports the final maturation process, consisting of stabilization of cell cell junctions, matrix deposition and strong pericyte adhesion[130].

III.A.1. Pro- and anti- angiogenic factors

The initial step leading to angiogenesis is strictly regulated by a local balance between pro- and anti-angiogenic factors. Under physiological conditions, in adults, vessels are quiescent due to the preponderance of anti-angiogenic signals. Several factors and conditions can induce a proangiogenic switch, such as hypoxia, hypoglycemia, mechanical stress or inflammation.

Numerous pro-angiogenic molecules have been identified, including enzymes, soluble factors and macromolecules of the ECM that provide an environment for endothelial cell migration and differentiation. Ischemia and hypoxia, via hypoxia-inducible factors, help coordinate the pro-angiogenic response by inducing the expression of several growth factors/cytokines and their respective receptors. Among the members of the VEGF family, VEGFA is the key factor in angiogenesis, since it modulates the survival, proliferation, migration and invasion of vascular

endothelial cells through its binding to VEGFR1 and VEGFR2. Fibroblasts growth factor (FGF) 1 and 2 also promote an angiogenic phenotype by regulating proteolysis of the extracellular matrix[131]. Proteases, mainly MMPs, participate in the progression of the angiogenic process by degrading the sub-endothelial basement membrane and the surrounding extracellular matrix, to promote migration of endothelial cells.

Several factors, including thrombospondins 1 (TSP1) and 2 (TSP2), inhibit angiogenesis in their native form[132]. Conversely, many inhibitors are formed by the cleavage of matrix macromolecules devoid of anti-angiogenic activity in their native form. Examples are endostatin (which consists of the C-terminal domain of type XVIII collagen), canstatin and tumstatin (derived from type IV collagen), endorepellin (C-terminal fragment of perlecan) and angiostatin (fragment of plasmin)[133]. Other endogenous angiogenesis inhibitors are factors regulating the immune system (interferon α and β, interleukin-1β, -4, -12 and-18)[134].

III.A.2. ADAMTS and angiogenesis

ADAMTS1 and ADAMTS8 were the first members of the ADAMTS family to be identified as anti-angiogenic agents through the inhibition of the VEGFA- and FGF-induced angiogenesis[135]. ADAMTS1 inhibits angiogenesis via proteolytic and non-proteolytic mechanisms. It can bind VEGF165 (the most abundant isoform of VEGFA) and limit its interaction with VEGFR2[136]. It has been shown that the TSR1 domains and the intact catalytic site of ADAMTS1 are essential for its inhibitory activity[137]. Further studies have however identified ADAMTS1 as a "tip-cell" specific protease promoting endothelial cell sprouting in collagen invasion assays[138]. Other members of the ADAMTS family are also capable of inhibiting angiogenesis. ADAMTS12 is anti-angiogenic *in vivo* and *in vitro* by a mechanism independent of its catalytic activity[59]. In contrast, the catalytic activity of ADAMTS9 is required for its antiangiogenic activity[139]. Our laboratory has also demonstrated that ADAMTS2 is also a potent inhibitor of angiogenesis[119].

III.B. Lymphangiogenesis

The lymphatic system is a network of vessels running parallel to the bloodstream. It begins with dead-end capillaries that collect excess interstitial fluid. This fluid is then drained through lymphatic vessels of increasing diameter to the lymph nodes, where it is filtered, before passing through the thoracic duct and returning to venous circulation via the subclavian veins (Figure 13). Lymphatic vessels are present in most organs, with the exception of non-vascularized tissues (such as cartilage, cornea and the epidermis) and a few vascularized tissues such as the retina. The lymphatic system is involved in the drainage of interstitial fluids, the absorption of fats in the intestine and play a key role in the immune response by mediating the trafficking and maturation of immune cells (antigen-presenting cells and lymphocytes) from tissues to lymph nodes.

In the skin, lymphatics begin in the papillary dermis, then extend parallel to the dermal venous plexus into the inner layers of the dermis, where they connect to larger vessels. Lymphatic

capillaries lack valves, basal lamina, pericytes and smooth muscle cells. Anchoring fibers attach them to the ECM, enabling them to modify their organization and increase extracellular fluid resorption in the event of excessive tissue pressure. Collecting vessels, found in the hypodermis, are equipped with valves and lined by a basal lamina. They are surrounded by a layer of smooth muscle cells that provide a peristaltic movement of lymphatic fluids[140].

Lymphatic vessels are formed after the blood vessels vascular network. During embryogenesis, a group of endothelial cells (derived from embryonic veins of the jugular and perimesonephric region) engage in lymphatic differentiation under the induction of Prox1 expression, which, in turn, induces the expression of VEGFR3. Since VEGFC, the main ligand for VEGFR3, is produced by surrounding mesenchymal cells, this establishes a chemotactic gradient orchestrating lymphatic vessel formation and progressive maturation. As in the vascular system, adult lymphatic vessels are physiologically stable, and activation of neo-lymphangiogenesis is only observed under certain conditions such as wound healing, inflammation or cancer. The mechanisms of lymphangiogenesis are quite similar to those of angiogenesis, with enlargement and vascular budding leading to the formation of neo-vessels. As in vasculogenesis, the incorporation of precursors into lymphatic vessels has also been demonstrated under conditions of pathological lymphangiogenesis. The maintenance and activation of the lymphatic network involve numerous signaling pathways regulated by growth factors, receptors, co-receptors and inhibitors[141].

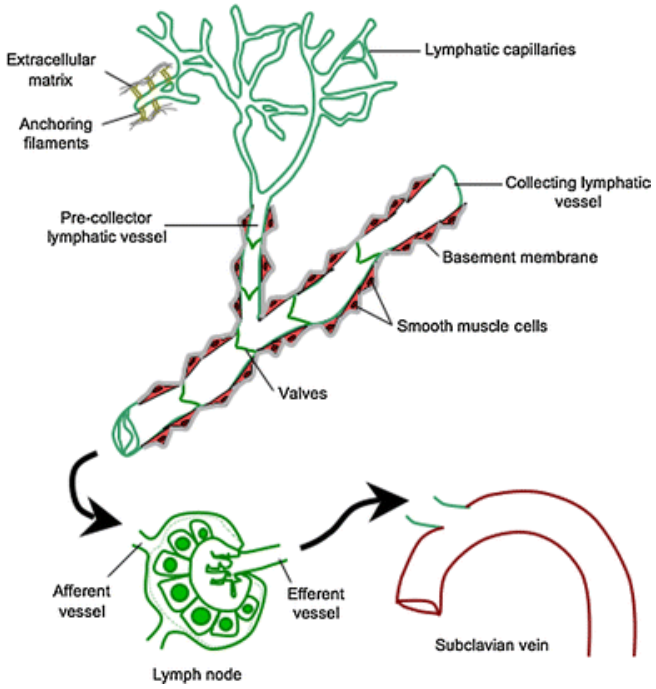

Figure 13: Organization of the lymphatic vascular system. Lymph is collected by lymphatic capillaries. It then travels to the pre-collecting and collecting lymphatic collectors, passes through the lymph nodes and finally empties into the subclavian vein in the jugular region. The lymphatic capillaries are formed by a layer of lymphatic endothelial cells interacting together and anchoring to the ECM. Precollector vessels have a basal lamina, surrounded by smooth muscle cells (red) and contain valves preventing lymph reflux[142].

III.B.1. VEGFC

VEGFC, the most important soluble mediator of lymphangiogenesis, is synthesized as a 58 kDa (after signal peptide cleavage) antiparallel homodimeric precursor stabilized by disulfide bridges. The C-terminal and N-terminal propeptides are then cleaved to produce mature VEGFC with much higher affinity for its VEGFR2 and VEGFR3 receptors. As a result, these cleavages are critical for the initiation and regulation of the lymphangiogenic process (Figure 14). The absence of VEGFC (model of VEGFC-KO mice) prevents lymphatic vessel formation, causing massive edema and embryonic lethality[143]. Conversely, its ectopic overexpression in the epidermis leads to hyperplasia of local vessels, demonstrating its central role in lymphatic vessel formation and homeostasis[144]. At the end of embryonic development, VEGFC expression declines in most tissues except in lymph nodes[145]. In experimental models, overexpression of VEGFC promotes lymphangiogenesis and metastasis dissemination[146].

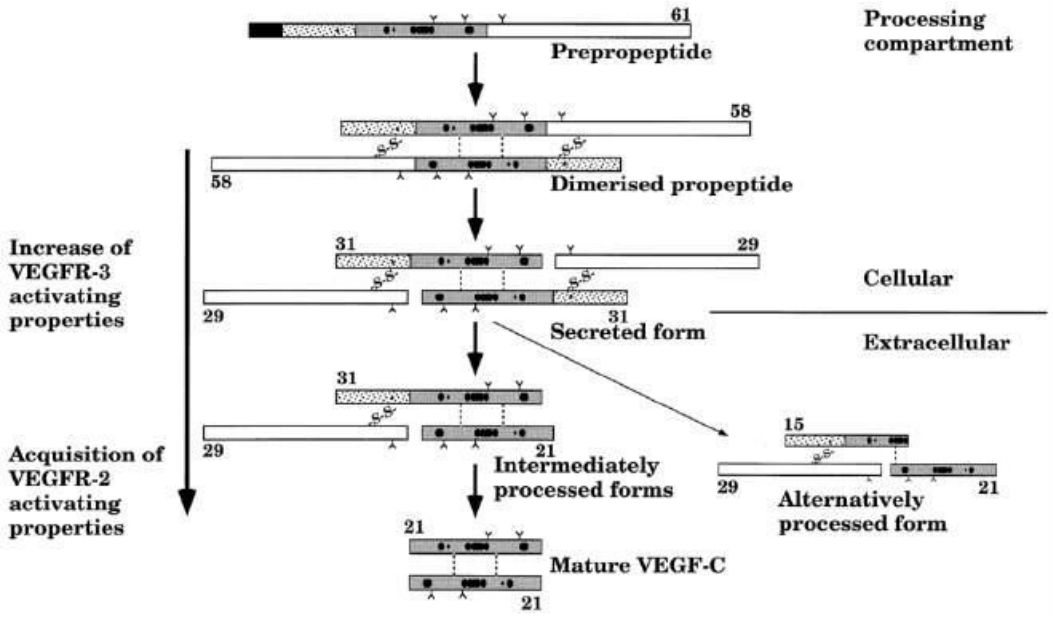

Figure 14: Schematic model of VEGFC proteolytic activation. Numbers indicate the molecular mass (kDa) of the corresponding polypeptide in reduced condition (non-covalent bonds are shown as dotted lines)[147].

III.B.2. ADAMTS and lymphangiogenesis

Hennekam lymphangiectasia–lymphedema syndrome (HKLLS) is a genetically heterogeneous lymphatic dysplasia with characteristics of facial dysmorphism, neurocognitive impairments, and abnormalities of the pericardium, intestinal tract, and extremities. This autosomal recessive condition is caused by biallelic mutations in the gene incoding CCBE1 (Collagen and Calcium Binding EGF domain 1) (HKLLS1)[148] or in protocadherin Fat 4 (HKLLS2).

CCBE1 knockout mouse embryos die prenatally due to fluid accumulation and edema, in line with human data[149]. It was later shown that CCBE1 acts as a cofactor increasing pro-VEGFC processing[150]. The proteolytic activation of pro-VEGFC is performed by endopeptidic proteases. The carboxypropeptide is processed by furin, plasmin and similar enzymes. The aminopropeptide can be cleaved by multiple proteases such as plasmin[151], thrombin[152], kallikrein-related peptidase 3 (KLK3, also known as prostate-specific antigen (PSA)) and cathepsin D[153]. However, the key enzyme in this cleavage is ADAMTS3[81,154] as its absence in mice leads to embryogenic lethality (14 to 15 days post coitus) due to impaired placental vascularization and complete absence of lymphatic vessel leading to generalized massive edema[81]. Based on these data, mutations in ADAMTS3 were searched in human patients with primary lymphedema displaying similarities with diagnostic criteria of Hennekam lymphangiectasia–lymphedema syndrome. These studies led to the identification of two siblings presenting primary lymphedema in the lower limb and abnormal facial features, due to compound heterozygosity for mutations drastically affecting ADAMTS3 activity[82]. The inherited disease is now known as HKLLS3, and an additional patient with homozygous nonsense mutation in ADAMTS3 was later described[155].

Based on these data concerning the role of ADAMTS3 in lymphangiogenesis and knowing the many similarities between ADAMTS2, 3 and 14, our laboratory decided to investigate the potential involvement of ADAMTS2 and ADAMTS14 in lymphatic homeostasis. I took part in this study, which will be described in greater details in the "Results" section.

IV. The tumor micro-environment

IV.A. Cancer development

Cancer is a life threatening disease mostly due to the metastatic spread from the primary tumor causing multiple organs failure or deterioration of a vital organ. Cancer is the leading cause of death in the European Union (Figure 15) and its prevalence is expected to increase with the aging populations of European countries.

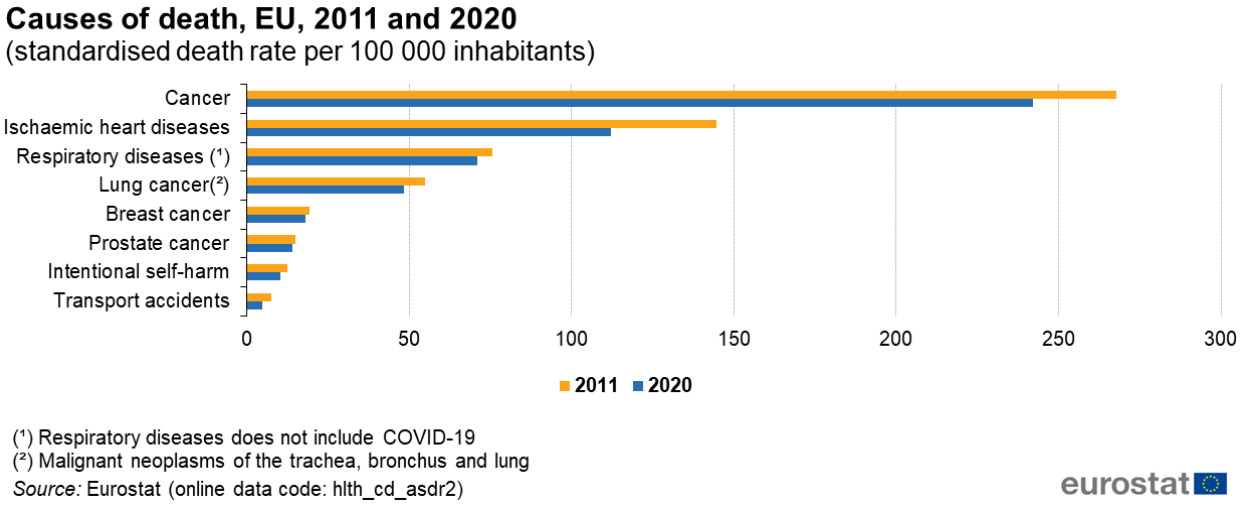

Figure 15: All-cause mortality rate in the European Union countries in 2011 and 2022 (Eurostat)

Cancer is initiated by the transformation of a normal cell into a cancer cell. To form a tumor, cancer cells bypass regulatory checkpoints, leading to excessive proliferation. This phenomenom can arise from the acquired expression of oncoproteins (e.g papillomavirus E6 and E7) or from acquired mutations affecting proteins involved in cell proliferation (e.g. TP53, PIK3CA, BRAF or KRAS).

Different types of factors can increase the risk of cancer. UVB, inflammation or reactive oxygen species (ROS) can induce DNA damages that can increase the mutation rate, and thus the likelihood of activating proto-oncogenes or inactivating tumor suppressor genes. Genetic factors (such as mutations in the tumor suppressor genes BRCA1/2) can also drastically increase the risk of cancer (e.g. breast and ovarian cancers with BRCA1/2 mutations).

These cancer cells acquire other characteristics such as, among others, de-differentiation or shift in the metabolism signature. As soon as the tumor reaches a volume of 1 or 2 mm^3, cancer cells trigger the formation of new blood vessels (angiogenesis) that irrigate and feed the tumor, allowing it to grow further. In addition, cancer cells gradually invade the surrounding healthy

tissues and, at the same time, recruit other cells such as fibroblastic cells and immune cells. The tumor becomes, then, a complex mass with multiple cell types intertwined.

From the initial tumor site, cancer cells can enter the lymphatic or blood vessels which provide pathways to colonize distant tissues where they will form new tumors called metastases. It should be noted that some cancer types preferentially form metastases in particular tissues. As an example, breast cancer tends to metastasize into the lungs, liver, bones or the brain. The multiple steps and mechanisms that allow cancer cells to metastasize into distant organs have been, and still are, the subject of intense research, as this knowledge is essential to the search of innovative therapies. The process involves profound phenotypic changes affecting metabolism and ECM- and cell-cell interactions which ultimately favor migration of cancer cells outside the primary tumor. The following steps involve intravasation, blood or lymph transport, immune escape and survival in the blood, extravasation, phenotypic adaptation to the new environment up to recovery of the proliferative capacity. Although highly interesting, these different aspects of tumor progression will not be detailed here for reasons of conciseness.

IV.B. Components of the TME

The tumor microenvironment (TME) comprises all non-cellular and cellular components of solid tumors, excluding the cancer cells themselves. Non cancer tumor cells are essentially composed of endothelial cells, fibroblastic cells and immune cells, either tissue-resident or recruited from the blood (Figure 16).

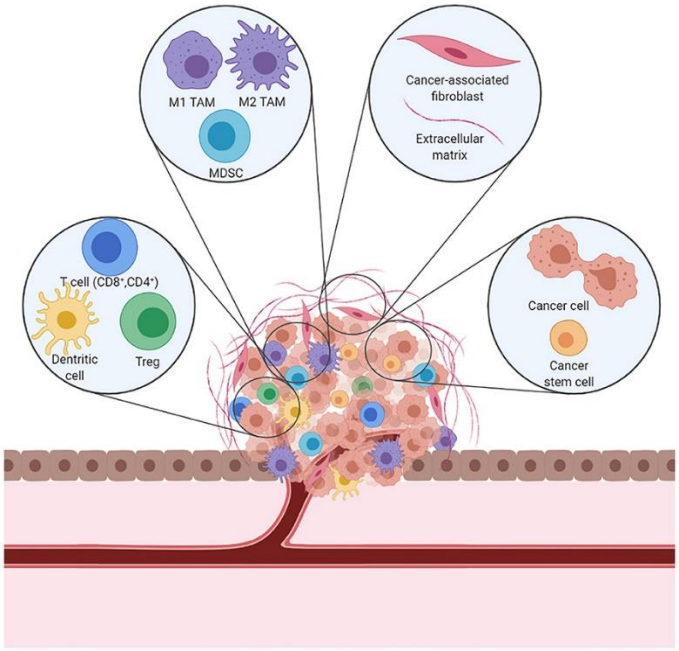

Figure 16: Schematic representation of the different cell types present in the tumor micro-environment[156]

IV.A.1. Endothelial cells

Endothelial cells are present in all solid tumors with a size larger than about 1 mm^3 as they form the inner layer of the blood and lymphatic vessels. Angiogenesis is very active in tumor, because of local hypoxia and through the secretion of pro-angiogenic factors by tumor cells. Blood vessels are needed to fuel tumor growth by providing nutrients and allowing the elimination of metabolic waste. They also allow the recruitment of progenitor cells (endothelial and fibroblastic), facilitate the infiltration of immune cells and the metastatic dissemination of cancer cells. Lymphangiogenesis is also active in some types of tumors where lymphatic vessels, besides lymph drainage, constitute routes for immune cell trafficking and spread of cancer cells to the lymph node. Tumor lymphatic drainage is associated with pre-metastatic niche formation, a process characterized by ECM modification and immune infiltration affecting a distant organ where it promotes the formation and growth of metastases[157]. A process called vascular mimicry has been described as the ability of cancer cells to organize themselves into vessel like structures potentially providing blood flow into poorly vascularized regions, but these cells are not considered as endothelial cells[158].

IV.A.2. Cancer associated fibroblasts

Fibroblastic cells in the TME are collectively called “cancer associated fibroblasts” (CAFs). CAFs can be identified by the expression of fibroblastic activation markers such as high expression of alpha smooth muscle actin (αSMA). They were initially thought to represent a homogenous population of cells possessing the same characteristics, mainly ECM production and remodeling. It is now well established that they can display different types of “polarizations”, either promoting or restraining tumor growth, resulting from diverse functions (including matrix deposition and remodeling, extensive reciprocal signaling interactions with cancer cells and crosstalk with infiltrating leukocytes)[159,160]. As such, they are a potential targets for optimizing therapeutic strategies against cancer and efforts are being made for advancing our understanding of their regulation and functions (Figure 17)[161].

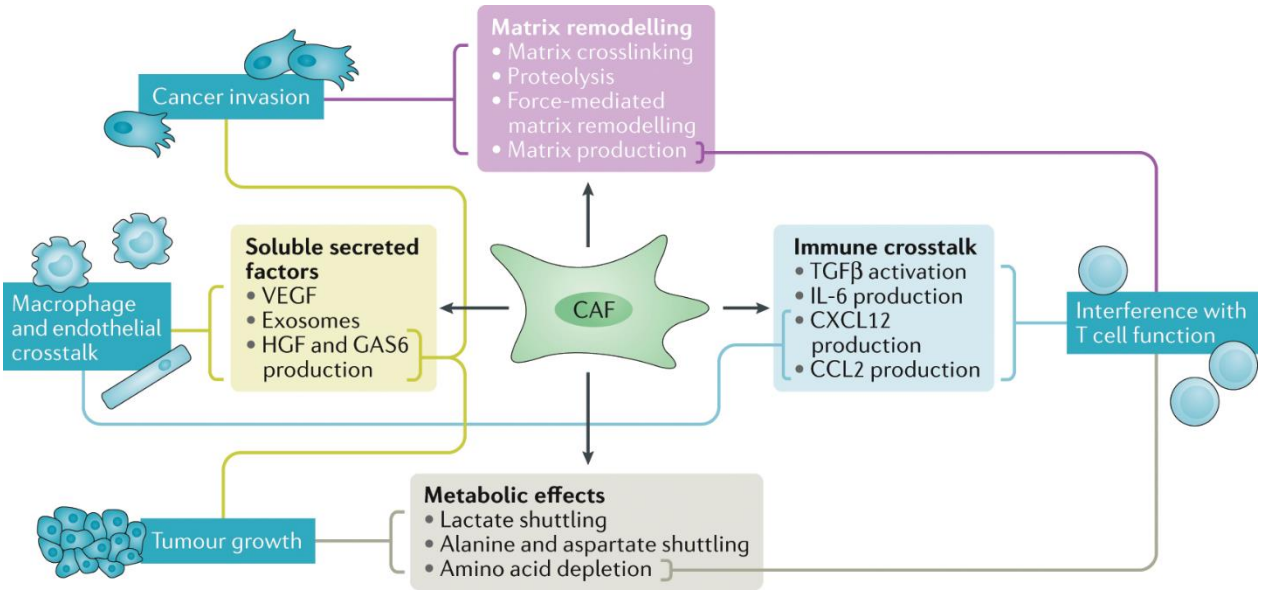

Figure 17: Schematic representation of the interplay of CAFs with the other cells in the TME through secreted factors[161]. CAFs produce cytokines, exosomes, modify the amino acids and metabolites content and remodel the ECM. That may lead to alterations in the immune response against cancer cells, and promote tumor development and cancer cell invasion.

Although they are probably quite plastic and able to display intermediate phenotypes, several subtypes of CAFs have been classified. CAFs sub-classification differs based on the involved cancer types (colorectal cancer, pancreatic cancer or breast cancer). In pancreatic cancer, three CAFs sub-types have been identified: myCAFs, iCAFs and apCAFs. Myofibroblastic CAFs (myCAF) display a continuously active phenotype and are responsible for the deposition and remodeling of the ECM. Inflammatory CAFs (iCAFs) are distinct from myCAFs by the loss of myofibroblastic makers (e.g.αSMA, TGF-β response genes) and the expression of inflammatory markers (e.g. IL6, IL1). *In vitro*, iCAFs are only found when fibroblastic cells are placed in coculture with cancer cells which may indicate that cancer cells are responsible for the iCAFs activation/polarisation[162]. Antigen presenting CAFs (apCAFs) are characterized by the expression of MHCII family genes that indicate a role in antigen presentation[163]. Breast cancer study highlighted another classification for CAFs (S1, S2, S3 and S4 CAFs)[159]. CAF-S1 are distinct from the other CAFs subtypes by its expression of FAP and are linked to the attraction, retention and differentiation of T cell into regulatory T cells ($CD25^+$ $FoxP3^+$) indicating an immunosuppressive role. CAF-S1 represent a bigger proportion of CAFs in triple negative breast cancer (absence of expression of estrogen receptor, HER2, and progesterone receptor) than in HER2 or LumA breast cancer, and may therefore correlate with patient overall survival[164]. A better characterization of CAFs may reveal key interplay between CAFs and other tumor cells, and therefore drive the identification of biomarkers, the development of personalized medicine and the discovery of strategies to overcome resistance to treatment.

High proportions of myCAFs result in desmoplasia, a name referring to the formation of a stiff and abundant ECM within the tumor, as usually found in pancreatic and breast cancer. The functional consequence of desmoplasia is not easy to decipher, as it may impact multiple opposing phenomena. Collagen deposition creates a stiff ECM around cancer cells that may restrict their local growth, while, however, promoting their metastatic phenotype switch[165]. A dense ECM can limit tumor neovascularization but also impair the recruitment of immune cells and tumor infiltration. In addition, the impact of desmoplasia on tumor progression is probably specific to the type and the stage of cancers.

IV.B.3. Extracellular matrix

The extracellular scaffold within the tumors is mainly secreted by CAFs and, to some extent, by cancer cells and endothelial cells (basement membrane). The main constituent of the tumor ECM is fibrillar collagens, especially in desmoplastic cancers such as breast and pancreatic cancer. Collagen deposition has now been shown to be more than a passive marker of tumor progression. In breast cancer, evidences link collagen density to tumor growth and metastasis[166]. Cancer cells can reorganize collagen fiber orientation[167], which favors their migration[168]. Other components of the tumor ECM have been shown to also promote cancer cell migration (e.g. fibronectin)[169], be involved in angiogenesis (e.g. fibronectin and tenascin-c)[170] or immune suppression (e.g. tenascin-c)[171]. The tumor ECM modulates immune cell infiltration at many levels. As examples, type I collagen and its proteolytic fragments are chemotactic for monocytes[172,173], the ECM modulates macrophage polarization and functions[174,175] and, conversely, macrophages can modulate ECM organization[176].

While initially considered to form a barrier limiting the proliferation of cancer cells, it is now evident that collagen must be considered as a double-edged sword in tumor progression since it can either promote or repress tumor progression, depending on tumor type and stage. Changes in the composition, abundance and organization of collagen fibers alter biochemical and biomechanical signals within the tumor microenvironment, with major effects on both cancer and non-transformed (stromal, immune) cells, thus triggering a cascade of interacting biological events modifying the long term of tumor progression[177]. Collagen fibrils are resistant to many types of proteases, and can be efficiently cleaved only by some metalloproteinases (MMP1, 8, 13, 14) that cleave the mature collagen trimeric molecules at specific sites. After this primary cleavage, other proteases (as MMP2 and MMP9) can degrade further the collagen scaffold into smaller fragments, disturbing the structure and density of fibers and generating pro-inflammatory matrikines (such as the P-G-P tripeptide)[178].

IV.B.4. Immune response against cancer

Another component of the TME are immune cells. They mostly originate from the recruitment from the systemic circulation but can also come from tissue-resident immune cells "invaded" by the tumor. Immune cells distribution is massively heterogeneous between cancer types and between patients[179–181]. B cells, T cells (CD4, CD8, Treg), macrophages, monocytes,

natural killer cells and dendritic cells can all be found within tumors. T cells and macrophages are often the dominant immune cell population within the TME.

The immune system is the major mean of defense against cancer through the detection and killing of virus-infected cells and cancer cells. Cancer cell lysis can be mediated by both the adaptive and the innate immune system. The adaptive immune system includes the processes of antigen recognition and presentation, the interplay between lymphocytes and antigen presenting cells, and between helper T cells and cytotoxic T and B cells. The adaptive immunity leads to CD8 T cell activation, antibody production and memory T cells. It provides a mean to directly kill infected or cancer cells (perforins and granzymes from CD8 T cells) and a long-term protection by the production of long-lived antibodies. The acute (IgM) or lasting (IgG) production of antibodies allows other means of cancer cell lysis than a direct cancer cells killing by cytotoxic lymphocytes (CTLs). Through processes called antibody-dependent cellular cytotoxicity (ADCC) and antibody-dependent cellular phagocytosis (ADCP), innate immune cells, mostly natural killer (NK) cells for ADCC and myeloid cells for ADCP recognize the Fc domain of antibodies bound on the surface of cancer cells and lyse (perforins and granzymes from NK cells) or phagocyte (myeloid cells) them[182]. This interplay between the adaptive and innate immunity in cancer cell killing can be exploited for cancer treatment using monoclonal antibodies[183].

The complement system is an innate immune response that can also lead to cancer cell lysis. Complement activation arises from three possible pathways i) the classical pathway triggered by antibody binding to C1q ii) the lectin pathways triggered by the binding of MASPs to "foreign" sugar and iii) the alternative pathway, a constitutive pathway that is amplified by pathogens and cell lysis. The complement cascade leads to the formation of inflammatory (anaphylatoxins C3a and C3b), opsonization (C3b) and membrane attack complex proteins (C5B, C6, C7, C8 and C9). Cell lysis by the membrane attack complex is an acellular process called CDC for Complement-dependent cytotoxicity while opsonisation lead to an ADCP-like process resulting in the phagocytosis of the target cell by myeloid immune cells (called CDCC for complement-dependent cellular cytotoxicity)[184–186].

Another cancer cell killing pathway related to the immune system is mediated by TNF-related family receptors with a death domain[187] including TNFα-TNFR[188] or TRAIL-TRAILR[189]. TNFα is a pro-inflammatory cytokine mostly expressed by immune cells. TNFα binds to its receptor TNFR1 and induces pro-inflammatory genes expression by the nuclear translocation of NF-κB. This pathway can also directly induce cell death by apoptosis or necroptosis. Dying cells release damage-associated molecular patterns (DAMPs) that further propagate the inflammatory signaling. Alteration in the TNF signaling by mutation in genes coding for proteins involved in its regulation have been linked to inflammatory pathologies like autoimmune diseases, and systemic and chronic inflammation[188]. TRAIL (tumor-necrosis-factor related apoptosis inducing ligand) is also mostly expressed by immune cells. It forms a trimeric complex before interacting with its receptors and result in a response relatively similar to that of TNFα-TNFR. TRAIL-mediated cell death seemed to have a greater effect on cancer cells as compared to healthy cells[190], may elicit

tumor suppression[191] and M1 macrophage polarization[192]. TRAILR activation by antibodies (Mapatumumab) were clinically investigated in combination with sorafenib (pan-kinase inhibitor) in advanced hepatocellular carcinoma by GSK (NCT01258608). The addition to Mapatumumab did not improve patient outcome as compared to sorafenib alone[193]. The same conclusion was drawn from a clinical trial looking at the added value to use Mapatumumab with chemotherapy in advanced non-small-cell lung cancer patients (NCT00583830)[194].

FAS-FASL pathway is a TNF receptor superfamily pathway that is mostly involved in T cells apoptosis. FAS molecules can be expressed on cancer cells[195,196] but regulatory mechanisms prevent their sensibility for FAS mediated apoptosis and, instead, may allow cancer cells to induce apoptosis in CTLs and NK cells[197].

IV.B.5. Immunosuppression in the TME

While immune cells from both the innate and adaptive immunity participate in the cancer cell lysis, the efficiency of cancer cell recognition and killing by the immune system is progressively altered in the TME.

Throughout the growth of the primary tumor, the TME remains under chronic inflammation due to the expression of pro-inflammatory cytokines (e.g. IL-6, CCL2, CCL5) by cancer cells and under hypoxia due to a deficiency of angiogenesis[198]. This environment promotes immunosuppression through cytokines (e.g. IL10, TGFβ, IL4) and checkpoint inhibitors (e.g. PD1-PDL1, CTLA4) expression by cancer cells, Treg and myeloid cells. Another mediator of immunosuppression are tumor derived exosomes[199]. Exosomes engulf part of the parent cells including mRNA, miRNA, proteins and surface receptors. Exosomes production by cancer cells allow the "distant" contact of inhibitory checkpoints (PDL1) with immune cells, the depletion of key amino acids (CD39, CD73)[200] and/or directly impact gene expression (mRNA and miRNA)[201]. As previously described in section IV.B.3, some components of the ECM in the TME have also been linked to immune suppression.

While the infiltration of some immune cells in the tumor (neutrophils[202,203], B cells[204], NK cells[205] and CD8 T cells[206]) seems to be beneficial for patients, others like macrophages[207–209] or myeloid derived suppressor cells (MDSC)[210], seem to correlate with a poorer survival for patients. Thus, some immune cells appear to be more sensitive to the immunosuppression of the TME resulting to a net negative effect on tumor control by the immune system.

Macrophages are myeloid cells of embryogenic ($CD11b^-$) or bone marrow ($CD11b^+$) origin present early on during inflammation or infection. They display multiple roles based on the pathologic state of its residing host tissue. Macrophages have been classified as M1-macrophages (as mediator of inflammation and cancer cell lysis) and M2-macrophages (displaying pro-fibrotic, pro-angiogenic, wound healing and anti-inflammatory properties). This initial classification was based on *in vitro* studies and, although useful for some purposes, multiple subclasses of macrophages have now been highlighted (M2a, M2b, M2c, M2d). These phenotypes do not represent a terminal polarization but rather transient states that may shift from one to the other

based on the on-going or resolving infection or inflammation[211]. In tumors, macrophages are collectively named "TAM" (for tumor-associated macrophages), they display an overall immune-suppressive and pro-tumor properties[212]. TAMs are not a homogeneous population and can display M1-like and M2-like phenotypes. Their polarization status progressively switches from M1-like to M2-like and end-up participating in the immunosuppression of the TME. TAMs recruitment and M2-like polarization promote immunosuppression through the expression of IL10, arginase 1 (ARG1), TGFβ, PD1 or CCL22 (Treg recruitment)[213].

MDSC are immune cells that accumulate in the blood, organs and tumors in response to inflammatory cues like infection, stress or cancer[214]. MDSC have a potent immunosuppressive function linked to the expression of IL10, ROS[215], PDL1, ARG1 and inducible nitric oxide synthase (INOS, NOS2)[216] leading to the inhibition of NK cells[217] and T cells[218].

NK cells are cytotoxic lymphocytes considered part of innate immunity because their function does not require immunization. A striking difference between NK cells and CTLs is their MHCI responsiveness: while TCR-mediated recognition of MHCI by CTLs is required for their cytotoxic activity, NK cells are inhibited up binding to MHCI[219]. Cancer cells frequently develop immune escape strategies including downregulation of MHCI molecules, thereby reducing their susceptibility against CTLs. This downregulation of MHCI at the surface of cancer cells increase their sensitivity for NK cells killing. However, NK cells are no exception to the immunosuppressive properties of the TME: TGFβ, adenosine and checkpoint inhibitors expression (e.g. PDL1 and CD155) downregulate activating receptors (e.g. NKG2D) in NK cells and prevent their activation. Ligands of activation receptors of NK cells (MICA and MICB for NKG2D) can be cleaved leading to the release of soluble forms causing a continuous activation of NK cells and subsequent desensitization. Soluble MICA and MICB are increased in the blood of cancer patients that may lead to generalized desensitization[220]. ADAM17 (for ULBP2[221], MICA[222], MICB[223]), ADAM9 (for MICA[224]) and ADAM10 (for MICA[222]) have been identified as NKG2D ligand sheddase. Alternatively, soluble MULT1 competes with other soluble NKG2D ligands and prevents NK cells desentitization[225] (Figure 18).

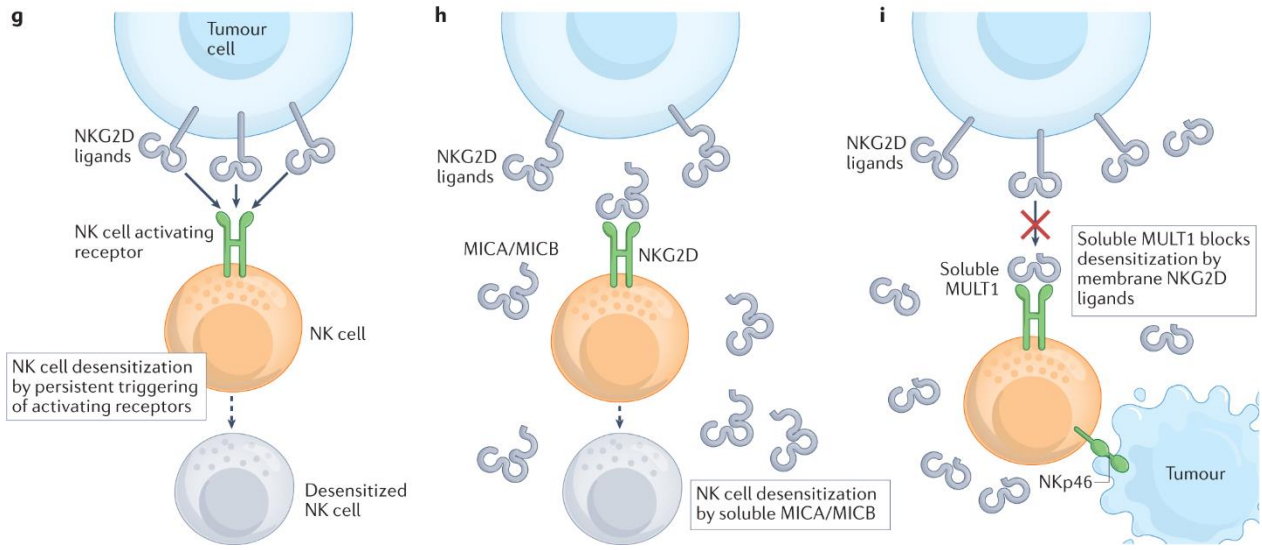

Figure 18: Regulatory functions of cleaved NKG2D ligands on NK cells activation. Continuous activation of NK cells receptors like NKG2D leads to NK cells desensitization**.** Both full length and soluble MICA and MICB are involved in NKG2D mediated desensitization of NK cells. MULT1 has a high affinity of NKG2D, competes with MICA and MICB and prevents NK cells desensitization[219].

T cells are the lymphoid cells that are central to the adaptive immune system. They have the particularity of maturing within specialized lymphoid organs (lymph nodes, thymus, …) up on the exposure to antigens "presented" by dendritic cells migrating into lymphoid organs. They express granzymes and perforins that are released upon the identification of the antigen specific to the T cell receptor (TCR) of the cell. Cancer cell lysis by CTLs can be repressed at different levels. First, since cancer cells originate from the "self", they are unlikely to express a wide variety of specific immunogenic antigens, which restricts the variety of cancer cell specific TCR. Secondly, an increase in inhibitory immune checkpoint proteins expression by cancer cells, macrophages and dendritic cells reduces T cells activation and prevents cancer cell killing[226]. Additionally, receptor-receptor inhibitory signals and paracrine secretion of immunosuppressive cytokines, such as TGFβ1, can prevent T cell activation. Finally, overstimulation by antigens derived from the overwhelming amount of cancer cells can lead to T cell exhaustion, a final irreversible inactivation of T cells[227].

Treg (regulatory T cells) are a subset of $CD4^+$ T cells expressing Foxp3 and CD25. They are key regulators of immunological self-tolerance and thus play a key role in preventing autoimmune disease development. In human, mutations in the gene of Foxp3 induce a syndrome characterized by multiple auto-immune pathologies (type I diabetes, dermatitis, enteropathy, …)[228]. Tregs can infiltrate tumors and lead to immunosuppression. Depletion of Tregs *in vivo* can be sufficient to reduce tumor growth and improve CD8 T cells tumor infiltration[229,230]. Furthermore, a reduced ratio of tumor infiltration $CD8^+$ T cells to Tregs correlate with a poor

prognosis in several cancers[231–233]. Tregs mediate immunosuppression by the expression of CTLA4, IL10, TGFβ, glucocorticoid-induced TNF receptor (GITR) and the production of adenosine. Tregs can lead to NK cells inhibition[234] and effector T cell anergy or apoptosis[235].

Dendritic cells (DCs) are myeloid immune cells first characterized by their expression of MHCII and their antigen presentation function. They are produced from hematopoietic stem cells and circulate in the blood as immature DCs displaying an increased endocytic activity and a reduced MHCII expression. Antigens and stimulatory signaling induce their maturation process by increasing their MHCII expression, reducing their endocytic capacity and increasing their migratory phenotype allowing migration into lymphoid organs (mostly lymph nodes)[236]. They are mostly residing within the lymphoid organ and participate in the priming and stimulation of T cells. DCs have been further sub-categorized based on the level of MHCII and other surface marker expression, their morphology, their migratory potential[237] or their ability to cross-present antigens[238]. Within the TME, DCs present tumor-associated antigens on their MHC molecules allowing T cells responses against cancer cells. T cells response to tumor-associated antigens is mediated by the TCR of T cells along co-stimulatory signaling that can take the form of receptor-receptor interaction between DCs and T cells (ICOL-ICOS, CD80/CD86-CD28 or OX40L-OX40) or soluble factors (INF or IL12) produced by DCs. However, inhibitory signals produced by cancer cells and other immune cells (IL10, IL6, M/GM-CSF or VEGF) impairs DCs maturation[236]. Additionally, cancer cells produce "tumor antigens" such as MUC1 that may alter DC maturation and prevent effector T cell activation[239].

V. ADAMTS in cancer progression

Studies demonstrating direct implications of ADAMTS enzymes in the TME are scarce. ADAMTS1 has been described to be anti-angiogenic by repressing endothelial cell proliferation by both direct sequestration of VEGF165 and generation of anti-angiogenic peptides from ECM macromolecules[240]. In the same line, it was also shown that ADAMTS1 overexpression reduces subcutaneous tumor growth in multiple cell line models, potentially through reduction of blood vessel density[241]. The hypothesis of ADAMTS1 being an anti-cancer factor has been however challenged in a model of spontaneous mammary tumor (MMTV-PyMT model). This study showed that both tumor growth and metastases formation are repressed in the absence of ADAMTS1 (MMTV-PyMT-ADAMTS1$^{-/-}$) as compared to wild type (MMTV-PyMT-ADAMTS1$^{+/+}$) and heterozygote mice (MMTV-PyMT-ADAMTS1$^{+/-}$). This was not linked to any change in blood vessel density, but related to an increased cancer cells apoptosis and immune cells infiltration[38]. These contradictory results concerning the role of ADAMTS1 in tumor progression illustrate the critical importance of which experimental models are used (*in vitro* vs *in vivo*, repression vs overexpression).

High expression of ADAMTS12 is of bad prognosis in liver cancer. However, ADAMTS12$^{-/-}$ mice are more sensitive to CCl4-induced liver fibrosis, which suggests, as for ADAMTS1, that ADAMTS12 has several and perhaps antagonistic functions[242]. This hypothesis is further substantiated by previous data showing that the absence of ADAMTS12 (ADAMTS12$^{-/-}$ mice) results in increased angiogenesis and tumor growth *in vivo*[59]. ADAMTS12 overexpression was reported to increase cancer cell proliferation through increased glycolysis[243] and mTOR signaling[244]. ADAMTS12 overexpression in MCF7 breast cancer cells increased their proliferation, an effect that is suppressed by coexpression with fibuline 2[60]. Again, contradictory results at the *in vitro* and *in vivo* levels prevent to define the role of ADAMTS12 in cancer development.

ADAMTS2 was found to have potent anti-angiogenic properties *in vitro*, with the addition of recombinant ADAMTS2 causing endothelial cell apoptosis within hours and impairing vessel formation in a model of embryoid bodies. *In vivo*, ADAMTS2 expression drastically reduces the growth, in nude mice, of sub-cutaneous implanted HEK293T cells[119]. Several studies established a correlation between the level of expression of ADAMTS2 and poor prognosis in different cancers. However, these studies are based on immunohistochemistry (IHC) analyses, while we know that the antibodies that have been used are unreliable and non-specific. Therefore, these publications will not be cited here. At the mRNA level, ADAMTS2 has been identified as a marker to differentiate thyroid lesions and tumor sub-types[245]. It is strongly expressed in renal carcinoma tumors, which was correlated with reduced overall survival[246]. In tongue tumor, high expression of ADAMTS2 is part of a signature associated with metastasis formation[247]. Mass spectrometry analysis has also correlated ADAMTS2 protein expression in colorectal cancer with tumor progression, metastases and poorer survival[248]. Outside of the study performed in our lab[119], the pool of the evidence regarding ADAMTS2 and tumor development seemed to indicate that ADAMTS2 has a pro-tumor role.

Scientific context and aims of the project

Our laboratory pionereed the discovery, purification and characterization of the aminoprocollagen peptidases (ADAMTS2, ADAMTS3 and ADAMTS14). These long-term and still ongoing studies allowed to identify their involvement in genetic diseases such as the dermatosparactic type of Ehler-Danlos Syndrome and the Hennekam lymphangiectasia-lymphedema syndrome 3, to unravel the mechanistic determinants of these pathologies (altered type I collagen processing and defect in pro-VEGFC activation) and to discover a new array of potential functions in the regulation of angiogenesis, TGFβ signaling, lysyl oxidase activation, tumor repression and immune system regulation.

The aim of this work was to pursue these fruitful discoveries in order to identify potential "new" functions for these enzymes and elucidate the mechanism involved.

1) The first part of this work aimed to establish a more comprehensive list of ADAMTS2 and ADAMTS14 substrates. To do so, we applied the laboratory experience of *in vitro* N-TAILS analysis to *in vivo* tissues, which increased the complexity of the experimental approach but significantly improved the relevance of the data.

2) The second part aimed to evaluate the specific role of ADAMTS2 and ADAMTS14 in the context of lymphangiogenesis at adulthood.

3) The third and main objective of this project was to investigate and characterize the involvement of ADAMTS2 in cancer progression by developing and using new models aiming to indentify the mechanisms and pathways involved.

Results

Chapter 1: Study of ADAMTS2 and 14 by N-terminomic *in vivo*

The development of the N-TAILS provided the first dedicated tool for the discovery of protease substrates[123,124]. This proteomic approach suffers however from some limitations such as reduced sensitivity and specificity which explains why it was first applied to low complexity samples like conditioned media[123,124,249–258] or cell lysates[259,260]. *In vivo* samples have also been used, but only those with limited complexity and/or heterogeneity, such as bronchoalveolar fluid[123], wound fluid[127], dental pulp[249,261,262], epidermis[263], sputum[264], colonic mucosal biopsies[265] and alveolar bone[266].

After establishing a first list of substrates for ADAMTS2 and ADAMTS14 on skin fibroblasts *in vitro* (using active recombinant ADAMTS2 and 14)[267], our laboratory wanted to go one step further by studying skin samples of wild type, ADAMTS2 knockout, ADAMTS14 knockout and ADAMTS2-ADAMTS14 double knockout mice. The goals were multiple and consisted in:

- Confirming and validating the relevance of *in vitro* data obtained with fibroblasts;
- Identifying additional substrates that could have been missed *in vitro*;
- Determining whether ADAMTS14 can rescue ADAMTS2 deficiency, especially for aminopropeptide cleavages of fibrillar collagens;
- Identifying ADAMTS14-specific substrates.

The most significant or interesting data are provided below, together with short explanations about their relevance. The full article is inserted in the manuscript thereafter. In this work, I mainly participated in the extracellular substrate validations as well as paper manuscript reviewing.

A. The skin N-terminomes of ADAMTS2 and ADAMTS14 greatly overlap and revealed new potential substrates of both enzymes

The comparison of peptides identified by N-TAILS in the skin of WT, TS2-KO, TS14-KO and TS2-TS14-KO mice shows that both enzymes are involved in the cleavage of similar proteins**.**

Substrates were identified by the comparison of the abundance of peptides from the skin of WT mice as compared to knockout mice. 59 % (40) of the 68 extracellular and cell surface substrates identified are common for ADAMTS2 and ADAMTS14 (Figure 19).

Surprisingly, while often processing identical proteins, each protease is unable to fully compensate for the absence of the other. Indeed, for several substrates such as cystatin-3, annexin A1, annexin A2 or collagens, the protease/control ratio (indicating cleavage when >1) is higher when comparing TS2-TS14-KO skin to WT skin than when evaluating TS2-KO and TS14-KO separately. This additive, rather than compensatory, effect indicate that both proteases cleave their substrates independently of the other. (Figure 20).

In addition, this N-TAILS analysis on skin extracts identified new potential substrates for both ADAMTS2 and ADAMTS14 which have never been described before, such as annexins, complement factors and cathepsins (Figure 20).

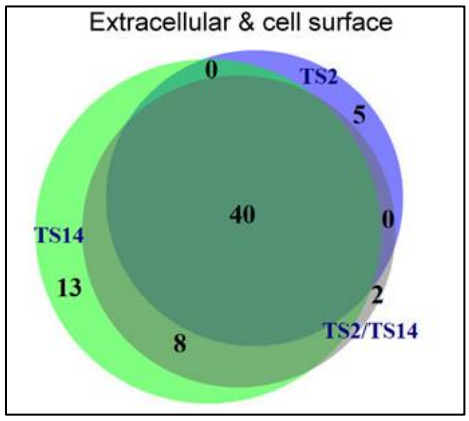

Figure 19: Venn diagram representing the extracellular and cell surface proteins identified as ADAMTS2 and/or ADAMTS14 substrates by N-TAILS. Most of these proteins (40/68) were identified as substrates when comparing the WT skin to TS2-KO mice skin (TS2), to TS14-KO mice skin (TS14) and to TS2-TS14-KO mice skin (TS2/TS14).

Name	TS2	TS14	TS2TS14	Name	TS2	TS14	TS2TS14
Inter alpha-trypsin inhibitor	1.2 ± 0.7	1.9 ± 0.7	1.6 ± 0.5	Galectin-1	1.3 ± 0.3	1.9 ± 0.4	2.1 ± 0.4
AE-binding protein 1	0.7 ± 0.2	2.0 ± 0.5	1.2 ± 0.3	Galectin-7	2.0 ± 0.6	2.8 ± 0.8	4.8 ± 1.4
Alpha-2-HS-glycoprotein	0.7 ± 0.3	2.2 ± 1.3	0.9 ± 0.3	Gc-globulin	1.7 ± 0.8	4.1 ± 2.0	6.0 ± 3.7
Alpha-2-macroglobulin	1.7 ± 1.0	2.0 ± 0.6	2.2 ± 0.6	Gelsolin	2.6 ± 0.7	2.4 ± 0.9	5.0 ± 1.7
Annexin-8	6.4 ± 2.2	5.5 ± 1.9	15.0 ± nd[a]	H2-Q9	1.9 ± 1.3	2.7 ± 1.1	2.9 ± 1.1
Apolipoprotein A-I	2.7 ± 1.8	3.3 ± 1.9	4.5 ± 1.8	Hemopexin	1.0 ± 0.4	1.9 ± 0.5	1.5 ± 0.5
Apolipoprotein H	1.6 ± 0.8	2.6 ± 1.2	2.3 ± 0.8	Ig gamma-2B	1.8 ± 0.5	2.3 ± 0.8	3.5 ± 1.2
Beta-globin	2.2 ± 0.6	2.9 ± 1.1	6.7 ± 3.3	Ig gamma-3	1.1 ± 0.4	1.9 ± 0.4	1.8 ± 0.4
Biglycan	2.8 ± 2.4	3.0 ± 1.6	3.6 ± 1.8	Ig kappa chain V-V	1.2 ± 0.8	5.1 ± 2.7	2.9 ± 1.1
Carboxypeptidase A3	1.6 ± 0.4	2.1 ± 0.5	3.2 ± 1.1	Kallikrein j	2.0 ± 0.8	2.4 ± 0.6	5.1 ± 0.6
Cathepsin B heavy chain	1.3 ± 0.6	1.9 ± 0.6	1.6 ± 0.3	Kininogen-1	2.2 ± 0.5	2.9 ± 0.6	5.5 ± 0.2
Cathepsin H	1.2 ± 0.6	2.4 ± 0.8	2.0 ± 0.6	Lumican	1.6 ± 0.7	2.6 ± 1.3	2.3 ± 0.4
Cathepsin S	1.0 ± 0.5	2.2 ± 0.7	1.5 ± 0.4	Mast cell protease 4	1.5 ± 0.2	1.7 ± 0.2	2.4 ± 0.5
Caveolin-1	2.0 ± 0.8	3.1 ± 1.4	3.1 ± 0.0	MIF	1.1 ± 0.6	2.7 ± 1.1	1.8 ± 0.5
Cavin-1	2.1 ± 0.4	3.5 ± 0.9	8.7 ± 0.4	Myelin protein zero	1.6 ± 0.7	2.1 ± 1.1	1.7 ± 0.4
Coagulation factor XIIIa	2.5 ± 1.0	3.8 ± 1.5	7.8 ± nd[a]	Osteoglycin	2.3 ± 0.7	2.3 ± 0.9	4.5 ± 1.6
Collagen alpha-1(I) chain	4.2 ± 0.5	1.7 ± 0.2	6.8 ± 1.0	p24 gamma-1	2.1 ± 1.1	3.3 ± 1.7	1.4 ± 1.0
Collagen alpha-1(III) chain	3.7 ± 2.2	2.8 ± 1.3	5.8 ± 2.7	p35/Annexin A1	2.7 ± 1.2	2.7 ± 0.9	7.4 ± 3.7
Collagen alpha-1(IV) chain	1.6 ± 0.6	1.8 ± 0.6	2.2 ± 0.4	p36/Annexin A2	2.7 ± 1.2	2.7 ± 0.9	7.4 ± 3.7
Collagen alpha-1(V) chain	3.9 ± 1.7	4.1 ± 1.6	9.3 ± 0.8	PCPE-1	2.2 ± 0.4	1.9 ± 0.4	3.6 ± 0.5
Collagen alpha-1(VI) chain	2.2 ± 0.8	1.9 ± 0.6	3.4 ± 0.9	PDI A6	1.8 ± 0.7	2.1 ± 0.7	2.9 ± 0.9
Collagen alpha-1 (XIV) chain	3.6 ± 0.7	2.3 ± 0.5	8.2 ± 2.5	Periostin	1.0 ± 0.5	2.2 ± 0.8	1.3 ± 0.4
Collagen alpha-2(I) chain	3.1 ± 0.7	1.6 ± 0.2	4.6 ± 0.6	Proapolipoprotein A-II	3.5 ± 2.5	4.9 ± 3.2	11.9 ± 7.9
Collagen alpha-2(V) chain	1.8 ± 0.3	1.7 ± 0.3	2.8 ± 0.3	Prolargin	2.9 ± 0.9	2.6 ± 0.8	5.8 ± 1.3
Collagen alpha-2(VI) chain	2.5 ± 0.7	2.2 ± 0.6	4.1 ± 0.0	Protein unc-80 homolog	1.8 ± 0.6	2.0 ± 0.2	3.5 ± 1.4
Collagen alpha-3(VI) chain	4.7 ± 1.3	2.1 ± 0.6	8.0 ± 1.2	Serpin A1c	1.1 ± 0.3	2.4 ± 1.0	2.1 ± 0.5
Complement C3	1.8 ± 1.4	4.3 ± 3.4	2.3 ± 0.8	Serpin A1d	0.8 ± 0.5	2.8 ± 1.3	1.0 ± 0.4
Complement C4-B	0.3 ± 0.1	2.7 ± 1.0	0.6 ± 0.2	Serpin B6	4.7 ± 2.5	3.9 ± 2.4	8.0 ± 1.9
Complement factor B	0.9 ± 0.2	2.0 ± 0.4	1.8 ± 0.5	Protein serpinb6e	1.3 ± 0.3	2.3 ± 0.6	2.5 ± 0.1
Complement factor H	1.0 ± 0.3	1.8 ± 0.5	1.7 ± 0.6	Serum albumin	3.2 ± 1.7	4.2 ± 2.4	12.6 ± 9.7
Corneodesmosin	1.5 ± 0.4	1.7 ± 0.4	2.2 ± 0.4	Siderophilin	2.2 ± 0.7	2.8 ± 1.1	5.2 ± 2.5
Cystatin-3	2.4 ± 0.6	2.7 ± 0.8	7.0 ± 3.7	Stromelysin-1/MMP3	0.4 ± 0.1	1.5 ± 0.3	0.5 ± 0.1
Dermatopontin	2.0 ± 0.4	1.6 ± 0.2	3.1 ± 0.6	Susd 4	2.3 ± 0.7	2.4 ± 1.1	3.9 ± 1.1
Dermokine	1.1 ± 0.3	1.4 ± 0.3	1.4 ± 0.2	Transcobalamin II	0.8 ± 0.5	2.2 ± 1.1	0.8 ± 0.2

Figure 20: List of proteins identified by N-TAILS as cleaved by ADAMTS2 and/or ADAMTS14 and abundance ratio of peptides from these proteins between the control and the knockout mice. Values are ratio (± SD) established by comparing N-terminal peptide abundance in the skin of WT mice (which contains ADAMTS2 and ADAMTS14) to the skin of TS2-KO mice, TS14-KO mice and TS2-TS14 double knockout mice. Values > 1 indicate a cleavage. For more details, please see the publication at the end of chapter 1.

B. Both ADAMTS2 and ADAMTS14 may be involved in C-propeptide processing of type I collagen and N-propeptide processing of type V collagen

Regarding the identified cleavage sites for ADAMTS2 and ADAMTS14 in collagens, this N-TAILS analyses: (i) confirmed the aminoprocollagen peptidase activity of ADAMTS2 (Figure 21.A); (ii) indicated that ADAMTS14 has limited aminoprocollagen peptidase activity on type I collagen *in vivo* as compared to ADAMTS2 (1.7 vs 4.2 p/c ratio, Figure 20); (iii) generated the first evidence that ADAMTS2 and ADAMTS14 have carboxypropeptide peptidase activity on type I collagen *in vivo* (Figure 21.A); (iv) confirmed the activity of ADAMTS2 (and ADAMTS14) on the N-propeptide of type V collagen (Figure 21.B).

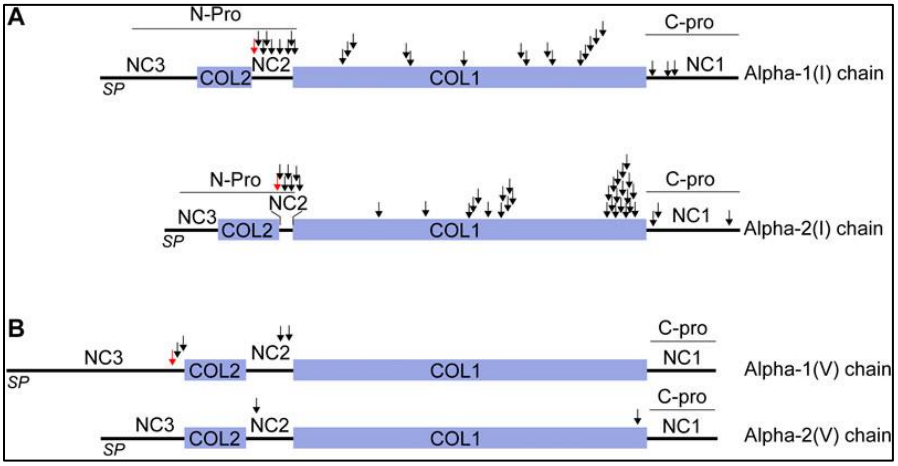

Figure 21: Schematic representation of the identified cleavage site of ADAMTS2 and/or ADAMTS14 on the peptidic sequence of α1 and α2 type I and V collagen. Arrows correspond to the identified cleavage by ADAMTS2 and/or ADAMTS14 and red arrows correspond to already identified cleavage site for ADAMTS2.

C. ADAMTS2 and ADAMTS14 may process extracellular actin and vimentin

While substrates of secreted enzymes are expected to be extracellular, several peptides of actin and vimentin have been identified as resulting from the activity of ADAMTS2 and ADAMTS14 (Figure 22.A) These totally unexpected data were therefore verified *in vitro* by incubating the enzymes with fibroblasts extracts in the presence or absence of EDTA (used as a metalloproteinase inhibitor).

These experiments confirmed that actin and vimentin can be cleaved by ADAMTS2 and ADAMTS14 as pictured by the identification of lower molecular weight products of actin and vimentin by Western blot after incubation with ADAMTS2 and ADAMTS14 (Figure 22.B). Interestingly, the incubation of cell extracts with ADAMTS2 and with ADAMTS14 gave different cleavage patterns for actin and vimentin, indicating different cleavage sites. The biological relevance of these data, on the other hand, still needs to be defined.

A

Cleavage sites	TS2	TS14	TS2TS14
Alpha-ACTIN-1			
VCDN(14).(15)GSGL	1.4 ± 0.3	2.1 ± 0.6	2.5 ± 0.5
SGLV(19).(20)KAGF	2.1 ± 0.4	2.2 ± 0.4	4.5 ± 1.1
LVKA(21).(22)GFAG	2.1 ± 0.7	2.2 ± 0.8	3.6 ± 0.8
PTLL(107).(108)TEAP	2.0 ± 1.0	3.9 ± 2.4	3.2 ± 3.1
KDLY(296).(297)ANNV	1.8 ± 0.6	2.4 ± 0.9	3.5 ± 1.1
KQEY(364).(365)DEAG	2.4 ± 0.7	2.6 ± 0.6	5.8 ± 1.7
Gamma-ACTIN			
KDLY(294).(295)ANTV	1.6 ± 1.0	3.5 ± 1.6	2.7 ± 2.0
QQMW(356).(357)ISKQ	1.8 ± 0.6	1.9 ± 0.5	2.6 ± 0.4
KQEY(362).(363)DESG	1.8 ± 0.3	1.9 ± 0.3	3.4 ± 0.2
VIMENTIN			
SNRS(29).(30)YVTT	1.7 ± 0.5	1.7 ± 0.5	3.0 ± 1.5
RSLY(53).(54)SSSP	1.9 ± 0.5	1.9 ± 0.5	3.8 ± 0.6
SVDF(86).(87)SLAD	1.1 ± 0.3	1.9 ± 0.5	1.8 ± 0.6
DFSL(88).(89)ADAI	1.2 ± 0.4	1.7 ± 0.6	1.3 ± 0.1
SLAD(90).(91)AINT	1.4 ± 0.5	1.5 ± 0.5	1.6 ± 0.4
NKIL(131).(132)LAEL	1.7 ± 0.6	1.9 ± 0.6	2.4 ± 0.8
KILL(132).(133)AELE	1.8 ± 0.6	2.3 ± 0.5	3.4 ± 0.5
LQSF(206).(207)RQDV	2.1 ± 0.5	2.0 ± 0.5	3.5 ± 0.2
KSKF(295).(296)ADLS	1.6 ± 0.7	2.0 ± 0.6	2.2 ± 0.7
SLTC(328).(329)EVDA	2.8 ± 1.0	2.2 ± 0.7	4.7 ± 0.5

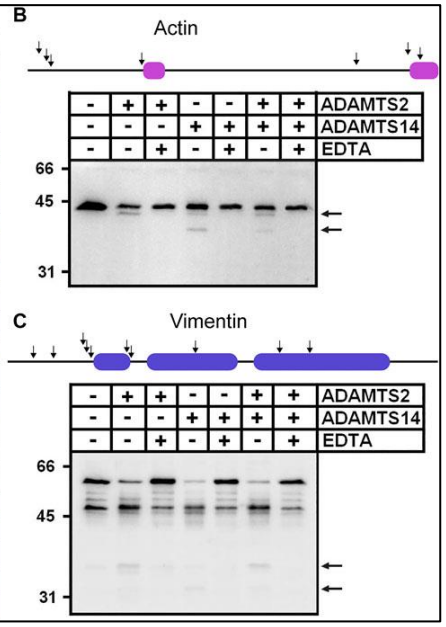

Figure 22: A) Actin and vimentin peptides identified by N-TAILS associated with ADAMTS2 and/or ADAMTS14 activity. B) Western blot analysis of actin and vimentin (from fibroblast extracts) after incubation with ADAMTS2 and/or ADAMTS14 in the presence or absence of EDTA used as inhibitor.

Overall, this study demonstrated that N-TAILS analysis (i) can be performed on complex tissues, (ii) identified novel roles for ADAMTS2 and ADAMTS14 during collagen processing, (iii) showed extensive redundancy between the proteins cleaved by ADAMTS2 and ADAMTS14, (iv) indicated the absence of compensatory roles between ADAMTS2 and ADAMTS14, and (v) established the skin N-terminome associated with the two enzymes, which could be the starting point for the discovery of some of their new function yet to be discovered.

frontiers in Molecular Biosciences

ORIGINAL RESEARCH
published: 19 March 2021
doi: 10.3389/fmolb.2021.643178

In vivo N-Terminomics Highlights Novel Functions of ADAMTS2 and ADAMTS14 in Skin Collagen Matrix Building

Cédric Leduc[1], *Laura Dupont*[1], *Loïc Joannes*[1], *Christine Monseur*[1], *Dominique Baiwir*[2], *Gabriel Mazzucchelli*[2], *Christophe Deroanne*[1], *Alain Colige*[1†] *and Mourad Bekhouche*[1,3,4*†]

[1]*Laboratory of Connective Tissues Biology, GIGA-Cancer, University of Liège, Liège, Belgium,* [2]*GIGA Proteomic Facility, GIGA–Interdisciplinary Cluster for Applied Genoproteomics, University of Liège, Liège, Belgium,* [3]*Tissue Biology and Therapeutic Engineering, Centre National de la Recherche Scientifique/University of Lyon Unité Mixte de Recherche 5305, Lyon, France,* [4]*Faculté d'Odontologie de Lyon, Université de Lyon, Université Lyon 1, Lyon, France*

OPEN ACCESS

Edited by:
Kazuhiro Yamamoto, University of Liverpool, United Kingdom

Reviewed by:
Fransiska Malfait, Ghent University, Belgium
Paripok Phitsuwan, King Mongkut's University of Technology Thonburi, Thailand

***Correspondence:**
Mourad Bekhouche
mourad.bekhouche@univ-lyon1.fr

[†]*These authors share last authorship*

Specialty section:
This article was submitted to Protein Chemistry and Enzymology, a section of the journal Frontiers in Molecular Biosciences

Received: *17 December 2020*
Accepted: *08 February 2021*
Published: *19 March 2021*

Citation:
Leduc C, Dupont L, Joannes L, Monseur C, Baiwir D, Mazzucchelli G, Deroanne C, Colige A and Bekhouche M (2021) In vivo N-Terminomics Highlights Novel Functions of ADAMTS2 and ADAMTS14 in Skin Collagen Matrix Building. Front. Mol. Biosci. 8:643178. doi: 10.3389/fmolb.2021.643178

A disintegrin and metalloproteinase with thrombospondin type I motif (ADAMTS)2 and ADAMTS14 were originally known for their ability to cleave the aminopropeptides of fibrillar collagens. Previous work using N-terminomic approach (N-TAILS) *in vitro* led to the identification of new substrates, including some molecules involved in TGF-β signaling. Here, N-TAILS was used to investigate the substrates of these two enzymes *in vivo*, by comparing the N-terminomes of the skin of wild type mice, mice deficient in ADAMTS2, in ADAMTS14 and in both ADAMTS2 and ADAMTS14. This study identified 68 potential extracellular and cell surface proteins, with the majority of them being cleaved by both enzymes. These analyses comfort their role in collagen matrix organization and suggest their implication in inflammatory processes. Regarding fibrillar collagen, this study demonstrates that both ADAMTS2 and ADAMTS14 are involved in the processing of the aminopropeptide of alpha1 and alpha2 type V collagen. It also revealed the existence of several cleavage sites in the Col1 domain and in the C-propeptide of type I collagens. In addition to collagens and other extracellular proteins, two major components of the cell cytoskeleton, actin and vimentin, were also identified as potential substrates. The latter data were confirmed *in vitro* using purified enzymes and could potentially indicate other functions for ADAMTS2 and 14. This original investigation of mouse skin degradomes by N-terminomic highlights the essential role of ADAMTS2 and ADAMTS14 in collagen matrix synthesis and turnover, and gives clues to better understand their functions in skin pathophysiology. Data are available via ProteomeXchange with identifier PXD022179.

Keywords: ADAMTS, collagen, Ehlers-Danlos Syndrome (EDS), degradomics, TAILS, N-Terminomics

INTRODUCTION

Ehlers-Danlos syndrome (EDS) encompasses a group of inherited diseases caused by mutations affecting genes involved in the homeostasis of connective tissues (Beighton et al., 1998). A significant number of these genes are directly related to the biology of fibrillar collagens. Mutations in type V and type III procollagens are the main causes of, respectively, the "classical" and the "vascular" types of EDS. Missense mutations in type I procollagens can also lead to rare forms of classical and vascular

EDS, while complete or partial skipping of exon six in alpha1 type I (COL1A1) or alpha2 type I (COL1A2) is responsible for arthrochalasia EDS, a condition mainly characterized by congenital bilateral hip dislocation, severe generalized joint hypermobility with multiple dislocations/subluxations and skin hyperextensibility (De Paepe and Malfait, 2012; Malfait and De Paepe, 2014). Electron microscopy of skin specimens shows loosely and randomly organized collagen fibrils with a smaller and variable diameter, and an irregular outline (Colige et al., 2004). The molecular basis behind this clinical picture is the absence of aminopropeptide cleavage of the mutated chain (either alpha1 or alpha2) since exon six encodes the cleavage site cleaved by aminoprocollagen peptidases (ADAMTS2, 3 and 14) (Colige et al., 1999). Null mutations in ADAMTS2, the main aminoprocollagen peptidase, lead also to EDS, but, surprisingly, not to the arthrochalasia EDS as reported for its mutated substrates. Instead, absence of ADAMTS2 activity causes dermatosparaxis EDS presenting with extreme skin fragility, characteristic craniofacial features, redundant skin with excessive skin folds at the wrists and ankles, umbilical hernia and severe bruising with a risk of subcutaneous hematomas and hemorrhages (Colige et al., 1999). In these patients and in animal models of deficiency in Adamts2 ($TS2^{-/-}$) electron microscopy shows collagen fibrils with a highly typical hieroglyphic or ribbon-like pattern. These differences in the morphology of collagen fib rils in arthrochalasia and dermatosparaxis, while persistence of N-propeptides is observed in both diseases, suggested that ADAMTS2 has possibly substrates other than type I procollagens.

Because of their close similarities with ADAMTS2, the consequences of mutations affecting ADAMTS3 and ADAMTS14 have been evaluated in mouse models (Janssen et al., 2016; Dupont et al., 2018). ADAMTS3 has been shown to be required for the formation of lymphatic network by its capacity to cleave pro-VEGF-C into fully active VEGF-C able to bind its receptors (Janssen et al., 2016). Regarding ADAMTS14, KO-mice do not display obvious specific phenotype despite the fact that biallelic null mutations have been predicted to be pathogenic using dedicated browser such as "GnomAD". In the same line, mice deficient for both Adamts2 and Adamts14 ($TS2^{-/-}TS14^{-/-}$) display an aggravated phenotype as compared to $TS2^{-/-}$ mice, again indicating further roles and substrates for ADAMTS14 (Dupont et al., 2018). In order to have first indications about the diversity of the substrates of ADAMTS2, 3 and 14, a proteomic analysis dedicated to the identification of protease substrates (N-TAILS) was performed in cell culture models (Bekhouche et al., 2016). This study showed that the repertoire of substrates of these "so-called" aminoprocollagen peptidases extends beyond fibrillary procollagens. Although most useful because of their relatively low complexity, these *in vitro* models do not recapitulate the *in vivo* situation. As an example, fibrillary procollagens are secreted in the culture medium as uncleaved precursors, whereas in connective tissues *in vivo* they stay concentrated close to the producing cells and are fully matured.

In order to clarify why arthrochalasia and dermatosparaxis EDS display different clinical phenotypes (Van Damme et al., 2016) and to investigate the diverse functions of ADAMTS2 and ADAMTS14 *in vivo* (Dupont et al., 2018), N-Tails analysis has been performed on skin samples from wild-type mice (Wt) and $TS2^{-/-}$, $TS14^{-/-}$ and $TS2^{-/-}TS14^{-/-}$.

MATERIALS AND METHODS

Reagents

The hyperbranched polyglycerol-aldehyde polymer was purchased from Flintbox (University of British Columbia, Vancouver, BC, Canada). Isobaric tag for relative and absolute quantitation (iTRAQ) labels are from AB Sciex (Concord, ON, Canada). Porcine trypsin was purchased from Promega (#V511A; Madison, WI, United States). Ultrafiltration devices were purchased from Merck Millipore. All other reagents were purchased from Sigma-Aldrich (Saint-Quentin Fallavier, France).

Cell Lines

Fibroblasts were obtained from the dermis of healthy donors (normal fibroblasts, NF) and of a patient suffering from the dermatosparactic type of the Ehlers-Danlos syndrome (dermatosparactic fibroblasts, DF) (Nusgens et al., 1992). Cells were cultured in DMEM (Lonza) supplemented with 10% fetal bovine serum (FBS, Lonza). For collagen production, cells were cultured in DMEM supplemented with 1% FBS and 50 µg/ml 2-phospho-L-ascorbic acid (Sigma Cat#49752). The conditioned medium was collected after 48h, centrifuged for 15 min at 4,000 rpm at 4°C. The supernatant was conserved at −80°C before collagen purification.

Skin Proteome Preparation

The experiment was conducted in triplicate using twelve 8-week-old adult mice (2 males and one female of each genotype (Wt, $TS2^{-/-}$, $TS14^{-/-}$ and $TS2^{-/-}/TS14^{-/-}$)). The investigation on mice was reviewed and approved by Ethics Committee for Animal Use and Care of the University of Liege (Belgium) (protocol N°1,109). A square (1 cm^2) of shaved skin was collected from the anteroventral part of the mice and incubated 1 h at 4°C under shaking in 3 ml of 50 mM HEPES sodium salt (pH 7.5), 2 mM $CaCl_2$ and 150 mM NaCl containing a cocktail of inhibitors of proteases and phosphatases (MS-SAFE, Sigma). Skin pieces were harvested and crushed with ceramic beads (MagNA Lyser Green Beads, Roche, n°03358,941,001) using the MagNA Lyser Instrument (Roche) in 90% (V/V) tissue protein extraction reagent (Thermo Scientific #78510), 10% (V/V) HEPES sodium salt (pH 7.5), 2 mM $CaCl_2$, 150 mM NaCl containing the MS-SAFE inhibitors cocktail. Crushed samples were centrifuged 5 min at 8,000 rpm at 4°C and the protein concentrations estimated (Bradford assay (Bradford, 1976)) in the collected supernatants and adjusted to 1.0 mg/ml. Samples of 500 µg of proteins for each condition were used for iTRAQ-TAILS labeling (Kleifeld et al., 2011; Bekhouche et al., 2016). Proteomic analyses were performed at the GIGA Proteomic platform on the ESI-Q Exactive (ThermoFisher) coupled with a 2D-RP/RP liquid chromatography (2D-RP/RP NanoAcquity

UPLC, Waters, Milford, United States) for the peptide fractionation in three fractions.

Proteomic Data Analysis

Proteomic data analysis was previously described (Bekhouche et al., 2016). Briefly, in a first step, peptides were identified using Mascot (version 2.2.06; Matrix Science Inc., Boston, MA, United States) and allowing non-tryptic cleavages and two missed cleavages/peptide. Carbamidomethyl cystein was set as a fixed modification, and other modifications were set as variable: N-terminal acetyl, deamidation (NQ), Pyro-glu (N-term E), Pyro-Gln (N-term Q), Oxidation (M), iTRAQ (K), iTRAQ (Y) and iTRAQ (N-term). Peptide tolerance was set at 0.02 Da.

The tandem mass spectrometry (MS/MS) data were analyzed using the TransProteomicPipeline (TPP). The PeptideProphet and ProteinProphet software programs, embedded into TPP, were used to validate protein and peptide assignment. The nontryptic model was omitted in the PeptideProphet parameters. The error rate to validate proteins or peptides was respectively set at 2 and 5%. Then, Clipper software was used to determine the upper and lower cutoffs corresponding to 3-sigma calculated from the normal distribution of the log2(P:C ratio) from natural mature N termini. A Gaussian error function was used to calculate a *p* value that reflects the probability of a peptide to be a false-positive. A peptide with a P:C ratio above or below the 3-sigma cutoff has 99,8% chance to be dependent of the studied protease (auf dem Keller and M Overall, 2012). The cutoffs for each experiment are reported in **Supplementary Table S4**. The mass spectrometry proteomics data have been deposited to the ProteomeXchange Consortium via the PRIDE (Perez-Riverol et al., 2019) partner repository with the dataset identifier PXD022179 and 10.6019/PXD022179.

Biological Process Analysis

The biological processes have been investigated using the Panther database (PANTHER version 14: more genomes, a new PANTHER GO-slim and improvements in enrichment analysis tools (Mi et al., 2019)). Statistical overrepresentation tests were performed using the whole *Mus musculus* genome as reference dataset. The *p*-Values are determined using the Fisher's Exact test corrected by the determination of the false discovery rate (fdr). The fdr was below 0.05 for all the reported biological process.

The Venn diagram were drawn using the BioVenn software (BioVenn—a web application for the comparison and visualization of biological lists using area-proportional Venn diagrams (Hulsen et al., 2008)).

Purification of Recombinant ADAMTS2 and 14

Recombinant ADAMTS2, its inactive mutant, or ADAMTS14 were produced in HEK293 cells, purified and quantified as previously described (Colige et al., 2005). Briefly, recombinant proteases were purified, using Concanavalin A-Sepharose and Heparin-Sepharose columns, from 1 L of serum-free medium conditioned during 48 h. Proteases were recovered in 50 mM Tris, pH 7.5, 1 M NaCl, 2 mM $CaCl_2$.

Analysis of Fibrillar Collagens Degradation

Collagen from dermatosparactic or normal calf skin was extracted and purified according to a reported procedure (Nusgens and Lapiere, 1979; Colige et al., 1995). Collagen from fibroblasts cultures, was concentrated by adding ethanol to the conditioned medium (see above, 2.2) at a final concentration of 33% (V/V). After overnight incubation at 4°C, precipitated collagen was recovered by centrifugation (7,000 rpm, 40 min, 4°C). Pellets were solubilized in 0.1 M acetic acid (pH 2.9) under shaking at 4°C for 18 h. Non-solubilized contaminants were excluded by centrifugation (17,000 rpm, 40 min, 4°C) and the supernatant containing the collagen was neutralized by adding 1 M Tris base solution (at 1/10 of the final volume). Collagen cleavage was analyzed by incubation of 10 µg of type I collagen with recombinant ADAMTS2 or 14 (200 nM for 16 h at 37°C) in 50 mM Tris (pH 7.5), 0.5 M NaCl, 2 mM $CaCl_2$, in the presence or absence of 25 mM EDTA used as inhibitor of ADAMTS metalloproteinase activity. Collagens were used in native form or after thermal denaturation at 95°C for 10 min. Digestion products were separated by SDS-PAGE and stained with Coomassie Blue.

Analysis of Cleavage of Intracellular Substrates

Cell lysates from human normal fibroblasts (NF) were prepared by sonication and incubated with recombinant human ADAMTS2 and/or 14 (200 nM for 16 h at 37°C) in 50 mM Tris (pH 7.5), 0.5 M NaCl, 2 mM $CaCl_2$, in the presence or absence of 25 mM EDTA. Actin and vimentin cleavages were analyzed by Western blot using polyclonal anti-alpha-actin-1 (A2066, Sigma) and polyclonal anti-vimentin (VI008–01, Quartett).

Determination of Cleavage Site Specificity

Amino acid sequence logos, corrected by the natural abundance of amino acids in the human proteome, were generated using the iceLogo software package (Colaert et al., 2009). Analyses were based on the cleavage sites determined by proteomics for all the potential extracellular substrates, without type I collagen cleavage sites or without all fibrillar collagens.

RESULTS

N-Terminomic Analysis of ADAMTS2 and ADAMTS14 Skin Degradome

ADAMTS2 and ADAMTS14 are clearly implicated in several physio-pathological processes (Colige et al., 1999; Kesteloot et al., 2007; Dubail et al., 2010; Dupont et al., 2018; Wang et al., 2020). To better understand their *in vivo* roles in skin physiology and extracellular matrix homeostasis, N-terminomic experiments have been performed on skin of mice, either wild type (Wt), deficient in Adamts2 ($TS2^{-/-}$), deficient in Adamts14 ($TS14^{-/-}$)

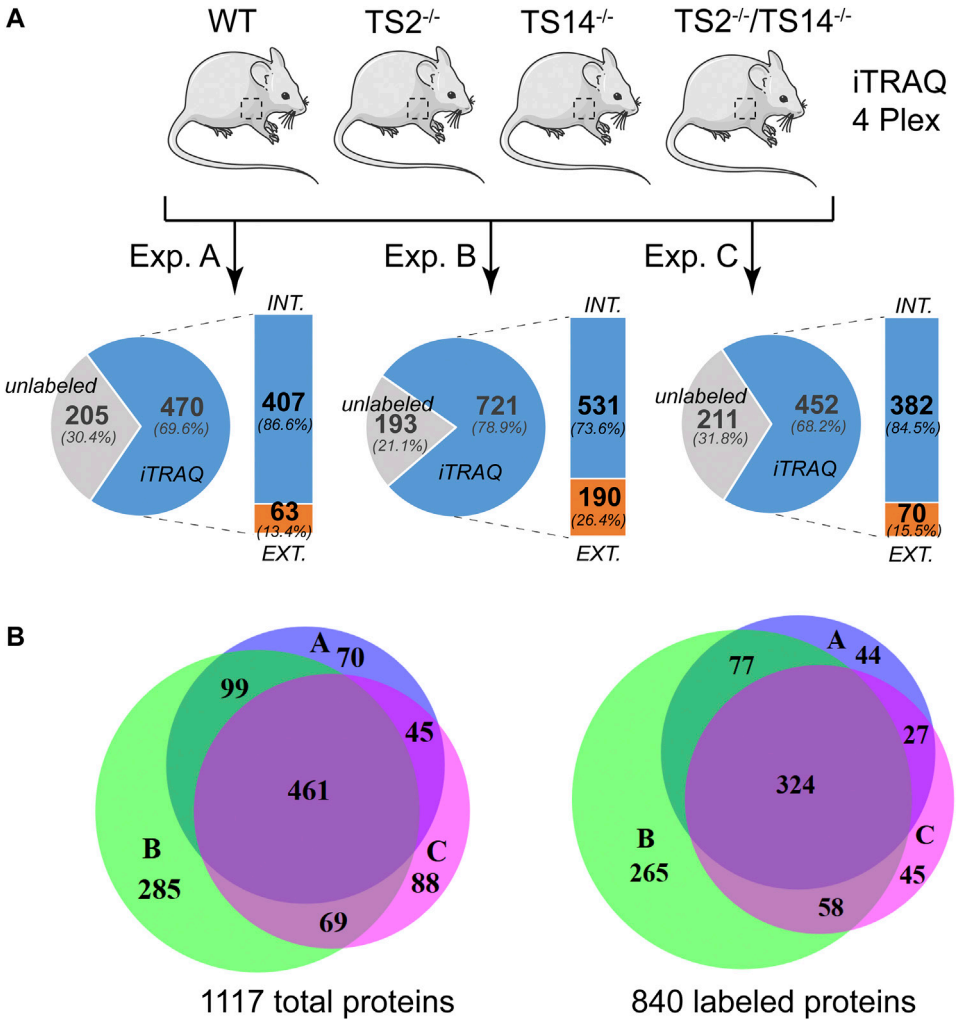

FIGURE 1 | N-terminomic analysis of ADAMTS2 and 14 in mouse skin. **(A)** Schematic view of the experimental method to assess the potential substrates of ADAMTS2 and/or ADAMTS14 in mouse skin and to investigate their biological function *in vivo*. Three independent iTRAQ-TAILS analyses using skin proteome of each genotypes (4-plex) have been performed. As a general procedure, a protease/control (P/C) ratio above or below the three sigma cutoff from the normal distribution of natural N-termini is considered to be related to the studied protease. Here, the ratio Wt/TS2$^{-/-}$ and TS14$^{-/-}$/TS2$^{-/-}$TS14$^{-/-}$ were used to investigate the ADAMTS2 substrates, the ratios Wt/TS14$^{-/-}$ and TS2$^{-/-}$/TS2$^{-/-}$TS14$^{-/-}$ were used to investigate the ADAMTS14 substrates and the ratio Wt/TS2$^{-/-}$TS14$^{-/-}$ was used to investigate the substrates common to ADAMTS2 and ADAMTS14. **(B)** Venn diagram showing the number of specific or common total **(left)** or labeled **(right)** proteins identified in each experiment. Experiment A is in blue, B in green and C in purple. Venn diagrams were generated using the online BioVenn software (Hulsen et al., 2008).

and deficient in both Adamts2 and Adamts14 (TS2$^{-/-}$TS14$^{-/-}$) (**Figure 1A**). For each experiment, proteins extracted from the four genotypes were labeled with specific iTRAQ labels for quantification by mass spectrometry (MS/MS). This 4-plex experiment was performed in triplicate. The proteomic analysis shows that between 68 and 79% of the proteins were labeled and have therefore been used for relative quantification. Among the labeled proteins between 13 and 26% are extracellular. By using Venn diagrams as analytical tool, a total of 1,117 proteins, including 840 with an iTRAQ labeled peptide, were identified in the three experiments, but only 41 and 38% of them were common to the three experiments, for unlabeled and labeled proteins, respectively (**Figure 1B**). As actual substrates might have been missed during the proteomic analyses, especially when their abundance is low, the data of these three experiments can be considered as complementary. In order to take this limitation into account but to generate also high confidence data, a labeled peptide was considered to identify a candidate substrate when it was observed in at least two experiments with a similar Protease/Control (P/C) fold change (either increased or decreased).

The degradomes (proteolytic events related to a proteolytic enzyme) are determined from the Protease/Control (P/C) ratios significantly different from the normal distribution of the natural N-termini. They include the proteins cleaved directly by the studied protease and also indirectly by the activation of other proteases or regulatory pathways. In this study, any N-terminally iTRAQ labeled peptide was considered to be part of the

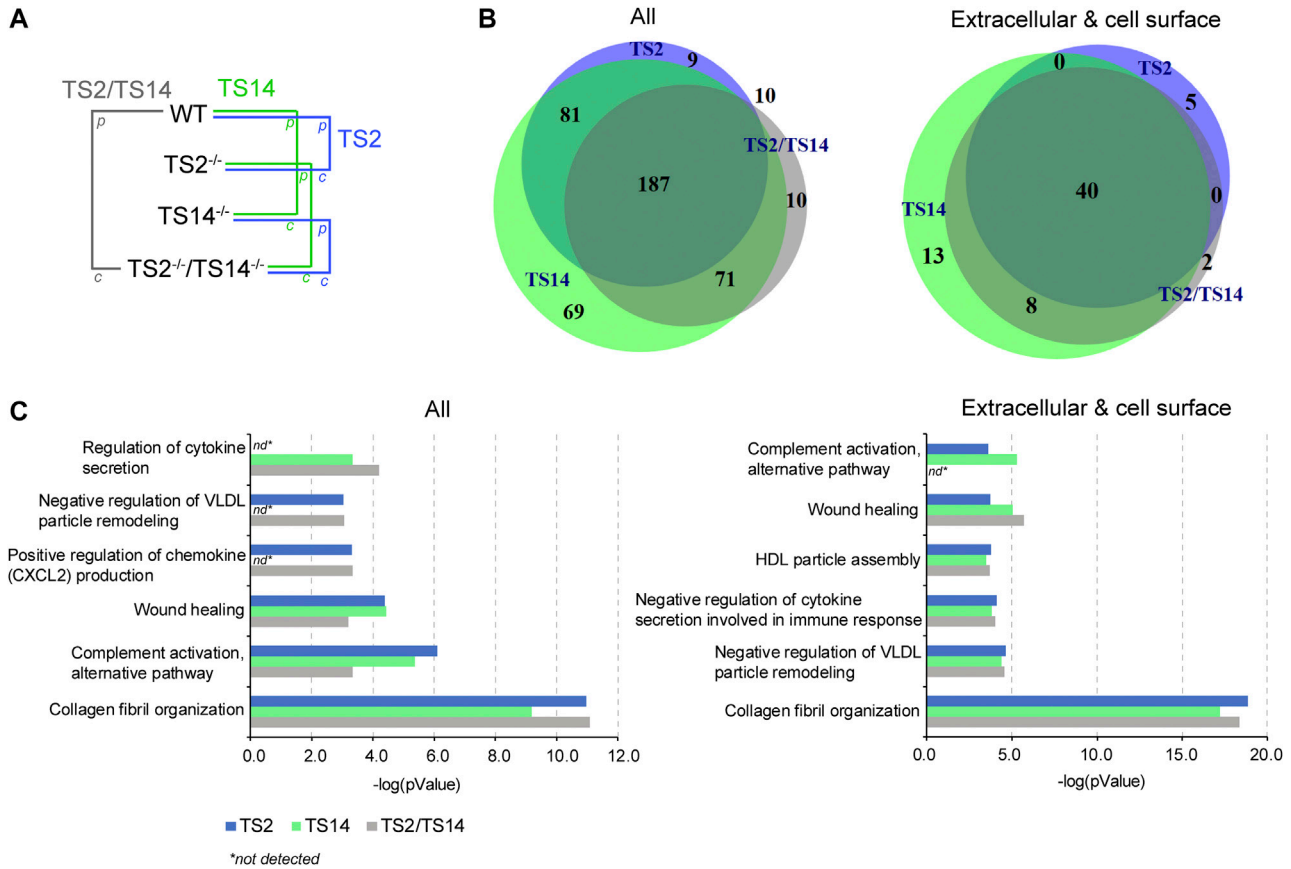

FIGURE 2 | ADAMTS2 and 14 degradomes in mouse skin and their biological processes. **(A)** Schematic view of the multiple comparisons of the P/C ratios analyzed for each iTRAQ-TAILS experiment (n = 3). The function of the ADAMTS2 (in blue) is investigated by the comparison of wild type (Wt) mice with those deficient for ADAMTS2 ($TS2^{-/-}$) and from the comparison of the mice deficient for ADAMTS14 ($TS14^{-/-}$) with those deficient for ADAMTS2 and ADAMTS14 ($TS2^{-/-}TS14^{-/-}$). The potential substrates of ADAMTS14 (in green) were identified from the comparison of Wt mice with the mice deficient for ADAMTS14 ($TS14^{-/-}$) and from the comparison of the mice deficient for ADAMTS2 ($TS2^{-/-}$) with those deficient for ADAMTS2 and ADAMTS14 ($TS2^{-/-}TS14^{-/-}$). The common substrates of ADAMTS2 and 14 (red) were obtained from the comparison between Wt mice and $TS2^{-/-}TS14^{-/-}$ mice, and by combining data obtained specifically for Adamts2 and for Adamts14. **(B)** Venn diagram showing the common and specific N-terminally labeled proteins related to ADAMTS2 (blue), ADAMTS14 (green) or ADAMTS2 and ADAMTS14 (green). All the 437 unique proteins (287 identified by comparing Wt to $TS2^{-/-}$, 408 by comparing Wt to $TS14^{-/-}$ and 278 by comparing Wt to $TS2^{-/-}TS14^{-/-}$) showing a P/C ratio above or below three sigma cutoff from the normal distribution of natural N-termini are reported on the left. The 68 extracellular and cell surface proteins related to ADAMTS2 or ADAMTS14 activities (45 by comparing Wt to $TS2^{-/-}$, 61 by comparing Wt to $TS14^{-/-}$ and 50 by comparing Wt to $TS2^{-/-}TS14^{-/-}$) are reported on the right. **(C)** Biological processes related to all the proteins affected by ADAMTS2 and ADAMTS14 in mouse skin **(left panel)** or related to the extracellular and cell surface substrates **(right panel)**. The biological processes have been identified using the Panther database (Mi et al., 2019). Statistical Overrepresentation test was performed using the whole *Mus musculus* as reference dataset, the pValue is determined using the Fisher's Exact test and corrected by the determination of the false discovery rate (fdr). The fdr is below 0.05 for all the biological processes reported. nd: not detected.

ADAMTS2 and/or ADAMTS14 degradomes when its P/C ratio was above or below a 3-sigma cut-off from the normal distribution of natural N-termini, including those obtained after the removal of the signal peptide. The degradome of ADAMTS2 has been determined from Wt vs $TS2^{-/-}$ and from $TS14^{-/-}$ vs $TS2^{-/-}TS14^{-/-}$ ratios, and that of ADAMTS14 has been determined from Wt vs $TS14^{-/-}$ and from $TS2^{-/-}$ vs $TS2^{-/-}TS14^{-/-}$ ratios, while that of ADAMTS2 and ADAMTS14 together has been determined from Wt vs $TS2^{-/-}TS14^{-/-}$ ratios (**Figure 2A**). In this analysis, the whole degradome of ADAMTS2 and/or ADAMTS14 was found to be composed of 437 proteins, including 68 proteins secreted or anchored at the cell surface. Forty extracellular and cell surface proteins were related to both ADAMTS2 and ADAMTS14 activities, while five are specific of ADAMTS2 and 21 (13 + 8) of ADAMTS14. Of note, two proteins were detected only when comparing Wt and $TS2^{-/-}TS14^{-/-}$, the coagulation factor XIIIa and the mast cell protease 4 (**Figure 2B**). The degradomes of ADAMTS2 and ADAMTS14 are common at 59% (40/68) when considering specifically the extracellular and cell surface proteins, while only a 40% (148/369) overlap is found when considering all the other proteins, showing an enrichment for common extracellular substrates (**Figure 2B**). Investigation of the biological processes (pantherdb.org) related to these degradomes clearly illustrated a fundamental role for these two enzymes in collagen fibril organization, which was

TABLE 1 | Potential extracellular substrates specific or common of ADAMTS2 and/or ADAMTS14.

Name	TS2	TS14	TS2TS14	Name	TS2	TS14	TS2TS14
Inter alpha-trypsin inhibitor	1.2 ± 0.7	1.9 ± 0.7	1.6 ± 0.5	Galectin-1	1.3 ± 0.3	1.9 ± 0.4	2.1 ± 0.4
AE-binding protein 1	0.7 ± 0.2	2.0 ± 0.5	1.2 ± 0.3	Galectin-7	2.0 ± 0.6	2.8 ± 0.8	4.8 ± 1.4
Alpha-2-HS-glycoprotein	0.7 ± 0.3	2.2 ± 1.3	0.9 ± 0.3	Gc-globulin	1.7 ± 0.8	4.1 ± 2.0	6.0 ± 3.7
Alpha-2-macroglobulin	1.7 ± 1.0	2.0 ± 0.6	2.2 ± 0.6	Gelsolin	2.6 ± 0.7	2.4 ± 0.9	5.0 ± 1.7
Annexin-8	6.4 ± 2.2	5.5 ± 1.9	15.0 ± nd[a]	H2-Q9	1.9 ± 1.3	2.7 ± 1.1	2.9 ± 1.1
Apolipoprotein A-I	2.7 ± 1.8	3.3 ± 1.9	4.5 ± 1.8	Hemopexin	1.0 ± 0.4	1.9 ± 0.5	1.5 ± 0.5
Apolipoprotein H	1.6 ± 0.8	2.6 ± 1.2	2.3 ± 0.8	Ig gamma-2B	1.8 ± 0.5	2.3 ± 0.8	3.5 ± 1.2
Beta-globin	2.2 ± 0.6	2.9 ± 1.1	6.7 ± 3.3	Ig gamma-3	1.1 ± 0.4	1.9 ± 0.4	1.8 ± 0.4
Biglycan	2.8 ± 2.4	3.0 ± 1.6	3.6 ± 1.8	Ig kappa chain V-V	1.2 ± 0.8	5.1 ± 2.7	2.9 ± 1.1
Carboxypeptidase A3	1.6 ± 0.4	2.1 ± 0.5	3.2 ± 1.1	Kallikrein j	2.0 ± 0.8	2.4 ± 0.6	5.1 ± 0.6
Cathepsin B heavy chain	1.3 ± 0.6	1.9 ± 0.6	1.6 ± 0.3	Kininogen-1	2.2 ± 0.5	2.9 ± 0.6	5.5 ± 0.2
Cathepsin H	1.2 ± 0.6	2.4 ± 0.8	2.0 ± 0.6	Lumican	1.6 ± 0.7	2.6 ± 1.3	2.3 ± 0.4
Cathepsin S	1.0 ± 0.5	2.2 ± 0.7	1.5 ± 0.4	Mast cell protease 4	1.5 ± 0.2	1.7 ± 0.2	2.4 ± 0.5
Caveolin-1	2.0 ± 0.8	3.1 ± 1.4	3.1 ± 0.0	MIF	1.1 ± 0.6	2.7 ± 1.1	1.8 ± 0.5
Cavin-1	2.1 ± 0.4	3.5 ± 0.9	8.7 ± 0.4	Myelin protein zero	1.6 ± 0.7	2.1 ± 1.1	1.7 ± 0.4
Coagulation factor XIIIa	2.5 ± 1.0	3.8 ± 1.5	7.8 ± nd[a]	Osteoglycin	2.3 ± 0.7	2.3 ± 0.9	4.5 ± 1.6
Collagen alpha-1(I) chain	4.2 ± 0.5	1.7 ± 0.2	6.8 ± 1.0	p24 gamma-1	2.1 ± 1.1	3.3 ± 1.7	1.4 ± 1.0
Collagen alpha-1(III) chain	3.7 ± 2.2	2.8 ± 1.3	5.8 ± 2.7	p35/Annexin A1	2.7 ± 1.2	2.7 ± 0.9	7.4 ± 3.7
Collagen alpha-1(IV) chain	1.6 ± 0.6	1.8 ± 0.6	2.2 ± 0.4	p36/Annexin A2	2.7 ± 1.2	2.7 ± 0.9	7.4 ± 3.7
Collagen alpha-1(V) chain	3.9 ± 1.7	4.1 ± 1.6	9.3 ± 0.8	PCPE-1	2.2 ± 0.4	1.9 ± 0.4	3.6 ± 0.5
Collagen alpha-1(VI) chain	2.2 ± 0.8	1.9 ± 0.6	3.4 ± 0.9	PDI A6	1.8 ± 0.7	2.1 ± 0.7	2.9 ± 0.9
Collagen alpha-1 (XIV) chain	3.6 ± 0.7	2.3 ± 0.5	8.2 ± 2.5	Periostin	1.0 ± 0.5	2.2 ± 0.8	1.3 ± 0.4
Collagen alpha-2(I) chain	3.1 ± 0.7	1.6 ± 0.2	4.6 ± 0.6	Proapolipoprotein A-II	3.5 ± 2.5	4.9 ± 3.2	11.9 ± 7.9
Collagen alpha-2(V) chain	1.8 ± 0.3	1.7 ± 0.3	2.8 ± 0.3	Prolargin	2.9 ± 0.9	2.6 ± 0.8	5.8 ± 1.3
Collagen alpha-2(VI) chain	2.5 ± 0.7	2.2 ± 0.6	4.1 ± 0.0	Protein unc-80 homolog	1.8 ± 0.6	2.0 ± 0.2	3.5 ± 1.4
Collagen alpha-3(VI) chain	4.7 ± 1.3	2.1 ± 0.6	8.0 ± 1.2	Serpin A1c	1.1 ± 0.3	2.4 ± 1.0	2.1 ± 0.5
Complement C3	1.8 ± 1.4	4.3 ± 3.4	2.3 ± 0.8	Serpin A1d	0.8 ± 0.5	2.8 ± 1.3	1.0 ± 0.4
Complement C4-B	0.3 ± 0.1	2.7 ± 1.0	0.6 ± 0.2	Serpin B6	4.7 ± 2.5	3.9 ± 2.4	8.0 ± 1.9
Complement factor B	0.9 ± 0.2	2.0 ± 0.4	1.8 ± 0.5	Protein serpinb6e	1.3 ± 0.3	2.3 ± 0.6	2.5 ± 0.1
Complement factor H	1.0 ± 0.3	1.8 ± 0.5	1.7 ± 0.6	Serum albumin	3.2 ± 1.7	4.2 ± 2.4	12.6 ± 9.7
Corneodesmosin	1.5 ± 0.4	1.7 ± 0.4	2.2 ± 0.4	Siderophilin	2.2 ± 0.7	2.8 ± 1.1	5.2 ± 2.5
Cystatin-3	2.4 ± 0.6	2.7 ± 0.8	7.0 ± 3.7	Stromelysin-1/MMP3	0.4 ± 0.1	1.5 ± 0.3	0.5 ± 0.1
Dermatopontin	2.0 ± 0.4	1.6 ± 0.2	3.1 ± 0.6	Susd 4	2.3 ± 0.7	2.4 ± 1.1	3.9 ± 1.1
Dermokine	1.1 ± 0.3	1.4 ± 0.3	1.4 ± 0.2	Transcobalamin II	0.8 ± 0.5	2.2 ± 1.1	0.8 ± 0.2

[a]*nd: not determined.*

The 68 extracellular and cell surface potential substrates are reported together with the average P/C ratio from at least two experiments for ADAMTS2, ADAMTS14 or ADAMTS2 and ADAMTS14. When several peptides were identified for a protein, the ratios from the peptide giving the highest value are reported for illustration. All the peptides and ratios are reported in supplemental.

expected for ADAMTS2 but was more surprising for ADAMTS14 since collagen fibrils in TS14$^{-/-}$ mice appear to be normal. This analysis also shed light on their implication in lipoprotein regulation and assembly, notably by the cleavage of the proapolipoprotein A-II and apolipoprotein A-I, and in immune response by the regulation of cytokines and chemokines secretion and complement activation, notably through the cleavage of complement proteins (C3C, C4-B) and of the macrophage migration inhibitory factor (**Figure 2C**, **Table 1**, **Supplementary Figure S1**).

Proteomic Analysis of Type I Collagen Processing by ADAMTS2 And/or ADAMTS14 in Mouse Skin

Cleavage of the Aminopropeptide of Fibrillar Collagens

As a positive control assessing the quality and the specificity of our technical approach, we first focused on the cleavages of the aminopropeptides of type I procollagens, the primary substrates of ADAMTS2. For Col1A1 and Col1A2, the highest P/C ratios were detected at sequences corresponding to the published cleavage sites in the NC2 domain: S_{151}-$_{152}$Q for Col1A1 and A_{85}-$_{86}$Q for Col1A2 (**Table 2**). Peptides corresponding to more upstream sequences have P/C ratios largely below 1, evidencing the near absence of intact N-propeptide in Wt skin (**Supplementary Table S2**). These data clearly validate the reliability of our experimental setting.

Surprisingly, several additional potential cleavage sites were also identified in the NC2 domain (**Figure 3A**; **Table 2**), some with a P/C ratio >2. Some were a few amino acids downstream the "canonical" cleavage site and could therefore result from exopeptidase activity, but several others were at longer distance suggesting that ADAMTS2 cleaves within a preferred region and not exclusively at the previously reported single cleavage site.

Regarding ADAMTS14, no clear activity could be evidenced at sites cleaved by ADAMTS2, which is in line with previous studies

TABLE 2 | Type I collagen processing in mouse skin.

Collagen α1(I) chain				Collagen α2(I) chain			
Peptide Sequence	**TS2**	**TS14**	**TS2TS14**	**Peptide Sequence**	**TS2**	**TS14**	**TS2TS14**
NC2 (A150-P167)				*NC2 (A75-P96)*			
NFAS(151).(152) QMSYGYDEKSAGVSVPGPMGPSGPR	4.2 ± 0.5	1.7 ± 0.2	6.8 ± 1.0	NFAA(85).(86)QYSDKGVSSGPGPMGLMGPR	3.1 ± 0.7	1.6 ± 0.2	4.6 ± 0.6
FASQ(152).(153) MSYGYDEKSAGVSVPGPMGPSGPR	2.0 ± 0.3	1.5 ± 0.2	2.9 ± 0.4	FAAQ(86).(87)YSDKGVSSGPGPMGLMGPR	2.0 ± 0.3	2.0 ± 0.3	1.5 ± 0.2
QMSY(155).(156) GYDEKSAGVSVPGPMGPSGPR	2.4 ± 1.0	1.6 ± 0.3	3.3 ± 1.1	YSDK(90).(91)GVSSGPGPMGLMGPR	2.9 ± 0.4	1.4 ± 0.2	2.9 ± 0.6
SYGY(157).(158) DEKSAGVSVPGPMGPSGPR	3.0 ± 1.0	1.8 ± 0.3	5.2 ± 2.0	SDKG(91).(92)VSSGPGPMGLMGPR	1.9 ± 0.3	1.4 ± 0.2	2.6 ± 0.3
DEKS(161).(162)AGVSVPGPMGPSGPR	2.0 ± 0.3	1.5 ± 0.2	2.9 ± 0.5	DKGV(92).(93)SSGPGPMGLMGPR	1.9 ± 0.2	1.5 ± 0.1	2.8 ± 0.1
EKSA (162).(163)GVSVPGPMGPSGPR	1.9 ± 0.3	1.4 ± 0.1	2.6 ± 0.4	*Triple helix (G97-G1113)*			
KSAG(163).(164)VSVPGPMGPSGPR	3.7 ± 0.3	1.4 ± 0.1	5.1 ± 0.2	SSGP(96).(97)GPMGLMGPR	1.9 ± 0.3	1.5 ± 0.2	2.7 ± 0.5
Triple helix (<I>G168-P1181</I>)				GPGP(98).(99)MGLMGPR	2.5 ± 0.8	1.8 ± 0.5	3.9 ± 1.6
VSVP(167).(168)GPMGPSGPR	1.8 ± 0.5	1.6 ± 0.4	2.5 ± 0.6	RGIP(336).(337)GPAGAAGATGAR	2.5 ± 0.7	1.7 ± 0.4	3.6 ± 1.0
VPGP(169).(170)MGPSGPR	1.8 ± 0.5	1.5 ± 0.4	2.6 ± 1.0	RPGP(485).(486)IGPAGPR	2.4 ± 0.7	1.6 ± 0.4	3.5 ± 1.3
TGPP(332).(333) GFPGAVGAKGEAGPQGAR	2.1 ± 0.6	1.7 ± 0.3	3.5 ± 1.1	RGTP(600).(601)GESGAAGPSGPIGSR	2.1 ± 0.6	1.6 ± 0.3	3.2 ± 1.1
PPGF(334).(335)PGAVGAKGEAGPQGAR	2.3 ± 0.8	1.7 ± 0.5	3.5 ± 1.7	GESG(604).(605)AAGPSGPIGSR	2.0 ± 0.2	1.3 ± 0.1	2.5 ± 0.4
PGFP(335).(336)GAVGAKGEAGPQGAR	2.4 ± 0.8	1.9 ± 0.5	4.0 ± 1.3	ESGA(605).(606)AGPSGPIGSR	2.0 ± 0.4	1.4 ± 0.2	2.7 ± 0.5
RGFP(485).(486)GADGVAGPKGPSGER	2.6 ± 1.0	1.7 ± 0.4	3.8 ± 1.5	VGAP (636).(637)GSAGASGPGGLPGER	2.3 ± 0.8	1.7 ± 0.4	3.5 ± 1.2
GFPG(486).(487)ADGVAGPKGPSGER	1.8 ± 0.3	1.4 ± 0.2	2.3 ± 0.2	SGDR(699).(700)GEAGAAGPSGPAGPR	1.9 ± 0.4	1.6 ± 0.3	3.0 ± 0.7
AGAQ(608).(609)GAPGPAGPAGER	2.2 ± 0.4	1.6 ± 0.3	3.1 ± 0.3	GDRG(700).(701)EAGAAGPSGPAGPR	1.9 ± 0.3	1.5 ± 0.2	2.8 ± 0.3
PGPI(842).(843)GNVGAPGPKGPR	2.4 ± 0.3	1.9 ± 0.3	4.3 ± 0.2	DRGE(701).(702)AGAAGPSGPAGPR	2.4 ± 0.6	1.7 ± 0.4	3.8 ± 1.1
PPGP(889).(890)VGKEGGKGPR	2.4 ± 0.6	1.4 ± 0.3	3.1 ± 0.8	GEAG(703).(704)AAGPSGPAGPR	2.0 ± 0.2	1.3 ± 0.1	2.5 ± 0.4
AGSP(935).(936)GTPGPQGIAGQR	2.2 ± 0.6	1.6 ± 0.3	3.1 ± 1.0	EAGA(704).(705)AGPSGPAGPR	2.1 ± 0.4	1.5 ± 0.2	3.0 ± 0.7
PGTP(938).(939)GPQGIAGQR	2.6 ± 0.8	1.6 ± 0.4	3.8 ± 1.3	AGAP(969).(970)GPHGSVGPAGKHGNR	2.2 ± 0.5	1.6 ± 0.3	3.4 ± 0.7
KNGD(1,054).(1,055) RGETGPAGPAGPIGPAGAR	2.1 ± 0.5	2.0 ± 0.4	3.6 ± 0.1	RGEP(987).(988)GPAGSVGPVGAVGPR	2.5 ± 0.8	1.6 ± 0.4	3.7 ± 1.4
NGDR(1,055).(1,056) GETGPAGPAGPIGPAGAR	2.0 ± 0.4	1.4 ± 0.2	2.6 ± 0.5	EPGP(989).(990)AGSVGPVGAVGPR	2.2 ± 0.6	1.5 ± 0.3	3.2 ± 1.1
RGET (1,058).(1,059) GPAGPAGPIGPAGAR	1.7 ± 0.2	1.2 ± 0.1	2.1 ± 0.1	PGPA(990).(991)GSVGPVGAVGPR	1.9 ± 0.2	1.3 ± 0.1	2.4 ± 0.4
ETGP(1,060).(1,061)AGPAGPIGPAGAR	2.4 ± 0.7	1.6 ± 0.4	3.5 ± 1.1	AGSV(993).(994)GPVGAVGPR	2.3 ± 0.5	1.5 ± 0.2	3.3 ± 0.9
PAGP(1,063).(1,064)AGPIGPAGAR	2.6 ± 0.8	1.5 ± 0.4	3.7 ± 1.5	SVGP(995).(996)VGAVGPR	1.7 ± 0.2	1.6 ± 0.2	2.6 ± 0.3
NC1 (S1182-V1453)				LKGY(1,031).(1,032) SGLQGLPGLAGLHGDQGAPGPVGPAGPR	2.2 ± 0.6	1.9 ± 0.5	3.6 ± 1.1
GYDF(1,187).(1,188) SFLPQPPQEKSQDGGR	4.4 ± 0.4	9.5 ± 3.6	24.3 ± 7.6	YSGL(1,034).(1,035) QGLPGLAGLHGDQGAPGPVGPAGPR	2.6 ± 1.2	1.7 ± 0.5	3.1 ± 1.0
DTTL(1,224).(1,225)KSLSQQIENIR	2.5 ± 0.9	2.0 ± 0.9	3.4 ± 0.8	GLPG (1,039).(1,040) LAGLHGDQGAPGPVGPAGPR	2.9 ± 0.6	1.9 ± 0.5	5.6 ± 2.4
LKSL(1,227).(1,228)SQQIENIR	2.3 ± 0.6	1.7 ± 0.5	3.2 ± 0.8	LPGL(1,040).(1,041) AGLHGDQGAPGPVGPAGPR	2.3 ± 0.4	1.3 ± 0.2	2.8 ± 0.3
				PGLA(1,041).(1,042) GLHGDQGAPGPVGPAGPR	2.8 ± 1.2	2.5 ± 1.2	6.1 ± 2.9
				LAGL(1,043).(1,044)HGDQGAPGPVGPAGPR	2.0 ± 0.3	1.6 ± 0.2	2.9 ± 0.5
				GLHG(1,045).(1,046)DQGAPGPVGPAGPR	1.5 ± 0.4	1.8 ± 0.2	2.7 ± 0.9
				LHGD(1,046).(1,047)QGAPGPVGPAGPR	2.2 ± 0.3	1.5 ± 0.2	3.2 ± 0.1
				HGDQ(1,047).(1,048)GAPGPVGPAGPR	1.8 ± 0.2	1.3 ± 0.1	2.4 ± 0.4
				GDQG(1,048).(1,049)APGPVGPAGPR	2.0 ± 0.2	1.4 ± 0.2	2.7 ± 0.5
				RSGQ(1,076).(1,077)PGPVGPAGVR	2.2 ± 0.3	1.5 ± 0.2	3.2 ± 0.1
				NC1 (Y1114-K1372)			
				DATL(1,145).(1,146)KSLNNQIETLLTPEGSR	3.9 ± 3.4	6.0 ± 5.6	3.2 ± 1.0
				LKSL(1,148).(1,149)NNQIETLLTPEGSR	1.6 ± 0.4	2.0 ± 0.6	2.7 ± 0.8
				RLPF(1,347).(1,348)LDIAPLDIGGADQEFR	3.0 ± 0.7	2.0 ± 0.6	5.3 ± 1.2

Cleavage sites observed by proteomics of ADAMTS2 (TS2) and ADAMTS14 (TS14) within α1 and α2 chains of type I collagen. Each cleavage site has been observed at least in two experiments. The sequences of the cleavage sites are reported in bracket according to the UniprotKB numbering. The classical N-propeptide cleavage sites are highlighted in grey.

(Dupont et al., 2018) showing that type I collagen is fully processed in the $TS14^{-/-}$ mice, and further confirming the specificity of our analyses. Most interestingly, the P/C ratios were, however, higher in $TS2^{-/-}TS14^{-/-}$ than in $TS2^{-/-}$ mice suggesting that, in the absence of ADAMTS2, ADAMTS14 can display some aminoprocollagen peptidase activity *in vivo* (**Table 2**).

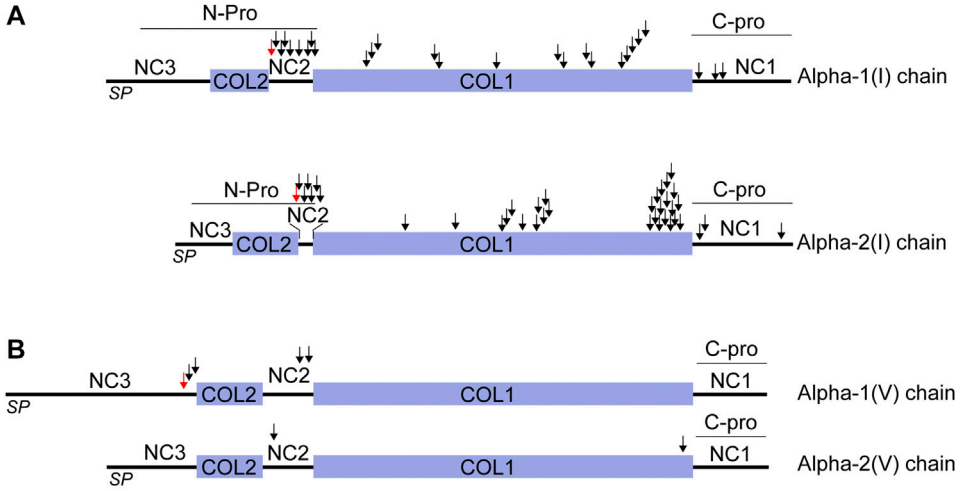

C

Cleavage sites	TS2	TS14	TS2TS14
Alpha-1(V) chain			
PGMP(435).(436)ANQD	3.9 ± 1.7	4.1 ± 1.6	9.3 ± 0.8
MPAN(437).(438)QDTI	2.5 ± 0.6	1.9 ± 0.4	3.9 ± 0.3
QDTI(441).(442)FEGI	2.2 ± 0.6	1.8 ± 0.5	3.4 ± 0.7
AGSK(535).(536)GPMV	1.5 ± 0.4	2.1 ± 0.5	3.0 ± 0.8
MVSA(541).(542)QESQ	1.6 ± 0.3	1.8 ± 0.3	2.7 ± 0.7
Alpha-2(V) chain			
SRPF(189).(190)SAQM	1.8 ± 0.3	1.7 ± 0.3	2.8 ± 0.3
QGPP(903).(904)GATG	2.6 ± 0.9	1.8 ± 0.4	4.3 ± 1.6

FIGURE 3 | ADAMTS2 and/or ADAMTS14 cleavages of type I and V collagens. Schematic view of the pro alpha-1(I) and alpha-2(I) chains showing the signal peptides (PS), the main triple helix collagenous domain (COL1) and the short triple helix collagenous domain (COL2) and the N- and C-propeptides (N- and C-Pro) **(A)**. Schematic view of the pro alpha-1(V) and alpha-2(V) chains showing the collagenous (COL) and non collagenous (NC) domains **(B)**. The ADAMTS2 and ADAMTS14 cleavage sites are indicated by arrows. The red arrows correspond to the already reported ADAMTS2 cleavage sites (Colige et al., 2005; Bekhouche and Colige, 2015). Table showing the P/C ratio for type V collagens, according to the cleavage sites observed by proteomic. Ratios above the average 3σ cut-offs are highlighted in green. The previously described ADAMTS2 cleavage site within alpha-1(V) chain is in bold **(C)**.

The processing of the aminopropeptide of type V procollagens is still a matter of controversy, especially *in vivo*. Processing of Col5A1 has been reported to be performed by BMP1 (within the NC3 domain) and by ADAMTS2 (within the NC3 domain upstream of the Col2 domain) (**Figure 3B**). However, no cleavage has been reported in the NC2 domains of Col5A1 or Col5A2, while their sequence and localization between two collagen domains are similar to those of type I, II and III fibrillar procollagens which are all processed in this region. Several peptides N-terminally iTRAQ labeled were identified in the large N-terminal domain of Col5A1 encompassing the Col2, NC2 and NC3 domains (**Figure 3B**). As opposed to what was observed for type I procollagens, the P/C ratios were usually similar for ADAMTS2 and ADAMTS14, suggesting that both enzymes can process Col5A1 with the same efficacy (**Figure 3C**). Accordingly, the P/C ratios were much higher when comparing Wt and $TS2^{-/-}TS14^{-/-}$ samples. The main processing site ($P_{435\cdot436}A$, upstream of the Col2 domain) was identical to that described previously using recombinant proteins (Colige et al., 2005). As for Col1A1 and Col1A2, other cleavage sites were also identified in this region of Col5A1, two with P/C > 2 ($N_{437\cdot438}Q$ and $I_{441\cdot442}F$) and one with a P/C of 0.4 ($Q_{438\cdot439}D$) reflecting a preferential cleavage at $N_{437\cdot438}Q$. The P/C of the other labeled peptides was not affected by the presence or absence of ADAMTS2 and ADAMTS14, which confirms the specificity of the cleavages with a P/C ratio >2.

Most interestingly, two cleavage sites were also identified in the NC2 domain of Col5A1, including one at an A. Q site as in Col1A2 (**Figure 3B**). Altogether these data indicate that ADAMTS2 and ADAMTS14 can process the N-terminal portion of Col5A1 at three different sites, meaning that Col5A1 is present in the skin under forms (including that generated by BMP1 cleavage) having N-terminal non-collagenous extremity of different size and bulkiness.

N-terminally iTRAQ-labeled peptides corresponding to the NC2 domain of Col5A2 were also detected. Although the P/C

ratios were lower than for Col1A1, Col1A2 and Col1A5, it clearly indicates that the N-propeptide of Col5A2 can be processed by ADAMTS2 and ADAMTS14, but probably at a reduced rate.

Similar to our previous study *in vitro*, the cleavage of the N-propeptide of Col3A1 was not seen in this experiment, probably because the corresponding peptide was not isolated and therefore not analyzed during the MS/MS step.

Cleavages Outside of the Aminopropeptide

Having confirmed and further documented the processing of the aminopropeptides of fibrillar collagens, we were also intrigued by the presence of potential cleavage sites elsewhere in type I collagen chains. In a previous work performed *in vitro* using human cells (Bekhouche et al., 2016), we identified several peptides corresponding to the Col1 domain and the C-propeptide of Col1A1 and Col1A2 that were possibly generated by ADAMTS2 or ADAMTS14 (**Supplementary Table S3**). However, we hypothesized that this could be an artifact linked to the *in vitro* conditions, such as incomplete folding of the triple helical domains leading to an increased sensitivity to proteases. Here, dozens of peptides corresponding to the Col1 domain of Col1A1 and Col1A2 were found to be N-terminally iTRAQ labeled. For both Col1A1 and Col1A2, the P/C ratios were, on average, between 1.5 and two when considering ADAMTS2, and between 1.0 and 1.5 for ADAMTS14 (**Supplementary Tables S2, S3**). However, similarly to what was observed for the processing of the aminopropeptides, these ratios were significantly higher when comparing Wt and $TS2^{-/-}TS14^{-/-}$ skin samples, suggesting that ADAMTS2 and ADAMTS14 can cleave at identical sites. Some "hot spot" regions characterized by several contiguous cleavage sites were found, as, for example, at positions 333 to 337 and 827 to 838 of Col1A1 as well as at positions 988 to 996 of Col1A2 (**Table 2**). They can be generated by direct cleavages operated by ADAMTS2 and 14 in more sensitive domains or, alternatively, by a single cleavage followed by progressive degradation by exopeptidases. In both cases however, it means that the observed individual P/C ratios give an underestimation of the actual cleavage activity in the concerned region.

Finally, peptides corresponding to cleavages in the C-propeptides were also found. As opposed to our observations for Col1 domain, the P/C ratios were similar for both ADAMTS2 and ADAMTS14, again illustrating the specificity in the identification of potential cleavage sites. For Col1A1, one site ($F_{1187\text{-}1188}S$) is located upstream of the C-propeptide cleavage site by BMP1 ($A_{1207\text{-}1208}D$) while the two others are located about 20 amino acids downstream. For Col1A2, three sites were identified, all after the cleavage site for BMP1 (**Table 2**).

Confirmation of the Cleavage of Type I Collagen Within the Col1 Domain and the C-Propeptide

To confirm our iTRAQ data showing multiple cleavages in the Col1 triple helical domain and in the C-propeptide of type I collagens, we performed *in vitro* assays using recombinant enzymes and collagen purified from the skin of dermatosparactic calf which is characterized by the persistence of the aminopropeptides in about 80% of type I collagen molecules (**Figure 4A**, lane 1). This particular substrate was chosen because it provides the opportunity to have an internal control consisting in the processing of the aminopropeptide of Col1A1 and Col1A2. This cleavage (conversion of pNa1 and pNa2 into a1 and a2 chains) was almost complete in the presence of recombinant ADAMTS2, but much reduced in the presence of ADAMTS14 in accordance with its lower aminoprocollagen peptidase activity (**Figure 4A**, lanes 2 and 4, respectively). When looking at lower molecular weight products (**Figures 4C,E**), the released pNa1 propeptide was observed with an apparent 30 kDa MW and was mainly found in the presence of recombinant active ADAMTS2 (lanes 2 and 6). The presence of other bands and of "trails", covering the entire migration lanes and corresponding to cleavages of collagen in multiple sites, were also identified (lane 2), including in the presence of recombinant ADAMTS14 (lane 4). Since ADAMTS14 has only a reduced aminoprocollagen peptidase activity, it shows that the two types of activity are not related.

The same type I collagen preparation was also used as substrate after heat denaturation to verify whether disruption of the triple helical folding impacts the sensitivity to cleavage. Processing of the aminopropeptides by ADAMTS2 or ADAMTS14 was still observed, but marked differences were also visible as compared to gels obtained with native collagen (compare panels a, c, e to panels b, d, f of **Figure 4**), such as the presence of products at 97 and 110 kDa observed in the presence of ADAMTS2 and 14 (lanes 2, 4 and 6 on each panel), and at 105 kDa specifically in the presence of ADAMTS14 (lanes four on each panel). Additional discrete degradation products of lower MW were also identified as well as more pronounced degradation trails along the entire migration lanes (**Figure 4**, lanes 2, 4, 6; panels d and f).

The presence of cleavage sites within the C-propeptide of Col1A1 and Col1A2 was also evidenced by our iTRAQ analyses on *in vitro* assays. Since collagen purified from dermatosparactic skin lacks the C-propeptide, we used collagen produced by human dermatosparactic fibroblasts in culture which is mainly secreted as complete procollagen still retaining its two propeptides (pro-alpha one and pro-alpha 2). After incubation with active ADAMTS2 (**Figure 5**, lane 2), proa1 and proa2 are converted into pCa1 and pCa2, respectively, as a result of the aminoprocollagen peptidase activity of ADAMTS2. Fully processed alpha1 was also observed while similar amount of pNa1 was absent in the control (lane 1) suggesting that it is produced by cleavage of the N- and C-propeptides of the proa1 chain. In line with this hypothesis, the amount of alpha2 chain recovered after incubation with ADAMTS2 exceeded the amount of pNa2 in the control. Moreover, the relative intensity of pCa2 was lower after incubation with ADAMTS2 (lane 2) than expected from the intensity of proa2 in the control. These two observations clearly suggest some cleavage of the C-propeptide of proa2.

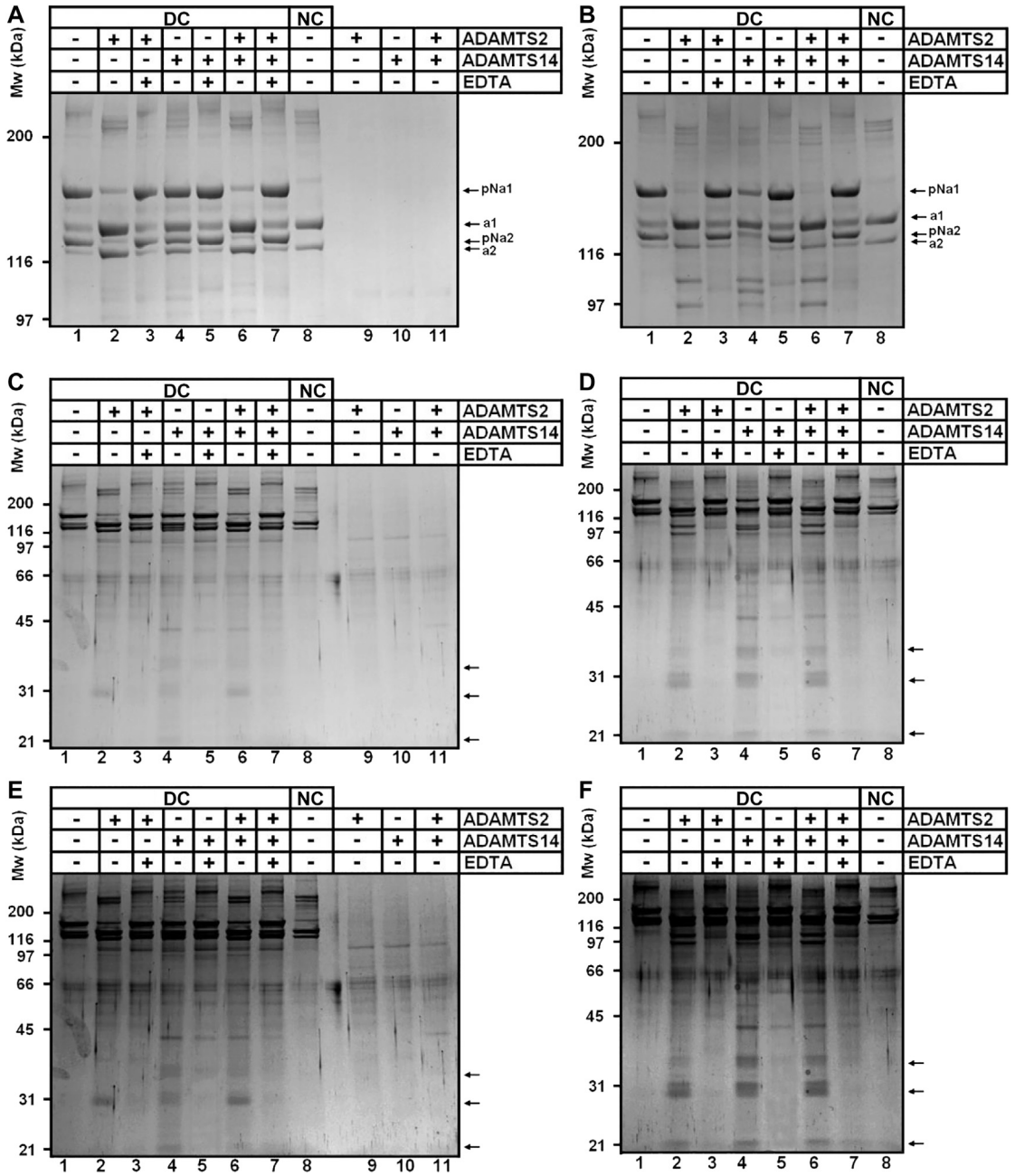

FIGURE 4 | Collagen digestion from calf skin by recombinant human ADAMTS2 and/or ADAMTS14 **(A–F)** Collagen from dermatospatactic calf (DC) skin has been heat denatured (10 min at 95°C) **(B, D, F)** or not **(A, C, E)** before addition of recombinant human TS2 and/or TS14 overnight at 37°C. Digestion products have been analyzed by 6.25% **(A, B)** or 10% **(C–F)** SDS-PAGE stained by Coomassie blue. Pictures at **(E)** and **(F)** correspond respectively to **(C)** and **(D)** with a higher contrast to emphasize the degradation trail. Collagen from normal calf skin (NC) have been used as control for the identification of the fully processed α1 and α2 chains. Products at 31 kDa **(C, E)** correspond to the N-terminal propeptide released mainly by ADAMTS2 when type I collagen is in its native form. Additional low MW products can be observed after incubation of denatured collagen with ADAMTS14 and ADAMTS2.

Regarding ADAMTS14, only a low aminoprocollagen peptidase activity was observed, as expected, as illustrated by the presence of low amounts of pCa2 generated from proa2 (lane 3). However, accumulation of pNa2 was clearly observed indicating that ADAMTS14 can cleave the C-propeptide of Col1A2 more efficiently than its N-propeptide.

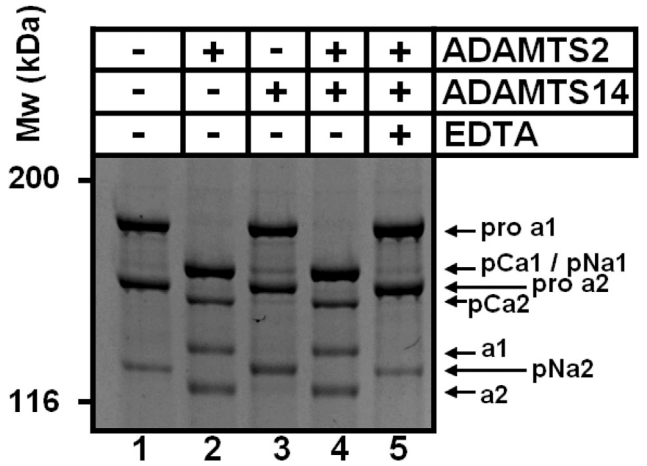

FIGURE 5 | Cleavage of type I procollagen. The collagen substrate, mainly in the form of pro-α1I and pro-α2I, was recovered from culture medium conditioned by dermatosparactic fibroblasts, and then incubated with recombinant human ADAMTS2 and/or ADAMTS14 during 18 h at 37°C. Digestion products were analyzed by 6.25% SDS-PAGE stained by Coomassie blue. The cleavage of pro-α2 into pCα2 and mature α2 demonstrates that ADAMTS2 displays a procollagen C-proteinase activity in addition to its aminoprocollagen peptidase property.

Other Potential Substrates Involved in Collagen Fibril Formation

Several proteoglycans, non-fibrillar collagens and matricellular proteins are known to be involved in the regulation of collagen fibril formation and functions. Some of them were found to be potential substrates of ADAMTS2 and/or ADAMTS14 based on P/C ratios significantly >2 (**Table 1**). They are therefore mentioned, although cleavages were not confirmed by other methods, since their processing could be involved in the clinical features found in dermatosparactic EDS and other connective tissue disorders.

Two sites of cleavage in type XIV collagen were found for both ADAMTS2 and ADAMTS14: at positions 630 (AQQY.LEID) within the fifth fibronectin type-III domain and 1,636 (MARY.TAIL) within the third collagen like domain. Identical sites for both enzymes strongly suggest that the cleavages are real and that type XIV collagen is a true substrate. Potential cleavages were also found in COL4A1 ($G_{1438\cdot1439}T$), at a position corresponding to the release of the arresten cryptic bioactive fragment and in type VI collagens: (1) in the first VWFA domain of COL6A1 ($F_{186\cdot187}S$); (2) in the VWFA1 and VWFA2 domains of COL6A2 ($F_{116\cdot117}S$ and $F_{141\cdot142}A$) and (3) in the VWFA6 domain of COL6A3 ($F_{1051\cdot1052}A$). Besides collagens, potential proteolytic cleavages were also found in PCPE-1 (a co-factor stimulating the processing of the C-propeptide of fibrillar collagens by BMP-1) and in three proteoglycans regulating matrix assembly: biglycan, lumican and osteoglycin. Finally, the degradomes of ADAMTS2 and ADAMTS14 in mouse skin point out several proteins involved in the immune system such as immunoglobulins, complement proteins (C3, C4-B, factor B, factor H), the macrophage inhibitory factor or annexins A8, A1 and A2 known to be involved in leukocyte recruitment and activation (Swisher et al., 2007; Poeter et al., 2014; Sugimoto et al., 2016).

Potential Intracellular Cleavages

This work was primarily focused on extracellular and cell surface degradome since ADAMTS2 and ADAMTS14 are secreted proteases. Unexpectedly however, numerous cleavage sites related to the presence/absence of ADAMTS2 and/or ADAMTS14 were found in intracellular proteins (**Supplementary Table S1**), including actins and vimentin (**Figure 6A**). On average, P/C ratios for actin were higher for ADAMTS14 than for ADAMTS2, as opposed to what was seen for the N-propeptides cleavages, and even higher when comparing Wt skin and $TS2^{-/-}TS14^{-/-}$ skins. Of note also, cleavage sites in actin-2, also known as gamma-actin, are identical to the corresponding cleavage sites in actin-1 which suggests their specificity. In order to confirm these surprising observations, fibroblasts extracts were incubated in the presence of purified ADAMTS2 and/or ADAMTS14 with or without a saturating concentration of EDTA used as inhibitor (**Figure 6B**). In the absence of ADAMTS and EDTA, actin was detected as a single band of 42 kDa with an antibody raised against the C-terminal decapeptide of alpha-actin-1, demonstrating absence of cleavage by intracellular endogenous proteases, while a second product of about 40 kDa was observed after incubation with ADAMTS2, which would correspond to cleavages at positions $V_{19\cdot20}K$ and/or $A_{21\cdot22}G$ in alpha-actin-1 (**Figure 6A**). This product was also seen with ADAMTS14, in addition to a second one at about 34–35 kDa which was not observed with ADAMTS2. Remarkably, only discrete bands were seen, with no trace of smear which would indicate multiple cleavages at specific positions.

Regarding vimentin, several peptides with N-terminal iTRAQ labeling were detected, some with P/C ratio slightly but significantly higher in the presence of ADAMTS2 or ADAMTS14 (**Figure 6A**). For confirmatory purposes Western blot analysis was performed on fibroblast extracts incubated or not with purified ADAMTS2 or ADAMTS14. In the control samples, vimentin appeared as two major bands at 48 kDa and at 58 kDa the latter likely corresponding to the full-length protein. Additional minor products at 53, 50, 46 and 39 kDa were also visible (Romano et al., 2020) (**Figure 6C**). Upon incubation with ADAMTS2 or 14, the intensity of bands at 58 and 53 kDa were markedly reduced, accompanied by an increased intensity of the products at 48 and 39 kDa and the presence of additional bands at 37 and 32 kDa. These data clearly suggest the existence of several cleavage sites by ADAMTS2 and ADAMTS14 but were not investigated further.

Cleavage Site of ADAMTS2 and ADAMTS14 in Mouse Skin

The cleavage sites observed by N-terminomics were used to evaluate cleavage sites enrichment linked to the presence of ADAMTS2 and ADAMTS14. All the potential cleavage sites were used, in a first step, to establish the privileged consensus

A

Cleavage sites	TS2	TS14	TS2TS14
Alpha-ACTIN-1			
VCDN(14).(15)GSGL	1.4 ± 0.3	2.1 ± 0.6	2.5 ± 0.5
SGLV(19).(20)KAGF	2.1 ± 0.4	2.2 ± 0.4	4.5 ± 1.1
LVKA(21).(22)GFAG	2.1 ± 0.7	2.2 ± 0.8	3.6 ± 0.8
PTLL(107).(108)TEAP	2.0 ± 1.0	3.9 ± 2.4	3.2 ± 3.1
KDLY(296).(297)ANNV	1.8 ± 0.6	2.4 ± 0.9	3.5 ± 1.1
KQEY(364).(365)DEAG	2.4 ± 0.7	2.6 ± 0.6	5.8 ± 1.7
Gamma-ACTIN			
KDLY(294).(295)ANTV	1.6 ± 1.0	3.5 ± 1.6	2.7 ± 2.0
QQMW(356).(357)ISKQ	1.8 ± 0.6	1.9 ± 0.5	2.6 ± 0.4
KQEY(362).(363)DESG	1.8 ± 0.3	1.9 ± 0.3	3.4 ± 0.2
VIMENTIN			
SNRS(29).(30)YVTT	1.7 ± 0.5	1.7 ± 0.5	3.0 ± 1.5
RSLY(53).(54)SSSP	1.9 ± 0.5	1.9 ± 0.5	3.8 ± 0.6
SVDF(86).(87)SLAD	1.1 ± 0.3	1.9 ± 0.5	1.8 ± 0.6
DFSL(88).(89)ADAI	1.2 ± 0.4	1.7 ± 0.6	1.3 ± 0.1
SLAD(90).(91)AINT	1.4 ± 0.5	1.5 ± 0.5	1.6 ± 0.4
NKIL(131).(132)LAEL	1.7 ± 0.6	1.9 ± 0.6	2.4 ± 0.8
KILL(132).(133)AELE	1.8 ± 0.6	2.3 ± 0.5	3.4 ± 0.5
LQSF(206).(207)RQDV	2.1 ± 0.5	2.0 ± 0.5	3.5 ± 0.2
KSKF(295).(296)ADLS	1.6 ± 0.7	2.0 ± 0.6	2.2 ± 0.7
SLTC(328).(329)EVDA	2.8 ± 1.0	2.2 ± 0.7	4.7 ± 0.5

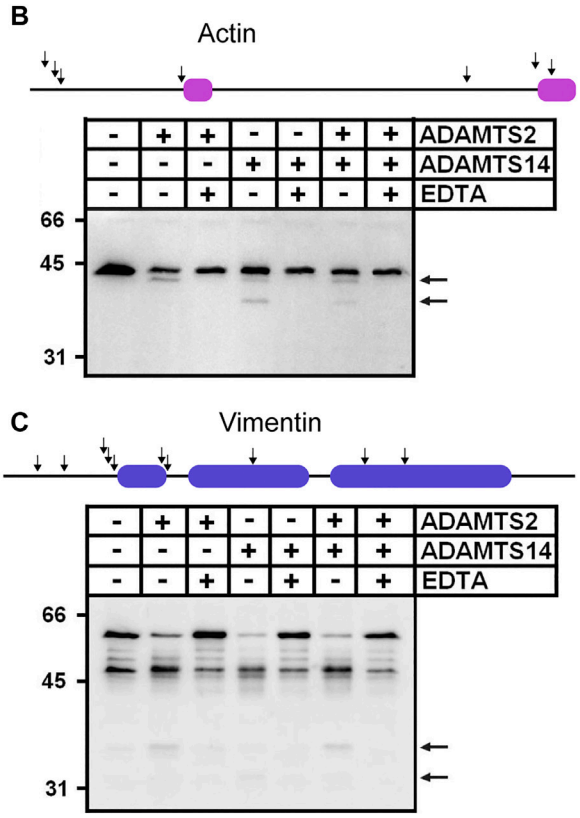

FIGURE 6 | *In vitro* cleavage of actin and vimentin by ADAMTS2 and ADAMTS14. Table showing the P/C ratios according to the cleavage sites observed by proteomic. Ratios above the average 3σ cut-offs are highlighted in green **(A)**. Western blot analysis of *in vitro* cleavage of actin **(B)** and vimentin **(C)** by ADAMTS2 and/or ADAMTS14. The schematic representation of actin and vimentin are reported on the top of the western blots with their respective actinin binding (magenta) and coiled coil (blue) domains. Human fibroblasts lysates were incubated in the presence of recombinant ADAMTS2 and/or ADAMTS14 (200 nM, 16 h at 37°C). EDTA was used as an inhibitor of metalloproteinases. Degradation products are indicated by black arrows.

cleavage sites (**Figure 7**, upper panel). This revealed an overrepresentation of G and P that could be linked, at least in part, to the abundance of these amino acids in collagens. In addition, Y, F and A were often found at P1 and A and S at P1', which is similar to previously described cleavage sites for aminoprocollagen peptidases (Bekhouche et al., 2016; Janssen et al., 2016) (**Figure 7**, upper panel). Considering all the potential extracellular substrates, excluding type I collagen (middle panel) or all fibrillar collagens (lower panel), it was shown that ADAMTS2 and ADAMTS14 display common preferential cleavage sites, enriched in small nonpolar, amphipatic or slightly hydrophobic amino acids (G, P, F, Y, A, L and M). Of note also was the presence of acidic amino acids at P2', P3' and P4'.

DISCUSSION

The procollagen N-proteinases were originally described only for their ability to specifically excise the N-terminal propeptide of fibrillar collagens (Bekhouche and Colige, 2015). However, more recently, we and others have demonstrated their roles in TGFβ signaling (Bekhouche et al., 2016) and in lymphangiogenesis through the proteolytic activation of pro-VEGF-C into VEGF-C able to interact with its receptors (Janssen et al., 2016; Brouillard et al., 2017; Dupont et al., 2018; Wang et al., 2020). The existence of marked differences between the phenotype of patients with arthrochalasia EDS (caused by the absence of the ADAMTS2 cleavage sites in type I collagen) and the phenotype of patients with dermatosparactic EDS (null mutations in ADAMTS2) is another observation arguing for additional functions of ADAMTS2. Finally, the peculiar atopic dermatitis-like skin phenotype of mice deficient in both ADAMTS2 and ADAMTS14 (Dupont et al., 2018) also points to yet to be discovered new substrates of these two related enzymes. In order to search for such potential substrates using a large-scale unbiased approach, we have compared N-terminomes of the skin of Wild type, $TS2^{-/-}$, $TS14^{-/-}$ and $TS2^{-/-}TS14^{-/-}$ mice, an experimental approach never tried before because its inherent difficulties, such as the dynamic nature of the cleavage events that could be hidden by cellular uptake, rapid degradation of the generated peptides, and potential variations in protein composition or cell abundance. Moreover, the deficiency of a protease *in vivo* can be compensated by another protease cleaving near or at the same cleavage site (Fortelny et al., 2014). As an additional challenge, skin is formed by several

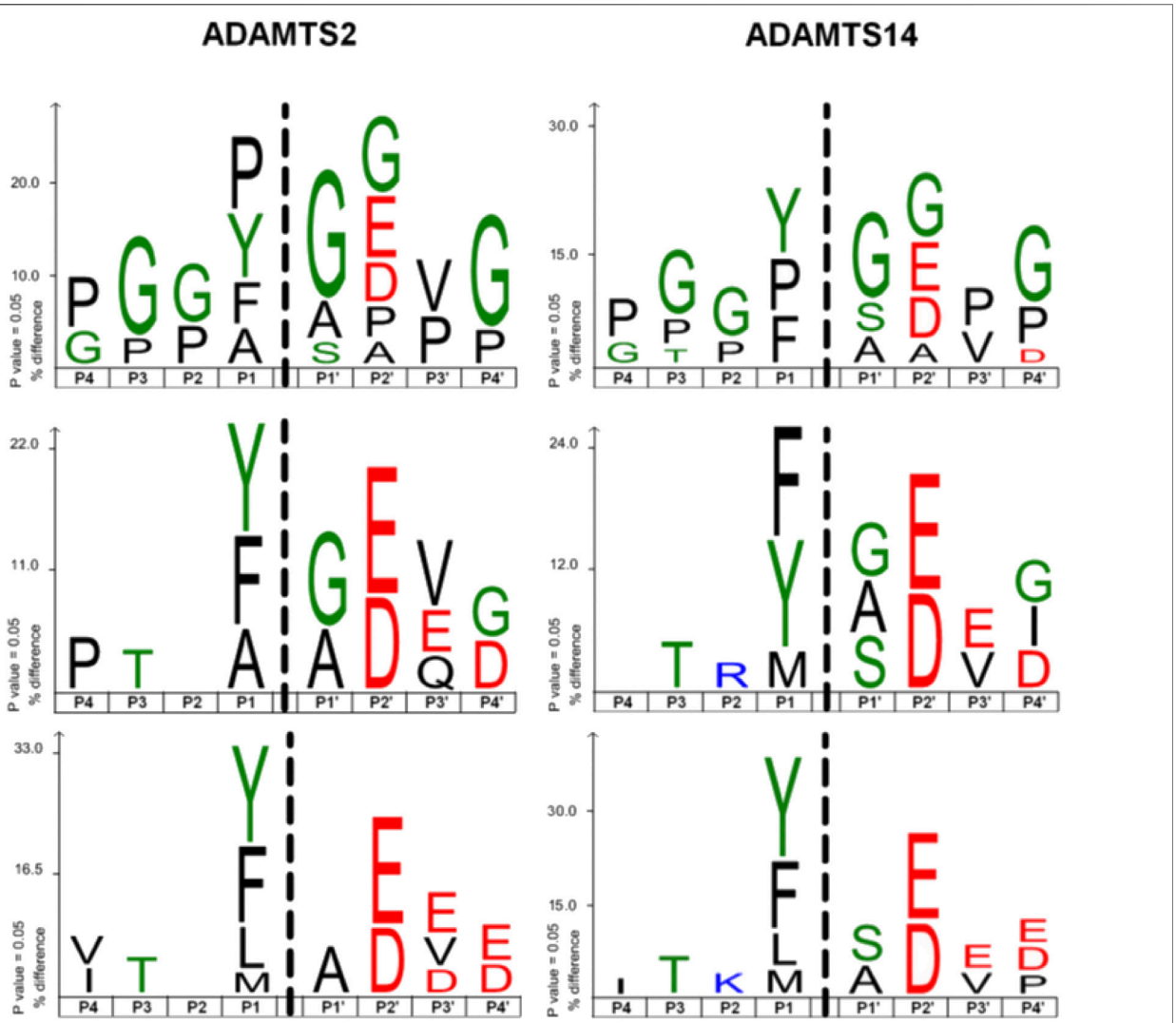

FIGURE 7 | Cleavage site specificity of ADAMTS2 and ADAMTS14 in mouse skin. The cleavage site specificity of ADAMTS2 **(left panels)** or ADAMTS14 **(right panels)** was determined using all the extracellular or extracellular transmembrane cleavage sites **(top)**, without type I collagen **(middle panels)** or without all the fibrillar collagens **(down panels)**. The amino acid sequence logos, corrected by the natural abundance of amino acids in the human proteome, were generated using the iceLogo software package (Colaert et al., 2009). The height of the amino acids represents their frequency regarding their natural abundance; the color reflects its physicochemical properties.

compartments such as *epidermis*, dermis, and muscular, nerve and blood vessels elements which may vary in abundance, a situation susceptible to induce modifications in the relative abundance of a specific protein. The use of a high throughput method and the complexity of the skin samples led to variations between the three individual experiments which prevented the identification of potential gender differences. In this study, three individual experiments have therefore been analyzed independently, in order to increase the likelihood of identifying new substrates, and have been compared between each other in a second step for validations purposes. Potential substrates were identified by taking into account only peptides harboring a P/C ratio above or below the 3-sigma cutoff from the normal distribution of natural N-termini, which constitutes a very stringent threshold. Sixty-eight proteins located at the cell surface or being part of the extracellular matrix were identified as potential substrates of ADAMTS2 and/or ADAMTS14, from which fibrillary collagens were the most represented in terms of identified peptides.

The previously described cleavage sites by ADAMTS2 of the N-propeptide of COL1A1 and COL1A2 were clearly identified, confirming the relevance of our experimental model. Of notes, however, these cleavages seem to occur within a preferential sequence rather than at a specific cleavage site as always reported so far, which illustrates that ADAMTS2 is capable to cleave multiple peptide bonds. As an additional evidence of the specificity of the N-TAILS data, cleavages of the N-propeptide of COL1A1 and COL1A2 by ADAMTS14 were only marginal, which was expected from previous *in vitro* and *in vivo* data showing that ADAMTS14 displays only a very low aminoprocollagen peptidase activity (Colige et al., 2002; Dupont et al., 2018). Having clearly demonstrated the reliability of our experimental design, we then

investigated the cleavages of the N-propeptides of type V procollagens which are still incompletely defined. For COL5A1, a cleavage by BMP1 was previously identified within the NC3 domain (Imamura et al., 1998; Bonod-Bidaud et al., 2007) but could not be identified here as expected when using models comparing Wt to Adamts2 and/or Adamts14 deficient skins. The $P_{435\text{-}436}$A site previously found for ADAMTS2 at the end of the variable domain (Colige et al., 2005) was identified here for Adamts2 but also for Adamts14. Accordingly, the P/C ratio was much higher by comparing Wt skin to $TS2^{-/-}TS14^{-/-}$ skin, indicating that both enzymes display this activity *in vivo* and, therefore, identifying a new function for ADAMTS14. Some cleavages by both enzymes were also identified in the NC2 domain of COL5A1 and COL5A2 separating the small and the large central triple helical domains, at a location similar to the ones reported for type I, type II and type III procollagens, which was never described before. The existence of several cleavage sites generating type V collagens with N-propeptides of different size and bulkiness is a new observation and is probably part of the regulation operated by type V collagen on collagen fibril formation (Linsenmayer et al., 1993; Marchant et al., 1996; Wenstrup et al., 2004) as observed *in vitro* and *in vivo* in EDS. It would also explain why arthrochalasic and dermatosparactic EDS have different clinical manifestations since both type I and type V collagen processing are altered in dermatosparaxis while only type I collagen is affected in arthrochalasia.

Besides cleavages of the N-propeptides, N-TAILS identified also several cleavages in the central COL1 domain of both alpha one and alpha 2 type I collagens. While some sites were not, or only barely, affected by the presence of ADAMTS2 or 14 (P/C < 1.5), some others were characterized by higher ratios, especially in some clusters, and when comparing Wt to $TS2^{-/-}TS14^{-/-}$ skin, which suggested specificity in these cleavages. This hypothesis was evaluated *in vitro* using purified enzymes and purified collagen, either native or heat denatured. It showed that ADAMTS2 and ADAMTS14 can cleave within the COL1 triple helical domain, but mainly (or only) when collagen is unfolded. This "collagenase" activity was similar for ADAMTS2 and ADAMTS14, while ADAMTS14 displays only a limited capacity to cleave the aminopropeptide of non-denatured procollagen which demonstrates that the two activities are independent. The existence of such function was never described before and its biological relevance will have to be further investigated. An attractive hypothesis would be that, when ADAMTS2 (or ADAMTS14) meets and interacts with its type I procollagen substrate, it cleaves the N-propeptide but it also degrades collagen trimers that are not correctly folded, therefore preventing their integration in fibrils. This quality control function of aminoprocollagen peptidases, if confirmed, would also explain why collagen fibrils have a so irregular and abnormal shape in dermatosparaxis. Indeed, in the absence of ADAMTS2, aminoprocollagen but also collagen with defects in the triple helix domains can both accumulate in fibrils and hamper the highly organized polymerization process of collagen fibrils.

Excision of the C-propeptide of type I procollagen was originally attributed to BMP1, and later extended to meprins α and β (Kessler et al., 1996; Jefferson et al., 2013). Here, our degradomic analysis has revealed major cleavage sites for ADAMTS2 and ADAMTS14 in the C-propeptide of both COL1A1 and COL1A2. This was also confirmed *in vitro* using purified enzymes and type I procollagen, and is reminiscent to what was already demonstrated for type III procollagen (Bekhouche et al., 2016). However, the functional relevance of these observations *in vivo*, when BMP1 is present and active, is not clear yet since, except for one site in COL1A1, they are located downstream of the BMP1 site. In these conditions, these ADAMTS-dependent cleavages should not affect the maturation of type I collagen and its polymerization. Since the C-propeptide of type I collagen can inhibit collagen synthesis when released in the extracellular space (Mizuno et al., 2000), an intriguing hypothesis would be that its cleavage by ADAMTS2 or 14 would affect its regulatory function.

The main purpose of this study was to get a better insight into the overall implications of ADAMTS2 and ADAMTS14 in collagen fibril homeostasis. In addition of cleavages at multiple sites in fibrillary collagens, other proteins regulating collagen fibrillogenesis were also found to be potential substrates, similarly to what was found previously regarding the cleavage of Lox (Rosell-García et al., 2019), a crucial enzyme for the formation of crosslinks stabilizing collagen fibrils. Two cleavages were found in COL14A1, a FACIT (Fibril Associated Collagen with Interrupted Triple helix) known for its capacity to interact with collagen fibrils and regulate their formation (Young et al., 2002; Agarwal et al., 2012). Similarly, type VI collagen was also identified as a likely substrate regulating fibril formation (Lamandé and Bateman, 2018; Wu and Ge, 2019). However, the functional relevance of these cleavages was not investigated further but would deserve additional characterizations.

Lumican, biglycan and osteoglycin are members of the Small Leucin-rich Proteoglycan (SLRP) family (Frikeche et al., 2016). They are considered as collagen fibril-regulating proteins, and are also emerging as factors controlling immune response. It is interesting to note that these three proteoglycans have been identified here as potential substrates of ADAMTS2 which is also implicated in immune response as previously described (Hofer et al., 2008) and further illustrated here by the specific enrichment in biological processes linked to complement activation and regulation of cytokines involved in immune response. Although still to be considered as a working hypothesis and having to be confirmed by complementary approaches, these observations could pave the way to better understand the multiple roles of ADAMTS2 and 14 in extracellular matrix formation and functions.

Analysis of the skin degradome also identified cytoplasmic proteins, such as actin and vimentin, as potential substrates of ADAMTS2 and 14. These surprising data were confirmed *in vitro* using skin fibroblasts extracts incubated with recombinant purified enzymes, but not by comparing the electrophoretic pattern of actin and vimentin in Wt and ADAMTS2-deficient fibroblasts. This could suggest that these cleavages occur only after secretion or release in the extracellular space, as observed after cell death for example. We cannot however completely rule out the possibility that ADAMTS2 and 14 could display intracellular activities, either during the secretion process, as described for procollagen processing, or after their internalization when bound to cell membrane (Dubail et al.,

2010). The proteomic identification of intracellular substrates has already been reported for MMP2(auf dem Keller et al., 2013) and by studies reporting the intracellular functions of MMPs(Jobin et al., 2017), such as α-actinin cleavage, or the transcriptional regulation of NF-kappa-B inhibitor alpha by MMP12(Marchant et al., 2014). Interestingly, these intracellular activities are related to the innate immunity system (Marchant et al., 2014) with a propensity for MMPs to regulate negatively the pro-inflammatory response (Dufour and Overall, 2013; Khokha et al., 2013). Further studies are needed to precisely assess the role the cleavage of proteins by ADAMTS2 and ADAMTS14 either in the extracellular and/or in the intracellular space, with a potential implication in cytoskeleton dynamic, gene expression and inflammatory response.

CONCLUSION

Our N-TAILS analysis of mouse skin degradomes has extended our knowledge regarding the roles of ADAMTS2 and 14 well beyond the previously known cleavage of the N-propeptide of type I, type II and type III procollagens. The identification *in vivo* of several cleavage sites in the N-terminal region of type V collagen, generating N-terminal propeptides of different size and bulkiness, is a new finding possibly explaining how type V collagen can finely tune collagen fibril formation and structure. In the same context, other molecules involved in fibrillogenesis, such as SLRPs and non-fibrillar collagens, have also been identified as likely substrates of ADAMTS2 and 14.

Another intriguing observation is the potential quality control activity leading to the degradation of incorrectly folded collagen trimers before their assembly in collagen fibrils. If this hypothesis is confirmed, this would represent a key activity of ADAMTS2 and 14 for maintaining the structural integrity of collagen fibers and connective tissues.

DATA AVAILABILITY STATEMENT

The datasets presented in this study can be found in online repositories. The names of the repository/repositories and accession number(s) can be found in the article.

ETHICS STATEMENT

The animal study was reviewed and approved by the Ethics Committee for Animal Use and Care, University of Liège, Belgium.

AUTHOR CONTRIBUTIONS

Conceptualization, AC and MB; methodology, MB; formal analysis, AC DB and MB; investigation, CL CM LD CD and LJ; data curation, DB GM and MB; writing original draft preparation, MB and CL; writing review and editing, AC and MB; visualization, MB and AC; supervision, MB and AC; project administration, AC and MB; funding acquisition, AC and MB. All authors have read and agreed to the published version of the manuscript.

FUNDING

The authors are grateful for support by the Incoming Postdoctoral–Marie Curie (COFUND) fellowship (Brussels, Belgium), the Télévie (7.4602.14; 7.4608.19; 7.4566.16), Fonds de la Recherche Scientifique–Fonds National de la Recherche Scientifique (FRS-FNRS; T.0183.13; CDR J003220 F).

ACKNOWLEDGMENTS

The authors thank Ulrich auf dem Keller (Technical University of Denmark, Denmark) for his help in running the analysis of N-terminomics data, and Antoine Heyres for its technical support. We thank the Betty Nusgens for critical reading of the manuscript.

SUPPLEMENTARY MATERIAL

The Supplementary Material for this article can be found online at: https://www.frontiersin.org/articles/10.3389/fmolb.2021.643178/full#supplementary-material.

REFERENCES

Agarwal, P., Zwolanek, D., Keene, D. R., Schulz, J. N., Blumbach, K., Heinegård, D., et al. (2012). Collagen XII and XIV, new partners of cartilage oligomeric matrix protein in the skin extracellular matrix suprastructure. *J. Biol. Chem.* 287, 22549–22559. doi:10.1074/jbc.M111.335935

auf dem Keller, U., Prudova, A., Eckhard, U., Fingleton, B., and Overall, C. M. (2013). Systems-level analysis of proteolytic events in increased vascular permeability and complement activation in skin inflammation. *Sci. Signal.* 6, rs2. doi:10.1126/scisignal.2003512

auf dem Keller, U., and M Overall, C. (2012). CLIPPER: an add-on to the Trans-Proteomic Pipeline for the automated analysis of TAILS N-terminomics data. *Biol. Chem.* 393, 1477–1483. doi:10.1515/hsz-2012-0269

Beighton, P., De Paepe, A., Steinmann, B., Tsipouras, P., and Wenstrup, R. J. (1998). Ehlers-danlos syndromes: revised nosology, villefranche, 1997. Ehlers-danlos national foundation (United States) and ehlers-danlos support group (United Kindom). *Am. J. Med. Genet.* 77, 31–37. doi:10.1002/(sici)1096-8628(19980428)77:1<31::aid-ajmg8>3.0.co;2-o

Bekhouche, M., and Colige, A. (2015). The procollagen N-proteinases ADAMTS2, 3 and 14 in pathophysiology. *Matrix Biol.* 44-46, 46–53. doi:10.1016/j.matbio.2015.04.001

Bekhouche, M., Leduc, C., Dupont, L., Janssen, L., Delolme, F., Vadon-Le Goff, S., et al. (2016). Determination of the substrate repertoire of ADAMTS2, 3, and 14 significantly broadens their functions and identifies extracellular matrix organization and TGF-β signaling as primary targets. *FASEB J.* 30, 1741–1756. doi:10.1096/fj.15-279869

Bonod-Bidaud, C., Beraud, M., Vaganay, E., Delacoux, F., Font, B., Hulmes, D. J., et al. (2007). Enzymatic cleavage specificity of the proalpha1(V) chain

processing analysed by site-directed mutagenesis. *Biochem. J.* 405, 299–306. doi:10.1042/BJ20070051

Bradford, M. M. (1976). A rapid and sensitive method for the quantitation of microgram quantities of protein utilizing the principle of protein-dye binding. *Anal. Biochem.* 72, 248–254. doi:10.1006/abio.1976.9999

Brouillard, P., Dupont, L., Helaers, R., Coulie, R., Tiller, G. E., Peeden, J., et al. (2017). Loss of ADAMTS3 activity causes Hennekam lymphangiectasia-lymphedema syndrome 3. *Hum. Mol. Genet.* 26, 4095–4104. doi:10.1093/hmg/ddx297

Colaert, N., Helsens, K., Martens, L., Vandekerckhove, J., and Gevaert, K. (2009). Improved visualization of protein consensus sequences by iceLogo. *Nat. Methods* 6, 786–787. doi:10.1038/nmeth1109-786

Colige, A., Beschin, A., Samyn, B., Goebels, Y., Van Beeumen, J., Nusgens, B. V., et al. (1995). Characterization and partial amino acid sequencing of a 107-kDa procollagen I N-proteinase purified by affinity chromatography on immobilized type XIV collagen. *J. Biol. Chem.* 270, 16724–16730. doi:10.1074/jbc.270.28.16724

Colige, A., Sieron, A. L., Li, S. W., Schwarze, U., Petty, E., Wertelecki, W., et al. (1999). Human Ehlers-Danlos syndrome type VII C and bovine dermatosparaxis are caused by mutations in the procollagen I N-proteinase gene. *Am. J. Hum. Genet.* 65, 308–317. doi:10.1086/302504

Colige, A., Vandenberghe, I., Thiry, M., Lambert, C. A., Van Beeumen, J., Li, S. W., et al. (2002). Cloning and characterization of ADAMTS-14, a novel ADAMTS displaying high homology with ADAMTS-2 and ADAMTS-3. *J. Biol. Chem.* 277, 5756–5766. doi:10.1074/jbc.M105601200

Colige, A., Nuytinck, L., Hausser, I., Van Essen, A. J., Thiry, M., Herens, C., et al. (2004). Novel types of mutation responsible for the dermatosparactic type of Ehlers-Danlos syndrome (Type VIIC) and common polymorphisms in the ADAMTS2 gene. *J. Invest. Dermatol.* 123, 656–663. doi:10.1111/j.0022-202X.2004.23406.x

Colige, A., Ruggiero, F., Vandenberghe, L., Dubail, J., Kesteloot, F., Van Beeumen, J., et al. (2005). Domains and maturation processes that regulate the activity of ADAMTS-2, a metalloproteinase cleaving the aminopropeptide of fibrillar procollagens types I-III and V. *J. Biol. Chem.* 280, 34397–34408. doi:10.1074/jbc.M506458200

De Paepe, A., and Malfait, F. (2012). The Ehlers-Danlos syndrome, a disorder with many faces. *Clin. Genet.* 82, 1–11. doi:10.1111/j.1399-0004.2012.01858.x

Dubail, J., Kesteloot, F., Deroanne, C., Motte, P., Lambert, V., Rakic, J. M., et al. (2010). ADAMTS-2 functions as anti-angiogenic and anti-tumoral molecule independently of its catalytic activity. *Cell. Mol. Life Sci.* 67, 4213–4232. doi:10.1007/s00018-010-0431-6

Dufour, A., and Overall, C. M. (2013). Missing the target: matrix metalloproteinase antitargets in inflammation and cancer. *Trends Pharmacol. Sci.* 34, 233–242. doi:10.1016/j.tips.2013.02.004

Dupont, L., Ehx, G., Chantry, M., Monseur, C., Leduc, C., Janssen, L., et al. (2018). Spontaneous atopic dermatitis due to immune dysregulation in mice lacking Adamts2 and 14. *Matrix Biol.* 70, 140–157. doi:10.1016/j.matbio.2018.04.002

Fortelny, N., Cox, J. H., Kappelhoff, R., Starr, A. E., Lange, P. F., Pavlidis, P., et al. (2014). Network analyses reveal pervasive functional regulation between proteases in the human protease web. *PLoS Biol.* 12, e1001869. doi:10.1371/journal.pbio.1001869

Frikeche, J., Maiti, G., and Chakravarti, S. (2016). Small leucine-rich repeat proteoglycans in corneal inflammation and wound healing. *Exp. Eye Res.* 151, 142–149. doi:10.1016/j.exer.2016.08.015

Hofer, T. P. J., Frankenberger, M., Mages, J., Lang, R., Meyer, P., Hoffmann, R., et al. (2008). Tissue-specific induction of ADAMTS2 in monocytes and macrophages by glucocorticoids. *J. Mol. Med.* 86, 323–332. doi:10.1007/s00109-007-0284-0

Hulsen, T., de Vlieg, J., and Alkema, W. (2008). BioVenn—a web application for the comparison and visualization of biological lists using area-proportional Venn diagrams. *BMC Genomics* 9, 488. doi:10.1186/1471-2164-9-488

Imamura, Y., Steiglitz, B. M., and Greenspan, D. S. (1998). Bone morphogenetic protein-1 processes the NH2-terminal propeptide, and a furin-like proprotein convertase processes the COOH-terminal propeptide of pro-alpha1(V) collagen. *J. Biol. Chem.* 273, 27511–27517. doi:10.1074/jbc.273.42.27511

Janssen, L., Dupont, L., Bekhouche, M., Noel, A., Leduc, C., Voz, M., et al. (2016). ADAMTS3 activity is mandatory for embryonic lymphangiogenesis and regulates placental angiogenesis. *Angiogenesis* 19, 53–65. doi:10.1007/s10456-015-9488-z

Jefferson, T., Auf dem Keller, U., Bellac, C., Metz, V. V., Broder, C., Hedrich, J., et al. (2013). The substrate degradome of meprin metalloproteases reveals an unexpected proteolytic link between meprin β and ADAM10. *Cell. Mol. Life Sci.* 70, 309–333. doi:10.1007/s00018-012-1106-2

Jobin, P. G., Butler, G. S., and Overall, C. M. (2017). New intracellular activities of matrix metalloproteinases shine in the moonlight. *Biochim. Biophys. Acta Mol. Cell Res.* 1864, 2043–2055. doi:10.1016/j.bbamcr.2017.05.013

Kessler, E., Takahara, K., Biniaminov, L., Brusel, M., and Greenspan, D. S. (1996). Bone morphogenetic protein-1: the type I procollagen C-proteinase. *Science* 271, 360–362. doi:10.1126/science.271.5247.360

Kesteloot, F., Desmoulière, A., Leclercq, I., Thiry, M., Arrese, J. E., Prockop, D. J., et al. (2007). ADAM metallopeptidase with thrombospondin type 1 motif 2 inactivation reduces the extent and stability of carbon tetrachloride-induced hepatic fibrosis in mice. *Hepatology* 46, 1620–1631. doi:10.1002/hep.21868

Khokha, R., Murthy, A., and Weiss, A. (2013). Metalloproteinases and their natural inhibitors in inflammation and immunity. *Nat. Rev. Immunol.* 13, 649–665. doi:10.1038/nri3499

Kleifeld, O., Doucet, A., Prudova, A., auf dem Keller, U., Gioia, M., Kizhakkedathu, J. N., et al. (2011). Identifying and quantifying proteolytic events and the natural N terminome by terminal amine isotopic labeling of substrates. *Nat. Protoc.* 6, 1578–1611. doi:10.1038/nprot.2011.382

Lamandé, S. R., and Bateman, J. F. (2018)Collagen VI disorders: insights on form and function in the extracellular matrix and beyond. *Matrix Biol.* 71-72, 348–367. doi:10.1016/j.matbio.2017.12.008

Linsenmayer, T. F., Gibney, E., Igoe, F., Gordon, M. K., Fitch, J. M., Fessler, L. I., et al. (1993). Type V collagen: molecular structure and fibrillar organization of the chicken alpha 1(V) NH2-terminal domain, a putative regulator of corneal fibrillogenesis. *J. Cell Biol.* 121, 1181–1189. doi:10.1083/jcb.121.5.1181

Malfait, F., and De Paepe, A. (2014). The Ehlers-Danlos syndrome. *Adv. Exp. Med. Biol.* 802, 129–143. doi:10.1007/978-94-007-7893-1_9

Marchant, J. K., Hahn, R. A., Linsenmayer, T. F., and Birk, D. E. (1996). Reduction of type V collagen using a dominant-negative strategy alters the regulation of fibrillogenesis and results in the loss of corneal-specific fibril morphology. *J. Cell Biol.* 135, 1415–1426. doi:10.1083/jcb.135.5.1415

Marchant, D. J., Bellac, C. L., Moraes, T. J., Wadsworth, S. J., Dufour, A., Butler, G. S., et al. (2014). A new transcriptional role for matrix metalloproteinase-12 in antiviral immunity. *Nat. Med.* 20, 493–502. doi:10.1038/nm.3508

Mi, H., Muruganujan, A., Ebert, D., Huang, X., and Thomas, P. D. (2019). PANTHER version 14: more genomes, a new PANTHER GO-slim and improvements in enrichment analysis tools. *Nucleic Acids Res.* 47, D419–D426. doi:10.1093/nar/gky1038

Mizuno, M., Fujisawa, R., and Kuboki, Y. (2000). The effect of carboxyl-terminal propeptide of type I collagen (c-propeptide) on collagen synthesis of preosteoblasts and osteoblasts. *Calcif. Tissue Int.* 67, 391–399. doi:10.1007/s002230001150

Nusgens, B., and Lapiere, C. M. (1979). A simplified procedure for measuring amino-procollagen peptidase type I. *Anal. Biochem.* 95, 406–412. doi:10.1016/0003-2697(79)90747-4

Nusgens, B. V., Verellen-Dumoulin, C., Hermanns-Lê, T., De Paepe, A., Nuytinck, L., Piérard, G. E., et al. (1992). Evidence for a relationship between Ehlers-Danlos type VII C in humans and bovine dermatosparaxis. *Nat. Genet.* 1, 214–217. doi:10.1038/ng0692-214

Perez-Riverol, Y., Csordas, A., Bai, J., Bernal-Llinares, M., Hewapathirana, S., Kundu, D. J., et al. (2019). The PRIDE database and related tools and resources in 2019: improving support for quantification data. *Nucleic Acids Res.* 47. D442–D450. doi:10.1093/nar/gky1106

Poeter, M., Brandherm, I., Rossaint, J., Rosso, G., Shahin, V., Skryabin, B. V., et al. (2014). Annexin A8 controls leukocyte recruitment to activated endothelial cells via cell surface delivery of CD63. *Nat. Commun.* 5, 3738. doi:10.1038/ncomms4738

Romano, E., Rosa, I., Fioretto, B. S., Lucattelli, E., Innocenti, M., Ibba-Manneschi, L., et al. (2020). A two-step immunomagnetic microbead-based method for the isolation of human primary skin telocytes/cd34+ stromal cells. *Int. J. Mol. Sci.* 21, 5877. doi:10.3390/ijms21165877

Rosell-García, T., Paradela, A., Bravo, G., Dupont, L., Bekhouche, M., Colige, A., et al. (2019). Differential cleavage of lysyl oxidase by the metalloproteinases BMP1 and ADAMTS2/14 regulates collagen binding through a tyrosine sulfate domain. *J. Biol. Chem.* 294, 11087–11100. doi:10.1074/jbc.ra119.007806

Sugimoto, M. A., Vago, J. P., Teixeira, M. M., and Sousa, L. P. (2016). Annexin A1 and the resolution of inflammation: modulation of neutrophil recruitment, apoptosis, and clearance. *J. Immunol. Res.* 2016, 8239258. doi:10.1155/2016/8239258

Swisher, J. F., Khatri, U., and Feldman, G. M. (2007). Annexin A2 is a soluble mediator of macrophage activation. *J. Leukoc. Biol.* 82, 1174–1184. doi:10.1189/jlb.0307154

Van Damme, T., Colige, A., Syx, D., Giunta, C., Lindert, U., Rohrbach, M., et al. (2016). Expanding the clinical and mutational spectrum of the Ehlers-Danlos syndrome, dermatosparaxis type. *Genet. Med.* 18, 882–891. doi:10.1038/gim.2015.188

Wang, G., Muhl, L., Padberg, Y., Dupont, L., Peterson-Maduro, J., Stehling, M., et al. (2020). Specific fibroblast subpopulations and neuronal structures provide local sources of Vegfc-processing components during zebrafish lymphangiogenesis. *Nat. Commun.* 11, 2724. doi:10.1038/s41467-020-16552-7

Wenstrup, R. J., Florer, J. B., Brunskill, E. W., Bell, S. M., Chervoneva, I., and Birk, D. E. (2004). Type V collagen controls the initiation of collagen fibril assembly. *J. Biol. Chem.* 279, 53331–53337. doi:10.1074/jbc.M409622200

Wu, Y., and Ge, G. (2019). Complexity of type IV collagens: from network assembly to function. *Biol. Chem.* 400, 565–574. doi:10.1515/hsz-2018-0317

Young, B. B., Zhang, G., Koch, M., and Birk, D. E. (2002). The roles of types XII and XIV collagen in fibrillogenesis and matrix assembly in the developing cornea. *J. Cell Biochem.* 87, 208–220. doi:10.1002/jcb.10290

Conflict of Interest: The authors declare that the research was conducted in the absence of any commercial or financial relationships that could be construed as a potential conflict of interest.

The Supplementary Material for this article can be found online:

https://www.frontiersin.org/articles/10.3389/fmolb.2021.643178/full#supplementary-material.

Chapter 2: ADAMTS2 and 14 in lymphangiogenesis

The discovery of the ability of ADAMTS3 (potentiated by CCBE1 as cofactor) to process and activate pro-VEGFC into its mature form[150] was followed by the generation of an ADAMTS3-knockout model in our laboratory that revealed a profound alteration of the lymphatic system causing embryonic lethality[268].

At adulthood, ADAMTS3 expression is restricted to the brain and cartilage, which suggests that its activity is not mandatory for lymphangiogenesis after birth. Other enzymes such as plasmin or KLK3 are known to cleave pro-VEGFC into its active form[153]. Combining the high substrate similarity between the aminoprocollagen proteases, the widespread expression of ADAMTS2 and ADAMTS14, and the fact that multiple enzymes are capable to process the pro-VEGFC, it was hypothesized that ADAMTS2 and ADAMTS14 could also be involved in pro-VEGFC activation at adulthood.

In vitro studies were first performed to evaluate the ability of ADAMTS2 and ADAMTS14 to proteolytically activate pro-VEGFC into VEGFC.

In vivo, the lymphatic system of wild type, ADAMTS2 knockout, ADAMTS14 knockout and ADAMTS2-ADAMTS14 double knockout mice was evaluated in adulthood under physiological "resting" conditions and upon stimulation of lymphangiogenesis.

In this work, I took an active role in the purification of the aminoprocollagen peptidases, in the *in vitro* cleavage assays of pro-VEGFC by ADAMTS2,3 and 14, in the determination of the ADAMTS-cleaved VEGFC capacity to induce the phosphorylation of its receptors VEGFR3 and VEGFR2, and in the manuscript reviewing.

A. ADAMTS2, 3 and ADAMTS14 cleave and activate pro-VEGFC

Recombinant ADAMTS2, ADAMTS3, ADAMTS14 and pro-VEGFC were produced and purified in-house. Incubation of pro-VEGFC with each ADAMTS resulted in a molecular weight shift of the pro-VEGFC (61 kDa) and the aminopro-VEGFC (31 kDa) to the carboxypro-VEGFC (45 kDa) and mature VEGFC (21 kDa) (Figure 23.A). This processing was absent when ADAMTS when inhibited by EDTA (Figure 23.A lane 3, 5 and 7). This molecular weight shift indicates the processing of the aminopropeptide of pro-VEGFC by ADAMTS2, ADAMTS3 and ADAMTS14.

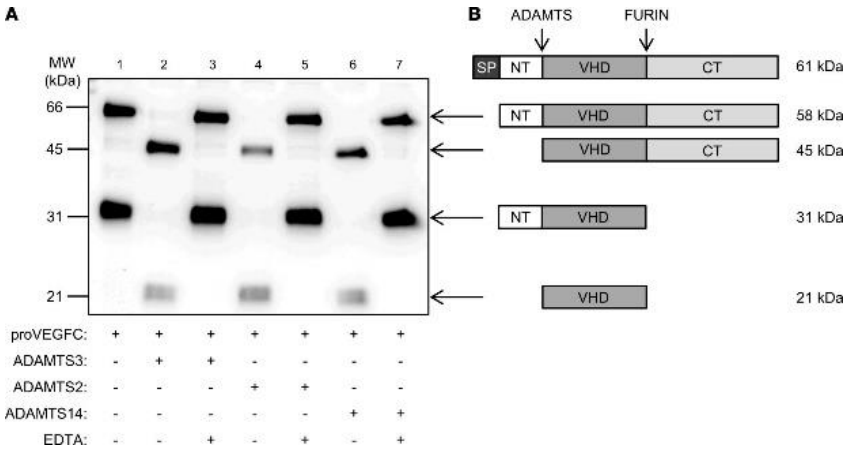

Figure 23: Western blot analysis of recombinant pro-VEGFC after incubation with ADAMTS2,3 or 14 in the presence or absence of EDTA used as inhibitor.

To further demonstrate that the ADAMTS-cleaved VEGFC is functional, we evaluated the phosphorylation of VEGFR3 present on lymphatic endothelial cells up on addition of recombinant pro-VEGFC preincubated with active or inactive (+/- EDTA) ADAMTS2, ADAMTS3 or ADAMTS14. VEGFR3 phosphorylation (pVEGFR3) was observed for each ADAMTS-cleaved VEGFC in a dose-dependent manner, showing a similar ability to cleave pro-VEGFC into its active form (Figure 24.A and B). Identical results were obtained for VEGFR2.

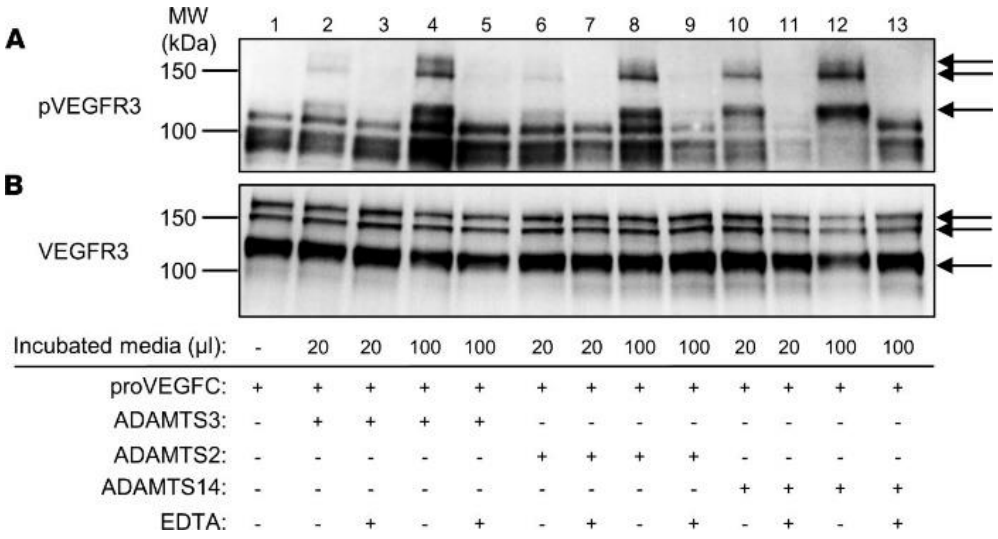

Figure 24: Western blot analysis of A) phosphorylated VEGFR3 and B) total VEGFR3 in lymphatic endothelial cell extracts collected 5 minutes after incubation with pro-VEGFC pretreated with active or inactive (+/- EDTA) ADAMTS2, ADAMTS3 or ADAMTS14. Black arrows indicate the VEGFR3 bands as detected by antibodies specific for phospho-VEGFR3 (pVEGFR3) (A) and VEGFR3 (B).

B. Absence of ADAMTS2, but not ADAMTS14, causes skin fluid retention

To evaluate *in vivo* the role of ADAMTS2 and ADAMTS14 on lymphangiogenesis, we compared the skin of adult TS2-KO, TS14-KO and TS2-TS14-KO mice to WT mice. Histological analyses showed widened and paler skin after hematoxylin and eosin (H&E) staining in the TS2-KO and TS2-TS14-KO mice (Figure 25, left), suggesting the presence of edema.

To test this hypothesis, we quantified the ratio between the weight of the skin immediately after sacrifice (wet) and that of the skin dried for 72 hours. The increased ratio observed for TS2-KO and TS2-TS14-KO skin confirms the presence of excessive water (edema) in the skin of these mice (Figure 25, right).

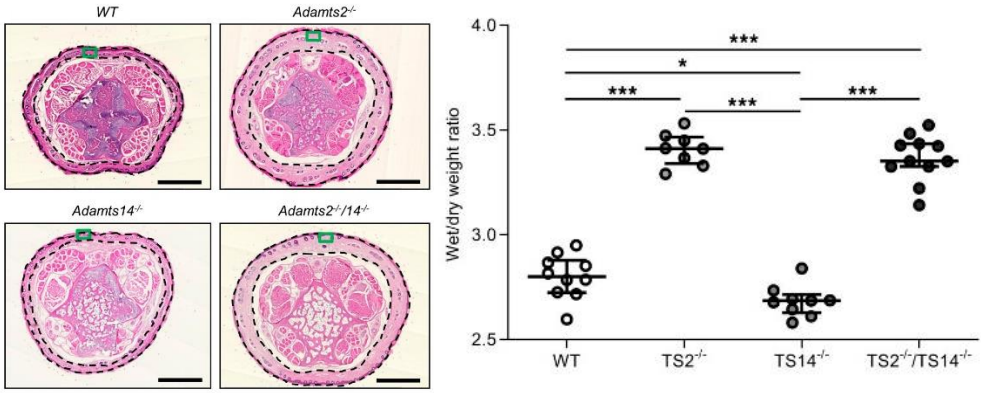

Figure 25: Left) H&E staining of the tail base of WT, TS2-KO, TS14-KO and TS2-TS14-KO mice. Right) Skin wet/dry weight ratio for WT, TS2-KO, TS14-KO and TS2-TS14-KO mice.

C. Absence of ADAMTS2, but not ADAMTS14, impairs lymphatic drainage

To assess the role of the lymphatic system in the abnormal fluid retention in the skin of TS2-KO mice, we evaluated the lymphatic drainage of a stained solution injected subcutaneously into the paw of adult WT, TS2-KO, TS14-KO and TS2-TS14-KO mice. As expected, the absence of ADAMTS2 significantly reduced lymphatic drainage as pictured by a reduced Evan blue staining in the draining lymph node 30 minutes after injection (Figure 26.A and B).

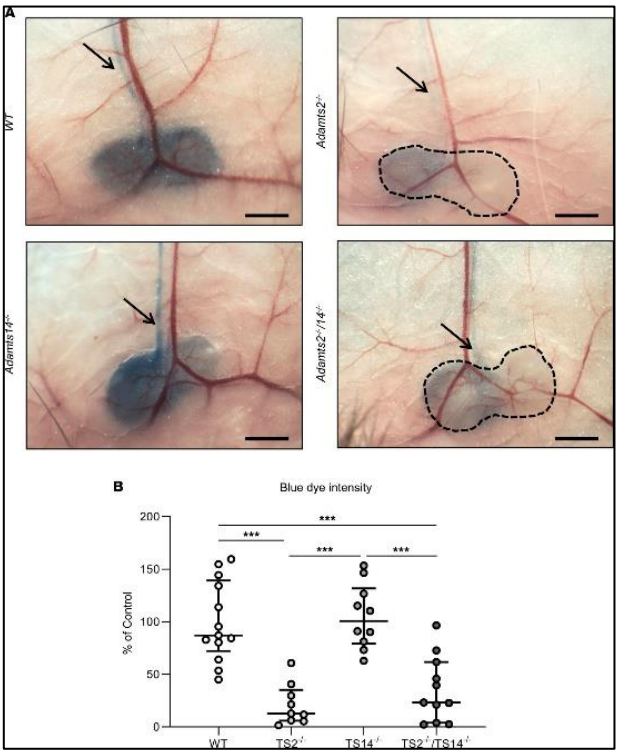

Figure 26: A) Visualisation of the draining inguinal lymph node after Evan blue subcutaneous injection in the footpad of WT, TS2-KO, TS14-KO and TS2-TS14-KO mice. B) Evan blue quantification in the draining inguinal lymph node of WT, TS2-KO, TS14-KO and TS2-TS14-KO mice.

In this study, we showed that ADAMTS2, 3 and 14 are similarly able to process the aminopropeptide of pro-VEGFC into its active form. We demonstrated that:

I) ADAMTS2 participates in the steady state fluid drainage by the lymphatic system at adulthood;

II) Both ADAMTS2 and ADAMTS14 are involved in lymphatic vessel network structure (see article below)

III) That neo-lymphangiogenesis is strongly impaired when both ADAMTS2 and ADAMTS14 are lacking (see article below).

This study revealed yet another function of ADAMTS2 (lymphatic homeostasis) that is likely to impact other physiological (fat absorption, immune cell trafficking, …) or pathological processes (metastasis dissemination, …).

JCI insight

RESEARCH ARTICLE

ADAMTS2 and ADAMTS14 can substitute for ADAMTS3 in adults for pro-VEGFC activation and lymphatic homeostasis

Laura Dupont,[1,2] Loïc Joannes,[2] Florent Morfoisse,[1,3] Silvia Blacher,[1] Christine Monseur,[2] Christophe F. Deroanne,[2] Agnès Noël,[1] and Alain C.M.A. Colige[2]

[1]Laboratory of Tumor and Developmental Biology and [2]Laboratory of Connective Tissues Biology, GIGA-R, University of Liège, Liège, Belgium. [3]Institute of Metabolic and Cardiovascular Diseases of Toulouse, INSERM UMR 1048, Toulouse, France.

The capacity of ADAMTS3 to cleave pro-VEGFC into active VEGFC able to bind its receptors and to stimulate lymphangiogenesis has been clearly established during embryonic life. However, this function of ADAMTS3 is unlikely to persist in adulthood because of its restricted expression pattern after birth. Because ADAMTS2 and ADAMTS14 are closely related to ADAMTS3 and are mainly expressed in connective tissues where the lymphatic network extends, we hypothesized that they could substitute for ADAMTS3 during adulthood in mammals allowing proteolytic activation of pro-VEGFC. Here, we demonstrated that ADAMTS2 and ADAMTS14 are able to process pro-VEGFC into active VEGFC as efficiently as ADAMTS3. In vivo, adult mice lacking *Adamts2* developed skin lymphedema due to a reduction of the density and diameter of lymphatic vessels, leading to a decrease of lymphatic functionality, while genetic ablation of *Adamts14* had no impact. In a model of thermal cauterization of cornea, lymphangiogenesis was significantly reduced in *Adamts2*- and *Adamts14*-KO mice and further repressed in *Adamts2/Adamts14* double-KO mice. In summary, we have demonstrated that ADAMTS2 and ADAMTS14 are as efficient as ADAMTS3 in activation of pro-VEGFC and are involved in the homeostasis of the lymphatic vasculature in adulthood, both in physiological and pathological processes.

Introduction

The lymphatic vasculature plays critical homeostatic functions, such as interstitial fluid and macromolecule drainage, local coordination of immunity, and immune cell trafficking (1, 2). The complete absence of lymphatic development leads to embryonic lethality, while lymphatic dysfunctions in adulthood are also implicated in several acquired pathologies, such as secondary lymphedema, psoriasis, and cancer. The most specific lymphatic molecular determinants have been identified through genetic studies of primary lymphatic defects in humans and through the use of transgenic animal models, especially in mice and fish (2, 3). These studies have identified the VEGFC/VEGFR3 axis as a central player in lymphangiogenesis. VEGFC is a ligand of VEGFR3, a receptor mainly expressed by lymphatic endothelial cells (LECs) but also present on blood vessel endothelial cells during angiogenic processes. VEGFD is also a VEGFR3 ligand that is able to stimulate lymphangiogenesis, but its loss in VEGFD-deficient mice and fish does not lead to an obvious phenotype (4). VEGFC and VEGFD are both synthesized as pro-molecules that require the cleavage of the amino- and carboxy terminal domains to acquire the capacity to bind and activate VEGFR3 efficiently (5). The C-propeptides of VEGFC and VEGFD are both cleaved by furin and similar enzymes. However, different processes are implicated in the removal of the N-propeptides. Serine proteases are the processing enzymes for VEGFD, while ADAMTS3 cleaves the N-propeptide of pro-VEGFC, with collagen and calcium-binding EGF domain-containing protein 1 (CCBE1) acting as a cofactor (6, 7). Accordingly, the genetic deletion of *Ccbe1* or *Adamts3* in mouse models leads to similar phenotypes, characterized by a total absence of primary lymphatic network formation, which causes embryonic lethality. In humans, missense hypomorphic mutations in *CCBE1* or *ADAMTS3* (8–10) lead to similar primary lymphedema diseases, Hennekam lymphangiectasia-lymphedema syndrome 1 and 3, respectively. In zebrafish, the absence of *adamts3*

Authorship note: AN and ACMAC contributed equally to this work.

Conflict of interest: The authors have declared that no conflict of interest exists.

Submitted: May 19, 2021
Accepted: March 16, 2022
Published: March 22, 2022

Reference information: *JCI Insight*. 2022;7(8):e151509. https://doi.org/10.1172/jci.insight.151509.

does not cause lymphatic defects, as seen in mammals, and only the simultaneous loss of *adamts3* and *adamts14* recapitulates the phenotype seen in the absence of *ccbe1* or *vegfc*. These findings suggest that Adamts3 and Adamts14 can display redundant functions in zebrafish embryo (11).

While the proteolytic activation of pro-VEGFC by ADAMTS3 is now well demonstrated during embryogenesis, it is not likely to occur in adults. Indeed, after birth, ADAMTS3 expression becomes mainly restricted to the central nervous system and the cartilage (12). On the other hand, the proteolytic activation of pro-VEGFC must occur in adulthood for lymphatic homeostasis, as highlighted by models in which the overexpression of pro-VEGFC in adult skin stimulates lymphangiogenesis (13). These observations clearly demonstrate that one or several enzymes can substitute for ADAMTS3 in adults and could therefore be implicated in lymphatic regulation. ADAMTS2 and ADAMTS14 share high sequence homology and an identical domain composition with ADAMTS3 (14). ADAMTS2 is expressed by cells of mesenchymal origin (fibroblasts, smooth muscle cells, adipocytes, etc.), while ADAMTS14 is moderately produced by several cell types, including mesenchymal cells and some immune cells. KO mice have been generated to investigate the in vivo functions of these 3 related ADAMTS proteins. Genetic ablation of *Adamts3* leads to embryonic lethality at 15 days after coitus due to the lack of lymphatic vessel development (7); this has a direct relationship with the capacity of ADAMTS3 to cleave pro-VEGFC into active prolymphangiogenic VEGFC. At birth, *Adamts2*-KO (TS2$^{-/-}$) pups are indistinguishable from their WT littermates. However, within 3 weeks, their skin becomes highly fragile because of the accumulation of incompletely processed procollagen molecules that form abnormal collagen fibrils (15). This clearly illustrates the critical role of ADAMTS2 for the cleavage of the amino-propeptide of fibrillary collagens, an activity at the origin of the name "aminoprocollagen peptidase" given to the subfamily of ADAMTS formed by ADAMTS2, ADAMTS3, and ADAMTS14. Finally, *Adamts14*-KO (TS14$^{-/-}$) mice do not display any obvious morphological phenotype. However, mice deficient for both *Adamts2* and *Adamts14* develop, during aging, skin lesions reminiscent of atopic dermatitis, which are not seen in single-KO mice and suggest dysregulation of the immune system (16). In addition to being able to cleave the amino-propeptide of fibrillar collagens, ADAMTS2, ADAMTS3, and ADAMTS14 can also cleave several common substrates at identical cleavage sites, usually after nonpolar or slightly hydrophobic amino acids, such as Pro, Gly, Ala, or Val (17).

Because ADAMTS2 and ADAMTS14 are mainly expressed in connective tissues where the lymphatic network extends, we reasoned that they could substitute for ADAMTS3 during adulthood in mammals, enabling proteolytic activation of pro-VEGFC at a site (A^{111}–A^{112} in humans, A^{107}–A^{108} in mice) fully compatible with a cleavage by ADAMTS2 and ADAMTS14. Here, we provide evidence that ADAMTS2 and ADAMTS14 are key actors of pro-VEGFC processing in adulthood.

Results

ADAMTS2 and ADAMTS14 control the processing of pro-VEGFC and are thus required to generate its biologically active form. In mice, ADAMTS3 is abundant in all connective tissues during embryonic development (12), explaining why, at that stage, it is the main enzyme processing pro-VEGFC into active VEGFC. However, its expression is reported to decrease after birth and to become restricted to brain and cartilage, while ADAMTS2 (mesenchymal cells in general, macrophages, etc.) and ADAMTS14 (fibroblasts, granulocytes, etc.) are more widely expressed (12) (see also The Human Protein Atlas, https://www.proteinatlas.org, and BioGPS, http://biogps.org). We investigated their respective expressions in embryos at 12.5 and 14 days after coitus (dpc) and in the skin of 18 dpc embryos, young pups, and adult mice (Supplemental Figure 1; supplemental material available online with this article; https://doi.org/10.1172/jci.insight.151509DS1). As expected, expression of *Adamts3* was high in 12.5 and 14 dpc embryos, but it was much reduced at 18 dpc and postnatally. In sharp contrast, *Adamts2* and *Adamts14* were produced from day 14 after coitus; their expression remained constant and at a higher level at later stages than the expression of *Adamts3*, suggesting that the activity of *Adamts2* and *Adamts14* could potentially substitute for that of *Adamts3* in their role in lymphangiogenesis during adulthood. To investigate a potential role of ADAMTS2 and ADAMTS14 in lymphangiogenesis, we first evaluated their capacity to activate pro-VEGFC in vitro. The conditioned medium from HEK293 cells overexpressing pro-VEGFC was collected and incubated with recombinant ADAMTS2, ADAMTS14, or ADAMTS3, which was used as a positive control (Supplemental Figure 2). When produced by HEK293 cells, VEGFC is secreted as 2 major forms that correspond to the full-size protein (at 61 kDa) after removal of the signal peptide (at 58 kDa) and to a product (around 31 kDa) resulting from the cleavage of the C-propeptide by pro-protein convertases, such as furin (Figure 1A, lane 1; see Figure 1B

for schematic illustration). Upon incubation with ADAMTS3, the cleavage of the N-propeptide was illustrated by the presence of products at 45 kDa and 21 kDa (Figure 1A, lane 2). The same migration pattern was observed after incubation with ADAMTS2 and ADAMTS14, demonstrating that these 2 enzymes can cleave pro-VEGFC (Figure 1A, lanes 4 and 6). EDTA-induced inhibition of ADAMTS3, ADAMTS2, or ADAMTS14 completely abolished pro-VEGFC processing (Figure 1A, lanes 3, 5, and 7). Localization of the cleavage site was determined and demonstrated to occur between Ala^{111} and Ala^{112} for the 3 ADAMTS proteins. Finally, a functional assay has been performed to confirm that this proteolytic processing can indeed activate pro-VEGFC into VEGFC. LECs were treated with pro-VEGFC–enriched medium preincubated with or without ADAMTS2, ADAMTS3, or ADAMTS14. After 5 minutes of treatment, cells were lysed and Western blot analysis was performed using an antibody specific for a phosphorylated form of VEGFR3, which was used as a readout of VEGFR3 activation by the fully processed VEGFC (Figure 2). Receptor phosphorylation was induced when pro-VEGFC was cleaved by ADAMTS3 (compare lane 1 with lanes 2 and 4) but not when ADAMTS3 was inhibited by the presence of EDTA (lanes 3 and 5) (Figure 2A). Most interestingly, the same levels of VEGFR3 phosphorylation were observed when ADAMTS2 (Figure 2A, lanes 6 and 8) or ADAMTS14 (Figure 2A, lanes 10 and 12) were used instead of ADAMTS3. Visualization of total VEGFR3 on the same blot revealed similar patterns for all the samples (Figure 2B), which confirmed that the increased signals observed when pro-VEGFC was incubated with active ADAMTS resulted from increased phosphorylation and not from an increased amount of VEGFR3. Similar results were observed with regard to the phosphorylation of VEGFR2 (Supplemental Figure 3).

Presence of lymphedema in TS2$^{-/-}$ mice. Having clearly demonstrated that ADAMTS2 and ADAMTS14 are as efficient as ADAMTS3 in vitro for activating pro-VEGFC, we investigated if their activity is also functionally important in vivo. We first evaluated signs of potential lymphedema by measuring the diameter of the tail base of adult TS2$^{-/-}$, TS14$^{-/-}$, and TS2$^{-/-}$ and TS14$^{-/-}$ (TS2$^{-/-}$TS14$^{-/-}$) mice. An increased diameter of the tail base was observed for single TS2$^{-/-}$ and double TS2$^{-/-}$TS14$^{-/-}$ mice, as compared with WT mice, but not for single TS14$^{-/-}$ mice (Figure 3A). Edema was associated with histological changes, with swelling of the dermis, as illustrated by an increase of its relative proportion on tissue sections (Figure 3B) and by decrease of its hematoxylin and eosin staining (Figure 3C). Moreover, tail skin samples were also weighed, fresh and after desiccation; this showed that water content was higher in TS2$^{-/-}$ and TS2$^{-/-}$TS14$^{-/-}$ mice (Figure 3D). Similar data were obtained when measuring edema at the level of paws (Supplemental Figure 4).

Impaired lymphatic network and function in absence of Adamts2 and/or Adamts14 in adult mice. In order to determine if the lymphatic network is altered in adults lacking *Adamts2* and/or *Adamts14*, whole mounts of dorsal ear skin were stained and evaluated by immunofluorescence. In this model, the structure of the lymphatic network varies according to the distance from the edge of the ear, the vessels being small, highly branched, and dense at the periphery, while being less numerous and larger toward the center. This specific distribution of the ear lymphatic vasculature was taken into account by determining the spatial distribution of normalized lymphatic vessel frequency starting at the ear border. This frequency was significantly reduced in TS2$^{-/-}$ and TS14$^{-/-}$ mice, and it was even more strongly reduced in TS2$^{-/-}$TS14$^{-/-}$ mice The analysis of the curves (Kolmogorov-Smirnov test) indicate that the spatial distributions of the lymphatic vessels were strongly affected in TS2$^{-/-}$TS14$^{-/-}$ mice but also modified in TS2$^{-/-}$ and TS14$^{-/-}$ mice as compared with WT mice (Figure 4, A and B). In sharp contrast, no difference was seen regarding blood vessels, showing that these alterations specifically affect the lymphatic vasculature (Supplemental Figure 5). A reduced diameter of the lymphatics in TS2$^{-/-}$ and TS2$^{-/-}$TS14$^{-/-}$ mice compared with WT and TS14$^{-/-}$ mice was also observed (Figure 4C).

As a complementary model, to get an insight into potential functional consequences of these alterations, we injected Evans blue dye in the footpads of mice of the 4 genotypes and evaluated its presence in inguinal lymph nodes. Thirty minutes after the injection, lymph nodes and the efferent lymphatic vessels had a marked blue color in WT and TS14$^{-/-}$ mice, whereas they were barely detectable in TS2$^{-/-}$ and TS2$^{-/-}$TS14$^{-/-}$ mice, demonstrating a delayed draining from the site of injection and, therefore, a clear reduction of the functionality of the lymphatic network (Figure 5).

Involvement of Adamts2 in postnatal lymphatic network homeostasis. In order to evaluate if *Adamts2* and *Adamts14* participate in the postnatal homeostasis of the lymphatic network in vivo, skin samples were collected from 6-day-old pups. In WT mice, LYVE1 staining revealed the presence of lymphatics in the upper dermis in close association with the bulge region of the hair follicle (Figure 6), as expected (18),

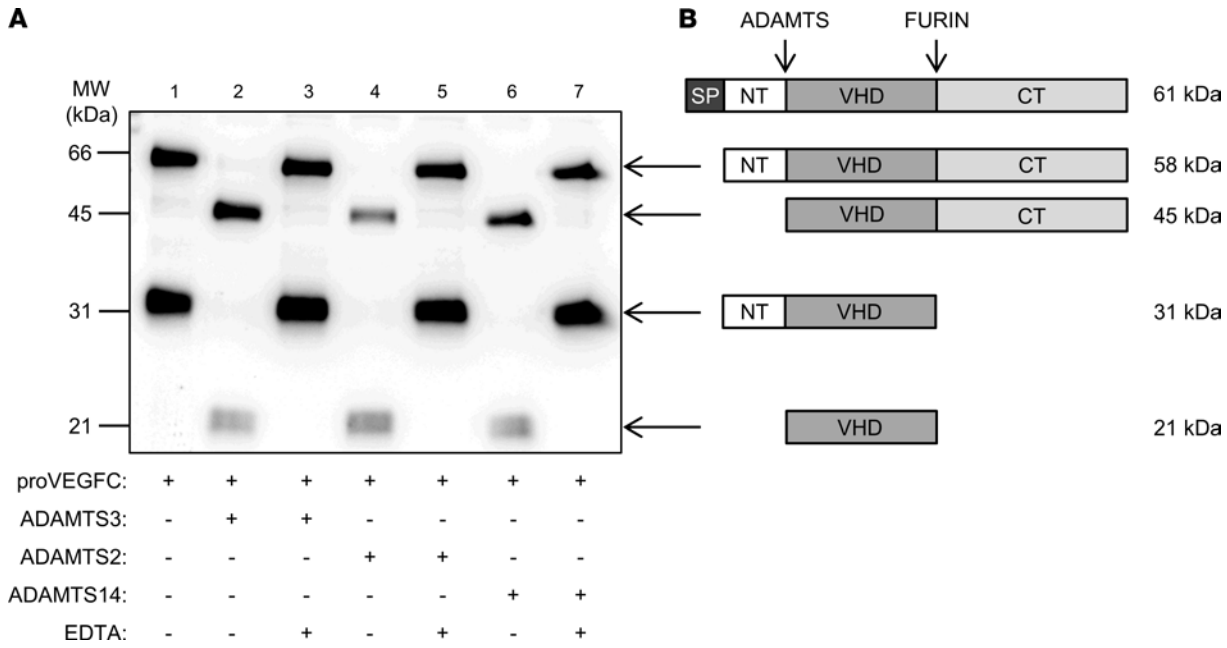

Figure 1. Processing of human pro-VEGFC by ADAMTS3, ADAMTS2, and ADAMTS14 proteases. (**A**) Conditioned medium from HEK293 cells expressing full-length pro-VEGFC was incubated with buffer (as negative control, lane1), ADAMTS3 (as positive control, lane 2), ADAMTS2, or ADAMTS14, in the presence or absence of EDTA used as inhibitor. The electrophoretic pattern of VEGFC was analyzed by Western blotting in reducing conditions. In absence of active enzymes (lane 1, 3, 5, and 7), VEGFC can be detected as a 58 kDa form (full-length pro-VEGFC without signal peptide) and a 31 kDa form generated by C-terminal processing by furin. In the presence of active ADAMTS3 (lane 2), ADAMTS2 (lane 4), and ADAMTS14 (lane 6), the 58 kDa form was totally converted into a 45 kDa polypeptide, whereas the 31 kDa form was processed into the fully mature 21 kDa VEGFC, which is in line with N-terminal processing of VEGFC proteins. (**B**) Schematic illustration of the different VEGFC forms, with their molecular weights provided (SP, signal peptide; NT, N-terminal propeptide; VHD, VEGF homology domain; CT, C-terminal propeptide).

while the LYVE1-positive cells identified in the lower dermis and in the adipose tissue were mainly macrophages (Supplemental Figure 6). The density of lymphatics was not modified in TS14$^{-/-}$ mice, but markedly reduced in TS2$^{-/-}$ and TS2$^{-/-}$TS14$^{-/-}$ mice (Figure 6), indicating that lymphedema observed in the adulthood most probably results from early postnatal defects.

ADAMTS2 and ADAMTS14 ablation affects pathological lymphangiogenesis. To investigate the mechanism leading to lymphatic vessel neoformation in adults, we used the model of thermal cauterization-induced corneal lymphangiogenesis, which relies on VEGFC signaling and mimics lymphangiogenesis induced upon inflammatory conditions such as keratitis, chemical burns, and graft rejection (19, 20). Although the cornea is an avascular tissue, it is rapidly colonized after thermal cauterization by lymphatic vessels arising perpendicularly from the limbal vascular arcade. In WT mice, *Adamts2* was expressed in control corneas, and its expression was still increased upon thermal cauterization (Figure 7A). While *Adamts3* remained poorly expressed under physiological and pathological conditions, *Adamts14* was clearly upregulated during the repair process. As compared with WT mice, a drastic reduction of neolymphangiogenesis was observed in TS2$^{-/-}$TS14$^{-/-}$ mice in terms of vessel length, number, and branching (Figure 7, B–E). Interestingly, intermediate values were observed in TS2$^{-/-}$ and TS14$^{-/-}$ mice, suggesting that the 2 enzymes are equally involved in the process. It is worth noting that the effect of ADAMTS deficiency was restricted to the lymphatic system, because the network of corneal blood vessels remained unaffected (Supplemental Figure 7).

Discussion

The processing of pro-VEGFC into VEGFC is a rate-limiting step for lymphangiogenesis, because it is required to endow VEGFC with its capacity to bind and activate VEGFR3 and VEGFR2. ADAMTS3 is involved in this crucial function during embryonic lymphangiogenesis (6, 7). However, given its restricted expression pattern in adults, it is unlikely that ADAMTS3 still performs this function in adulthood.

ADAMTS3 possesses high similarity with ADAMTS2 and ADAMTS14 in terms of sequence and domain composition. These 3 enzymes also share the capacity to cleave the amino-propeptide of fibrillar collagens but with different efficacy: ADAMTS2 is the most efficient, and ADAMTS3 and ADAMTS14

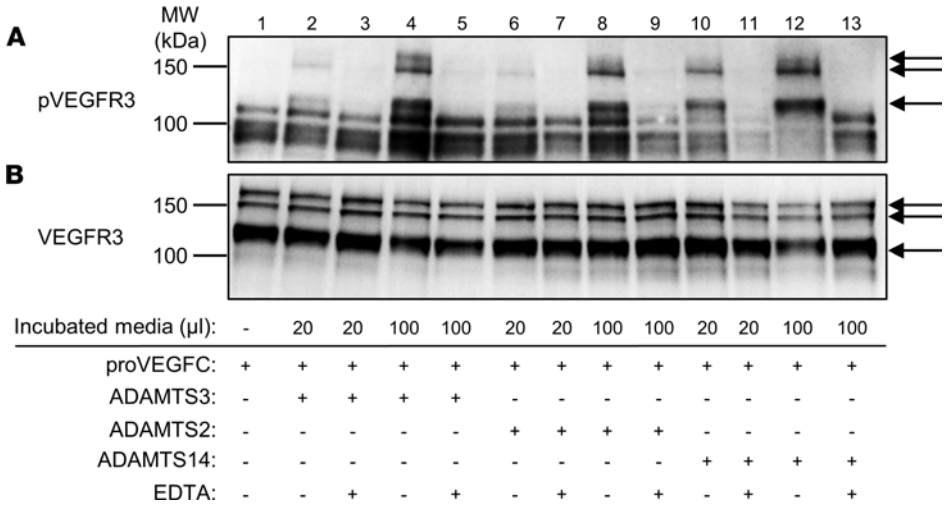

Figure 2. Phosphorylation of VEGFR3 by pro-VEGFC activated or not by ADAMTS3, ADAMTS2, or ADAMTS14. Conditioned medium from HEK293 cells expressing full-length pro-VEGFC was first incubated for 18 hours with buffer alone (lane 1, negative control), ADAMTS3 (as positive control), ADAMTS2, or ADAMTS14, in the presence or absence of EDTA used as inhibitor. These different pretreated media were then added (20 µL or 100 µL) into 1 mL of serum-free EBM-2 on LEC cultures. (**A**) After 5 minutes, cells were lysed, and phosphorylated VEGFR3 (pVEGFR3) was visualized by Western blotting. (**B**) After stripping of the antibodies, the same membrane was then used to visualize total VEGFR3. Treatment of the pro-VEGFC–rich conditioned medium with active ADAMTS3, ADAMTS2, and ADAMTS14 induced the phosphorylation of the 3 bands corresponding to VEGFR3 (arrows) in a dose-dependent manner, while the total amount of VEGFR3 was not affected, demonstrating that processing of pro-VEGFC by ADAMTS2, ADAMTS3, or ADAMTS14 leads to the activation of pro-VEGFC in a similar manner.

display only moderate and low activities, respectively (12, 14, 17, 21, 22). By sharp contrast, we have shown here that the 3 enzymes display similar processing activities when pro-VEGFC was used as substrate, showing that it might be a more physiological substrate for ADAMTS14 than fibrillar procollagens and, therefore, that ADAMTS14 activity could be more important for lymphangiogenesis than for collagen maturation. So far, TS2$^{-/-}$ or TS14$^{-/-}$ mice have been used mainly to determine their implications in collagen biology and were never specifically investigated for potential lymphatic defects. Of note, however, TS2$^{-/-}$TS14$^{-/-}$ mice display a peculiar phenotype, consisting of skin lesion formation caused by localized accumulation of inflammatory cells (16), a feature that could result from lymphatic defects because lymphatic vasculature plays a crucial role in resolving inflammation (23).

Potential existence of skin lymphedema was first evidenced by measuring the diameter of the tail base and of paw. Significant differences were found for TS2$^{-/-}$ and TS2$^{-/-}$TS14$^{-/-}$ mice, as compared with WT mice, which were further confirmed on histological tissue sections, by measurements of their skin water content and by the strong reduction of fluid drainage with both the inguinal lymph node and the efferent lymphatic vessel being barely stained after Evans blue dye injection in the footpad. In order to get better insight into the causes leading to reduced drainage, we performed ear skin whole-mount staining in order to get an overview of the lymphatic network. As compared with WT mice, we found a reduction of the density of lymphatic vessels in TS2$^{-/-}$ and TS14$^{-/-}$ mice that was even more pronounced in TS2$^{-/-}$TS14$^{-/-}$mice. This clearly indicates that both enzymes are involved and can partially compensate for each other in single-KO mice. In addition, in absence of *Adamts2* (TS2$^{-/-}$ and TS2$^{-/-}$TS14$^{-/-}$), vessels seem to have a smaller diameter, being shrunk or less swollen, as compared with WT and TS14$^{-/-}$ mice. These data suggest that edema found in TS2$^{-/-}$ and TS2$^{-/-}$TS14$^{-/-}$ mice is caused by decreased functionality of the lymphatic vessels and that their slightly reduced density and branching in TS14$^{-/-}$ mice is not sufficient to induce edema in physiological conditions. The skin of 6-day-old pups was also analyzed in order to determine if alteration of the lymphatic network takes place progressively in the adulthood or very early after delivery. For technical reasons related to the size and the fragility of samples, these analyses were performed on histological cross-sections of back skin. Skin lymphatics do not have specific orientations, and, as a result, their surfaces on histological sections vary strongly according to their local orientation. Therefore, we quantified the number of LYVE1-stained structures per mm² rather than the surface they covered, so that lymphatics studied

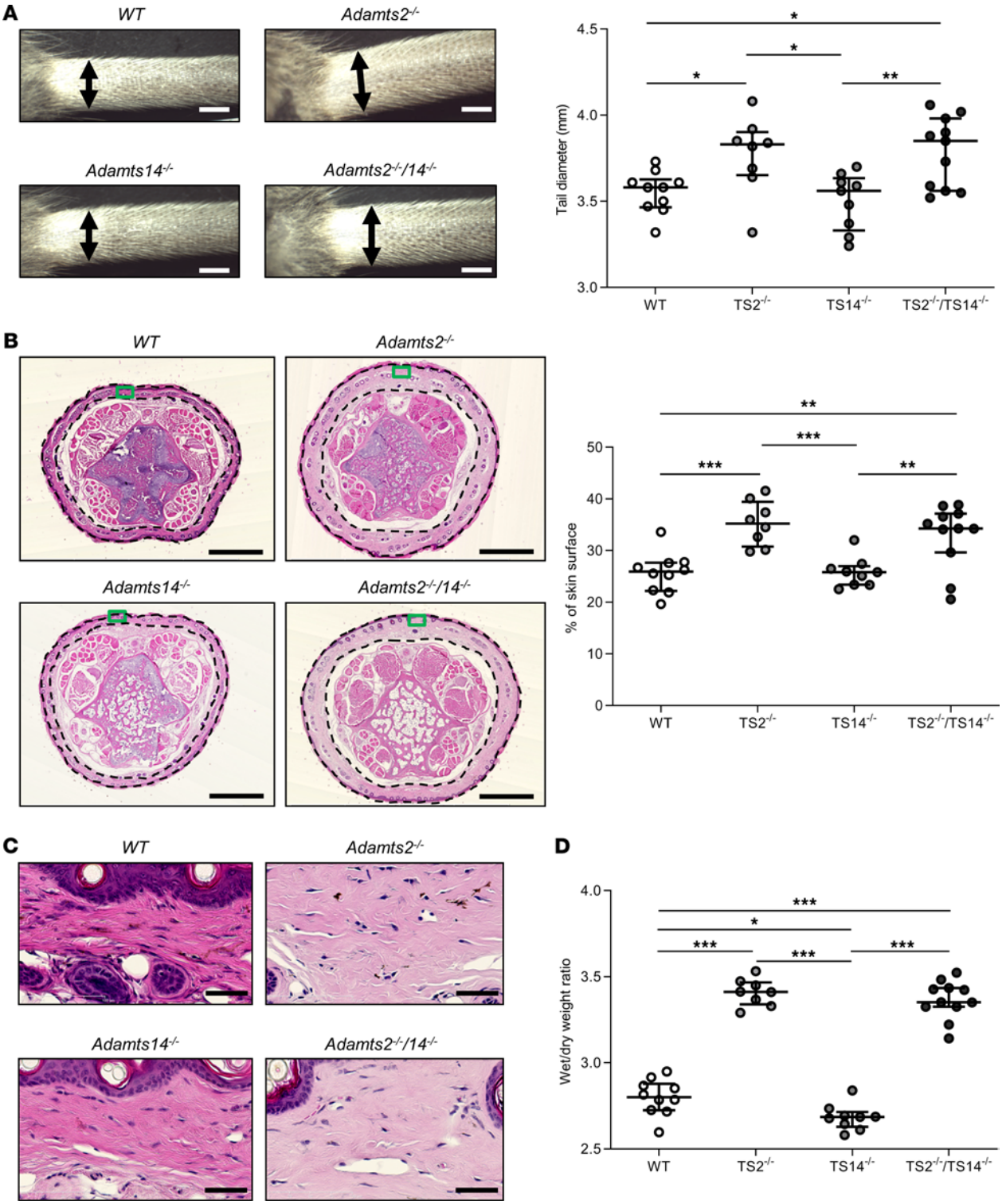

Figure 3. Tail swelling in absence of *Adamts2*. (**A**) Representative images of tails from 8-week-old WT, TS2$^{-/-}$, TS14$^{-/-}$, and TS2$^{-/-}$TS14$^{-/-}$ mice. Base tail diameters were measured (double arrows). Scale bar: 2 mm. As compared with those in WT mice, diameters were increased in TS2$^{-/-}$ and TS2$^{-/-}$TS14$^{-/-}$ mice, suggesting potential lymphedema. (**B**) Hematoxylin and eosin staining of paraffin-embedded sections of tails was performed to further characterize the tissue compartment responsible for the increased diameter. Scale bar: 1 mm. The percentage of surface covered by the dermis (delimited by black dotted lines) was determined (ImageJ software) and was found to be increased in TS2$^{-/-}$ and TS2$^{-/-}$TS14$^{-/-}$ mice. (**C**) Higher-magnification images of boxed regions in **B** show that the dermis is less stained in TS2$^{-/-}$ and TS2$^{-/-}$TS14$^{-/-}$ mice because it is swollen and less dense. Scale bar: 50 μm. (**D**) Tail skins were removed and weighed (wet weight) and then dried for 72 hours in an oven at 60°C before being reweighed (dry weight) to determine the ratios of wet-to-dry weight. An increase of water content was confirmed in TS2$^{-/-}$ and TS2$^{-/-}$TS14$^{-/-}$ mice. Statistical analyses were performed using Kruskal-Wallis test followed by Holm-Šidák post hoc test for multiple comparisons. *$P < 0.05$; **$P < 0.01$; ***$P < 0.001$.

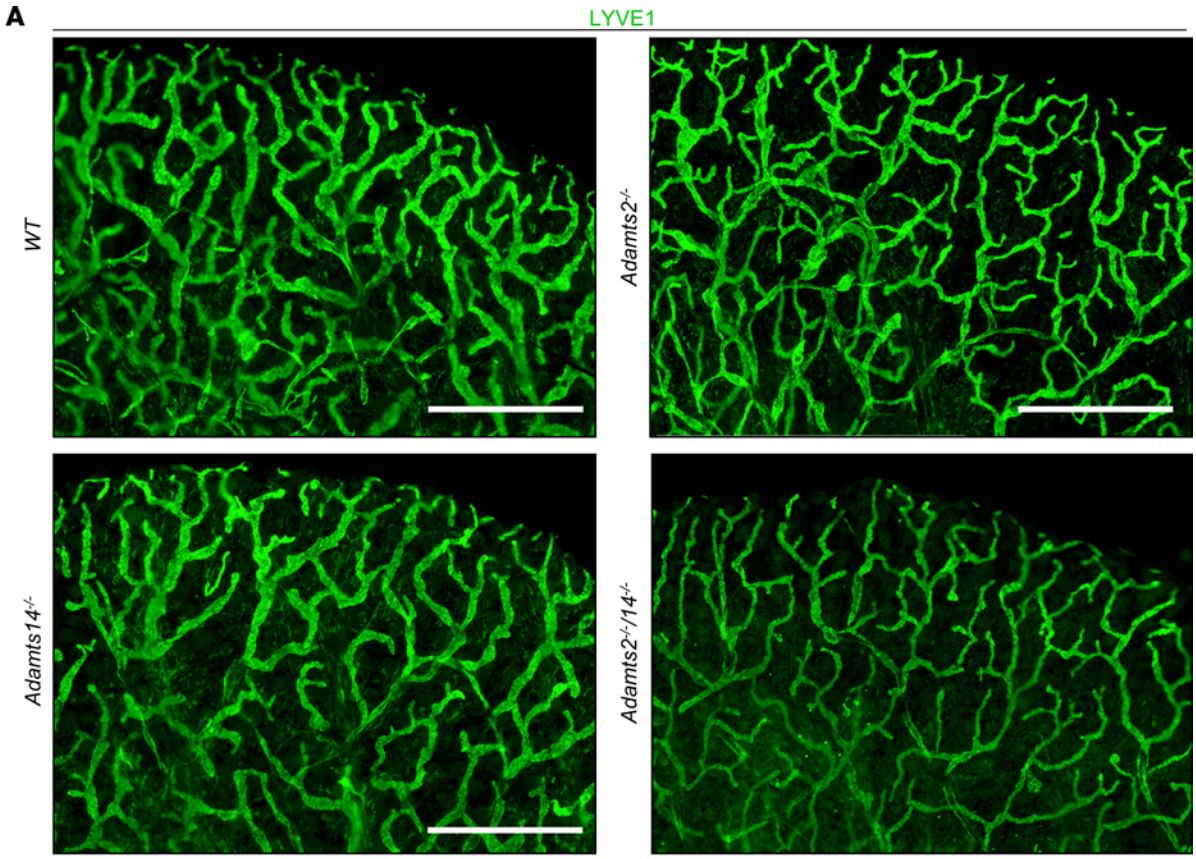

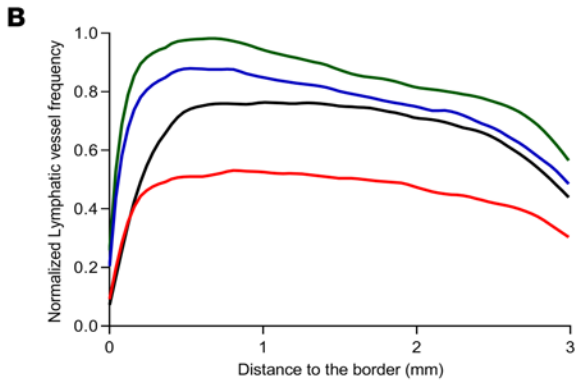

Kolmogorov-Smirnov test (Bonferroni's correction: significance level p<0,0125)			
	WT	TS2-/-	TS14-/-
TS2-/-	p=0.0057	/	/
TS14-/-	p<0.0001	p=0.0003	/
TS2-/-/14-/-	p<0.0001	p<0.0001	p<0.0001

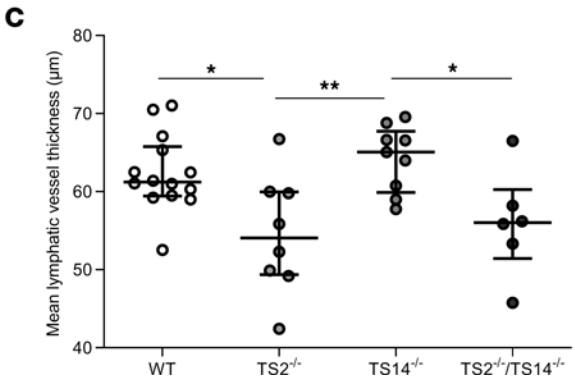

Figure 4. Absence of *Adamts2* and/or *Adamts14* affects the lymphatic network under physiological conditions in adult mice. (**A**) Whole mounts of dorsal ear skin were stained with an antibody specific for LYVE1 for immunofluorescence visualization of lymphatics. Scale bar: 1 mm. (**B**) For computerized quantification, lymphatic vessel frequencies were determined according to the distance from the border of the ear, because the structure and density of the lymphatic network vary according to the distance from the ear edge. The shapes of the distribution curves were found to be statistically different

(Kolmogorov-Smirnov test; significance levels were adjusted with Bonferroni's correction for multicomparison). The most dramatic reduction was observed in TS2$^{-/-}$TS14$^{-/-}$ mice, but it was also found to be reduced in TS2$^{-/-}$ and TS14$^{-/-}$ mice as compared with WT mice. By sharp contrast, no difference was seen regarding blood vessels, showing that these alterations affect lymphatics specifically (Supplemental Figure 5). (**C**) Computerized quantifications of mean diameter of the lymphatic vessels were also performed and demonstrated a smaller diameter in TS2$^{-/-}$ and TS2$^{-/-}$TS14$^{-/-}$ mice. Statistical analyses were performed using Kruskal-Wallis test followed by Holm-Šidák post hoc test for multiple comparisons. *$P < 0.05$; **$P < 0.01$.

in cross-sections or longitudinal sections would have the same values. Only the absence of *Adamts2* had an affect on lymphatic density, which could be attributed to the residual presence of *Adamts3* a few days after birth and to the fact that *Adamts2* is expressed much more than *Adamts14* around birth.

Having shown the effect of *Adamts2* on lymphatics in physiological conditions, we then used a model of acute neolymphangiogenesis occurring after injury. In the eye, lymphatic vessels are found in the conjunctiva and the limbus, in which lymphatic vasculature is a ring-shaped network with very small extensions directed toward the central avascular cornea (24). However, upon inflammatory stimuli, blood and lymphatic vessels rapidly extend from the limbus toward the cornea. The major advantage of the corneal neovascularization assay is that any vessel that grows into the corneal stroma is newly formed and can easily be detected, allowing the determination of several relevant parameters, such as vessel length, invasion distance, or vascular density (24). In the absence of *Adamts2* or *Adamts14*, a significant reduction of cornea invasion was observed, with lymphatics being shorter, less numerous, and less branched, as compared with WT mice. Remarkably, these alterations are more obvious in TS2$^{-/-}$TS14$^{-/-}$ mice, demonstrating that both enzymes actively participate in lymphangiogenesis during tissue inflammation and repair. Of note, angiogenesis was not affected, arguing for the involvement of the VEGFC/VEGFR3 pathway, as VEGFC is required for lymphangiogenesis but outcompeted by VEGFA for stimulating angiogenesis.

It was known that ADAMTS3 is required for embryonic lymphangiogenesis because of its capacity to process pro-VEGFC into active VEGFC. Here, we have demonstrated that ADAMTS2 and ADAMTS14 are as efficient as ADAMTS3 for processing pro-VEGFC into active VEGFC and that their absence in mouse models in vivo leads to alterations of the lymphatic network in adulthood.

These data open research avenues that are beyond the scope of the present study. As an example, it is not clear yet whether CCBE1 promotes the activity of ADAMTS2 and ADAMTS14, as has been reported for ADAMTS3 (6). The absence of ADAMTS2 or ADAMTS14 does not involve massive edema in our mouse models, suggesting that mutations in these genes should not be responsible for primary lymphedema. However, some reduction of their activity could be part of the numerous factors increasing the sensitivity to secondary lymphedema occurring after diverse types of injuries or trauma. This hypothesis is supported by our data showing that neolymphangiogenesis observed in healing cornea is almost completely prevented in absence of both ADAMTS2 and ADAMTS14. Efforts are being made now to develop inhibitors for specific ADAMTS, notably, for ADAMTS5, in order to find a medication able to limit cartilage degradation (25). Similar strategies could be used for ADAMTS2, ADAMTS3, and ADAMTS14 by focusing on their identical catalytic domain or on their ancillary domains, allowing their interactions with their substrates. If such inhibitors are obtained, they could help to fight conditions in which excessive or abnormal lymphangiogenesis is part of the pathological mechanisms, such as, for example, tumor aggressiveness and the formation of premetastatic niches in the lymph nodes.

Methods

Transgenic mice. WT, *Adamts14*$^{-/-}$, *Adamts2*$^{-/-}$, and *Adamts2*$^{-/-}$*Adamts14*$^{-/-}$ C57BL/6 mice were used for this study, either at postnatal day 6 or at 8 to 10 weeks of age (for descriptions, see refs. 15, 16). The animals were maintained on a 12-hour-light/dark cycle with free access to food and water.

RT-PCR. The different tissues were dissected and snap frozen. RNA was isolated using the Nucleospin RNA/protein extraction kit (Macherey Nagel, 740933.50). RT-PCR amplifications were performed using Tth DNA Polymerase (Roche). RT-PCR products were observed after electrophoresis in acrylamide gels and staining with Gel Star (Lonza, 50535). The following primers and cycles were used: 5′-CAGGCGCACACATAGTACCATCCA-3′ (reverse primer, sequence corresponding to exon 10) and 5′-CAGCCGCTACCTGCATTCCTATGA-3′ (forward primer, junction of exons 8 and 9) for *Adamts2* (28 cycles); 5′-GATACATCTCTGGGAGGCTGCTCCA-3′ (reverse primer, exon 22) and 5′-GCTGTGCCTATGTTGGTGACATCA-3′ (forward primer, junction of exons 20 and 21) for

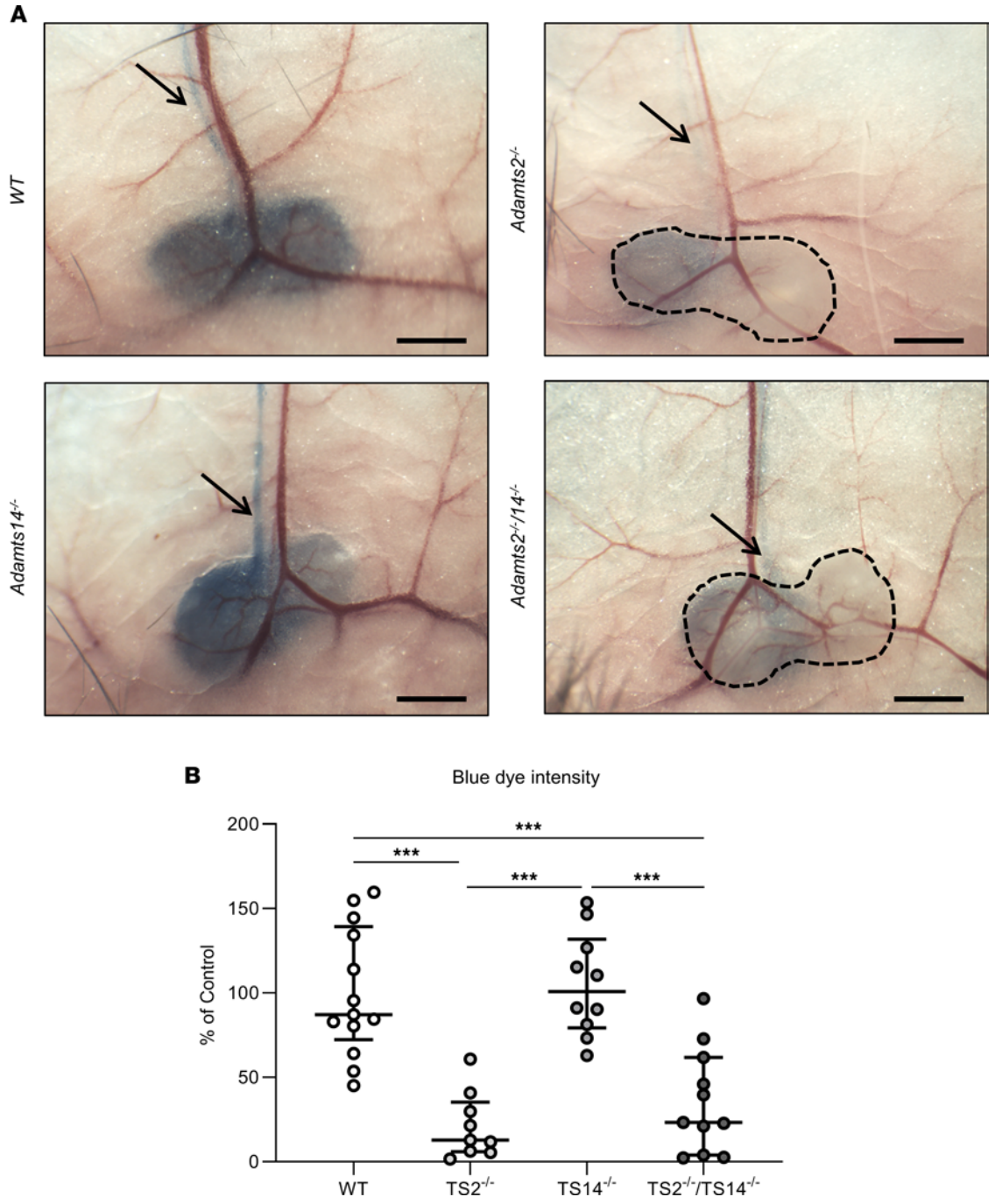

Figure 5. Impaired lymphatic function in absence of *Adamts2*. (**A**) Evans blue dye was injected into the footpad. After 30 minutes, mice were sacrificed and inguinal lymph nodes were visualized. Scale bar: 1 mm. In WT and TS14$^{-/-}$ mice, lymph nodes and the efferent lymphatic vessels (arrows) had a marked blue color. By contrast, they were barely detectable in TS2$^{-/-}$ and TS2$^{-/-}$TS14$^{-/-}$ mice, demonstrating a delayed draining from the site of injection. The images were acquired with a camera-equipped dissection microscope (Optika). (**B**) Computer-assisted quantification of the blue dye intensity in inguinal lymph nodes of WT, TS2$^{-/-}$, TS14$^{-/-}$, and TS2$^{-/-}$TS14$^{-/-}$ mice expressed as a percentage of WT control. Outliers were excluded based on Dixon's test for extreme values. Statistical analyses were performed using Kruskal-Wallis test followed by Holm-Šidák post hoc test for multiple comparisons. ***$P < 0.001$.

Adamts3 (30 cycles); 5′-CCATCCTCGTGGTTGAGGGCACA-3′ (reverse primer, exon 7) and 5′-CTGATCATGGTGGGCTACCGACA-3′ (forward primer, exon 5) for *Adamts14* (30 cycles); and 5′-GATTCTGACTTAGAGGCGTTCAGT-3′ (reverse primer) and 5′-GTTCACCCACTAATAGGGAACGTGA-3′ (forward primer) for *28S* (internal control) (16 cycles). Due to the localizations of the target sequences of the primers, only a single product was amplified by qRT-PCR for each Adamts gene (at 257 bp for *Adamts2*, at 155 bp for *Adamts3,* and at 236 bp for *Adamts14*).

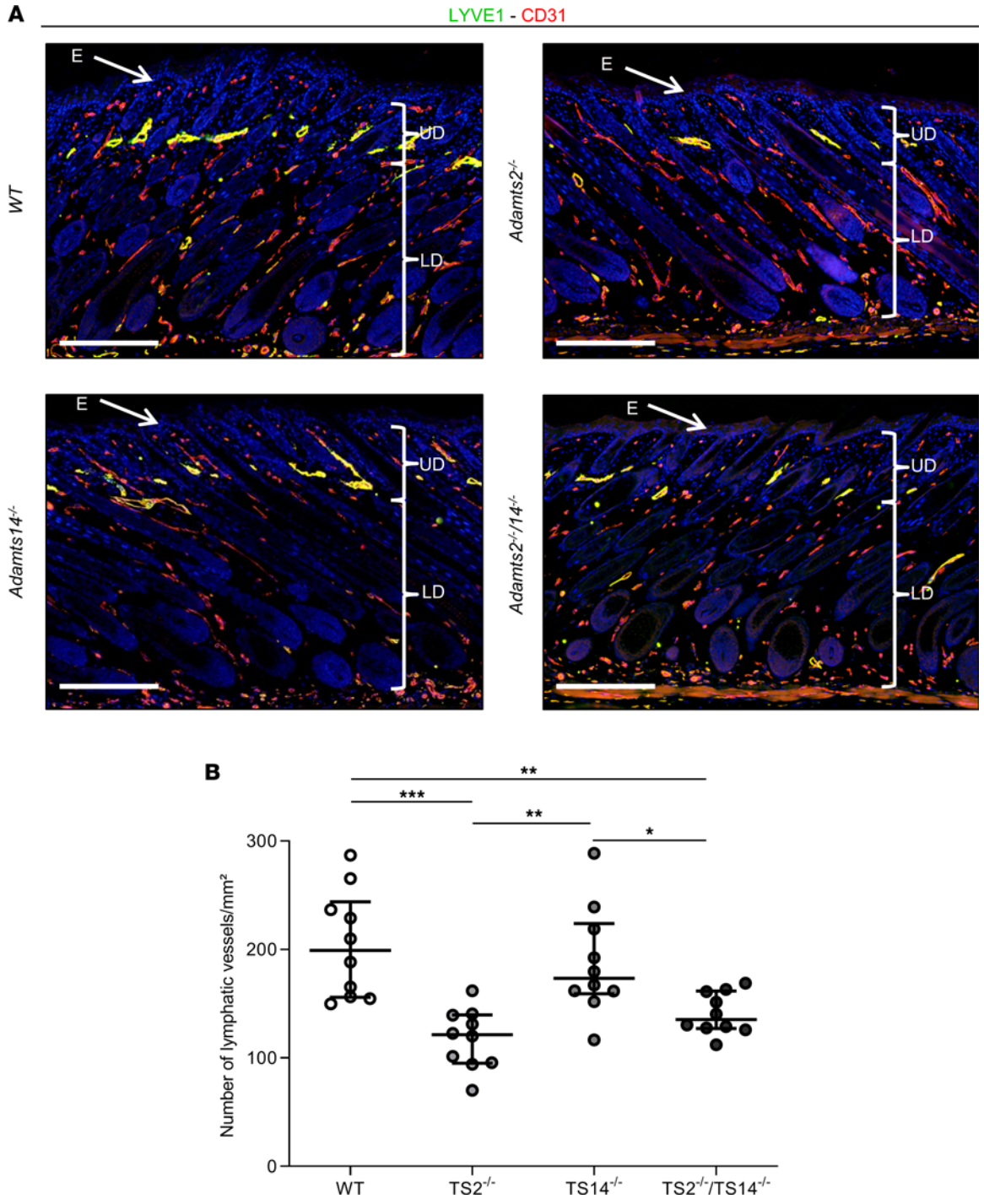

Figure 6. Absence of *Adamts2* affects lymphatic formation in postnatal day 6 mice. Skin sections were stained using antibodies for LYVE1 (green) and CD31 (red). Scale bar: 200 μm. (**A**) Because of coexpression of LYVE1 and CD31, lymphatics appear as yellow structures, mainly in the upper dermis and in close association with the bulge region of the hair follicle (18). LYVE1-positive cells identified in the lower dermis and in the adipose tissue were mainly macrophages (Supplemental Figure 6). (**B**) Computerized quantification of LYVE1 staining in the upper dermis. As compared with WT mice, fewer lymphatics were observed in $TS2^{-/-}$ and $TS2^{-/-}TS14^{-/-}$ mice. E, epidermis (white arrows); UD, upper dermis; LD, lower dermis. Statistical analyses were performed using Kruskal-Wallis test followed by Holm-Šidák post hoc test for multiple comparisons. $^{*}P < 0.05$; $^{**}P < 0.01$; $^{***}P < 0.001$.

Protein purification and VEGFC processing assay. Recombinant ADAMTS2, ADAMTS3, and ADAMTS14 were purified as previously described (26). Stably transfected cells were grown in DMEM supplemented with 10% fetal calf serum. Upon confluence, growth medium was replaced by serum-free DMEM containing soybean trypsin inhibitor (40 μg/mL), heparin (5 μg/mL), and $ZnCl_2$ (80 μM). After

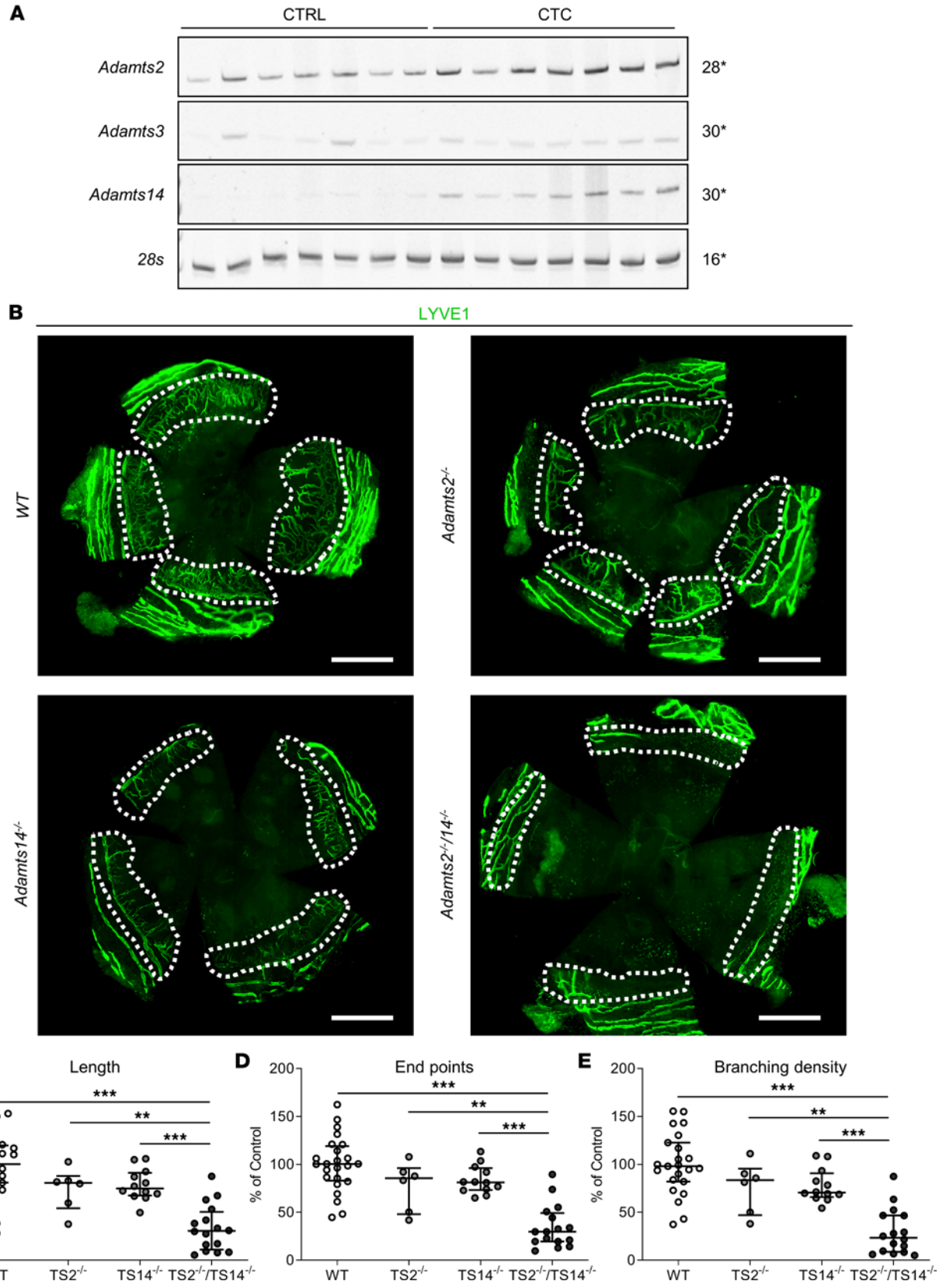

Figure 7. Absence of *Adamts2* or *Adamts14* inhibits inflammatory corneal lymphangiogenesis. (**A**) Expression of *Adamts2* (28 cycles), *Adamts3* (30 cycles), *Adamts14* (30 cycles), and *28s* (as control, 16 cycles) by RT-PCR on corneas collected from uninjured (CTRL) WT mice ($n = 7$) or from WT mice 7 days after corneal thermal cauterization (CTC) ($n = 7$). The expressions of *Adamts2* and *Adamts14*, but not of *Adamts3*, were increased during the healing process of the injured cornea. (**B**) Lymphatic vessel visualization using LYVE1 immunofluorescence on whole-mount corneas 7 days after thermal cauterization in WT, TS2$^{-/-}$, TS14$^{-/-}$, and TS2$^{-/-}$TS14$^{-/-}$ mice. Scale bar: 1 mm. A decrease of lymphatic vessels invading the injured corneas (white dotted lines)

were observed in KO mice as compared with WT mice. Computerized quantification of the (**C**) length, (**D**) end point numbers, and (**E**) branching density of lymphatic vessels in corneas 7 days after thermal cauterization in WT, $TS2^{-/-}$, $TS14^{-/-}$, and $TS2^{-/-}TS14^{-/-}$ mice expressed as a percentage of WT control (n = 23 WT, n = 6 $TS2^{-/-}$, n = 12 $TS14^{-/-}$, and n = 16 $TS2^{-/-}TS14^{-/-}$ corneas). Statistical analyses were performed using Kruskal-Wallis test followed by Holm-Šidák post hoc test for multiple comparisons. $^{**}P < 0.01$; $^{***}P < 0.001$.

48 hours, the medium was collected and the recombinant ADAMTS were purified through affinity chromatography (ConA-Sepharose [GE HealthCare, 17-0440-01] followed Heparin-Sepharose [GE HealthCare, 17-0467-01]). Note that this method leads to the purification of several ADAMTS polypeptides with different molecular weights (ref. 26 and Supplemental Figure 2) and different activities. In order to circumvent this problem, quantifications of recombinant ADAMTS were made after SDS-PAGE and staining with SYPRO Ruby using known concentrations of BSA as reference. Only the product around 100 kDa was taken into account, because this polypeptide corresponds to the expected molecular weight of the fully mature and most active form of ADAMTS2, ADAMTS3, and ADAMTS14. Concentrations of enzymes were adjusted around 10 ng per μL.

HEK293 cells (Invitrogen) expressing human pro-VEGFC were cultured for 48 hours in DMEM containing 0.1% FBS and 50 μM decanoyl-RVKR-CMK (furin inhibitor). For the processing assay, 20 μL conditioned medium was supplemented with NaCl (0.3 M final concentration) and 8 μL of either ADAMTS2, ADAMTS3, ADAMTS14, or control buffer, in the absence or presence of 25 mM EDTA (used as an inhibitor of metalloproteinases) in a total volume of 40 μL. After 18-hour incubation at 37°C, samples were denatured in reducing conditions (1× Laemmli sample buffer containing 200 mM DTT). Western blotting analyses were performed using a polyclonal goat anti-human VEGFC primary antibody (1:250, R&D Systems, AF752). Note that the VEGFC antibody does not react with the 29 kDa C-terminal domain of VEGFC and shows relatively low affinity for the fully processed mature 21 kDa form.

Determination of the cleavage site in pro-VEGFC by ADAMTS2, ADAMTS3, and ADAMTS14. HEK293 cells expressing human pro-VEGFC in a doxycycline-dependent manner were cultured for 60 hours in serum-free DMEM containing 1% nonessential amino acids (Biowest). The conditioned medium containing pro-VEGFC was collected with 0.1 mM AEBSF and concentrated on a 3 kDa cutoff filter (Amicon Ultra-15, PLBC, membrane Ultracel-PL, 3 kDa, MilliporeSigma). Total protein content was quantified (Micro BCA kit, Thermo Fisher Scientific) and 60 μg protein was incubated with control buffer or ADAMTS2, ADAMTS3, or ADAMTS14 for 18 hours at 37°C in 50 mM Tris-HCl, pH 8.0, containing 2 mM $CaCl_2$ and 0.6 M NaCl.

Samples were denatured in 4 M guanidine HCl and labeled with different ITRAQ labels (iTRAQ Reagents Multiplex Kit, Sciex) according to the manufacturer's instructions. Proteins were reduced with 1 mM TCEP and alkylated with 5 mM iodoacetamide. Ammonium bicarbonate buffer (pH 8) was added to reach 25 mM before methanol acetone precipitation. The protein pellets were dissolved in NaOH, and protein quantification was performed with Nanodrop. The different protein samples were precipitated using a 2D clean-up kit (GE Healthcare, 80648451) according to the manufacturer's instructions. Samples were resolubilized in ammonium bicarbonate and digested using multienzymatic limited digestion, as previously described (27). LC-MS/SM analyses were performed on an Acquity M-Class UPLC (Waters) in line with a Q Exactive Plus (Thermo Fisher Scientific), in nanoelectrospray-positive ion mode. The trap column was a Symmetry C18 5 μm (180 μm × 20 mm), and the analytical column was a HSS T3 C18 1.8 μm (75 μm × 250 mm) (Waters Corp.). The samples were loaded at 20 μL/min on the trap column in 98% solvent A over 3 minutes and subsequently separated on the analytical column at a flow rate of 600 nL/min, with the following linear gradient: initial conditions, 98% A; 5 minutes, 93% A; 60 minutes, 70% A; 70 minutes, 60% A; and 73 minutes, 15% A, before maintenance for 5 minutes, after which the column was reconditioned in initial conditions. Solvent A is 0.1% formic acid in water, and solvent B is 0.1% formic acid in acetonitrile. The total run time was 60 minutes. A TopN-MSMS mass spectrometer method was used, where N was set to 15; this means that the spectrometer acquired 1 full MS spectrum, selected the 15 most intense peaks in this spectrum (singly charged and unassigned charge precursors excluded), and made a full MS2 spectrum of each of these 15 compounds. The parameters for MS spectrum acquisition were as follows: mass range from 400 to 2000 m/z; resolution, 70,000; and automatic gain control (AGC) target of 1×10^6 or maximum injection time of 250 milliseconds. The parameters for MS2 spectrum acquisition were as follows: isolation window, 2.0 m/z; normalized collision energy, 30; resolution of 17,500; and AGC target of 2×10^5 or maximum injection time of 120 milliseconds and a fixed first mass set at 100 m/z. The main parameters for QExactive Plus tune were as follows: spray voltage, 2.3 kV; capillary

temperature, 270°C; and S-Lens RF level, 50.0. Data processing was performed by PEAKS X (BSI Bioinformatics Solutions). Relative quantitation was performed at the peptide level by considering the area under the curve of the corresponding extracted ion chromatograms.

Activation of VEGFC pathway. Primary human LECs (HMVEC-dLy, Lonza, CC-2810) were cultured in EGM2-MV medium in 6-well plate until confluence. HEK293 cells expressing human pro-VEGFC were cultured for 48 hours in DMEM containing 0.1% FBS. Conditioned medium (70 μL) was supplemented with NaCl (0.3 M final concentration) and 28 μL ADAMTS2, ADAMTS3, ADAMTS14, or control buffer in the absence or presence of 25 mM EDTA (used as an inhibitor of metalloproteinases) in a total volume of 140 μL. After a 18-hour incubation at 37°C, 20 μL or 100 μL of the incubation mixes were added to 1 mL serum-free EBM-2 medium (CC-3156, Lonza). LEC culture media were then replaced by the different digestion mixes. After 5 minutes, LECs were then lysed with cell lysis buffer 1× (9803, Cell Signaling) containing phosphatase and protease inhibitors (Complete and phosSTOP, Roche). Equivalent amounts of proteins were separated on polyacrylamide gels (7.5%) and transferred onto PVDF membranes. Membranes were then blocked, incubated overnight at 4°C with a pVEGFR3 (CY1115, Cell Applications) or a pVEGFR2-specific antibody (Tyr1175, no. 2478, Cell Signaling), washed extensively, and incubated for 1 hour at room temperature with horseradish peroxidase–coupled secondary antibody (P0217, Dako). After washing, the peroxidase activity was revealed with an enhanced chemiluminescence assay (ECL Prime Western Blotting System, MilliporeSigma) in an ImageQuant LAS 4000 (GE Healthcare). The membranes were then stripped, incubated with antibodies against total VEGFR3 (MAB3757 Merck Millipore) or total VEGFR2 (no. 2479 Cell Signaling), respectively, and revealed as described above.

Hind limb and tail thickness measurements. Images of hind limb and tail base from 8-week-old mice were acquired with a camera-equipped dissection microscope (Optika). The hind limb thickness was measured using the ImageJ software (NIH), just to the front of the first footpad, and the tail diameter was measured at the tail base.

Wet-to-dry weight ratio. Tail skins were removed and weighed (wet weight), dried for 72 hours in an oven at 60°C, and weighed again (dry weight). These measurements were used to determine the water content in the skin.

Immunohistological analyses. Tissues were fixed in a 4 % paraformaldehyde solution (and eventually decalcified in 0.5 m EDTA, pH 8, for 3 weeks in the case of hind limb and tail base samples) and paraffin embedded. Tissue sections (5 μm) were deparaffined, rehydrated, and stained with hematoxylin and eosin for general histological examination. The percentage of dermis area in hind limb and tail was quantified using ImageJ software as a percentage of the total tissue area.

For immunofluorescence, sections were treated (antigen retrieval, with Target retrieval solution, Dako) and then blocked with Universal blocking Reagent (HK085-5K BioGenex). Goat anti-LYVE1 antibody (1:100, AF2125, R&D Systems), and/or rat anti-CD31 antibody (1:150, DIA-310, Dianova), and/or rat anti-F4/80 antibody (1:100, Ab16911, Abcam) were incubated overnight at 4°C. After washes with PBS, Alexa Fluor 488–coupled rabbit anti-goat antibody (1:200; A21222, Invitrogen) was incubated at room temperature for 1 hour. After washes with PBS, Alexa Fluor 546–coupled goat anti-rat antibody (1:200; A11081, Invitrogen) was incubated at room temperature for 1 hour. Slides were then washed with PBS and mounted using Dako fluorescent mounting medium. Slides were scanned using a Nanozoomer 2.0 scanner (Hamamatsu) and visualized using NDPviewer (Hamamatsu). Dermal lymphatic count and dermal blood vessels per surface area were quantified using ImageJ software.

Staining of lymphatic vessels on whole-mount ear skins from adult mice. Ears from 8- to 10-week-old mice were collected and fixed in 4% paraformaldehyde overnight at 4°C. For each ear, the dorsal skin was separated from the rest of the tissue (central cartilage and the adhering ventral skin). Whole dorsal ear skins were fixed in methanol for 1 hour at –20°C and then blocked with 3% milk and 0.2% Triton X-100 for 1 hour at room temperature. They were then incubated with a polyclonal goat anti-LYVE1 antibody (1:200; AF2125, R&D Systems) and rat anti-CD31 antibody (1:150, DIA-310, Dianova) overnight at room temperature. After washing in PBS, an Alexa Fluor 488–coupled rabbit anti-goat antibody (1:200; A21222, Invitrogen) was added for 2 hours at room temperature. After washes with PBS, Alexa Fluor 546–coupled goat anti rat antibody (1:200; A11081, Invitrogen) was incubated at room temperature for 2 hours. Slides were then washed with PBS and mounted using Dako fluorescent mounting medium (Dako). Slides were scanned using a Nanozoomer 2.0 scanner (Hamamatsu) and

visualized using NDPviewer (Hamamatsu). The lymphatic vessel frequency, density, and thickness were quantified using ImageJ software.

Functional analysis of the lymphatic network in vivo. To evaluate lymphatic drainage, 30 μL of a 3% solution of Evans blue dye (MilliporeSigma) in PBS was injected into the footpads of anesthetized mouse hind limbs. Thirty minutes after injection, mice were sacrificed and dissected to expose the inguinal lymph node. The images were acquired with a camera-equipped dissection microscope (Optika). The blue dye intensity was measured using ImageJ software. Results are expressed as a percentage of WT control.

In vivo lymphangiogenesis. Thermal cauterization was induced on the corneas of 8 to 10-week-old mice. After 7 days, corneas were dissected and whole mounted for immunostaining as previously described (28–30) or snap frozen for RNA extraction. To visualize lymphatic and blood vessels, corneas were fixed in methanol at –20°C for 1 hour and then blocked with 3% milk for 1 hour at room temperature. Corneas were then incubated overnight at room temperature with a polyclonal goat anti-mouse LYVE1 antibody (1:200; AF2125, R&D Systems) and with a monoclonal rat anti-mouse CD31 (1:200; 553370, BD Biosciences). After washing in PBS, an Alexa Fluor 488–coupled rabbit anti-goat antibody (1:200; A21222, Invitrogen) was added for 2 hours at room temperature. After washing in PBS, an Alexa Fluor 546–coupled goat anti-rat antibody (1:200; A-11081, Thermo Fisher Scientific) was added for 2 hours at room temperature. After washing, the slides were scanned using a Nanozoomer 2.0 scanner (Hamamatsu) and visualized using NDPviewer (Hamamatsu). The lymphangiogenic responses were analyzed using a described computerized method (28, 31). All the results were normalized to the total cornea area and are expressed as a percentage of WT control.

Statistics. Results were illustrated with GraphPad Prism 8.0 and were expressed as medians with interquartile ranges for different experiments. Statistical analyses were carried out with SigmaPlot 14.0 software using the nonparametric Kruskal-Wallis test to test whether measurements performed on the 4 genotypes of mice have the same distribution. When tests revealed differences, Holm-Šidák post hoc test was conducted to determine which groups were different from others. The Kolmogorov-Smirnov test was used to compare the shapes of the distribution curves, and the significance levels were adjusted with Bonferroni's correction for multiple comparisons. *P* values of less than 0.05 were considered significant. The experiments were not randomized. Analysis and quantifications were not blinded.

Study approval. All animal experiments were conducted at the GIGA Animal Facility of the University of Liège in accordance with the Federation of European Laboratory Animal Science Associations and after approval from the local ethical committee at the University of Liège (approval no. 1964 and 2151).

Author contributions

LD designed, performed, and analyzed experiments and wrote the manuscript. LJ contributed to the pro-VEGFC activation analyses and to the determination of the cleavage site in pro-VEGFC by ADAMTS2, ADAMTS3, and ADAMTS14. FM designed, performed, and analyzed experiments. SB performed all computerized quantifications. CM contributed to immunostaining and mouse breeding. CFD participated in experimental design and data interpretation. AN funded and supervised the project. ACMAC supervised, funded, and designed the project; interpreted the data; and wrote the manuscript.

Acknowledgments

We thank all laboratory members for useful technical advice. We thank GIGA Animal Facility platforms of University of Liège for technical support and mouse housing. We thank the GIGA Proteomic Facility and, especially, Gabriel Mazzucchelli for technical support in determining the cleavage site in pro-VEGFC by ADAMTS2, ADAMTS3, and ADAMTS14. ACMAC is the Senior Research Associate of the Fund for Scientific Research — National Fund for Scientific Research (FRS-FNRS). LD is supported by a FNRS grant (FC96394), LJ is supported by a Télévie grant (7.4608.19), and CM is supported by a Télévie grant (7.6536.18). This work was supported by grants from FRS-FNRS (T.0183.13, PDR), the Fondation contre le Cancer (foundation of public interest, Belgium), the Fonds spéciaux de la Recherche (University of Liège), the Fondation Hospitalo-Universitaire Léon Fredericq (University of Liège), the Walloon Region through the FRFS-WELBIO strategic research program, and the Wallonia-Brussels Federation (grant for Concerted Research Actions, A.R.C. 19/23-21 "INovLYMPHATIC").

Address correspondence to: Laura Dupont, Avenue Hippocrate n° 13 B23/+3, 4000 Sart Tilman, Belgium. Phone: 32.43669293; Email: ldupont@uliege.be.

1. Petrova TV, Koh GY. Biological functions of lymphatic vessels. *Science*. 2020 Jul 10;369(6500):eaax4063.
2. Alitalo K. The lymphatic vasculature in disease. *Nat Med*. 2011;17(11):1371–1380.
3. Brouillard P, et al. Genetics of lymphatic anomalies. *J Clin Invest*. 2014;124(3):898–904.
4. Baldwin ME, et al. Vascular endothelial growth factor D is dispensable for development of the lymphatic system. *Mol Cell Biol*. 2005;25(6):2441–2449.
5. Künnapuu J, et al. Proteolytic cleavages in the VEGF family: generating diversity among angiogenic VEGFs, essential for the activation of lymphangiogenic VEGFs. *Biology (Basel)*. 2021;10(2):167.
6. Jeltsch M, et al. CCBE1 enhances lymphangiogenesis via A disintegrin and metalloprotease with thrombospondin motifs-3-mediated vascular endothelial growth factor-C activation. *Circulation*. 2014;129(19):1962–1971.
7. Janssen L, et al. ADAMTS3 activity is mandatory for embryonic lymphangiogenesis and regulates placental angiogenesis. *Angiogenesis*. 2016;19(1):53–65.
8. Alders M, et al. Mutations in CCBE1 cause generalized lymph vessel dysplasia in humans. *Nat Genet*. 2009;41(12):1272–1274.
9. Brouillard P, et al. Loss of ADAMTS3 activity causes Hennekam lymphangiectasia-lymphedema syndrome 3. *Hum Mol Genet*. 2017;26(21):4095–4104.
10. Scheuerle AE, et al. An additional case of Hennekam lymphangiectasia-lymphedema syndrome caused by loss-of-function mutation in ADAMTS3. *Am J Med Genet A*. 2018;176(12):2858–2861.
11. Wang G, et al. Specific fibroblast subpopulations and neuronal structures provide local sources of Vegfc-processing components during zebrafish lymphangiogenesis. *Nat Commun*. 2020;11(1):2724.
12. Le Goff C, et al. Regulation of procollagen amino-propeptide processing during mouse embryogenesis by specialization of homologous ADAMTS proteases: insights on collagen biosynthesis and dermatosparaxis. *Development*. 2006;133(8):1587–1596.
13. Jeltsch M, et al. Hyperplasia of lymphatic vessels in VEGF-C transgenic mice. *Science*. 1997;276(5317):1423–1425.
14. Colige A, et al. Cloning and characterization of ADAMTS-14, a novel ADAMTS displaying high homology with ADAMTS-2 and ADAMTS-3. *J Biol Chem*. 2002;277(8):5756–5766.
15. Li SW, et al. Transgenic mice with inactive alleles for procollagen N-proteinase (ADAMTS-2) develop fragile skin and male sterility. *Biochem J*. 2001 Apr 15;355(pt 2):271–278.
16. Dupont L, et al. Spontaneous atopic dermatitis due to immune dysregulation in mice lacking Adamts2 and 14. *Matrix Biol*. 2018;70:140–157.
17. Bekhouche M, et al. Determination of the substrate repertoire of ADAMTS2, 3, and 14 significantly broadens their functions and identifies extracellular matrix organization and TGF-β signaling as primary targets. *FASEB J*. 2016;30(5):1741–1756.
18. Peña-Jimenez D, et al. Lymphatic vessels interact dynamically with the hair follicle stem cell niche during skin regeneration in vivo. *EMBO J*. 2019;38(19):e101688.
19. Cursiefen C, et al. Time course of angiogenesis and lymphangiogenesis after brief corneal inflammation. *Cornea*. 2006;25(4):443–447.
20. Regenfuss B, et al. Corneal (lymph)angiogenesis--from bedside to bench and back: a tribute to Judah Folkman. *Lymphat Res Biol*. 2008;6(3-4):191–201.
21. Bekhouche M, Colige A. The procollagen N-proteinases ADAMTS2, 3 and 14 in pathophysiology. *Matrix Biol*. 2015;44-46:46–53.
22. Leduc C, et al. In vivo N-Terminomics highlights novel functions of ADAMTS2 and ADAMTS14 in skin collagen matrix building. *Front Mol Biosci*. 2021;8:643178.
23. Schwager S, Detmar M. Inflammation and lymphatic function. *Front Immunol*. 2019;10:308.
24. Hos D, et al. Antilymphangiogenic therapy to promote transplant survival and to reduce cancer metastasis: what can we learn from the eye? *Semin Cell Dev Biol*. 2015;38:117–130.
25. Santamaria S. ADAMTS-5: A difficult teenager turning 20. *Int J Exp Pathol*. 2020;101(1-2):4–20.
26. Colige A, et al. Domains and maturation processes that regulate the activity of ADAMTS-2, a metalloproteinase cleaving the aminopropeptide of fibrillar procollagens types I-III and V. *J Biol Chem*. 2005;280(41):34397–34408.
27. Morsa D, et al. Multi-enzymatic limited digestion: the next-generation sequencing for proteomics? *J Proteome Res*. 2019;18(6):The Next–2513.
28. Blacher S, et al. Additional parameters for the morphometry of angiogenesis and lymphangiogenesis in corneal flat mounts. *Exp Eye Res*. 2009;89(2):274–276.
29. Detry B, et al. Digging deeper into lymphatic vessel formation in vitro and in vivo. *BMC Cell Biol*. 2011;12:29.
30. Detry B, et al. Matrix metalloproteinase-2 governs lymphatic vessel formation as an interstitial collagenase. *Blood*. 2012;119(21):5048–5056.
31. Detry B, et al. Sunitinib inhibits inflammatory corneal lymphangiogenesis. *Invest Ophthalmol Vis Sci*. 2013;54(5):3082–3093.

The Supplementary Material for this article can be found online:

https://insight.jci.org/articles/view/151509/sd/1

Chapter 3: Study of ADAMTS2 in tumor development

It is now clearly established that ADAMTS2 is crucial for collagen fibrillogenesis by its capacity to cleave the aminopropeptide of several fibrillar procollagens[63,26,76]. Its expression and activities have also been associated to fibrosis progression[91], inhibition of angiogenesis[119] and lymphangiogenesis at adulthooh[269], while its absence (together with that of ADAMTS14) leads to a peculiar skin phenotype reminiscent of atopic dermatitis[87]. In addition to these publications from our laboratory, several studies have correlated ADAMTS2 expression to cancer progression[245–248].

With our expertise and knowledge of ADAMTS2 and the availability of ADAMTS2 knockout mice (TS2-KO) in our laboratory, we decided to try to elucidate the potential roles of ADAMTS2 in cancer development and to determine the underlying mechanism(s).

A. The absence of ADAMTS2 enhances tumor growth in distinct tumor models

We first used the available databases to draw correlations between ADAMTS2 expression in the primary tumor and overall survival of patients. A first analysis revealed that high expression of ADAMTS2 correlates with poorer prognosis in most cancers.

Desmoplasia corresponds to the accumulation of collagen within the TME. Since ADAMTS2 is involved in collagen fibril formation and homeostasis, and in order to get rid of the confounding effect of the desmoplastic reaction, we performed the same correlation analysis but included a normalization by the expression of COL1A1. Unexpectedly and newly interestingly, these new correlations clearly showed that ADAMTS2 expression was then associated with increased survival, suggesting that it probably displays anti-tumor functions besides its pro-tumor effects linked to desmoplasia.

To evaluate this hypothesis *in vivo*, we compared the formation of tumors in TS2-KO mice (of C57BL/6 genetic background) and in their wild type controls. Mice were subcutaneously injected with syngeneic Lewis lung carcinoma (LLC) or melanoma (B16F10) cancer cells, as these cells are known to form tumors lacking significant collagen accumulation. For both LLC (Figure 27.A) and B16F10 (Figure 27.B) cancer cells, tumor grew faster in TS2-KO mice indicating that ADAMTS2 may repress tumor growth independently of collagen deposition.

We also generated a model of spontaneous mammary cancer in mice known to develop desmoplasia. MMTV-PyMT (mouse mammary tumor virus-polyoma middle T tumor antigen) mice develop mammary tumors recapitulating several key characteristics of human breast cancer

development, including complexity of the TME and collagen accumulation. MMTV-PyMT WT and TS2-KO mice were generated, followed individually and sacrificed when the largest tumor reached around approximately 1 cm^3. TS2-KO had to be sacrificed significantly earlier than WT mice (Figure 27.C) indicating that tumors grew faster in TS2-KO mice, which was consistent with the results obtained with LLC and B16 tumors. These data also indicate that ADAMTS2 represses tumor growth in both non-desmoplastic and desmoplastic tumors.

Cultures of PyMT cancer cells were also established from MMTV-PyMT spontaneous tumors. Upon subcutaneous injection, they form homogenous and highly desmoplastic tumors, characterized by high collagen content which is produced by MMTV-PyMT cancer cells displaying a mesenchymal phenotype. In this model, again, tumor grew faster in TS2-KO mice than in WT mice (Figure 27.D).

Since similar results were obtained using different models, we concluded that ADAMTS2 is a tumor suppressor proteinase by a mechanism that is common to our models, despite their differences, and is therefore unlikely to be mediated by either CAFs or cancer cells.

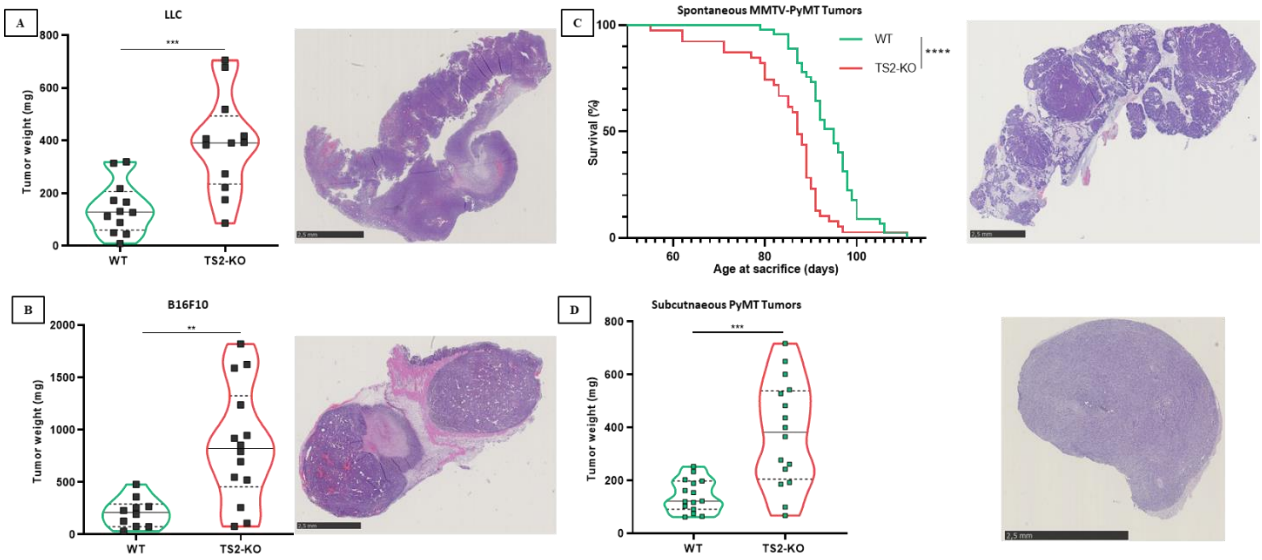

Figure 27: Weight of tumors generated by subcutaneous injection of LLC (A), B16F10 (B), PyMT cancer cells (D) after 14 (A and D) or 21 days (B) post-injection in WT and TS2-KO mice. (C) Survival of WT and TS2-KO MMTV-PyMT mice based on the age at sacrifice as determined by the time needed to reach a measurable 1 cm^3 tumor.

B. ADAMTS2 represses tumor growth through mechanism(s) independent of its already described functions

LLC and B16 subcutaneous tumors and PyMT spontaneous mammary tumors are highly heterogeneous, which could compromise the identification of the ADAMTS2-dependent regulations. On the contrary, subcutaneous tumors formed by the injection of PyMT cancer cells are highly homogeneous and this model was therefore privileged for additional characterizations.

We first hypothesized that ADAMTS2 might impact tumor growth through one of its known functions. Therefore, we compared collagen deposition (Sirius red staining, Figure 28.B), blood vessels (CD31 immunolabeling of endothelial cells, Figure 28.C) and lymphatic vessels (Lyve1 immunolabeling, none identified) in the parenchyma (H&E staining, Figure 28.A) of tumors generated in WT and TS2-KO mice. No significant differences were observed between tumors formed in WT and TS2-KO mice.

Additional investigations were then carried out. Neither proliferation (KI67 immunolabeling, Figure 28.D) nor apoptosis (cleaved caspased-3 immunolabeling, Figure 28.E) of cancer cells was affected by the absence of ADAMTS2, indicating that its impact on tumor growth may occur earlier in the development of the tumor.

Finally, we evaluated also ADAMTS2 expression and aminoprocollagen processing in tumors formed by subcutaneous injection of PyMT-WT and PyMT-KO cancer cells in WT and TS2-KO mice. While tumor growth was clearly increased in TS2-KO (Figure 28.F), as already seen, no correlations could be established between the size of the tumors and the level of collagen processing (Figure 28.H). It is also worth noting that the low expression of ADAMTS2 by cancer cells is not sufficient to repress tumor growth (Figure 28.G).

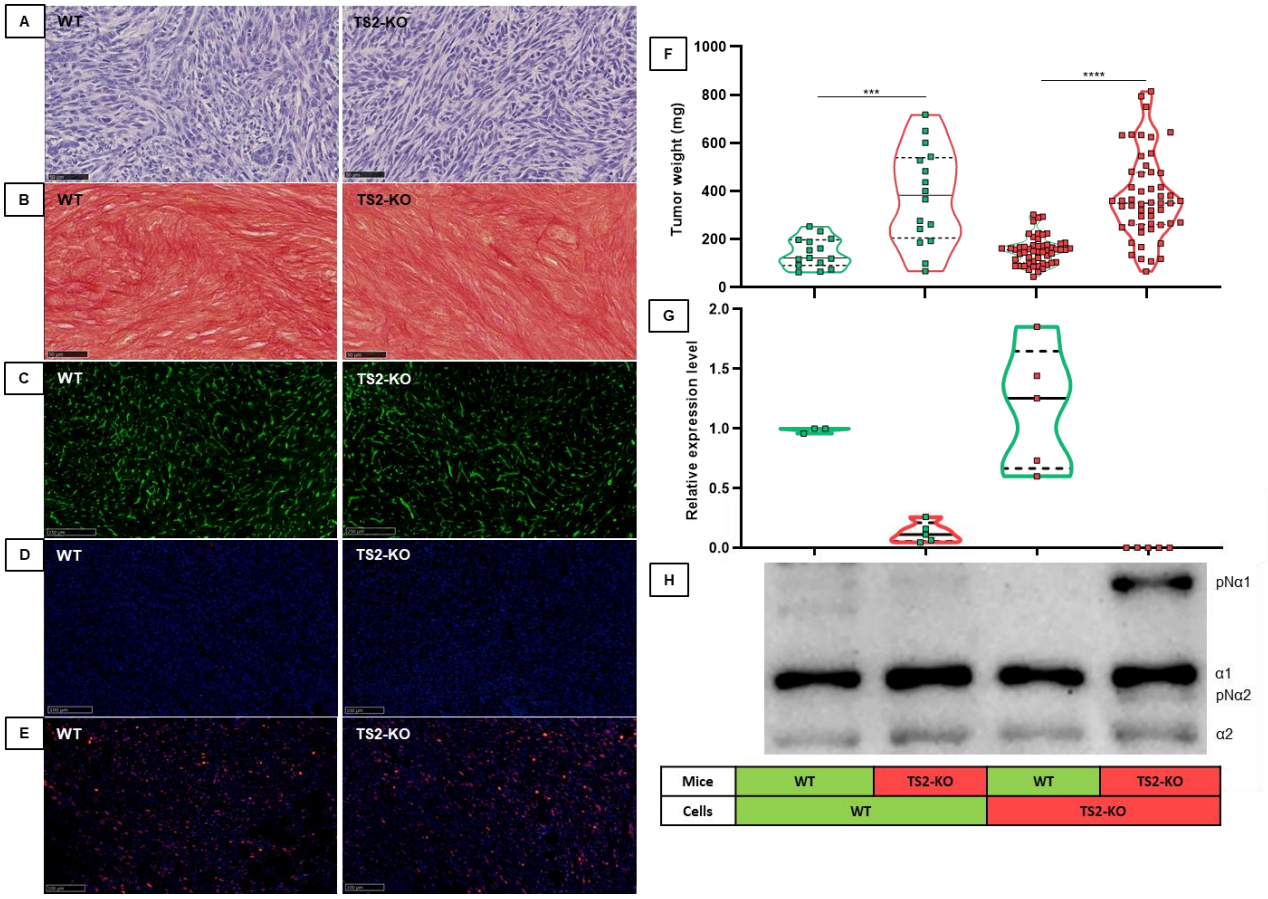

Figure 28: Representative pictures of sections of subcutaneous PyMT tumors formed by PyMT-TS2-KO cancer cells in WT and TS2-KO mice, after staining with H&E (A) or Sirius red (collagen) (B), or immunolabeling of CD31 (endothelial cells) (C), cleaved caspase-3 (D) and KI-67 immunolabeling (E). (F) Weights of tumors formed after subcutaneous injection of PyMT-WT and PyMT-TS2-KO cancer cells in WT and TS2-KO mice. (G) Relative ADAMTS2 expression measured by RT-qPCR and (H) evaluation of type I collagen processing (immunolabeling of type I collagens) in the different experimental tumor conditions. pNα1: type I aminoprocollagen alpha 1 chain; α1: type I mature collagen alpha; pNα2 : type I aminoprocollagen alpha 2 chain; α2: type I mature collagen alpha 2 chain.

C. The absence of ADAMTS2 expression by the host increases immuno-suppression in the TME

Having explored and excluded several mechanisms that would have explained the differences in tumor growth between WT and TS2-KO mice, we sought to verify wether the immune system might be involved in this phenotype. FACS analyses were used to characterize the profile of immune cells infiltrating the tumors at day 7 post-injection, an early timepoint when the difference in tumor growth is already significant (Figure 29.A). This analysis revealed a profound increase in immunosuppressive markers as well as modifications of the abundance of key immune populations in tumors formed in TS2-KO mice as compared to WT mice.

With regard to macrophages, we observed an increase in the proportion of M2-like population ($CD206^{high}$ and $CD11c^{low}$) in TS2-KO mice (Figure 29.B) as well as increased ARG1 expression (Figure 29.C), two indicators of high immunosuppressive status of macrophages. Additionnaly, we saw a reduction of dendritic cells (Figure 29.D), an increased expression of CD14 in monocytic (Figure 29.E) and granulocytic (Figure 29.F) MDSC, a decrease of T cells (Figure 29.G) and an increase of IL10 expressing T cells (Figure 29.G) in TS2-KO mice as compared to WT mice. These are all distinct markers that can be associated with immunosuppression. We concluded that the absence of ADAMTS2 leads to an increased immunosuppression in the TME.

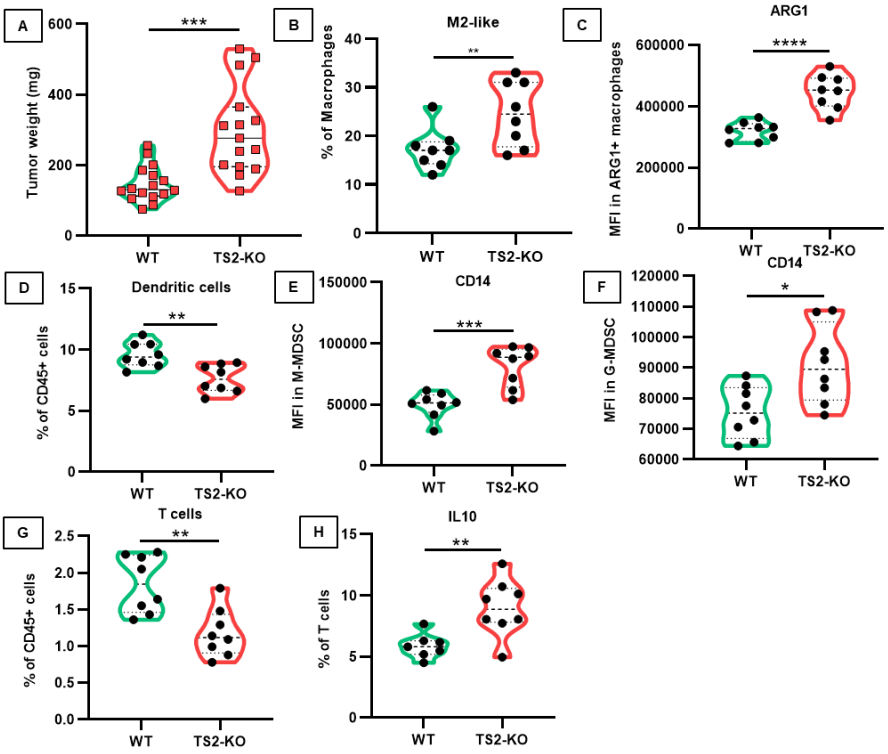

Figure 29: Immune cell populations infiltrating tumors 7 days after subcutaneous injection of PyMT cancer cells in WT and TS2-KO mice. Weights of tumors at sacrifice (7 days after injection) (A). Percentage among CD45+ cells of M2-like macrophages (B), dendritic cells (D) and T lymphocytes (G). Expression levels of arginase in macrophages (C) and of CD14 in M- and G-MDSC (E-F). Percentage of $IL10^{+}$ cells in T cells (H).

To confirm the involvement of the immune system in the repressive role of ADAMTS2 on tumor growth, we generated LLC conditionnally expressing ADAMTS2 or EGFP upon doxycycline treatment. These modified cell lines were injected subcutaneousy into NOD-SCID mice (lack of adaptive immunity), receiving or not doxycycline in their drinking water. Tumors from LLC able to conditionnally express ADAMTS2 (Figure 30.A) grew significantly slower in mice exposed to doxycycline. Such effects was not observed with cells conditionnally expressing EGFP (Figure 30.B), indicating that ADAMTS2 is able to repress tumor growth in the absence of adaptive immunity.

We repeated this experiment in NOD-SCID gamma (NSG) mice, which represent one of the most immunocompromised models due to the lack of IL2gamma receptor. In these mice, tumor growth was not repressed by the induction of ADAMTS2 expression (Figure 30.C), indicating that immune cells which are more affected in NSG than in NOD-SCID mice (NK cells, macrophages, …), are the likely mediators of the effect of ADAMTS2 on tumor growth.

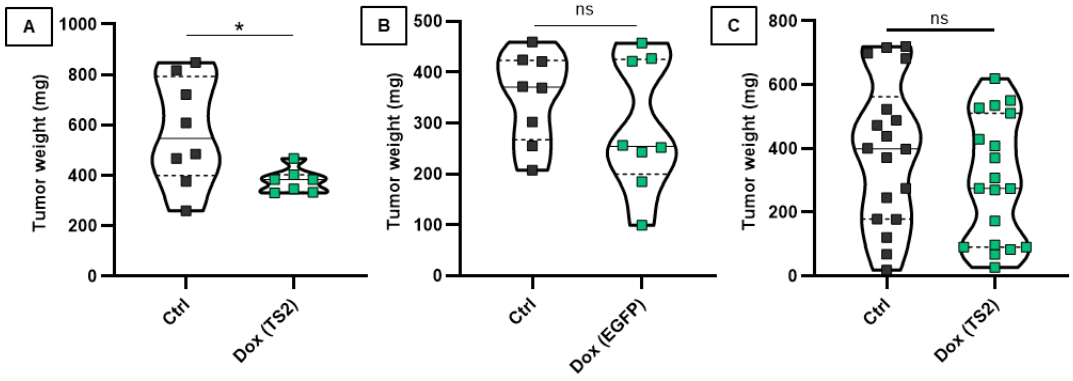

Figure 30: ADAMTS2 impacts tumor growth in an innate immune system dependent manner
Weights of tumors induced in NOD-SCID (A, B) or NSG (C) mice by subcutaneous injection of LLC cells conditionally expressing ADAMTS2 (A, C) or EGFP (B). Mice received or not doxycycline (Dox) in their drinking water.

In this work, multiple *in vivo* models have clearly showed that ADAMTS2 is a tumor suppressive enzyme, independently of the cancer type (lung carcinoma, melanoma, breast cancer) and the desmoplastic status (B16F10 and LLC vs PyMT tumors). This effect is not linked to previously known functions of ADAMTS2 (aminoprocollagen processing, angiogenesis, lymphangiogenesis). Instead, we showed that ADAMTS2 reduces tumor growth through the immune system by reducing the immunosuppression in the TME.

You can find the latest version of our manuscript for publication that includes the bulk of our research on the role of ADAMTS2 in tumor development from page 115 to page 160. The references of the thesis and the manuscript have been merged and can be found at the end of this document.

The ADAMTS2 Metalloproteinase Inhibits Tumor Growth By Regulating The Innate Immune System

Loïc Joannes[1], Laura Dupont[1,2], Louis Stock[1], Esther Arpigny[1], Pascale Hubert[3], Marie Ancion[3], Margaux Luyckx[3], Joan Abinet[4,5], Wen Peng[4,5], Christophe Deroanne[1], Agnes Noel[2], Thomas Marichal[4,5,6], Michael Herfs[3] and Alain Colige[1]

[1]Laboratory of Connective Tissues Biology, GIGA Institute, University of Liège, Liège, Belgium.

[2]Laboratory of Tumor and Development Biology, GIGA Institute, University of Liège, Liège, Belgium.

[3]Laboratory of Experimental Pathology, GIGA Institute, University of Liège, Liège, Belgium.

[4]Laboratory of Immunophysiology, GIGA Institute, University of Liège, Liège, Belgium.

[5]Faculty of Veterinary Medicine, University of Liège, Liège, Belgium

[6]Walloon Excellence in Life Sciences and Biotechnology (WELBIO) Department, WEL Research Institute, 1300 Wavre, Belgium.

Authorship note: LJ and LD contributed equally to this work

Address correspondence to: Alain Colige. Avenue Hippocrate n° 13 B23/+3, 4000 Liège, Belgium. Phone: +32 4 366 27 38. Email: acolige@uliege.be

Abstract

ADAMTS2 is a metalloproteinase involved in fibrillar collagen maturation and lymphatic vessel homeostasis. Exploration of human cancer datasets shows correlations between ADAMTS2 expression in primary tumors and overall survival for several cancer types, suggesting its involvement in cancer progression. This hypothesis was evaluated here both *in vitro* and in several mouse models *in vivo*. We have demonstrated that the growth of primary tumors is strongly enhanced in ADAMTS2-KO mice, as compared to wild-type mice, identifying ADAMTS2 as an anti-tumor proteinase. In contrast, the spread of metastases is virtually prevented in ADAMTS2-KO mice, showing a dual role of ADAMTS2, either beneficial or detrimental, at different steps of cancer progression. Additional investigations have shown that the effect of ADAMTS2 on primary tumor is not related to collagen biology or to a direct effect on mesenchymal or cancer cells. Rather, we have demonstrated that the innate immune system is involved, and that tumor-infiltrating immune cells possess a more immunosuppressive polarization in the absence of ADAMTS2, explaining the increased tumor growth in ADAMTS2-KO mice. In summary, our data show that ADAMTS2 exerts anti-tumor activity by inducing an immunotolerant tumor microenvironment.

Background

The tumor microenvironment is now considered a key element regulating the growth of the primary tumor and also participating in metastasis spreading. In addition to cancer cells, it also contains endothelial cells, different types of cancer-associated fibroblasts (CAFs) and immune cells, notably macrophages. Tumor associated macrophages (TAMs) can, depending on their specific polarisations, either promote or inhibit cancer progression. Another crucial component of the TME is the extracellular matrix (ECM) since its composition (collagens …), structure (fibrils …) and properties (stiffness) strongly influence the phenotype of residing cells, resistance to therapy and the capacity of immune cells to counteract tumor progression. To add to the complexity, the TME evolves over time due to its continuous remodeling by complex feedback loops involving interactions between ECM components and resident cells.

ADAMTS2 is a metalloproteinase originally identified by its ability to excise the NH2-terminal domain of fibrillar procollagens, a critical step in the process of collagen fibril formation (62,65). It was later shown to be involved in liver fibrosis (91), lymphatics homeostasis (269) and atopic dermatitis (87). Other functions and features have been highlighted, such as its capacity to cleave additional substrates, including fibronectin, reelin and various factors of the TGF-β pathway (DKK3, LTBP1, TGFβ-R3) (120,84,128). Interestingly, ADAMTS2 is not only expressed by mesenchymal cells, but can also be produced by blood monocytes (105) and macrophages (108), especially following glucocorticoids treatment (110,270,271).

Considering that each of these properties could potentially affect the TME, and also the fact that several publications identified ADAMTS2 as a relevant prognosis biomarkers for several types of cancer (119,245,247,248,272), we decided to evaluate its involvement in cancer progression.

Methods

Cell culture

HEK293, B16F10, LLC, MMTV-PyMT cancer cells, L929 and BMDMs were cultured in normoxia at 5 % CO_2, 37°C in a water saturated environment. MMTV-PyMT CAFs were cultured in hypoxia (5 % O_2) at 5 % CO_2, 37°C in a water saturated environment. Unless specified, cells are cultured in DMEM (Biowest, L0103-500) with penicillin and streptomycin (Gibco, 15140-122), 10 % FBS (Gibco, 10270-1060) and non-essential amino acids (Biowest, X0557-100) in polystyrene (PE) culture plates. HEK293, LLC and B16F10 were modified by lentivirus containing a reverse tetracycline-controlled transactivator 3 (rtTA3) with cytomegalovirus (CMV) promotor plasmid (tetracycline TET on system) containing either an ADAMTS2 or EGFP transgene.

Transgenic mice

Male C57BL/6 WT and TS2-KO, FVB/N WT and TS2-KO, Nude mice, NOD scid mice and NSG mice were used in this study at 8 to 12 weeks of age. Female MMTV-PyMT FVB/N WT and TS2-KO mice were sacrificed when they reached the ethical endpoint for tumor size (from 55 to 111 days). C57BL/6 TS2-KO mice have been described previously (273). They were used to generated FVB/N TS2-KO (through 7 backcrossing). WT and TS2-KO mice are generated by the crossing of heterozygous male and female mice and are thus, for every experiment, littermates. The animals were maintained on a 12-hour-light/dark cycle with free access to food and water.

RT-qPCR

RNA from cells and tumors were isolated using Nucleospin RNA extraction kit (Macherey Nagel, 740955.50). Reverse transcription was performed using PrimeScript™ RT reagent Kit (Takara Bio, RR037A). qPCR analyses were performed using Mesa green qPCR Mastermix plus low Rox (Eurogentec, RT-SY2X-03+WOULR) and Quantstudio 1 (Applied Biosystems). cDNA amplifications were performed with primers (Eurogentec) listed in Supplementary table 5.

Visualization of collagen maturation

Tumors were crushed at liquid nitrogen temperature in a “dismembrator” (Braun) and washed in 10 mM EDTA (pH 8.0). After centrifugation (20 minutes, 20 000 g), pellets were suspended in 0.1 N acetic acid (10µl/mg) and incubated overnight at 4°C. After centrifugation (20 minutes, 20 000 g), supernatants were neutralized (1:10 volume of 1 M Tris) before ethanol precipitation (30 % final volume, centrifugation at 20000 g for 20 min). Pellets were then solubilized in 2 % SDS loading buffer and heat-denaturated. Proteins were separated by SDS-PAGE before in-gel Coomassie blue staining or transfer on nitrocellulose membrane (Perkin Elmer, NBA085B001EA) for Western blotting analysis. Membranes were blocked using milk proteins in Tris buffer saline with 0.1 % Tween-20. Type I collagen immunolabeling was performed using an anti-collagen I antibody (Merck, AB765) and anti-rabbit antibody coupled to HRP (Agilent, P0399) and incubation in ECL. Visualization of HRP activity was done with Image Quant800 (Cytiva, Amersham).

Subcutaneous tumor growth models

Cells were cultured during 48 hours in culture medium w/o or w/ 1 µg/ml doxycycline hyclate (Sigma #D9891, St. Louis MO, USA) in order to induce the expression of recombinant proteins (ADAMTS2 or EGFP). For subcutaneous injections, HEK 293 cells (2 X 10^6) were suspended in 200 µl of 1:1 solution of DMEM (Biowest, L0103-500) and Matrigel™. LLC (1 X 10^5 cells), B16F10 (1 X 10^5 cells) and PyMT cancer cells (5 X 10^5 (14-days tumors) or 1 X 10^6 (7-days tumors cells) were suspended in 100 µl of DMEM before injection. Mice received drinking water *ad libitum* containing (or not) 2 mg/ml doxycycline hyclate (Sigma #D9891, St. Louis MO, USA). The water was changed three times a week for the duration of the experiments. Tumor were weighted directly after their recovery. Once a tumor reached >1 cm^3 (measured using caliper), in accordance with the ethic comity, the experiments were stopped, mice were sacrificed and tumor weighted.

Flow cytometry analysis on tumors

Subcutaneous tumors from PyMT-TS2-KO cancer cells formed in FVB/N WT and TS2-KO mice were cut in small pieces before a 45-minutes digestion at 37°C in DMEM (Biowest, L0103-500) with 5 mg/ml collagenase (Sigma, C0130). The cell suspensions were centrifuged and erythrocytes lysis was performed with ACK buffer (Gibco, A10492-1) for 5 minutes at room temperature prior to filtration on 40 µm filters. Immune cells were enriched using CD45 positive selection kit (Invitrogen, 8802-686574). Anti-CD16/CD32 (clone 2.4G2, BD Biosciences) antibody was incubated with immune cells for 5 minutes on ice prior to extracellular protein hybridization with antibodies for 30 minutes in the dark on ice. Intracellular protein hybridization (40 minutes in the dark on ice) was performed after fixation of extracellular antibodies (eBiosciences, 00-822-49) and permeabilisation of cells (eBiosciences, 00-833-56). Cells were then incubated in 1% paraformaldehyde for 30 minutes and kept in 1% BSA 0.1% sodium azide. Flow cytometry analyses were performed using a Cytoflex flow cytometer and collected data were analyzed with CytExpert (Beckman Coulter). In order to properly segregate negative from positive cell populations, PMT voltages were set optimally. Cell fragments and debris were eliminated based on both forward-scatter and side-scatter values. Gating strategy has been previously described (274). Antibodies and associated fluorophores are listed in Supplementary table 5.

Immunofluorescence analyses:

Antigen de-masking was performed on fixed tissue section using Target Retrieval Solution (Dako, S1699) recommended procedure. Sections were then blocked with 10% BSA in PBS for 1 hour at room temperature prior to antibody hybridization. Cells plated on glass coverslip were fixed with 4% paraformaldehyde for 15 minutes at room temperature, blocked and permeabilized for 30 minutes at room temperature in 10% BSA 0.1% Triton X-100 in PBS prior to antibody hybridization. Primary antibodies were incubated overnight at 4°C and secondary antibodies for 1 hour at room temperature. Slides were mounted using Dako fluorescent mounting medium, scanned using a Nanozoomer 2.0 scanner (Hamamatsu) and visualized using NDPviewer (Hamamatsu). Coverslip

were mounted using Dako fluorescent mounting medium. Cells were visualized using Nikon Eclipe Ti.

Histological analyses:

Tissues were fixed in a 4 % paraformaldehyde solution and paraffin embedded. Tissue sections (5 µm) were deparaffined, rehydrated, and stained with hematoxylin and eosin (H&E) or picro-Sirius red for general histological examination.

The mean number of lung metastases for each condition was determined on 5 H&E stained sections of lung parenchyma, with a 25 µm spacing between each section.

Statistics:

Unless specified, statistical analysis was performed using T test. Results were illustrated with GraphPad Prism 8.0 and were expressed as medians with interquartile ranges. P values of less than 0.05 were considered significant (<0.0001 ****, 0.0001<0.001 ***, 0.001<0.01 **, 0.01<0.05 *). The experiments were not randomized. Analyses and quantifications were not blinded. Outliers were identified and removed with the ROUT Q=5% method.

Results

ADAMTS2 expression affects overall survival of cancer patients

As a first evaluation of the existence of a potential pro- or anti-tumor role of ADAMTS2, we screened the pan-cancer RNA-seq TCGA repository and correlated the ADAMTS2 expression level to the overall survival of patients using the Kaplan Meier plotter tool (275) and the GEPIA webserver. In these analyses, high expression of ADAMTS2 correlates with reduced overall survival for most cancers (Figure 1.A and 1.C) (Supplementary table 1). To evaluate the role of ADAMTS2 in cancer development apart from its implication in desmoplasia, a similar analysis was repeated but using COL1A1 expression for normalization purposes. For most cancer types, normalization completely reversed the correlations (Figure 1.B and 1.D) (Supplementary table 1), suggesting that ADAMTS2 has anti-cancer activities besides its indirect pro-tumor role related to desmoplasia.

Tumor growth is increased in ADAMTS2 knockout mice and repressed by expression of recombinant ADAMTS2.

To evaluate whether ADAMTS2 can regulate tumor growth independently of desmoplasia, we used syngeneic tumor models devoid of collagen accumulation and desmoplastic reaction. Lewis Lung Carcinoma (LLC) and B16F10 melanoma (B16) cells were first engineered to conditionally express ADAMTS2 upon exposure to doxycycline. Despite strong induction of ADAMTS2 expression by doxycycline, at both the mRNA and protein levels (Supplementary figure 1.A and 1.B), the proliferation and migration rates were not impacted (Supplementary figure 1.C and 1.D), suggesting that ADAMTS2 does not have a direct effect on cancer cells.

These cells were injected subcutaneously in either C57BL/6 *Adamts2*$^{+/+}$ (wild type, WT) or *Adamts2*$^{-/-}$ mice (TS2-KO). TS2-KO mice were further divided in two cohorts receiving either regular drinking water or water supplemented with doxycycline to induce the expression of

recombinant ADAMTS2. LLC and B16 tumors were collected and weighed after 14 days and 21 days, respectively. Tumors were almost twice as big in TS2-KO mice as compared to WT mice (Figure 2.A and 2.B). Induction of ADAMTS2 expression reduced tumor size in TS2-KO mice to a weight similar to that of WT mice (Figure 2.A and 2.B) suggesting that ADAMTS2 has anti-cancer properties. To rule out the possibility of a direct effect of doxycycline *in vivo*, a similar experiment was repeated with LLC cells conditionally expressing EGFP, rather than ADAMTS2. In this model, doxycycline treatment failed to reduce tumor growth in TS2-KO mice (Supplementary figure 2).

All the tumors were collected and evaluated on histological sections. They were, however, too heterogeneous to allow any further characterizations and comparisons (Supplementary figure 3.A and B).

The growth of spontaneous breast tumors is increased while lung metastatic spread is repressed in TS2-KO mice

Subcutaneous tumors resulting from the injection of cancer cells represent a convenient experimental model, but only partially mimic human pathology. We therefore used the MMTV-PyMT (PyMT) mouse model characterized by the development of spontaneous mammary tumors (276). Since this model is heterogeneous in terms of tumor growth, mice could not be sacrificed at the same time, but were instead followed individually and euthanatized once the ethical endpoint for tumor size was reached.

For PyMT-WT mice, the first mouse was sacrificed on day 79, and 50% of mice had to be sacrificed by day 95. In contrast, for PyMT-TS2-KO mouse, the first mouse was euthanized on day 55, and 90% of mice had already been sacrificed by day 95 (Figure 2.C), thus confirming that ADAMTS2 inhibits tumor growth.

In the PyMT model, lungs are the preferred sites of tumor dissemination. Metastatic spread was quantified by metastatic foci on H&E stained lung sections. Remarkably, the number of metastatic

foci was much higher in PyMT-WT mice (2.3 metastases per section, on average) than in PyMT-TS2-KO mice (0.18 metastases per section, with around 60% of sections being metastases-free) (Figure 2.D). These results indicate that ADAMTS2 is essential for efficient metastasis dissemination, although it limits the growth of the primary tumors.

Absence of ADAMTS2 does not affect the transcriptome of CAFs, nor that of MMTV-PyMT cells

PyMT cancer cells and CAFs from tumors formed in PyMT-WT and PyMT-TS2-KO were separated from each other (Supplementary figure 4.A and 4.B) and analyzed by bulk RNA-Seq. As expected, cancer cells and CAFs were characterized by high expression of, respectively, epithelial (e.g. EPCAM, KRT8, KRT18, KRT7) (Supplementary table 2) and mesenchymal (e.g. COL1a1, COL1a2, FN, LOX) markers (Supplementary table 3). However, no specific signature could be demonstrated in cancer cells and CAFs recovered from tumors formed in PyMT-TS2-KO mice compared to PyMT-WT mice (Supplementary figure 4.C and 4.D).

ADAMTS2 suppresses tumor growth independently of vascularization and collagen processing.

Long-term cultures of PyMT cancer cells were established as stable cell populations from PyMT-WT and PyMT-TS2-KO tumors (Supplementary figure 5). They were used to induce subcutaneous tumors in WT or TS2-KO FVB/N mice. Tumors formed by PyMT-WT cancer cells grew much faster in TS2-KO mice (median of 383 mg) as compared to WT mice (median of 122 mg). Similar data were obtained using PyMT-TS2-KO cancer cells (median of 349 mg in TS2-KO versus 156 mg in WT mice), again showing that ADAMTS2 present in the TME represses tumor growth (Figure 3.A).

On histological sections, all these tumors appear similar, being highly homogeneous and devoid of hemorrhages and necrosis (Supplementary figure 3.D). They also display a homogeneous desmoplastic reaction (Figure 4.A and 4.B) characterized by a dense extracellular matrix and the

presence of PyMT cancer cells with a clear mesenchymal phenotype, with most cells being vimentin-positive and only a few dispersed Epcam-positive epithelial clusters (Supplementary figure 6). No significant difference could be identified neither in terms of tumor vascularization (Figure 4.C) or apoptosis and proliferation of cancer cells (Figure 4.D and 4.E), suggesting that the primary cause of the observed tumor growth differences manifests earlier.

Collagen deposition was also evaluated since the primary described function of ADAMTS2 is directly linked to collagen processing and fibril formation. A similar dense collagen network was identified in the 4 experimental conditions (PyMT-WT or PyMT-TS2-KO cancer cells forming tumors in WT and TS2-KO mice), with thick fibrils widely aligned with each other as in fibrotic tissue (Figure 4.B). RT-qPCR quantifications also indicate that most of the ADAMTS2 expression originates from the host, although PyMT-WT cancer cells, due to their mesenchymal phenotype, can also express some levels (Figure 3.B). The pattern of type I collagen chains was also determined. Collagen was fully converted to alpha chains under all conditions, except in tumors formed by PyMT-TS2-KO cancer cells in TS2-KO mice where about 20% of type I collagen was found as pNIa1 and pNIa2 (Figure 3.C). Since the size of tumors formed from control PyMT-WT and PyMT-TS2-KO cancer cells are similarly increased in TS2-KO mice as compared to WT mice (Figure 3.A, lanes 2 and 4 compared to lanes 1 and 3), this proves that defects in aminoprocollagen processing are not the cause of the increased tumor growth in TS2-KO mice.

Single-cell RNA sequencing revealed that ADAMTS2 modifies macrophages polarization in the TME

Single cell suspension from PyMT tumors formed in WT and TS2-KO mice were separated into immune ($CD45^+$) and non-immune ($CD45^-$) cell populations (Supplementary figure 7.A) before single-cell RNA-Sequencing. An automatic clustering of cells independently of the genotype of the host revealed that most cells were cancers cells in the $CD45^-$ population and macrophages in the $CD45^+$ immune cells (Supplementary figure 7.B).

Re-clustering of macrophages and cancer cells were then performed to evaluate specifically potential differences between tumors formed in WT and TS2-KO mice. Cancer cells clustering revealed 6 largely overlapping sub-clusters, none of which displayed clear relative abundance variation between cancer cells from WT and TS2-KO mice (Supplementary figure 8.A), suggesting that cancer cells are unaffected by the absence of ADAMTS2 at this tumor stage. Seven macrophages sub-clusters were identified (Supplementary figure 8.B), of which two were slightly decreased (cluster 0 and 1) and one increased (cluster 3) in TS2-KO mice (Supplementary figure 8.C). Interestingly, clusters 0 and 1 display a M1-like polarization, whereas cluster 3 is composed of macrophages with a more M2-like polarization (Supplementary table 4) which is considered to favor tumor progression.

The TME is more immunosuppressive in TS2-KO mice

Based on these data, we then characterized immune cells present in tumors collected at day 14, as for scRNA-Seq, and at day 7, in order to identify potential earlier modulations. FACS analysis confirmed the high abundance of macrophages in “day-14” tumors. However, no difference could be highlighted between tumors formed in WT and TS2-KO mice, beside a trend ($p<0.06$) towards increased M2-like macrophages in TS2-KO (Supplementary figure 9.A), in line with our scRNA-Seq data. No other difference could be observed regarding dendritic cells abundance, activation (CD80 and CD86) or inhibition (ILT3) (Supplementary figure 9.B), or to T cells abundance (Supplementary figure 9.C).

As early as 7-day post-injection, tumor growth differences were already apparent between tumors formed in WT and TS2-KO mice (Figure 5.A), confirming the implication of an early mechanism. Overall immune cell infiltration was unchanged in tumors from WT and TS2-KO mice, with a high proportion of macrophages among $CD45^+$ cells (Figure 5.B and V.C). The percentage of M1-like macrophages was twice as high at day 7 as compared to day 14 (around 40% versus 20%), illustrating a less repressed immune response at this early stage (Figure 5.D and Supplementary

figure 9.A). Most interestingly, a more pronounced polarization towards an M2-like phenotype was observed in TS2-KO as compared to WT mice (25% vs 18%, $p<0.01$) (Figure 5.E). We also noted increased expressions of ARG1 by macrophages (Figure 5.F) and of CD14 by both M-MSDC and G-MDSC (Figure 5.G and V.H), a reduced abundance of dendritic cells (Figure 5.I) and T cells (Figure 5.J) and an increased proportion of $IL10^{+}$ lymphocytes (Figure 5.K), which indicates a globally suppressed immune system in tumors formed in TS2-KO mice that could explain the increased tumor growth.

ADAMTS2 has no direct effect on the differentiation and polarization of BMDMs *in vitro*

In order to determine whether ADAMTS2 has direct regulatory functions on macrophages, we used bone marrow-derived macrophages (BMDMs) from WT and TS2-KO mice. Polarization into M1- (treatment with LPS and IFN-y) and M2-like phenotypes (IL4) were similar for both genotype (Supplementary figure 10). Similarly, treatment of BMDMs with ADAMTS2 did not affect their phenotypes (Supplementary figure 11).

ADAMTS2 suppresses tumor growth via the innate immune system

We then evaluated tumor growth in mouse strains with increased immuno-deficiency. In nude mice, expression of ADAMTS2 represses tumor growth (Figure 6.A), showing that T lymphocytes are not involved. In NOD scid mice (absence of B and T lymphocytes, and some impairment of the innate immune system), induction of ADAMTS2 by doxycycline still significantly reduced tumor growth, while induction of EGFP, used as a negative control, had no effect (Figure 6.B and 6.C). When NSG mice were used, the growth inhibitory effect of ADAMTS2 could no longer be observed (Figure 6.D), likely suggesting a role for macrophages and/or NK cells in the anti-tumor properties of ADAMTS2.

Discussion

The tumor microenvironment, comprising the ECM and various types of “non-transformed” cells, is now recognized as an essential player in tumor progression and metastasis. The organization of the extracellular matrix and its regulatory functions depend not only on the production of extracellular matrix macromolecules by specific cells, but also on the secretion and activity of extracellular matrix-modifying enzymes such as metalloproteinases (MMPs, ADAMs and ADAMTSs). Several ADAMTS have been associated with oncogenic or tumor-protective functions, depending on the context (240), although most of these studies were purely correlative. In a similar context, various ADAMTS genes have been shown to be overexpressed, mutated or silenced in tumors of diverse origins, again suggesting their involvement in cancer development (277). The primary identified function of ADAMTS2 is its capacity to excise the aminopropeptide of fibrillar collagens (26,76,278), but it was later shown to be involved in a more diverse array of functions potentially linked to tumor progression (21,119,128,269,279).

The implication of ADAMTS2 in cancer was first evaluated through *in silico* correlation between its tumoral expression and overall survival of human patients. A trend or a significant association was found between high ADAMTS2 expression and reduced survival. As this could result from its increased expression during desmoplasia which is often of poor prognosis (177), similar analyses were therefore repeated after normalization of ADAMTS2 expression by that of COL1A1. This normalization not only abolished the negative correlation between ADAMTS2 expression and survival but even reversed it, suggesting antitumor activity of ADAMTS2, apart from its function linked to desmoplasia and extracellular matrix accumulation.

To evaluate this hypothesis, TS2-KO mice and their WT controls were subcutaneously injected with syngeneic B16 and LLC cancer cells, which are known to induce the formation of fast growing tumors lacking significant collagen deposition and extracellular matrix accumulation. For both cell lines, tumor growth was much faster in TS2-KO mice. Moreover, this phenotype could be

suppressed by induction of recombinant ADAMTS2 expression by cancer cells, which confirmed the anti-tumor activity of ADAMTS2. Interestingly, *in vitro* studies using these inducible LLC and B16 cell lines failed to show a direct effect of ADAMTS2 on cancer cell proliferation, suggesting that its anti-tumor function is mediated by the TME.

To evaluate the impact of ADAMTS2 on a slower and more physiological tumor growth model, we used MMTV-PyMT mice which develop spontaneous mammary tumors with relevance to breast cancer development stages found in human (276). 50% of MMTV-PyMT-WT mice were sacrificed at 13.5 weeks of age when reaching ethical endpoint for tumor size, in line with literature data (280). Remarkably, age at euthanasia was significantly reduced by more than a week in PyMT-TS2-KO mice. These data confirmed the antitumor properties of ADAMTS2 in a spontaneous cancer model, but also demonstrated that this effect is not tumor type-dependent, in line with our preliminary *in silico* data (Figure 1) (Supplementary table 1).

This model of spontaneous breast tumors was further studied to identify how ADAMTS2 might regulate tumor growth. However, high heterogeneity in the TME, in terms of collagen content and organization, angiogenesis or necrosis, among others, prevented the identification of the mechanisms regulated differently in PyMT-WT and PyMT-TS2-KO mice. Similarly, bulk transcriptomic analyses of cancer cells and CAFs isolated from primary tumors failed to reveal any differences induced by the absence of ADAMTS2. This suggests that CAF and cancer cells are not the primary targets of ADAMTS2-mediated regulation or that they exhibit polarization or differentiation diversities far too high to allow the identification of regulatory mechanisms affecting only sub-populations of cells.

To solve this problem, we generated a less heterogeneous tumor model. We first established cultures of MMTV-PyMT cancer cell from spontaneous tumors forming in several PyMT-WT and PyMT-TS2-KO mice. After stabilization in culture, WT and TS2-KO cell lines showed a similar epithelioid phenotype and identical proliferation rates. After injection in WT or TS2-KO mice, they

all lead to the formation of highly homogeneous tumors, characterized by the formation of a TME highly enriched in collagen and by a marked mesenchymal polarization of PyMT cancer cells. As in the other models, tumor growth was faster in TS2-KO mice, regardless of whether the cancer cells were WT or TS2-KO. This demonstrated that ADAMTS2 secreted by the host can inhibit tumor growth, even in a model characterized by desmoplastic reaction, confirming the existence of collagen-independent functions of ADAMTS2. Further immuno-histological characterizations failed to identify significant differences between tumors formed in WT and TS2-KO mice but revealed the presence of numerous immune cells. scRNA-Seq was performed on 2-week-old tumors, a time when tumors are well formed and reach the size ethical endpoint. Similar populations of MMTV-PyMT cancer cells were detected in WT and TS2-KO mice. Regarding immune cells, they were mainly composed of macrophages, whose sub-clustering was suggestive of a more immunosuppressive microenvironment in tumors harvested from TS2-KO mice.

These data prompted us to further characterize the tumor immune cell population, at two weeks as for scRNA-Seq, and at an earlier time point to possibly identify some earlier crucial but transient regulations. FACS analyses of two-week-old tumors confirmed some immunosuppressive environment in the absence of ADAMTS2, with a slight increase in the M2-type macrophage population, but failed to identify any marked differences. By day 7, however, several key factors repressing the anti-tumor response were increased in TS2-KO mice, suggesting that the absence of ADAMTS2 leads to a more rapid switch from an initial anti-tumor response to a more immune-tolerant TME. Identifying the key upstream pathway involved and how it can be regulated by ADAMTS2 could therefore lead to a better understanding of the global anti-tumor response program and, potentially, to improved immune therapy against cancer.

Additional experiments were therefore carried out to further characterize the anti-tumor function of ADAMTS2. As macrophages represent most of the infiltrating immune cells, their implication in the observed ADAMTS2-related regulation was therefore evaluated *in vitro*. “Bone marrow derived

macrophages" (BMDMs) were generated with similar efficiency from WT and TS2-KO mice, demonstrating that they are not intrinsically different and that their differential regulation by ADAMTS2 could occur at a later stage. They were incubated with recombinant ADAMTS2, but no significant effect on BMDM polarization could be identified, suggesting that regulations induced by ADAMTS2 on macrophages are indirect. It could result, for example, from the cleavage of a factor present in tumor *in vivo*, but absent *in vitro*, that would secondarily affect macrophage phenotype. As another hypothesis, it cannot be ruled out that the activity of ADAMTS2 could be greatly reduced *in vitro* due to the absence of a specific coactivator (150,281) or because the high local concentrations observed in tissues *in vivo*, notably close to the cell surface, cannot be reached *in vitro* in culture.

To validate the involvement of the immune system in the regulation of tumor growth by ADAMTS2, we then used mouse models with different degrees of immune system deficiency. In "Nude" mice, lacking T cells, tumor growth was found to be markedly inhibited in the cohort receiving doxycycline to induce ADAMTS2 expression. In NOD scid (lacking adaptive immunity and reduced innate immunity), reduction of tumor growth by ADAMTS2 was still significant, but seemed less efficient. Finally, this effect was completely absent in NSG mice (no functional B-, T- and NK-cells; strongly defective macrophages), demonstrating the implication of the innate immune system in the ADAMTS2-mediated repression of the primary tumor growth.

The data obtained in this study raise several related questions. Firstly, it would be very interesting to assess whether dysregulation of the innate immune system is limited to the tumor microenvironment or whether it is generalized to the whole organism. In some tissues, macrophages are abundant under physiological conditions, such as Kupffer cells in the liver or interstitial and alveolar macrophages in the lungs. Intriguingly, Kupffer cells and lung alveolar macrophages are among the cells expressing the highest levels of ADAMTS2, together with mesenchymal cells (see "The Human Protein Atlas" at www.proteinatlas.org). We characterized

the immune cells present in the lungs of WT and TS2-KO mice. These preliminary and exploratory data illustrate a significant increase in alveolar and interstitial macrophages in TS2-KO lungs (Supplementary figure 12.A), while monocytes and neutrophils are unaffected (Supplementary figure 12.C). Functionally, these macrophages appear to be slightly less pro-inflammatory (reduced iNOS) but also less anti-inflammatory (reduced Il10) (Supplementary figure 12.B). These data are intriguing, and efforts are currently underway to elucidate the mechanism involved. In these ongoing studies, we are attempting to identify ADAMTS2 substrates whose cleavage may be responsible for immune system dysfunction. Identifying “new” protease substrates is a difficult task without prior indication of their nature. This task is even more complicated in complex samples, such as tumors, containing different cell types and characterized by the presence of abundant proteins (from blood or the extracellular matrix) which prevent the identification of less abundant potential substrates. As examples of proteins that could be involved, COL5A1 is a minor fibrillar collagen recently identified as a key regulator of triple negative breast cancer growth by activating cancer cell-macrophage crosstalk (282). Several factors regulating the innate immune response (MBL, ficolins, MARCO, C1q) contain a triple helical domain such as found in collagens (6,283,284), and could therefore be considered as potential preferential substrates for ADAMTS2, with consequences for their functions.

Another surprising observation in our study is the near-absence of lung metastases in MMTV-PyMT-TS2-KO mice, despite significantly faster growth of the primary tumor. Identification of the process involved was hampered by the fact that a significant number of metastases were only observed in the spontaneous MMTV-PyMT model, and not in the more characterized and less heterogeneous subcutaneous models. Several hypotheses can be put forward regarding the link between ADAMTS2 and the spread of metastases. Lymph node endothelial cells and lung alveolar macrophages are amongst the few non mesenchymal cell types that express significant levels of ADAMTS2, and modifications of their phenotype could be involved (285). CD169/Siglec1^{+}

macrophages represent a specific subpopulation of macrophages that have been shown to be immuno-suppressive within the primary tumors, while protecting from metastases when present and active in the lymph nodes (286). Differential regulation of such specific macrophage populations in our different experimental models could contribute to our observation and will be further explored.

Overall, this study demonstrates that ADAMTS2 is a tumor-suppressive metalloproteinase *in vivo*. The mechanism involved is independent of a direct effect on cancer cells or stromal cells, or of modifications affecting the extracellular matrix. Rather, it depends on the innate immune system, probably through the cleavage of substrates that interact with macrophages or NK cells. Surprisingly, however, ADAMTS2 activity seems to be critically involved in metastasis spreading, identifying it as an enzyme with deleterious or beneficial functions for cancer patients, depending upon tumor stage.

Abbreviations

ARG1: arginase-1; **BMDM**: bone marrow derived macrophage; **CAF**: cancer-associated fibroblast; **ECM** : extracellular matrix; **GTEx**: genotype-tissue expression; **GEPIA**: gene expression profiling interactive analysis; **G-MDSC**: granulocytic myeloid derived suppressor cell; **iNOS**: inducible nitric oxide synthase; **LLC:** lewis lung carcinoma**; M-MDSC**: monocytic myeloid derived suppressor cell; **TCGA:** the cancer genome atlas; **TAILS**: terminal amine isotopic labeling of substrates; **TAM**: tumor-associated macrophage; **TS2-KO**: ADAMTS2 knockout

Declarations

Study approval:

All animal experiments were conducted at the GIGA Animal Facility of the University of Liège in accordance with the Federation of European Laboratory Animal Science Associations and after approval from the local ethical committee at the University of Liège (approval no. 1963,1964 and 2490).

Data availability:

All data relevant to the study are included in the article or can be uploaded as online supplemental information. Any further information about resources and reagents should be directly requested to the corresponding author and will be fulfilled on reasonable request.

Competing Interests

The authors declare that they have no competing interests.

Fundings

AC is “Senior Research Associate”, CD and MH are “Research Associate” of the Fund for Scientific Research — National Fund for Scientific Research (FRS-FNRS).

This work was supported by grants from Télévie (TLV7.65.12.2), FRS-FNRS (FC96394 and J.0034.24), the “Fonds spéciaux de la Recherche” (University of Liège), the “Fondation Hospitalo-Universitaire Léon Fredericq” (University of Liège), the “Walloon Region” through the “FRFS-WELBIO” strategic research program.

T.M. is supported by a FRFS-Welbio Advanced Grant (WELBIO-CR-2022A-10), by an ERC Starting Grant ERC StG 2018 (IM-ID: 801823) and by the Baillet Latour Biomedical Fund.

This work was also supported in part by the FNRS [CDR J.0088.21 (MH), AMG-ONCO P.A002.23 (MH)], the University of Liege [Crédits Sectoriels de Recherche en Sciences de la Santé 2021-2023 (MH)], the Télévie [PDR Televie 7.8505.22 (MH)] and the Leon Fredericq Foundation.

Author contributions

LJ designed, performed, and analyzed experiments and wrote the manuscript.

LD designed, performed, and analyzed experiments.

LS contributed to immunostaining and cell culture.

EA contributed to mouse breeding, handling and *in vivo* models

WP, PH, MA and ML contributed to flow cytometry analysis

JA performed the bioinformatics analysis on single cell RNA sequencing

CD, AN, TM and MH funded and supervised part of the project.

AC supervised, funded, and designed the project; interpreted the data; and wrote the manuscript.

Acknowledgments

We thank all laboratory members for useful technical advice.

We thank platforms of the GIGA Institute of the University of Liège (*In vitro* imaging, Viral vectors and gene editing, Bioinformatics, Genomics and Animal facility) for their technical support.

Expression of ADAMTS2 and overall survival

A

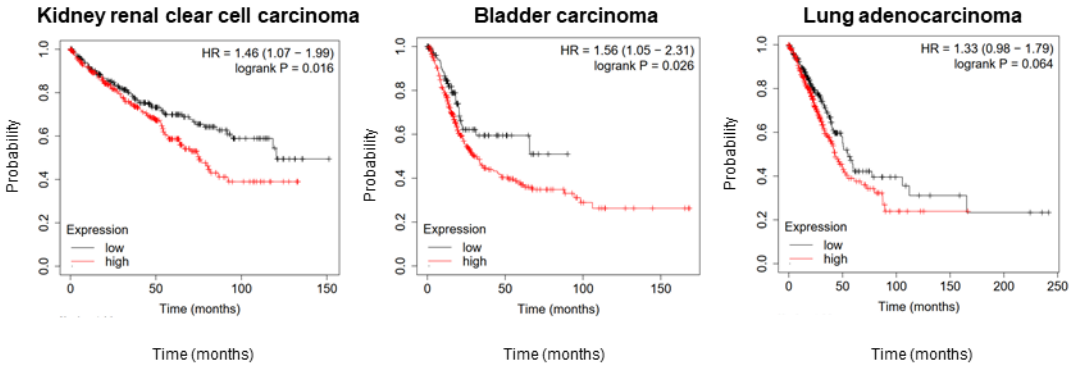

Expression of ADAMTS2 normalized to expression of COL1A1 and overall survival

B

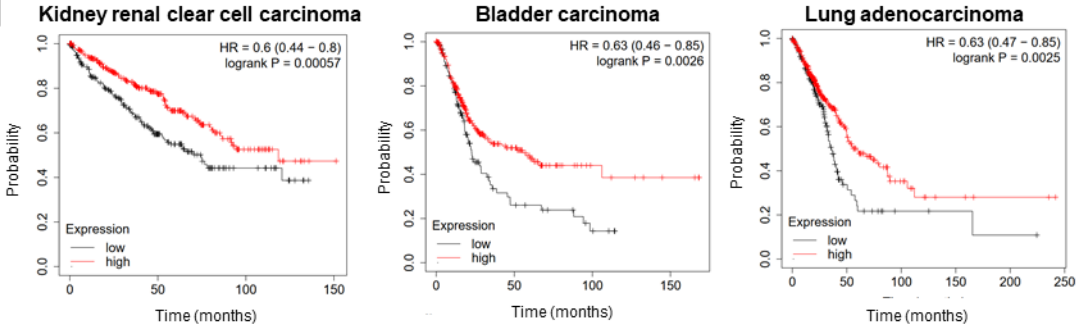

Pooled TCGA cancers

C

Expression of ADAMTS and overall survival

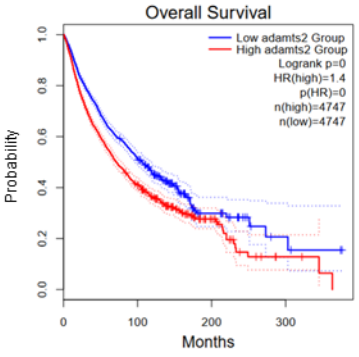

D

Expression of ADAMTS2 normalized to expression of COL1A1 and overall survival

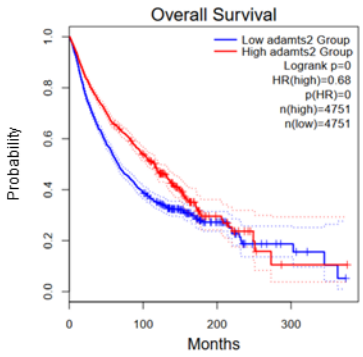

Figure 1

ADAMTS2 expression and patient overall survival

The “Kaplan Meier plotter” (Pan-cancer RNA-Seq) was used to evaluate overall survival of cancer patients expressing high (red) and low (blue) levels of ADAMTS2 in the primary tumors. (A) Data obtained for kidney renal clear cell carcinoma, bladder carcinoma and lung adenocarcinoma are provided as examples. (B) A similar correlation was established using COL1A1 as a reference for normalization purposes for desmoplasia. Correlations established for more cancer types are available as Supplementary table 1. Using “GEPIA” (a web server for cancer and normal gene expression profiling) all types of cancer were grouped as a single cohort and correlations between overall survival and ADAMTS2 expression were determined without (C) or with normalization to COL1A1 expression (D). HR: hazard ratio. OS: overall survival. P: p values.

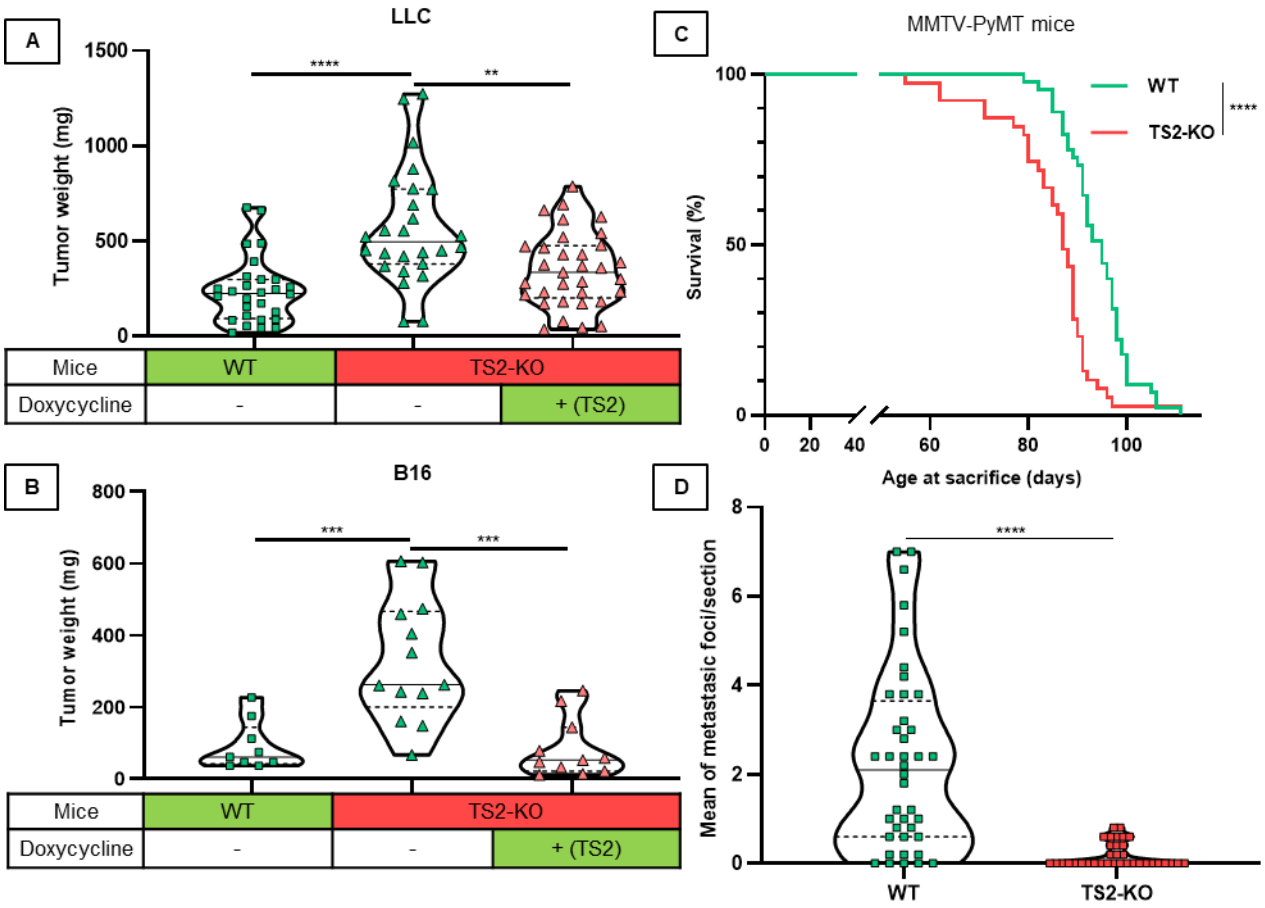
A
LLC
Tumor weight (mg)
1500
1000
500
0
****
**
Mice
WT
TS2-KO
Doxycycline
-
-
+ (TS2)
B
B16
Tumor weight (mg)
800
600
400
200
0
***
***
Mice
WT
TS2-KO
Doxycycline
-
-
+ (TS2)
C
MMTV-PyMT mice
Survival (%)
100
50
0
WT
TS2-KO
****
0
20
40
60
80
100
Age at sacrifice (days)
D
Mean of metastasic foci/section
8
6
4
2
0
****
WT
TS2-KO

Figure 2

ADAMTS2 is a tumor suppressor protein

LLC (A) and B16 (B) cells (modified to express recombinant ADAMTS2 upon treatment with doxycycline) were injected subcutaneously in WT or TS2-KO mice. Mice were given either control water or water supplemented with doxycycline to induce the expression of recombinant ADAMTS2 by cancer cells. Mice were sacrificed 14 days (A) or 21 days (B) after injection and tumors were weighed. Dots represent individual tumor weight, straight lines represent the median and dotted lines the quartiles. This experiment for LLC and B16 cells were performed 3 and 2 times respectively, the graph was made by pooling tumor weights from each experiments. Dox: doxycycline. (C) MMTV-PyMT mice expressing (WT, green) or not (TS2-KO, red) ADAMTS2 were followed individually and sacrificed once the ethical end point for tumor size was reached. Individual tumor weight at sacrifice are provided as Supplementary figure 12. The age at sacrifice (survival) was used to compare the rate of tumor growth between the two genotypes. Age at sacrifice was highly significantly reduced for TS2-KO mice. Statistical analysis were performed using Log-rank Mantel-Cox test (P value < 0.0001) and Gehan-Breslow-Wilcowon test (P value < 0.0001). (D) Comparison of the mean number of metastatic foci per representative lung section of PyMT-WT and PyMT-TS2-KO mice. Bars = 250 µm. A representative section stained for the presence of the MMTV-PyMT antigen is provided as Supplementary figure 3.E to confirm the metastatic nature of the cell clusters identified by HE staining.

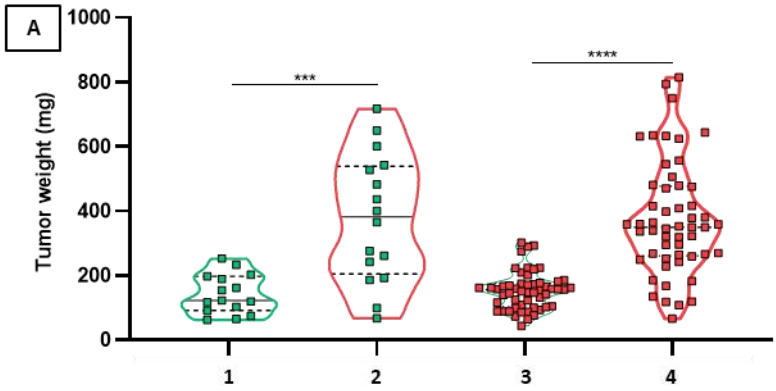

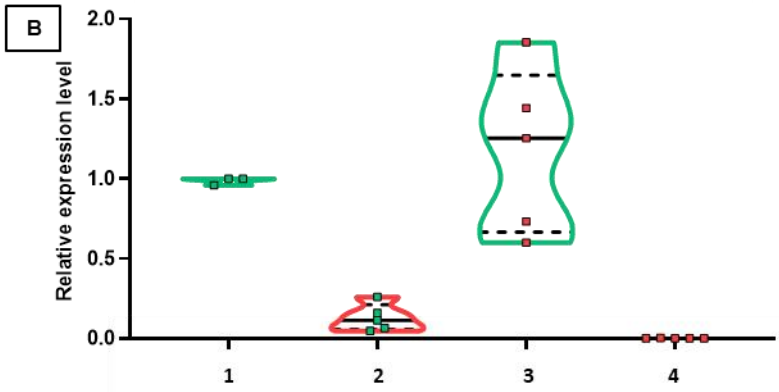

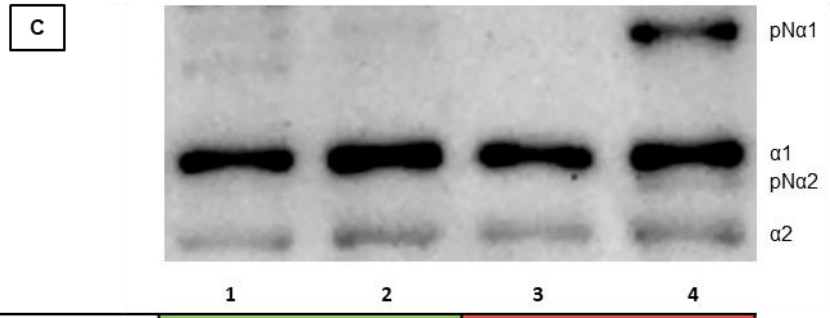

MMTV-PyMT cancer cells	WT		TS2-KO	
Mice	WT	TS2-KO	WT	TS2-KO

Figure 3

ADAMTS2 represses tumor growth independently of its aminoprocollagen activity

(A) Comparison of the subcutaneous tumor weight after injection of PyMT-WT and PyMT-TS2-KO cancer cells in WT and TS2-KO mice. (B) RT-qPCR evaluation of relative ADAMTS2 mRNA expression in subcutaneous tumors generated from PyMT-WT and PyMT-TS2-KO cancer cells in WT and TS2-KO mice. (C) Western blot analysis of the processing of type I collagen extracted from subcutaneous tumor generated by PyMT-WT and PyMT-TS2-KO cancer cells in WT and TS2-KO mice. pNα1: alpha 1 type I chain retaining its aminopropeptide. α1: fully processed alpha 1 type I chain. pNα2: alpha 2 type I chain retaining its aminopropeptide. α2: fully processed alpha 2 type I chain.

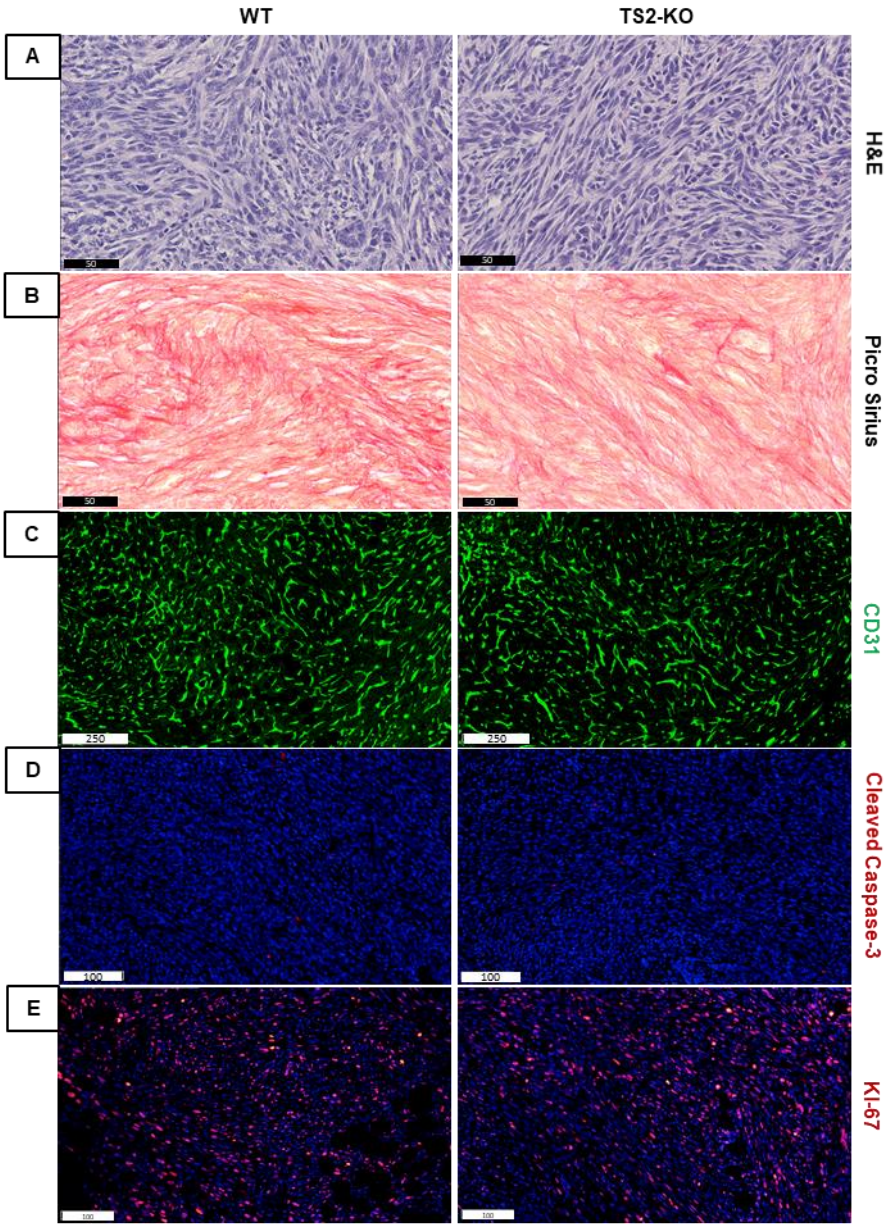
WT
TS2-KO
A
B
C
D
E
H&E
Picro Sirius
CD31
Cleaved Caspase-3
KI-67

Figure 4

The absence of ADAMTS2 does not impact collagen deposition, tumor vascularization, cancer cell proliferation or apoptosis

Representative picture of sections of subcutaneous PyMT tumors formed by PyMT-TS2-KO cancer cells in WT and TS2-KO mice, after H&E staining (A), Sirius red staining (for collagen fibrils) (B), CD31 immunolabeling (endothelial cells) (C), cleaved caspase-3 immunolabeling (D) and KI-67 immunolabeling (E).

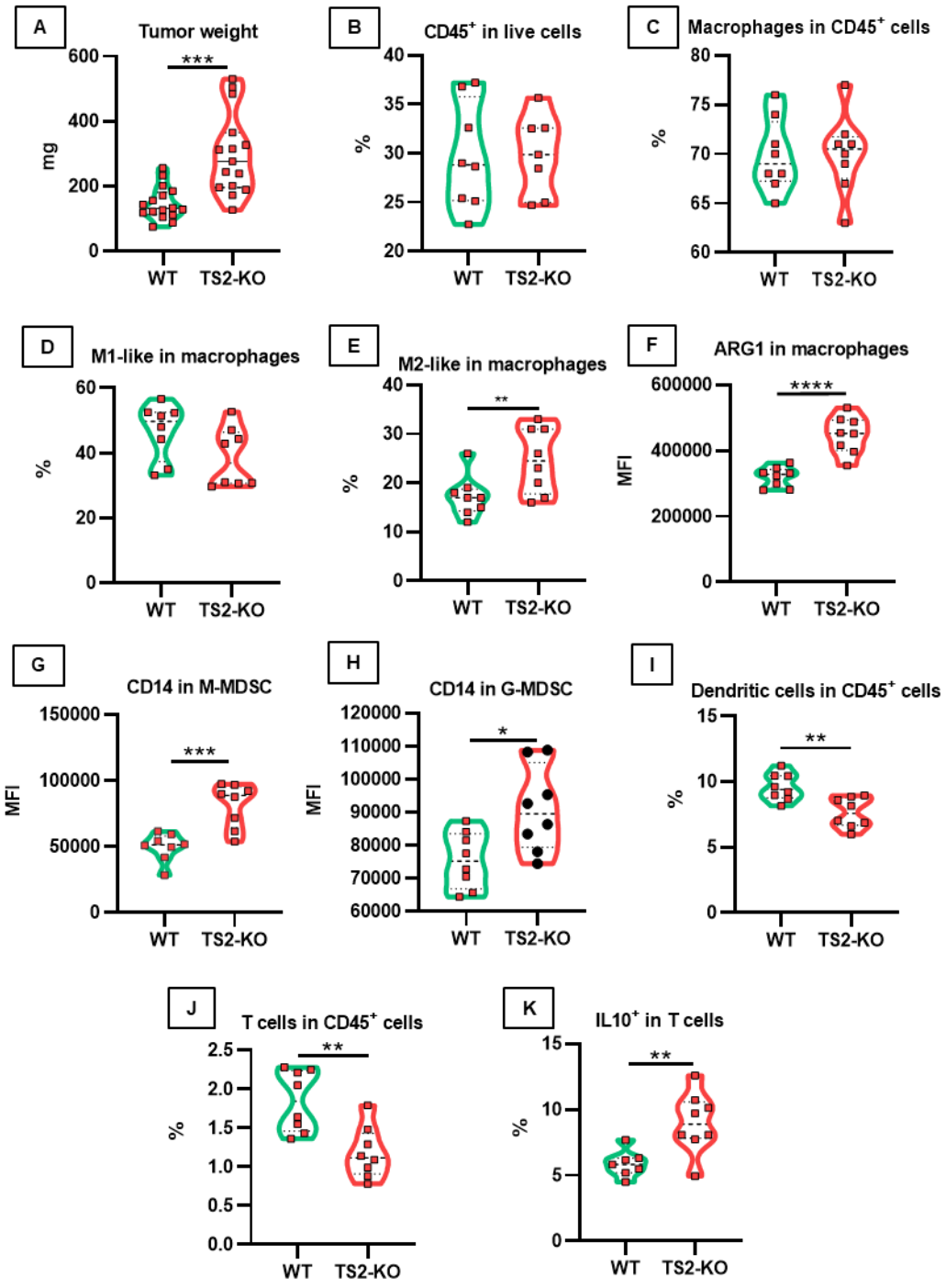
A
Tumor weight
***
mg
600
400
200
0
WT
TS2-KO
B
CD45+ in live cells
%
40
35
30
25
20
C
Macrophages in CD45+ cells
%
80
75
70
65
60
D
M1-like in macrophages
%
60
40
20
0
E
M2-like in macrophages
**
%
40
30
20
10
0
F
ARG1 in macrophages
****
MFI
600000
400000
200000
G
CD14 in M-MDSC
***
MFI
150000
100000
50000
H
CD14 in G-MDSC
*
MFI
120000
110000
100000
90000
80000
70000
60000
I
Dendritic cells in CD45+ cells
**
%
15
10
5
J
T cells in CD45+ cells
**
%
2.5
2.0
1.5
1.0
0.5
0.0
K
IL10+ in T cells
**
%
15
10
5

Figure 5

The absence of ADAMTS2 affects tumor growth and increases immunosuppressive markers in tumors formed after 7 days in TS2-KO mice

(A) Comparison of the subcutaneous tumor weight at 7 days post-injection of PyMT cancer cells in WT and TS2-KO mice. (B) Relative abundance (%) of $CD45^+$ cells within live cells. Relative abundance of (C) macrophages ($CD45^+$ $CD11b^+$ $F4/80^{high}$) within $CD45^+$ immune cells, and of (D) M1-like ($CD206^{low}$ $CD11c^{high}$) and (E) M2-like ($CD206^{high}$ $CD11c^{low}$) macrophages in the macrophage population present in 7-day tumors from WT and TS2-KO mice. (F) Mean fluorescence intensity (MFI) of arginase1 in macrophages, mean fluorescence intensity of CD14 in (G) M-MDSC and (H) G-MDSC, (I) relative abundance of dendritic cells within $CD45^+$ cells, (J) relative abundance of T cells in $CD45^+$ cells and (K) relative abundance of T cells expressing IL-10 in $CD3^+$ cells from subcutaneous PyMT tumors formed in WT and TS2-KO mice. ARG1: arginase1.

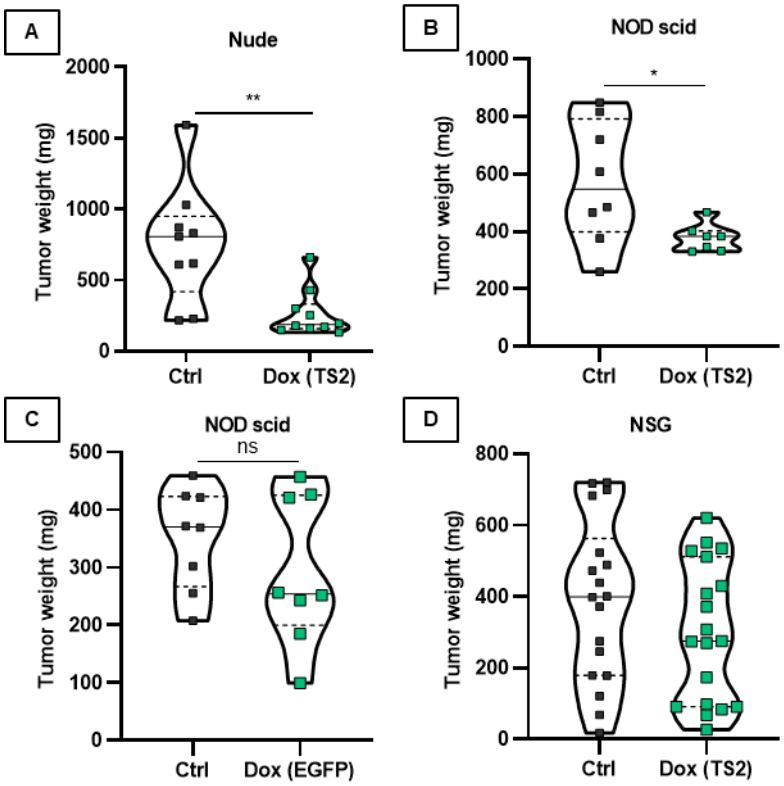

Figure 6

ADAMTS2 reduces tumor growth through a mechanism involving the innate immune system

Transformed cells conditionally expressing ADAMTS2 (A, B, D) or EGFP (C) were injected subcutaneously in nude mice (A), NOD scid (B-C) or NSG (D) mice. Mice were given either control water or water supplemented with doxycycline to induce the expression of recombinant ADAMTS2 (A-B-D) or EGFP (C) by cancer cells. HEK cells were injected in (A) and LLC in (B-D). Experiments were stopped and tumors were weighed at 21 days (A) or 14 days (B-D) after subcutaneous injection. Dots represent individual tumor weight, straight lines represent the median and dotted lines the quartiles. (A) and (D) graph results from the pooling of two distinct experiments. Dox: doxycycline.

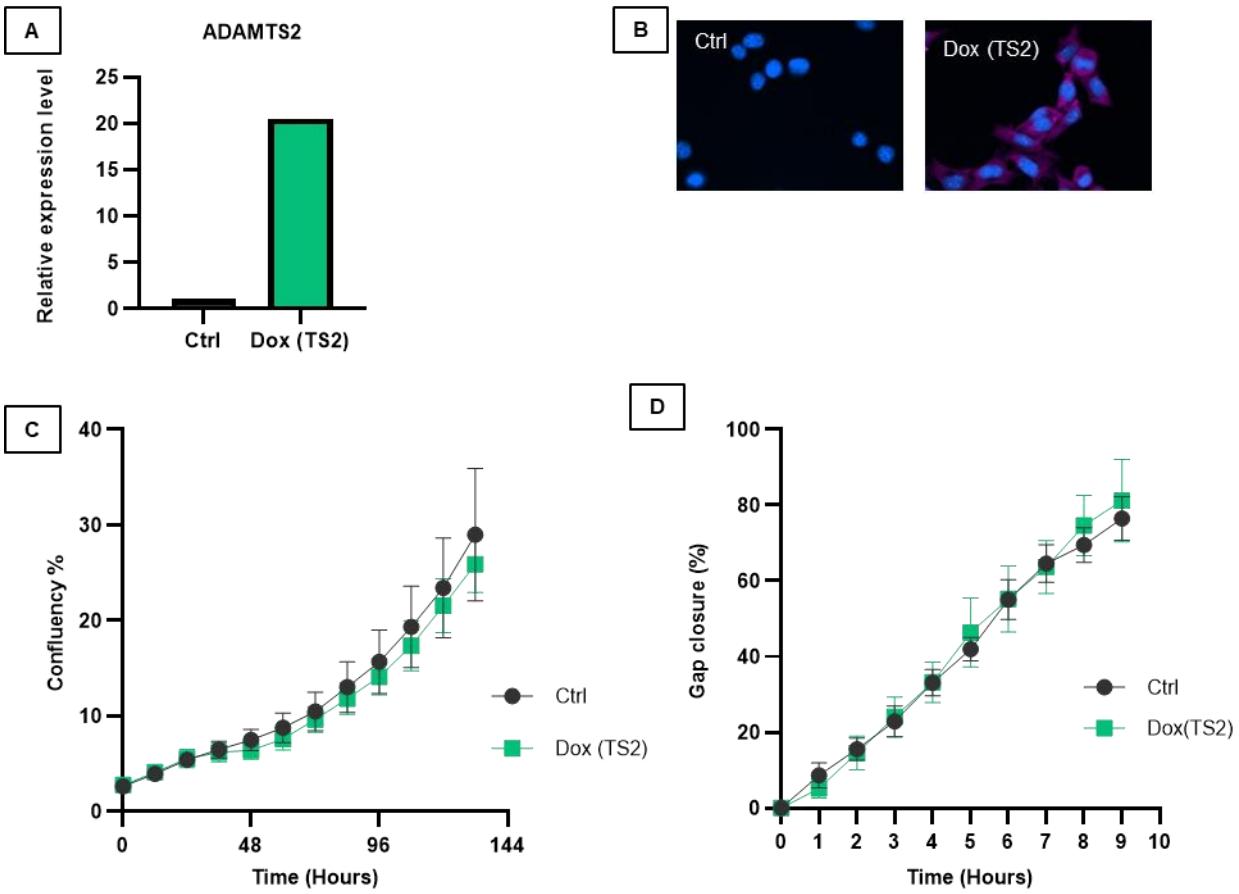

Supplementary figure 1

ADAMTS2 expression by cancer cells does not affect their migration or proliferation

(A) Quantification of ADAMTS2 expression by RT-qPCR in B16 cells cultured in absence (Ctrl) or presence of doxycycline (Dox) in the culture medium to induce the expression of recombinant ADAMTS2 (TS2). (B) Visualization, by immunofluorescence labeling, of ADAMTS2 expression in B16 cells in control condition or 48 h after addition of Dox. Quantification of B16 cell proliferation (C) and migration (D) with or without ADAMTS2 expression (Dox).

.

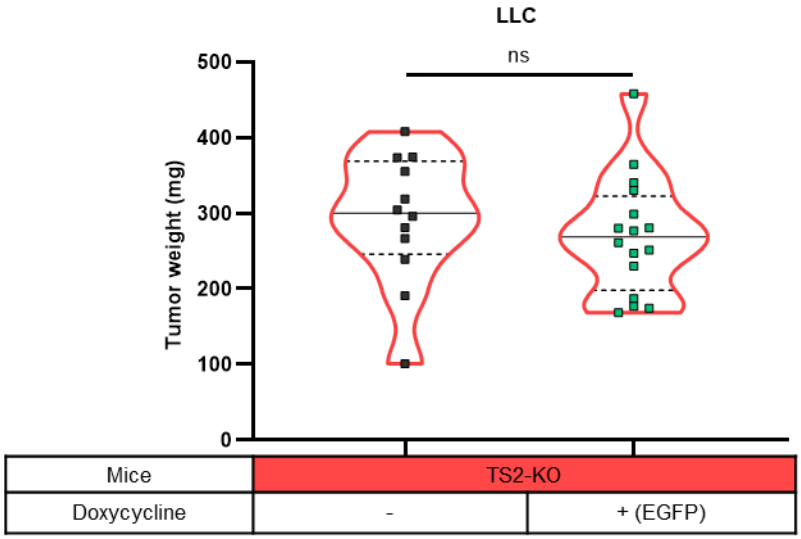

Supplementary figure 2

Doxycycline treatment does not affect tumor growth in TS2-KO mice

LLC cells able to conditionally express EGFP upon doxycycline treatment were injected subcutaneously in TS2-KO mice. Mice were given either control water or water supplemented with doxycycline to induce the expression of recombinant EGFP by cancer cells. Mice were sacrificed 14 days after injection and tumors were weighed. No difference was observed between the two cohorts. Dots represent individual tumor weight, straight lines represent the median and dotted lines the quartiles. Dox: doxycycline. ns: not significant

A

LLC tumors

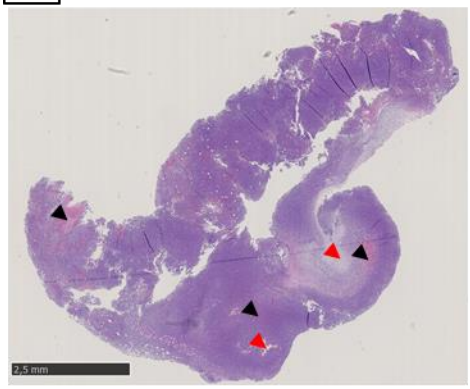

B

B16F10 tumors

C

Spontaneous PyMT tumors

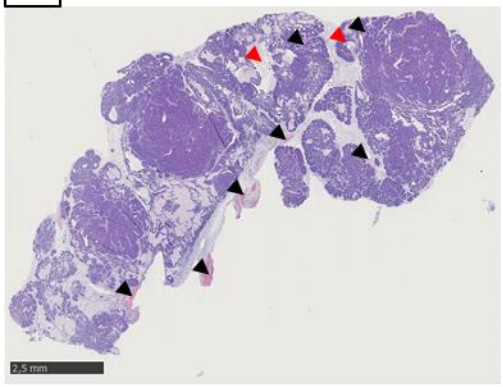

D

Subcutaneous PyMT tumors

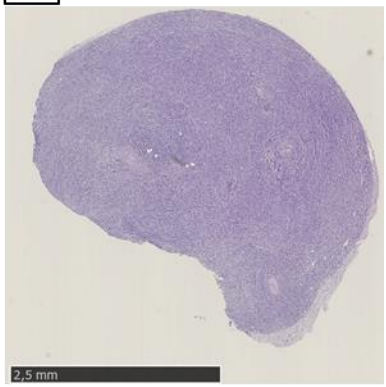

MMTV-PyMT lung metastasis by IHC

E

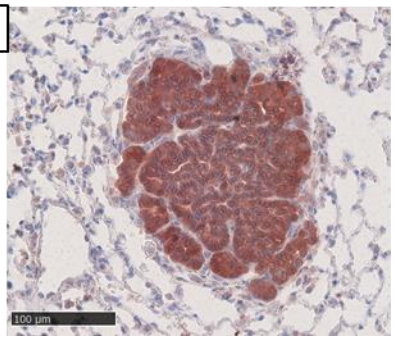

Supplementary figure 3

Heterogeneity of tumor models and MMTV-PyMT lung metastases

Representative pictures of hematoxylin and eosin stained sections of subcutaneous LLC tumors (A), B16 tumors (B), spontaneous PyMT tumors (C) and subcutaneous PyMT tumors (D). Only subcutaneous PyMT tumors are almost free of hemorrhage (black arrow) or necrosis (red arrow), and present a dense and homogenous extracellular matrix. Representative picture of MMTV-PyMT lung metastasis immunolabeled against the PyMT antigen (E).

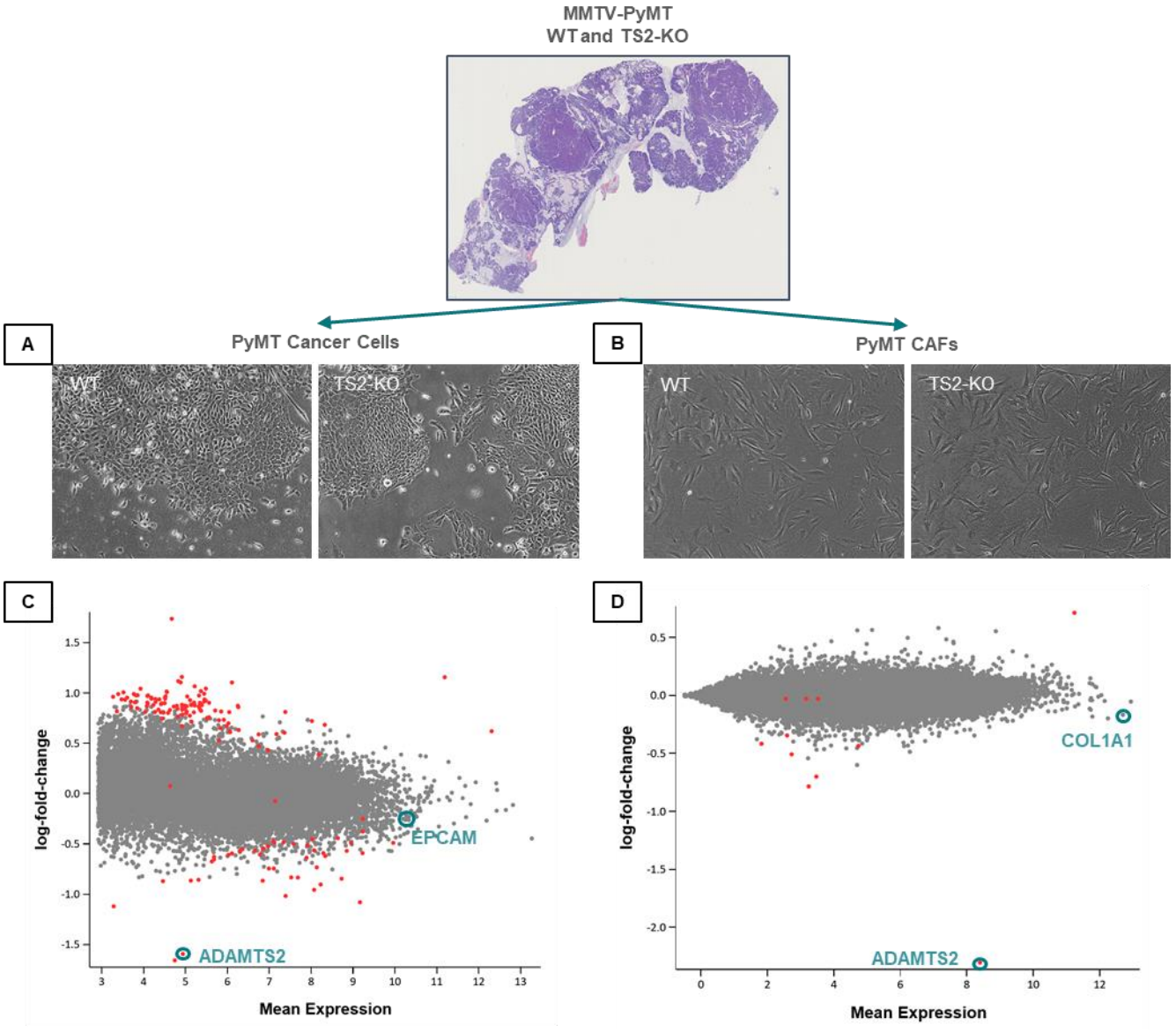

Supplementary figure 4

The transcriptomes of PyMT cancer cells and CAFs are not different in tumors developing in PyMT-WT mice and PyMT-TS2-KO mice

Representative bright field microscopy image of cancer cells (A) and CAFs (B) freshly isolated from spontaneous PyMT-WT and PyMT-TS2-KO tumors. Scatter plots of the mean gene expression to the expression fold changes in TS2-KO versus WT cancer cells (C) and in TS2-KO versus WT CAFs (D). Red dots correspond to genes associated with a significant p value. The associated fold changes remain low as well as their mean expression, suggesting that are not the primary cause of the differences in tumor growth. EPCAM (as a marker of epithelial cancer cells), COL1A1 (as a marker of CAFs) and ADAMTS2 are highlighted in green.

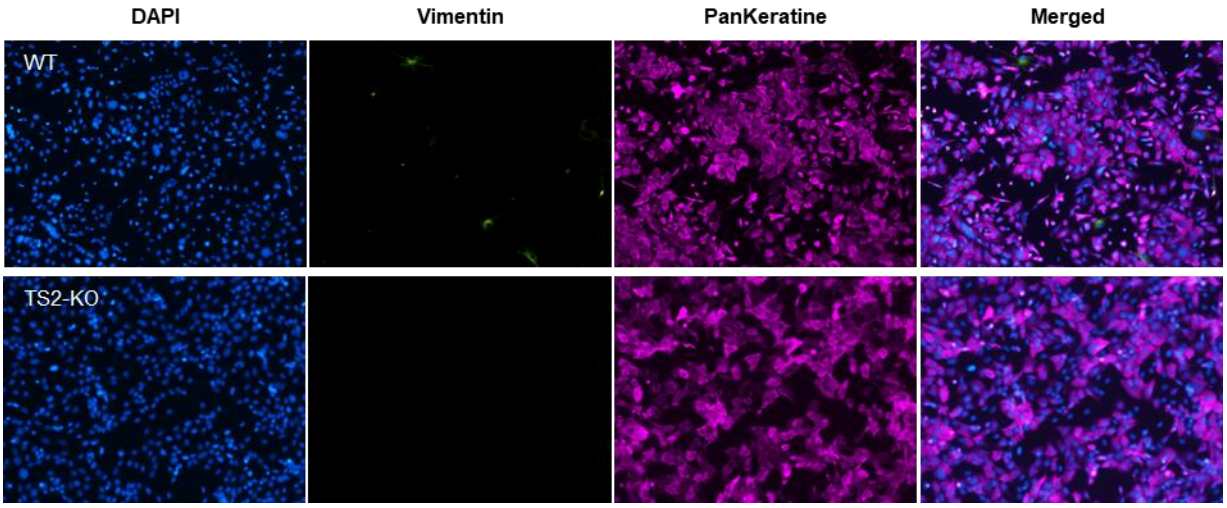

Supplementary figure V

PyMT cancer cells have an epithelial phenotype *in vitro*

Immunofluorescence microscopy of PyMT cancer cells staining DNA (blue), vimentin (green) and keratins (purple).

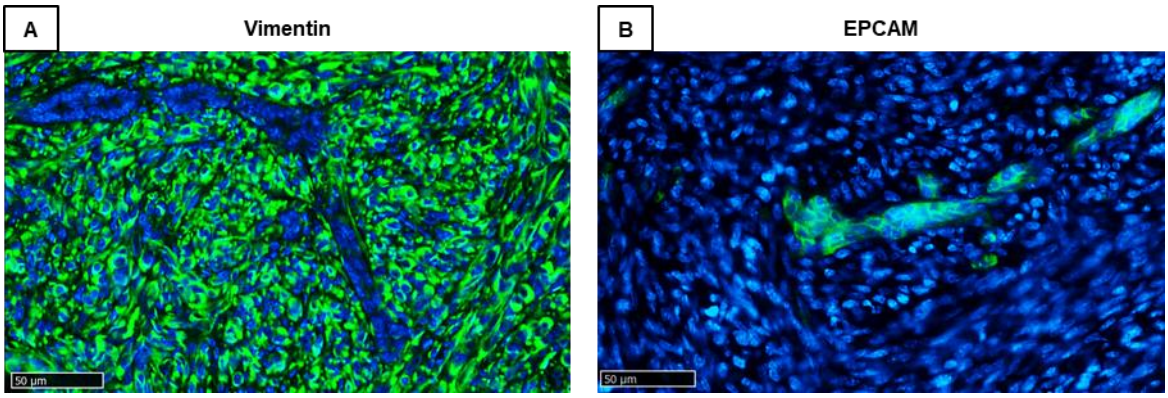

Supplementary figure 6

PyMT cancer cells have mostly a mesenchymal phenotype in subcutaneous tumors *in vivo*

Anti-Vimentin (A) and Anti-EPCAM (B) immunofluorescence labelling of subcutaneous PyMT tumor sections. Few clusters of epithelial EPCAM^{+} cancer cells are dispersed in a dense population of vimentin^{+} mesenchymal cancer cells.

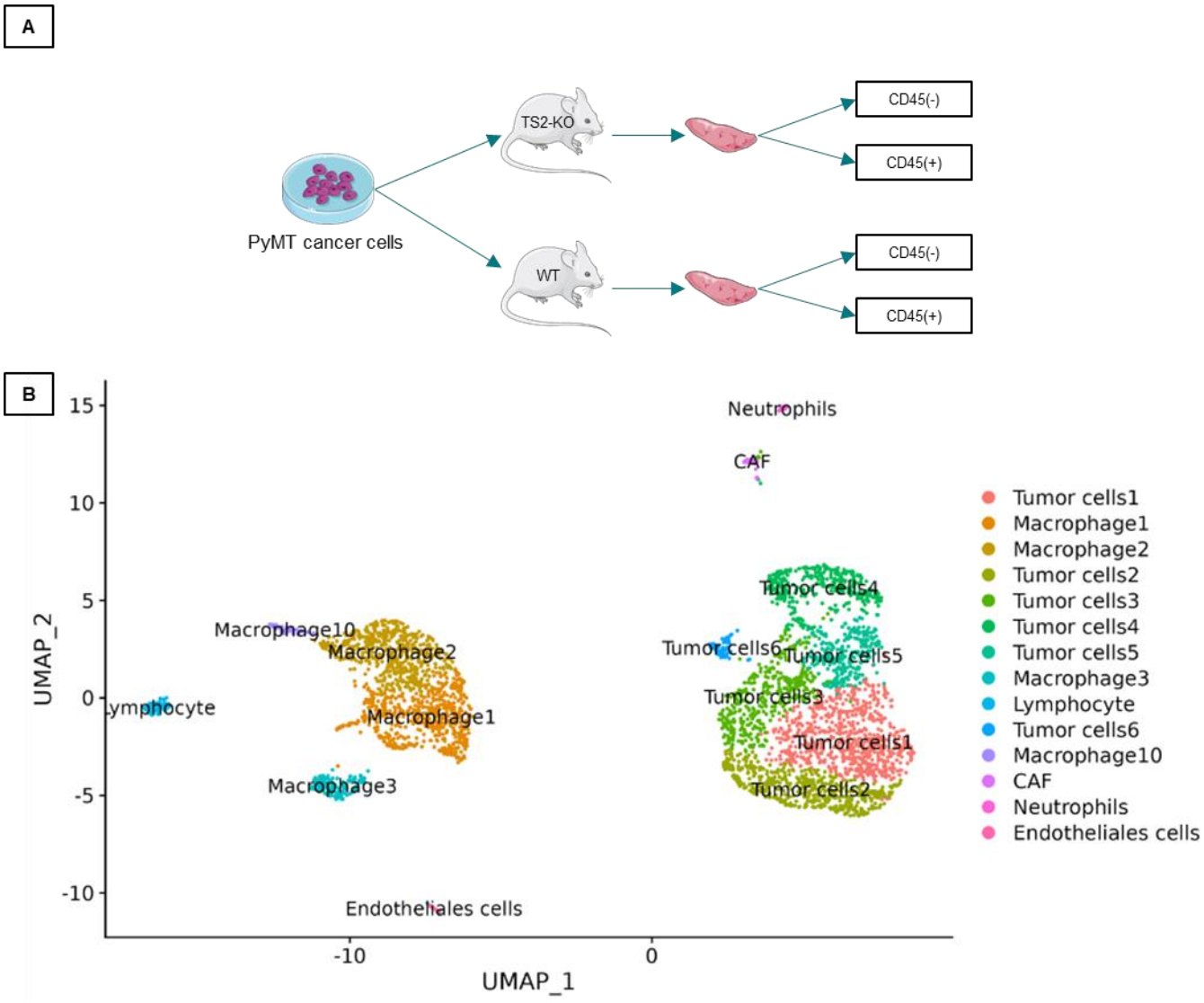

Supplementary figure 7

Single-cell transcriptomic of subcutaneous PyMT tumors

(A) Schematic representation of the single-cell RNA sequencing strategy allowing to process separately immune ($CD45^+$) and non-immune ($CD45^-$) cells present in subcutaneous PyMT tumors formed in WT and in TS2-KO mice. (B) UMAP representation of automatic clustering for the entire cell population. Each dot represents one cell.

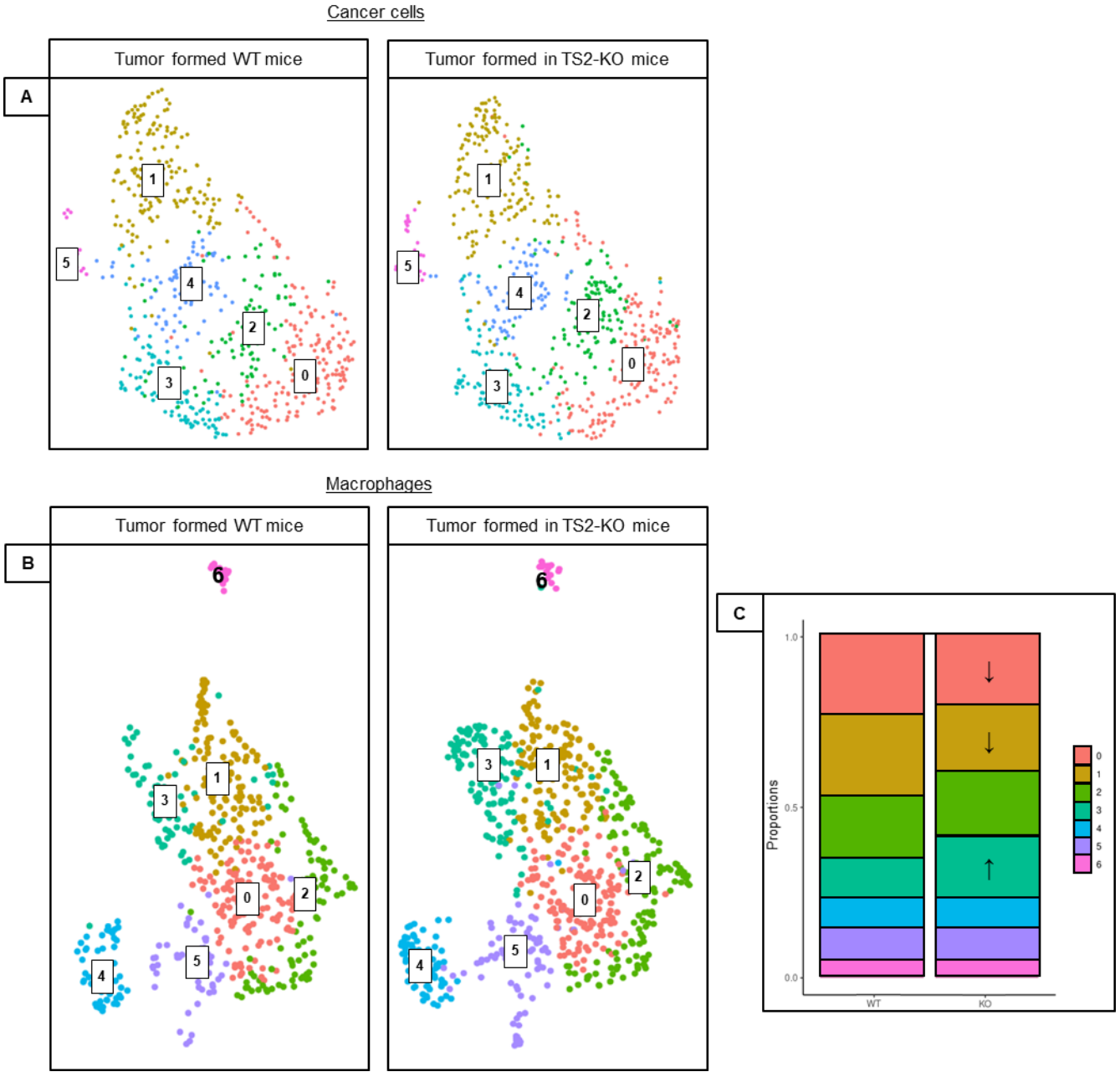

Supplementary figure 8

The absence of ADAMTS2 has no impact on the transcriptome of cancer cells *in vivo*, but increases macrophage polarization toward a M2-like phenotype

(A) UMAP representation after specific re-clustering of the different cancer cells subpopulations in tumors formed in WT and TS2-KO mice. Each dot represents one cell. (B) UMAP representation

after specific re-clustering of the different macrophage subpopulations in tumors formed in WT and TS2-KO mice. Each dot represents one cell. (C) Representation of the relative ratio of each identified macrophage specific cluster from subcutaneous PyMT tumor formed in WT and TS2-KO mice.

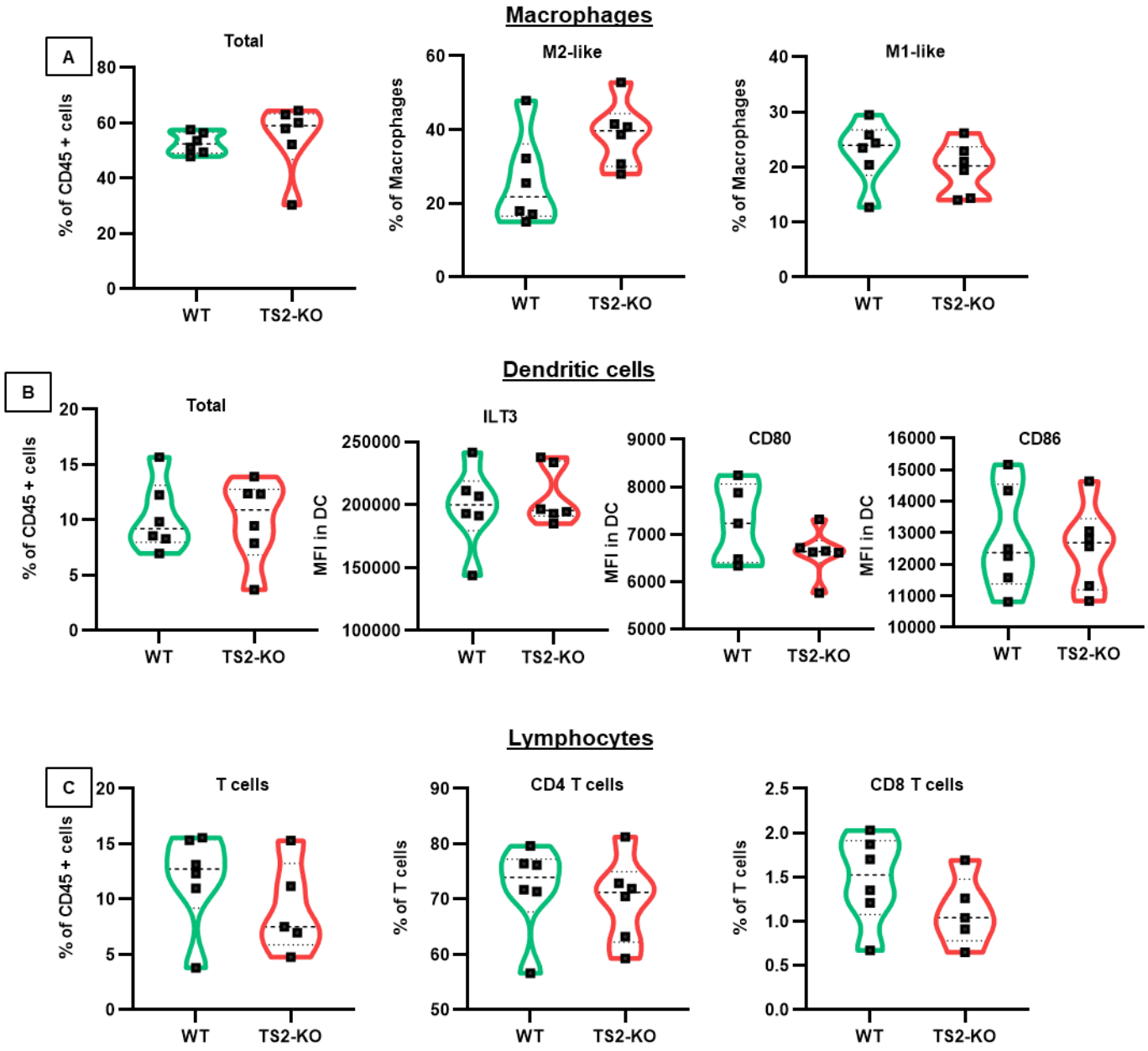

.

Supplementary figure 9

The absence of ADAMTS2 has a marginal effect on the immune cells infiltrating 14-day subcutaneous PyMT tumor

(A) Relative abundance (%) of macrophages ($CD45^+$ $CD11b^+$ $F4/80^{high}$) within $CD45^+$ immune cells and relative abundance of M1-like ($CD206^{low}$ $CD11c^{high}$) and M2-like ($CD206^{high}$ $CD11c^{low}$) within macrophages present in subcutaneous PyMT tumors formed in WT and TS2-KO mice. (B) Relative abundance of dendritic cells ($CD45^+$ $CD11b^+$ $F4/80^{low}$ IA/IE^{high}) within the $CD45^+$ immune cells and expression level of inhibition (ILT3) and activation (CD80 and CD86) markers. (C) Relative abundance of T cells ($CD45^+$ $CD3^+$) and relative abundance of CD4 T cells ($CD4^+$ $CD8^-$) and CD8 T cells ($CD4^-$ $CD8^+$) in $CD3^+$ immune cells.

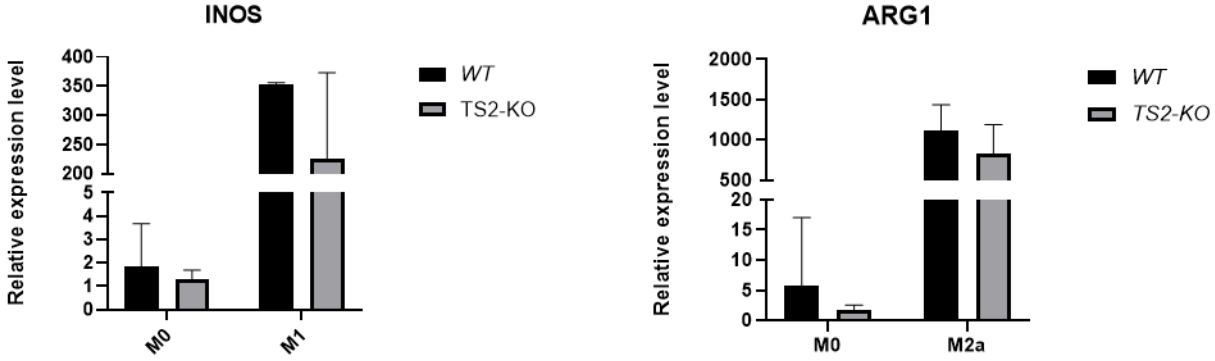

Supplementary figure 10

BMDMs from WT and TS2-KO mice respond similarly to inducers of polarization

BMDMs isolated from either WT or TS2-KO mice were treated with LPS and INFy (for inducing M1 polarization) or IL-4 (for inducing M2 polarization). The mRNA expression levels of inducible nitric oxide synthase (INOS) and arginase1 (ARG1) were quantified by RT-qPCR. No difference was observed between the regulations induced in BMDM-WT and –TS2-KO.

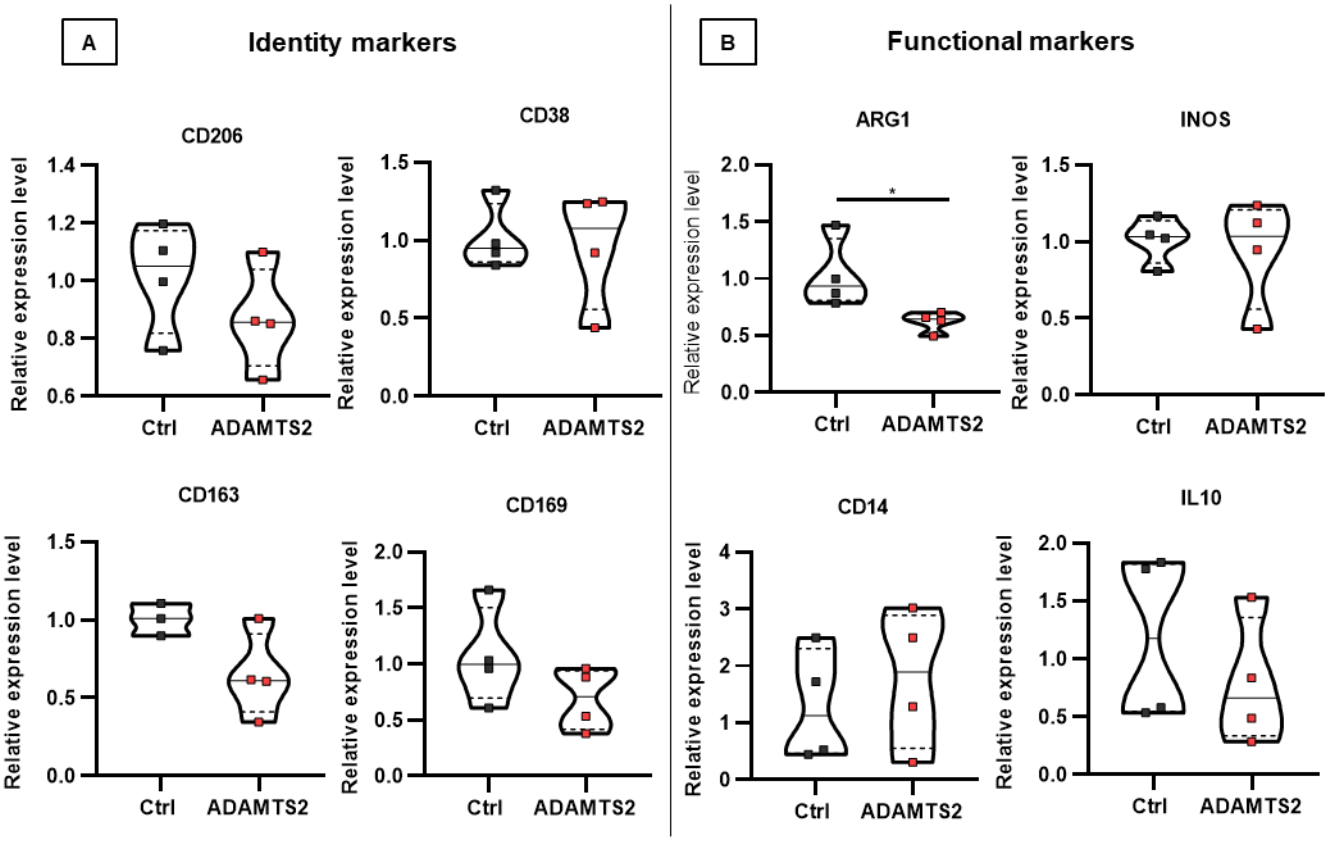

Supplementary figure 11

ADAMTS2 has a marginal effect on key macrophage polarization and functional genes on BMDMs

BMDMs were treated for 8 hours with a conditioned medium containing inactive ADAMTS2 (Ctrl) or active ADAMTS2 (ADAMTS2). The expression level of macrophages polarization (A) and functional (B) markers was quantified by RT-qPCR.

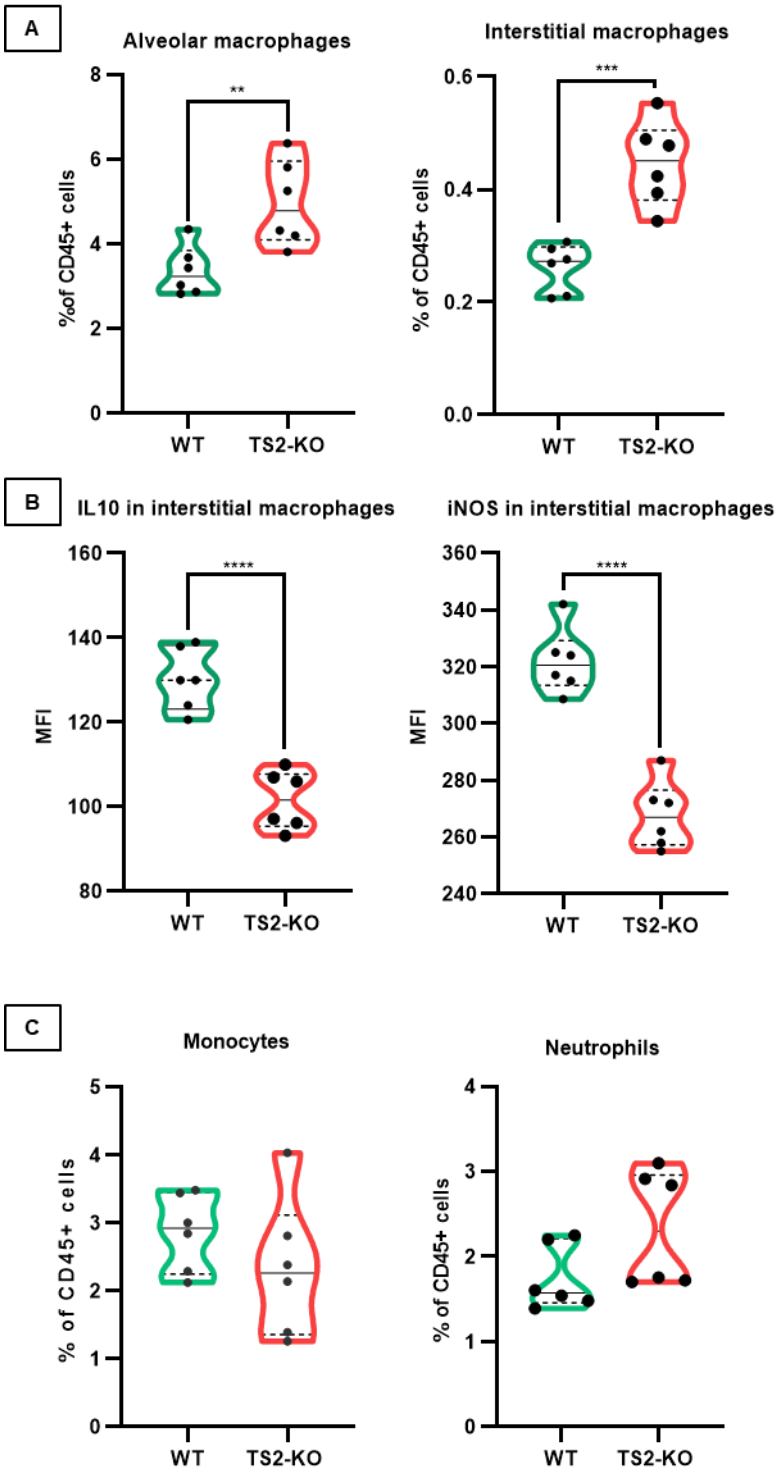
A
Alveolar macrophages
%of CD45+ cells
**
WT
TS2-KO
Interstitial macrophages
% of CD45+ cells
***
WT
TS2-KO
B
IL10 in interstitial macrophages
MFI
****
WT
TS2-KO
iNOS in interstitial macrophages
MFI
****
WT
TS2-KO
C
Monocytes
% of CD45+ cells
WT
TS2-KO
Neutrophils
% of CD45+ cells
WT
TS2-KO

Supplementary figure 12

The absence of ADAMTS2 affects macrophage abundance and polarization in the lung at steady state

(A) Relative abundance (%) of alveolar and interstitial macrophages (IM) within CD45+ cells in the lung of WT and TS2-KO mice. (B) Mean fluorescence intensity (MFI) of IL-10 and iNOS in IM in the lung of WT and TS2-KO mice. (C) Relative abundance (%) of monocytes and neutrophils within CD45+ cells in the lung of WT and TS2-KO mice.

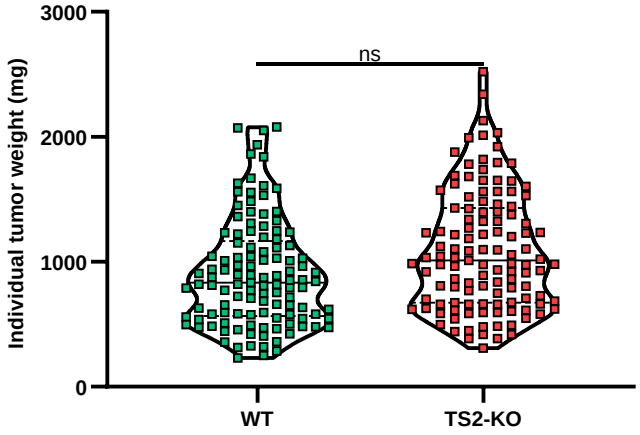

Supplementary figure 13

Tumor weights at sacrifice, and correlation between the age at sacrifice and lung metastatic foci in MMTV-PyMT mice, either WT or TS2-KO

Mice were followed individually and euthanatized when reaching the ethical endpoint for tumor burden. Individual tumor weight at sacrifice are similar in PyMT-WT and PyMT-TS2-KO mouse, showing that mice were euthanatized at a similar ethical endpoint.

Chapter 4: Ancillary works on ADAMTS2 in tumor development

To identify the underlying mechanisms of the tumor immunomodulatory role of ADAMTS2, many attempts have been made to produce *in vitro* models that would mimic the activity of ADAMTS2 within the tumor. These efforts were largely unsuccessful, likely suggesting that the complexity of the TME is required for ADAMTS2 to fulfill its roles. In this section, I will briefly describe some of our attempts and the issues related to the study of ADAMTS2 *in vitro* and ex vivo. I will then present the preliminary data we have obtained so far on the impact of ADAMTS2 on metastatic spread, a particularly interesting observation that we haven't had the opportunity to study in more detail due to a lack of time.

1) Problems related to the study of ADAMTS2 *in vitro*

To be fully active, ADAMTS2 requires specific conditions that are not found *in vitro*, which considerably hinders the elucidation of its various functions and activities. This is clearly illustrated in the specific context of procollagen processing and maturation.

In vivo, in the skin of WT mice, type I collagen is completely processed into mature alpha 1 (a1) and alpha 2 (a2) chains, whereas, as expected, a significant proportion of collagen still retains the aminopropeptide extension in TS2-KO mice (Figure 31.A).

However, the situation is completely different when we characterized the collagen produced by WT and TS2-KO fibroblasts in culture. In both the conditioned medium (Figure 31.B) and the cell layer (Figure 31.C), the majority of type I collagen consists of pro-alpha 1 (proa1) and pro-alpha 2 (proa2) chains, demonstrating that aminoprocollagen peptidase activity (by ADAMTS2) and carboxyprocollagen peptidase activity (by BMP1) are largely defective. Several mechanisms, not mutually exclusive, can explain this observation:

- Fibroblasts in culture are "hyperactivated", which could alter mechanisms that require complex and multifactorial interactions;
- In contrast to the *in vitro* situation, *in vivo* conditions in connective tissue allow very high local protein concentrations close to the cell membrane, favoring substrate-protease interactions. In the same context, it has been shown that ADAMTS2 requires proteolytic cleavages to display full activity, a mechanism that is likely to be enhanced at high concentrations;
- Finally, the presence of factors involved in the presentation of substrates to the enzyme, present *in vivo* but not *in vitro,* cannot be ruled out.

Whatever the cause of the reduction in ADAMTS2 activity *in vitro*, and if we generalize the results seen with collagen to other substrates, this indicates that some substrates, and therefore functions of ADAMTS2 cannot be highlighted or detected *in vitro*.

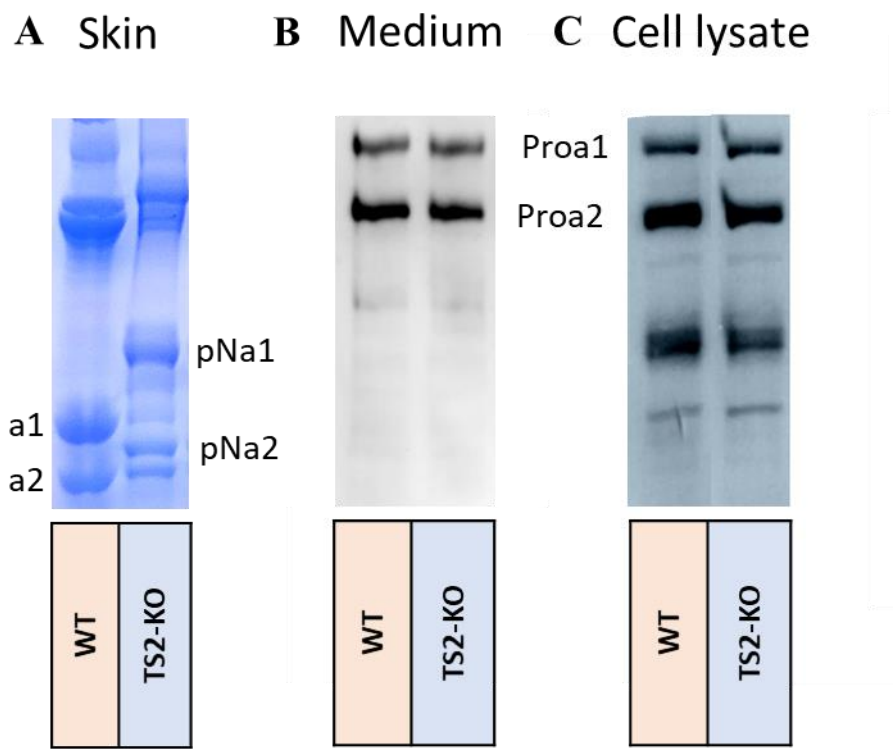

Figure 31: A) SDS-PAGE analysis of type I collagen bands (after in-gel Coomassie blue staining) from the skin of WT and TS2-KO mice. **B**) Western blotting analysis of collagen present in the conditioned medium (B) and in the cell layer (C) of WT and TS2-KO mouse skin fibroblasts. Proa1 and Proa2: alpha1 and alpha2 procollagens; pNa1 and a2: alpha 1 and alpha 2 amino-procollagens; alpha 1 and alpha 2: fully matured alpha 1 and alpha 2 collagens

2) Determination of ADAMTS2 substrates by iTRAQ N-TAILS on tumor models

Tumors forming after subcutaneous injection of LLC and B16F10 cancer cells develop more rapidly in TS2-KO mice than in WT mice, indicating that a conserved mechanism may be involved in both models, probably linked to ADAMTS2 enzymatic activity.

To evaluate this hypothesis, we first used a simplified experimental approach. We purified ADAMTS2, either active or inactive (due to a mutation in the catalytic domain) using a two-step chromatography process optimized at our laboratory[287,288]. Conditioned media from LLC and B16F10 cells in culture were then incubated with active or inactive ADAMTS2. N-TAILS analyses were then performed to identify potential substrates by comparing the N-terminomes in the samples treated with the active or inactive ADAMTS2. Sixty-one and 50 proteins were identified, with only

22 being common for LLC and B16F10 cells, of which only 2 are reported to be secreted or have transmembrane localization: Thrombospondine-2 and Neuronal Pentraxin Receptor (NPTXR) (Figure 32).

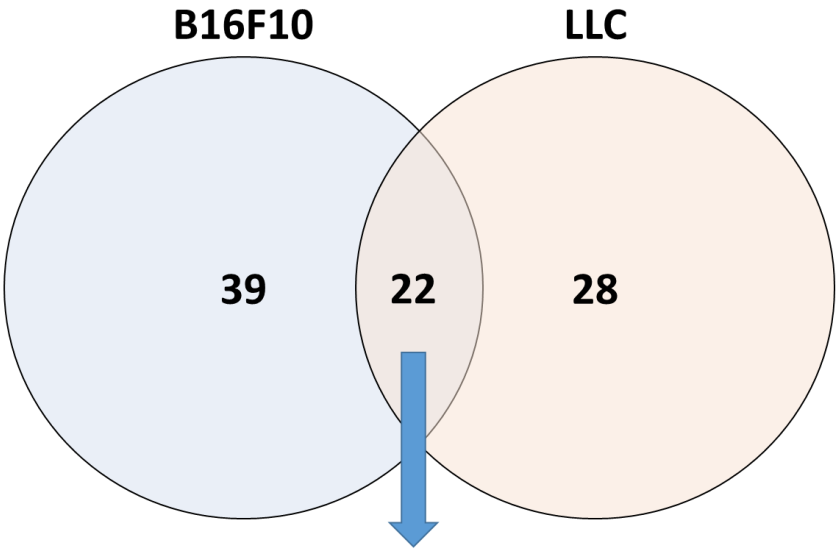

Protein	Peptide	B16F10	LLC
NPTXR_MOUSE	DTMA(175).(176)DGAWDSPALLLELEDAVR	4.27	2.25
TSP2_MOUSE	FLLE(306).(307)LIGGPLKTR	4.62	2.41

Figure 32: Venn diagram of the number of proteins identified as being cleaved by ADAMTS2 activity in B16F10 and LLC samples. Twenty-two proteins are common, of which only NPTXR and thrombospondin-2 are extracellular (transmembrane or secreted).

Thrombospondine-2 (TSP2) is an extracellular protein involved in fibrillogenesis, cell adhesion, angiogenesis, hemostasis, …[289]. TSP2 is much less known than TSP1 which has already been described as cleaved by several enzymes such as cathepsins, elastase, plasmin and ADAMTS1[290]. No functional link with the immune system could be made.

Neuronal pentraxin receptor is a poorly known member of the pentraxin family. It is very similar to NPTX1 and NPTX2, except for the presence of a transmembrane domain[291]. Pentraxins are involved in inflammation, complement activation and cancer. ADAMTS2 appears to cleave NPTXR just above the transmembrane domain, resulting in the loss of its cellular receptor function. Once cleaved, NPTXR is structurally similar to NPTX1 and NPTX2, two proteins described mainly in the brain, with no effect on immune system regulation reported.

Based on these disappointing data, iTRAQ N-TAILS experiment was carried on different types of extracts from subcutaneous PyMT tumors formed in WT and TS2-KO mice. Known ADAMTS2 substrates, such as collagens and several other ECM proteins, were identified,

validating our strategy, at least for abundant proteins (Figure 33). Newt, we mainly focused our analysis on proteins with known immuno-regulatory properties such as complement C3 (C3) and annexin A1 (Anxa1).

Like ADAMTS2, both proteins are expressed by macrophages. We therefore hypothesized that ADAMTS2 could directly regulate macrophage phenotype by cleaving locally secreted factors. However, confirmatory experiments *in vitro* failed to confirm the ability of ADAMTS2 to process complement C3 or annexin A1.

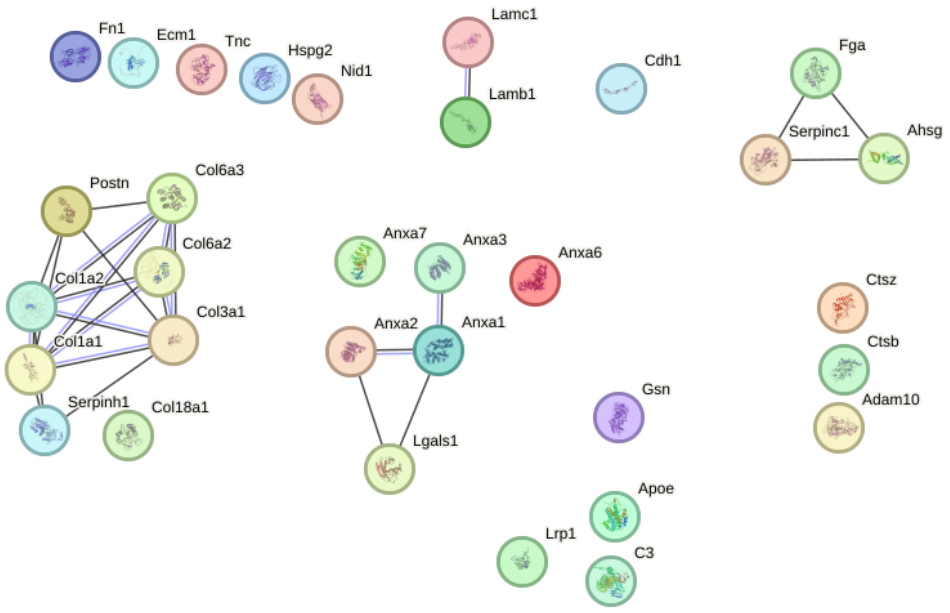

Figure 33: STRING schematic representation of potential ADAMTS2 substrates as identified by N-TAILS in subcutaneous PyMT tumors.

3) ADAMTS2 expression, binding and activity on macrophages

To evaluate the expression of ADAMTS2 from macrophages within the tumor, we performed an isolation of TAMs ($CD45^{+}$, CD11b+, $F4/80^{high}$) from subcutaneous PyMT tumors generated in WT mice from PyMT TS2-KO cancer cells previously modified to express EGFP. Cancer cells ($CD45^{-}$, $EGFP^{+}$) and stromal cells ($CD45^{-}$, $EGFP^{-}$) were also isolated, and the expression level of ADAMTS2 was quantified by RT-qPCR. We found that TAMs express less ADAMTS2 (at the mRNA level) than stromal cells, but much more than what is observed in bone marrow-derived macrophages (BMDMs), demonstrating the importance of taking macrophage polarization into account when studying the role of ADAMTS2 (Figure 34. A).

Confirming that macrophages have non negligible expression of ADAMTS2 within the tumor, attempts have been made to polarize BMDMs into ADAMTS2 expression macrophages.

IL-4, TGFβ, LPS and INF-Y all failed to induce ADAMTS2 expression in BMDMs while glucocorticoid treatment (1 week with methylprednisolone or dexamethasone) led to a significant increase in ADAMTS2 mRNA level. Even after 1 week of treatment, only a 5-fold increase in ADAMTS2 expression in BMDMs could be reached, which is still 6 times lower than in macrophages found within the tumor. The inability to generate ADAMTS2-expressing macrophages clearly indicates that a complex regulatory signaling within the tumor is required to generate this phenotype. The effect of the ADAMTS2 expressed by macrophages thus can't be evaluated *in vitro*.

Given that stromal cells express about 20 times more ADAMTS2 than macrophages in the tumor, it is possible that ADAMTS2 from stromal cells interacts with macrophages and remains functional.

To verify this hypothesis, BMDM were incubated in a medium conditioned by HEK293 cells expressing recombinant active HA-tagged ADAMTS2. By immunofluorescence, we observed that "exogenous" ADAMTS2 does accumulate at the surface of BMDMs (Figure 34.B).

Going a step further, we then tested whether this bound ADAMTS2 retained its activity, which is of crucial importance for studying the role of ADAMTS2 as a regulator of the immune system. BMDMs were first incubated in conditioned medium containing ADAMTS2 and washed to remove unbound ADAMTS2. pNcollagen substrate was then added (in the absence or presence of EDTA used as an inhibitor). After incubation (16 h at 37 ° C) to allow potential cleavage, samples were denatured. SDS-PAGE and Western blotting analyses clearly showed the conversion of pNcollagen alpha chains into mature alpha chains, but only in the absence of EDTA (Figure 34.C).

These data show that, even if TAMs have only a moderate ADAMTS2 expression, active ADAMTS2 secreted by other cells present in the TME could bind to their surface in an active form and thus participate in the regulation of their functions.

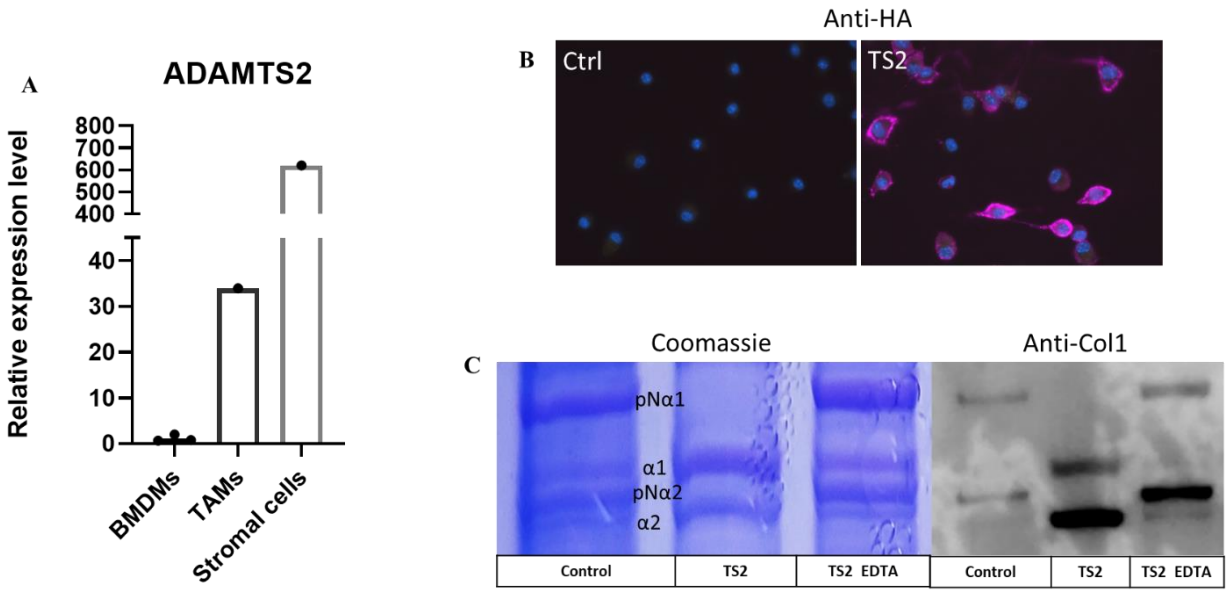

Figure 34: A) Quantification of the relative expression level of ADAMTS2 in BMDMs, in TAMs and stromal cells freshly isolated from subcutaneous PyMT tumor formed in WT mice by TS2-KO cancer cells. B) Immunofluorescence against HA-Tag on BMDMs incubated in conditioned medium containing or not recombinant active HA-tagged ADAMTS2. C) Evaluation of type I collagen pattern by in-gel Coomassie blue staining (left) and Western blotting (righ) after incubation in the medium of BMDMs left untreated (control), of BMDMs pretreated with recombinant active ADAMTS2 (TS2) or of BMDMs pretreated with inactive ADAMTS2 (TS2 EDTA).

4) ADAMTS2 knockout alters the population of lung resident macrophages

Given the impact of ADAMTS2 on tumor immunity and metastasis spread, we investigated whether the absence of ADAMTS2 could alter the overall immune landscape in the lung under physiological conditions, which could subsequently affect metastasis.

We performed an immuno-phenotyping by flow cytometry of lung alveolar and interstitial macrophages. It revealed a ~50% increase of both alveolar and interstitial macrophages in TS2-KO mice, as well as a significant but moderate decrease of both INOS and IL10, two markers of opposed phenotypes in macrophages. Although not yet understood, these data indicate, however, that macrophages may be functionally altered in TS2-KO mice, at least within the lungs (Figure 35).

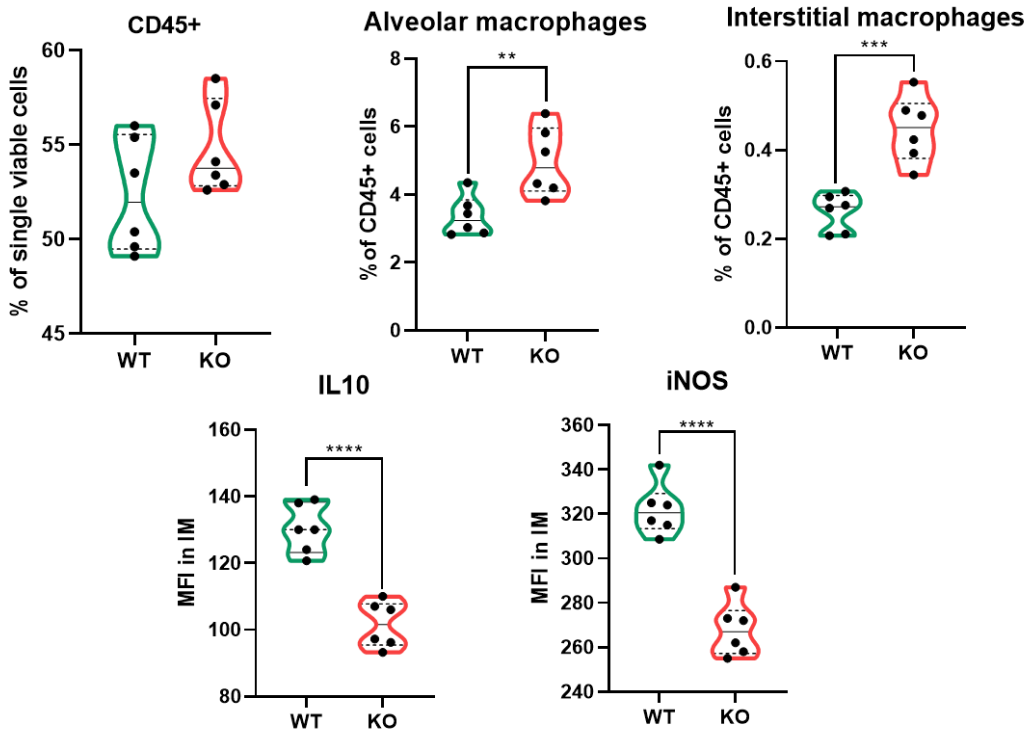

Figure 35: A) Percentage of CD45$^+$ cells among living cells recovered from the lungs of WT and TS2-KO mice. B) Percentage of alveolar and interstitial macrophages among CD45$^+$ cells in the lungs of WT and TS2-KO mice. C) Expression levels of IL-10 and INOS in interstitial macrophages of the lungs of WT and TS2-KO mice.

Next, we compared the lung immune cell population in the presence or absence of subcutaneous tumors developing in WT and TS2-KO mice. No difference could be identified in the lung immune cell with the presence of tumor. This is probably explained by the absence of lung pre-metastatic niche formation with this fast (14 days) model.

5) Hyperplasia of tumor-draining lymph nodes is reduced in TS2-KO mice

Given the ability of ADAMTS2 to activate pro-VEGFC and the importance of the lymphatic system for the spread of metastases, we compared the weight of control (tumor-free flank) and tumor draining lymph nodes in WT and TS2-KO mice. The weights of the control lymph nodes were similar in WT and TS2-KO mice (2.5 mg versus 2.4 mg). However, the increase in weight was significantly larger in WT (x 2.2) than in TS2-KO (x 1.8), while tumors were, on average, twice as large in TS2-KO mice (Figure 36). This effect could be due either to reduced tumor drainage in TS2-KO mice or to reduced inflammatory signaling from tumors formed in TS2-KO mice. These hypotheses are currently being addressed.

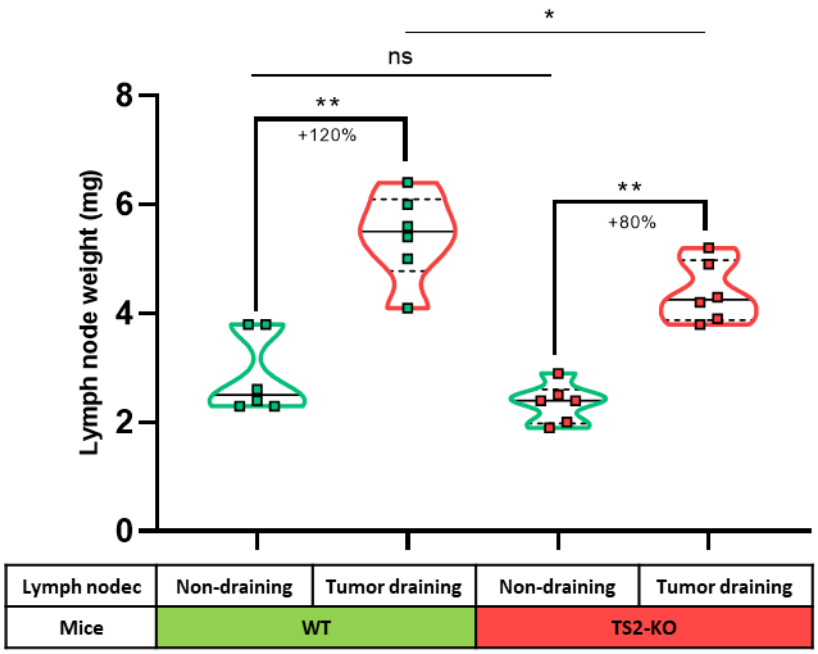

Figure 36: Wet weight of draining and non-draining (contralateral) lymph nodes 14 days after subcutaneous injection of TS2-KO PyMT cancer cells in WT and TS2-KO mice.

6) ADAMTS2 overexpression does not decrease tumor growth in WT immunocompetent mice

As described earlier in this manuscript, cells conditionally expressing ADAMTS2 (in the presence of doxycycline) were used to assess the effect of ADAMTS2 on tumor growth in mice with increasing severity of immune dysfunction.

Similar experiments were also performed in immuno-competent C57BL6 mice, either WT or TS2-KO. B16 and LLC cells conditionally expressing ADAMTS2 upon doxycycline treatment have been injected subcutaneously and mice were given water, either control or containing doxycycline. After 21 days (B16) or 14 days (LLC), tumors were collected and weighted. Tumor weights were not significantly different for mice receiving doxycycline (expression of recombinant ADAMTS2 by cancer cells), at the contrary of what was repeatedly observed with nude and NOD SCID mice (Figure 37).

The reasons for such differences have not been elucidated but could be related to differences in the anti-tumor immunity in the different models and to the innate immunity-dependent effect of ADAMTS2 on tumor growth. Our working hypothesis will be described in the Discussion section. These results do not change our conclusions about the implication of ADAMTS2 in the regulation of the innate immune system. These data were therefore not included in the manuscript (to be) submitted for publication.

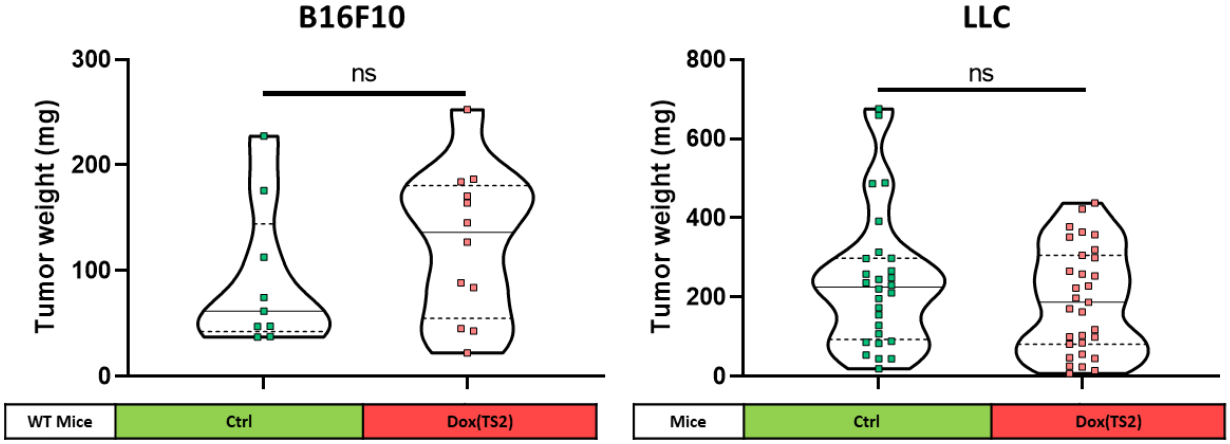

Figure 37: B16 and LLC cells were injected subcutaneously in WT mice. Mice were given either control water or water supplemented with doxycycline to induce the expression of recombinant ADAMTS2 by cancer cells. Mice were sacrificed 14 days (LLC) or 21 days (B16) after injection, and tumors were weighed. Dots represent individual tumor weight, straight lines represent the median and dotted lines the quartiles. These experiments for LLC and B16 cells were performed 3 and 2 times, respectively, and the graph was made by pooling tumor weights from all experiments. Dox: doxycycline.

Discussion and Perspectives

Discussion: Identification of the substrates of ADAMTS2 and 14 *in vivo* by N-TAILS

In this work, we performed the challenging task of iTRAQ N-TAILS analysis on *in vivo* tissues. We considered the skin to be sufficiently homogeneous and simple tissue to expect accurate results from this approach. Moreover, skin contains fibroblasts, which express high levels of ADAMTS2 and ADAMTS14, and is the tissue the most affected by the absence of these ADAMTSs[74,87]. Our two main goals with this study were to identify the different substrates of these enzymes *in vivo* and to determine if ADAMTS2 and ADAMTS14, which are structurally very similar, have a redundant or compensatory activities.

ADAMTS14, while part of the aminoprocollagen proteinases, has almost no activity against type I collagen aminopropeptide *in vitro*[77]. At the start of this study, the only known substrates of ADAMTS14 were identified by our laboratory using N-TAILS on *in vitro* models (LTBP1, DKK3, TGFβ-RIII and fibronectin)[120]. To date, two other *in vitro* substrates of ADAMTS14 have been confirmed: lysyl oxidases[292] and fibuline-2[293] which are also substrates initially identified by our iTRAQ N-TAILS analysis. The *in vivo* substrates of ADAMTS14 were, on the other hand, still unknown.

In this work, we took the unique opportunity of the availability of skin samples from WT, TS2-KO, TS14-KO and TS2-TS14-KO, which represent a unique and robust experimental model to evaluate specific and common substrates for these two enzymes.

Focusing on type I collagen, ADAMTS2 and ADAMTS14 showed activity against the aminopropeptide of both the alpha 1 and the alpha 2 chains of type I collagen. Moreover, additional cleavage sites by ADAMTS2 and ADAMTS14 were identified within the mature collagen domain as well as in the carboxypropeptide domain. The cleavages in the carboxypropeptide domain are not localized at the described cleavage site for BMP1. This observation, however, does not exclude the possibility that ADAMTS2 and ADAMTS14 can also process the carboxypropeptide of type I collagen *in vivo*. Indeed, in N-TAILS, trypsin is used to generate peptides before mass spectrometry analysis. Only 6 amino acids span between the reported aminopropeptide cleavage site and the next arginine (trypsin cleaves N-terminally at every arginine and lysine). In our mass spectrometry analysis, only peptides of minimum 8 to maximum 26 amino acids can be identified. Therefore, a peptide generated from cleavage at the previously reported BMP1 cleavage site could have been missed. The presence of cleavage at multiple sites indicates that the protease activity of ADAMTS2 and ADAMTS14 is not restricted to a highly specific amino acid sequence.

Comparing ADAMTS2 and ADAMTS14, we clearly see that most substrates (both collagens and non-collagen proteins) are processed by both enzymes (>1 ratio in both TS2-KO and TS14-KO skins) with some specificity for one or the other. For example, type I collagen is mostly cleaved

by ADAMTS2 while complement C3 is mostly cleaved by ADAMTS14. This observation indicates that both enzymes, while processing similar substrates, do not compensate for each other. Indeed, if ADAMTS2 could compensate for ADAMTS14 knockout and vice versa we would only see a > 1 ratio in the double knockout model.

The cleavage ratio in TS2-TS14-KO as compared to TS2-KO and TS4-KO was often higher confirming that, indeed, each enzyme is able to process the identified substrates causing an additive increase of the protease to control ratio in the double knockout skin.

It is important to mention that these results are far more complex and diverse than those previously obtained in our laboratory using fibroblasts *in vitro*[267]. In fact, the only substrates that are similar *in vitro* and *in vivo* for ADAMTS2 and ADAMTS14 are collagens. This discrepancy seems to indicate that *in vitro* models do not recapitulate the complexity of ADAMTS activity found *in vivo*.

In this analysis, the main and foremost identified substrates are fibrillar collagens that were the primary focus of the publication. The rest of the identified substrates can be split in multiple categories such as proteases and protease inhibitors (inter-alpha-tryspin inhibitor, alpha-2-macrogobulin, carboxypeptidase A3, cathepsins, cystatin-c, kalikrein, mast cell protease 4, serpin A1, serpin B6 and stromelysin-1), proteins involved in the coagulation process (annexin-8, coagulation factor XIIIa, kininogen-1) and immune system related proteins (complement proteins, galectin-1, CMHII, immunoglobulins, macrophage migration inhibitory factor, annexin A1).

The presence of protease inhibitors in these data could result from the mechanism of action of some protease inhibitors. For example, the alpha-2-macroglobulin serves as bait for proteases. Once it has been cleaved, it covalently binds the protease which ends up irreversibly inactive. The processing of these bait proteins may show up in N-TAILS analysis. Such cleavage in the bait region of alpha-2-macroglobulin were identified in our study, confirming that both ADAMTS2 and ADAMTS14 can be inhibited by alpha-2-macroglobulin.

As another hypothesis, the use of protease knockout models can lead to a significant reduction of the total amount of protease in the tissues, particularly for abundant proteases such ADAMTS2 and ADAMTS14 in the skin. The reduction of the protease pool could cause an increase of the inhibitors to proteases ratio therefore indirectly increasing the inhibition on other proteases. Consequently, the knockout of an enzyme could lead to the reduction of the activity of others, potentially confounding their activity. Additionally, the relative increase in the inhibitors to proteases ratio could indirectly reduce the stability of proteases causing their degradation[294] and leading to a disproportion of proteases peptides in our control condition falsly identifying these proteases as substrates for ADAMTS2/14.

The role of ADAMTS2 in the coagulation cascade has already been evaluated in our laboratory (unpublished). It rose from the identification of fibronectin as a substrate of ADAMTS2 and the identification of ADAMTS2 polymorphism in pediatric stroke[98]. By the addition of purified recombinant ADAMTS2 in blood sample, the formation of blood clot was drastically enhanced,

indicating that ADAMTS2 has pro-coagulant properties. The initial substrate of ADAMTS2 that triggers the blood clotting was not identified.

Regarding immune-related proteins, a previous study of the lab identified that immune dysregulation in the skin was associated with dermatitis-like lesion in ADAMTS2 and ADAMTS14 double knockout, while single knockout mice were unaffected[87]. At the time, only *in vitro* substrates of the enzyme were identified and did not include immune specific proteins. In this *in vivo* N-TAILS, however, we identified immune related proteins like complement proteins out of which complement C3 and annexin A1 stood out.

Complement C3 cleavage by ADAMTS2/14 was identified at the C3a C-terminal and C3c C-terminal region. C3a release leads to inflammation while C3c release comes from the IC3b domain which is an inhibitor of the C3 convertase. Both cleavages of the complement C3 would theoretically lead to an activation of the complement system and to inflammation[295]. Given that the complement cascade consist of a succession of proteolytic cleavages, the detection of complement C3 cleavage may be related to an activation that occurs upstream of complement C3 cleavage but could not be identified due to the technical limitation of N-TAILS mentioned above. Complement C3 cleavage may therefore indicate activation of this pathway by ADAMTS2. Complement activation starts through one of three different pathways: classical, lectin and alternative pathway. Classical pathway is initiated by the binding of C1q to immunoglobulins present on a pathogen. The lectin pathway starts by the binding of mannose binding lectins (MBL) to pathogen sugars present at the cell surface. C1q and MBL are part of the collectin family which are lectins containing a triple helical collagen domain which is susceptible to be cleaved by ADAMTS2 and ADAMTS14. Moreover, lectins are known binding partners of ADAMTS2 and ADAMTS14. There is thus theoretical basis for ADAMTS2/14 to play a role far up-stream in the complement cascade activation.

Annexin A1 was identified cleaved at the first N-terminal third of the protein and right in the middle of its sequence by ADAMTS2/14. Full length annexin A1 has a profound anti-inflammatory activity by its N-terminal domain binding to its cell surface receptor. Processing of the N-terminal tail of annexin A1 leads to a pro-inflammatory signaling[296]. The identified cleavage site of annexin A1 by ADAMTS2/14 is located c-terminaly to its known cleavages and its impact on annexin A1 function is unknown.

Annexin A1 is a glucocorticoid response gene much like ADAMTS2. While ADAMTS2 is upregulated at the mRNA level by glucocorticoids, annexin A1, which is stored in intracellular vesicles, is secreted up on glucocorticoid treatment meanwhile its mRNA level seems to be slightly repressed up on treatment (data not shown). If ADAMTS2 does cleave annexin A1 and leads to its inactivation. ADAMTS2 may be part of a regulatory mechanism allowing annexin A1 inactivation and the reduction of its anti-inflammatory activity.

However, we were unable to confirm that complement C3 and annexin A1 are cleaved by ADAMTS2. Using recombinant annexin A1 and ADAMTS2, no cleavage could be identified by

Western blot, and neither complement C3 nor annexin A1 were differentially processed in tumors from WT and TS2-KO mice.

The common substrates identified for ADAMTS2 and ADAMTS14, such as complement C3 and annexin A1, may be involved in the redundant immune regulatory role identified for these proteases[87].

Regarding the investigation of ADAMTS2/14 intracellular cleavages, we clearly showed, *in vitro*, that ADAMTS2 and ADAMTS14 are able to process actin and vimentin. This confirmatory experiment revealed that at least part of the intracellular protein found in N-TAILS (Figure 19) may be indeed substrates of ADAMTS2 and 14. Actin can be present extracellularly and in the blood[297]. Interestingly the scavenging of actin is performed by gelsolin[298] which has also been identified as substrate for both ADAMTS2 and ADAMTS14 (Figure 19). Vimentin has also been found extracellularly where it displays pro-angiogenic activity in tumors[299]. One can hypothesis that ADAMTS2 and ADAMTS14 could process actin and vimentin, and be part of a degradation process of these cytoskeleton proteins.

Discussion: ADAMTS2 and 14 in lymphangiogenesis

We pursued the characterization of both ADAMTS2 and ADAMTS14 *in vivo*, this time focusing on the lymphangiogenic process. This study was initiated by the observation that ADAMTS3 knockout mice died before birth due to severe edema formation caused by a lack of lymphatic vessel development[268]. Given the redundancy in collagen processing between ADAMTS2 and ADAMTS3, and the different patterns of expression between both enzymes, we hypothesized that ADAMTS2 and ADAMTS14 may replace the role of ADAMTS3 in the lymphangiogenic process at adulthood. Moreover, our laboratory collaborated with Stefan Schulte-Merker's team to show that ADAMTS14, much like ADAMTS3, is involved in the lymphangiogenic process in zebrafish[300].

In this work, we clearly showed that ADAMTS2, unlike ADAMTS14, is necessary for steady state lymphangiogenic fluid resorption while both enzymes are sufficient to allow proper neolymphangiogenesis during the healing process. This study revealed the profound role of ADAMTS2 in lymphangiogenesis which may directly affect other physiological mechanism such as fat absorption, immune cell transport and metastasis. The impact of ADAMTS2 on the lymphatic system may be involved in its immunoregulatory role[87] and the effect on metastasis we observed in the MMTV-PyMT mice model.

Lymph node metastasis is characteristic of many cancer types such as melanoma and breast cancer. The colonization of lymph node by cancer cells is thought to be a driver of the distant tissue metastasis[301]. Pre-metastatic niche established in lymph nodes has been extensively studied[302] and seems to rise form the capture of extracellular vesicles produced by cancer cells. It is characterized by vascular, ECM and immune alterations in the lymph node that favor cancer cell colonization.

We can hypothesize that the absence of metastases in ADAMTS2 knockout mice may originate from a deficiency of lymph node tumor drainage and subsequent impairment of the pre-metastatic niche formation which ultimately impairs distant tissue dissemination. This hypothesis is currently investigated in our laboratory as a stand-alone project and could explain why tumor draining lymph node hyperplasia is reduced in TS2-KO mice.

Discussion: ADAMTS2 in tumor development

With the ever expanding roles of ADAMTS2, we investigated its implication in tumor development. This study follows a previous work done at our lab which showed that the expression of ADAMTS2 by HEK293 nearly abolished their capacity to form subcutaneous tumors[119].

Multiple drawbacks affected this initial study: (i) immortalized cells rather than cancer cells were used to generate tumors, (ii) human cells were injected into immunocompromised mice, which may alter the immune system response to tumor development and (iii) engineered cells expressing ADAMTS2 were compared to unmodified parental cells, the comparison of the growth of tumors originating from different cell lines may be a confounding variable of the effect of ADAMTS2.

We first wanted to evaluate the effect of ADAMTS2 expression by cancer cells on tumor growth in immunocompetent mice. To do so, we used C57BL/6 mice WT and TS2-KO that were available at the laboratory to generate syngeneic subcutaneous models using lung squamous cancer cell (Lewis lung carcinoma, LLC) and melanoma (B16) cell lines. **Tumor from both LLC and B16 grew faster in TS2-KO mice indicating that ADAMTS2 has some suppressive function on tumor growth.**

Both LLC and B16, much like all non-mesenchymal cancer cell lines, do not express ADAMTS2. We do know that ADAMTS2 is mostly expressed by mesenchymal cells which are mainly present in tumors as CAFs. Thus, our starting hypothesis was that ADAMTS2, in the tumor, originates from CAFs. CAFs would therefore be the "mediator" of the ADAMTS2 repressive function on tumor growth. This hypothesis was, however, already challenged by the fact that LLC and B16F10 tumors have very low level desmoplastic reaction.

To evaluate the direct effect of ADAMTS2 on cancer cells and in an attempt to rescue this phenotype, cell lines were modified to conditionally express ADAMTS2 upon doxycycline treatment. The proliferation and migration of these cells were evaluated *in vitro,* and no significant differences could be identified, indicating that ADAMTS2 has no direct effect on cancer cells. Thus, ADAMTS2 appears to affect tumor growth indirectly, probably through the TME.

These engineered cell lines were injected in both WT and TS2-KO mice, and tumor weight was evaluated with and without induction of ADAMTS2 expression. **The induction of ADAMTS2 reduced tumor growth in TS2-KO mice back to the weight of tumors formed in WT mice, indicating a rescue of the TS2-KO phenotype.** The use of LLC conditionally expressing EGFP instead of ADAMTS2 confirmed that the doxycycline treatment is not responsible for the repression of tumor growth.

In contrast, induction of ADAMTS2 expression in tumors formed in WT mice had no effect on LLC and B16 tumors. Indicating that the amount of ADAMTS2 produced by the host is sufficient to mediate the tumor suppressive effect of ADAMTS2.

To confirm these results in a more relevant tumor model, we produced a MMTV-PyMT ADAMTS2 knockout model which took about 2 years to generate. We first changed the ADAMTS2 knockout mouse genetic background from C57Bl6 to FVB/N (for optimal MMTV-PyMT tumor growth), and then generated PyMT$^{-/+}$ FVBN ADAMTS2 knockout and wild type littermate mice. MMTV-PyMT mice develop tumors that recapitulate the physiopathological development of breast cancer, from mammary gland hyperplasia (8 week-old) and desmoplasia to lung metastasis (+/- 14 week-old). This model allowed the study of the absence of ADAMTS2 in relevant tumor development contexts, with the associated increased heterogeneity and complexity as compared to subcutaneous tumor models. Indeed within a single MMT-PyMT tumor, different tumor stages can be found associated with different vascular, necrosis, hemorrhagic and desmoplastic structures.

Study of tumor development in MMTV-PyMT mice is commonly performed by the sacrifice of mice at a defined time point, usually at 14 weeks which ensures enough metastatic dissemination to be quantifiable. Expecting an increase in tumor growth in TS2-KO mice, if both WT and TS2-KO mice were to be sacrificed at 14 weeks, (i) tumors from TS2-KO mice would be ethically too big and (ii) the change in tumor size between WT and TS2-KO mice could have affected metastatic dissemination and therefore prevent the evaluation of the role of ADAMTS2 in metastatic spread. To try to mitigate these issues, we took the challenge of following mice individually and to sacrifice them when the biggest of their tumors reached 1 cm³. The success of this approach can be appreciated by the equivalent weight distribution of WT and TS2-KO PyMT tumors.

To indirectly evaluate tumor growth, we therefore compared the age at sacrifice of WT and TS2-KO PyMT mice. TS2-KO PyMT mice were sacrificed earlier than WT PyMT mice indicating that **absence of ADAMTS2 increased tumor growth, as in the subcutaneous models.**

To evaluate the metastatic dissemination, we evaluated the presence of metastases in the lung of these mice. To avoid the biased of increased tumor growth in TS2-KO mice that may affect metastases growth, we quantified the number of metastatic foci instead of the surface area. We observed that **TS2-KO PyMT mice lungs were almost devoid of metastases.**

Due to our experimental settings, TS2-KO mice have been sacrificed, on average, earlier than WT mice which may be responsible for this severe reduction of metastatic foci number. However, no correlation was found between the age at sacrifice and the mean number of metastatic foci for each mouse. This indicates that the time gap between the sacrifice of WT and TS2-KO mice did not affect the number of lung metastases, and, therefore, that disseminations from the primary tumors that lead to the identified metastases occurred far earlier than the timing at which we started sacrificing the mice. Thus, our experimental approach is unlikely to have impacted the metastatic

dissemination. These data suggest that **ADAMTS2 has a key role in metastatic dissemination of mammary tumors into the lung, probably independently of its anti-tumor functions.**

Through the comparison of **subcutaneous (LLC and B16)** and *spontaneous MMTV-PyMT* tumors models, we can exclude some potential mechanisms underlying the role of ADAMTS2 in tumor development. The major differences between the two types of model are (i) the duration (**14 days** vs *14 weeks)*, (ii) the **absence** vs *presence* of desmoplastic reaction, (iii) the location of the tumor (**subcutaneous** vs *mammary orthotopic)* and (iv) the extent of hemorrhages and necrosis (**extensive** vs *moderate)*. Despite these multiple differences, the absence of ADAMTS2 results in increased tumor growth in both models, indicating that a common mechanism is at play independently of all these differing characteristics.

Given the high expression level of ADAMTS2 in fibroblasts compared to mammary gland epithelial cells, we first hypothesized that CAFs might be responsible for the production of almost all ADAMTS2 in MMTV-PyMT tumors, and therfore may be the likely effector of increased tumor growth in TS2-KO mice.

Fully exploiting our subcutaneous MMTV-PyMT tumor model, we optimized the isolation of both CAFs and epithelial cancer cells from spontaneous MMTV-PyMT tumors. We performed a fast and effective isolation of both cell types through differential plating. Cells were kept as short as possible in culture to retain as much as possible their *in vivo* phenotype.

To identify factors that could explain the differences in tumor growth observed between PyMT-WT and PyMT-TS2-KO mice, we decided to perform a transcriptomic analysis. Proteomic analysis was not planned as ADAMTS2 activity is inhibited in culture condition. This RNA sequencing, while clearly highlighting the epithelial phenotype of cancer cells and the mesenchymal phenotype of CAFs, was unsuccessful at highlighting a significant differential transcriptional pattern of these cells between WT and TS2-KO.

While the isolation of cancer cells and CAFs reduced complexity, it is clear that the *in vivo* heterogeneity and variability, that we aimed to reduce with cells isolation, have still affected our data and impaired the identification of faintly differentially expressed genes. Yet, ADAMTS2 serving as internal control for this experiment was in both cases clearly significantly shutdown in TS2-KO mice which indicates that big alterations of mRNA level were detectable.

Altogether, this RNA sequencing analysis highlights that **cancer cells and CAFs are transcriptionally unaffected by the absence of ADAMTS2,** at least once placed in culture. This experiment could be repeated using freshly isolated cancer cells or CAFs by cell sorting or immobilized anti-CD90.2 antibodies. These approaches would prevent cell plating on polystyrene dishes risking their subsequent phenotypic alterations.

Subcutaneous B16 and LLC tumors as well as spontaneous MMTV-PyMT tumors are too heterogeneous to provide relevant and robust data by histology or omics methods. In the hope of developing a better *in vivo* and fast tumor growth model, we undergo the strenuous task of MMTV-

PyMT cancer cell line isolation and stabilisation. The generation of a stable PyMT cancer cell line is a months-long process slowed by the high mortality of cancer cell after each passage. We were successful in this task for both PyMT-WT and PyMT-TS2-KO cancer cells. Both cell lines formed tumors after their subcutaneous injection in FVB/N mice reaching the tumor growth end point (1 cm^3) at 21 days for PyMT-WT cancer cells and 14 days for PyMT-TS2-KO cancer cells. We avoided drawing any conclusion about the differing growth rate of those cell lines, as the months of culture required for cancer cell stabilization may differentially affect each cell line.

Subcutaneous PyMT tumors are far more homogeneous than B16, LLC and spontaneous MMTV-PyMT tumors both in terms of tumor size and intra-tumoral content. This is likely due to the presence of many collapsed blood vessels (especially in the center of the tumor) that prevent the exponential growth of the tumor. We believe that the presence of an abundant collagen deposition (desmoplastic reaction) and subsequent rigidity of the parenchyma explain this phenomenon.

The desmoplastic reaction seems to originate, at least in part, from the cancer cells which mainly display a mesenchymal phenotype. This is a striking difference as compared to their phenotype *in vitro* which is predominantly epithelial. These observations highlight the ability of PyMT cancer cells to transdifferentiate from an epithelial to a mesenchymal phenotype. This sarcoma-like behavior greatly differs from spontaneous MMTV-PyMT tumors development but, while losing some of its relevance for breast tumor development, it produced our most homogeneous subcutaneous tumor model to date while retaining the phenotype of increased tumor growth in the absence of ADAMTS2.

The comparison of the weight of subcutaneous tumors formed by PyMT-WT and PyMT-TS2-KO cancer cells in WT and TS2-KO mice showed, once again, **that the absence of ADAMTS2 produced by the host, but not cancer cells, results in increased tumor growth.**

Armed with this new homogeneous *in vivo* model, we were able to evaluate the effect of ADAMTS2 knockout on the TME. In subcutaneous PyMT tumors, both collagen deposition and blood vessel distribution were visually unaffected by the knockout of ADAMTS2 from both the host and cancer cells, while lymphatic vessels were absent in all conditions (data not shown). From these histological analyses, we concluded that **the role of ADAMTS2 in fibrosis**[91,303]**, angiogenesis**[119] **and lymphangiogenesis**[269] **were unlikely to be involved in its tumor repressive function.**

Even with an unchanged amount of collagen in tumors, we hypothesized that the role of ADAMTS2 in collagen maturation may be at play in its anti-tumoral effect. First, we quantified the expression level of ADAMTS2 in subcutaneous tumors from PyMT-WT and PyMT-TS2-KO cancer cells formed in WT and TS2-KO mice. It revealed that 80% of ADAMTS2 expression in tumors is produced by the host while 20 % only is produced by cancer cells. Tumor formed by PyMT WT cancer cells, while expressing ADAMTS2, grow faster in TS2-KO mice as compared

to WT mice indicating that the **ADAMTS2 expressed by cancer cells is ineffective to rescue the lack of ADAMTS2 produced by the environment.**

This conclusion is opposite to that drawn from our rescue experiment in B16 and LLC subcutaneous tumors in which expression of recombinant ADAMTS2 by cancer cells reduced tumor growth in TS2-KO mice to levels similar to those observed in WT mice. We believe that, contrary to the high expression of recombinant ADAMTS2 in B16 and LLC tumors, the lower amount of ADAMTS2 and the high desmoplastic reaction found in subcutaneous PyMT tumor prevent ADAMTS2 from diffusing outside the vicinity of the cancer cells, and thus from affecting host cells.

We then evaluated the processing of the type I collagen in these tumors. In subcutaneous PyMT tumors formed by PyMT-WT cancer cells, type I collagen (both alpha 1 and alpha 2 chains) was completely processed in both WT and TS2-KO mice. From these observations, we concluded that (i) ADAMTS2 produced by cancer cells is sufficient to completely process type I collagen and that (ii) **collagen processing by ADAMTS2 is not involved in its tumor suppressive effect.**

Knowing that the absence of ADAMTS2 increases tumor growth in both non-desmoplastic (LLC and B16F10 subcutaneous tumors), moderately desmoplastic (MMTV-PyMT spontaneous tumors) and highly desmoplastic tumors (subcutaneous PyMT tumors), and also that the transcriptome of CAFs is unaffected by the knockout of ADAMTS2, we concluded **that it is highly unlikely that mesenchymal cells of the host are involved in this phenotype.**

To take a step back and evaluate our subcutaneous PyMT tumor model with a fresh view, we performed single-cell-RNA sequencing on whole tumors. We specifically focused our analysis on tumors generated from PyMT-TS2-KO so that only the ADAMTS2 produced by the host will be present.

In this analysis, very few CAFs have been identified. This was not anticipated since tumoral ADAMTS2 is mostly produced by the host and so, presumably, CAFs. Several hypotheses, not mutually exclusive, can be put forward: (i) CAFs could have been less efficiently recovered from tumors due to their embedding in a dense collagen matrix. (ii) CAFs could be present but mixed and "hidden" within the different cancer cell clusters. Indeed, because of the mesenchymal phenotype of PyMT cancer cells *in vivo*, bioinformatics clustering might be unable to differentiate the two populations. (iii) Inherent biases of scRNA sequencing may skew the relative abundance of cell types identification. Comparison between scRNA sequencing and single-nuclei RNA sequencing seems to indicate that scRNA sequencing is poorly effective to identify mesenchymal cells [304].

With no apparent changes in cancer cell clusters between WT and TS2-KO mice, we focused our analysis on immune cells ($CD45^+$) which were mostly identified as macrophages, although we could not exclude that dendritic cells, granulocytes and monocytes may be present within those clusters, but masked.

Reclusterisation of macrophages allowed a better segregation between the different sub-populations. We identified 7 clusters, out of which 3 were differentially abundant between tumors from WT and TS2-KO mice. Cluster 0 and 1, which are slightly reduced in TS2-KO mice, are disproportionately characterized by pro-inflammatory genes. In contrast, cluster 3, which is increased in TS2-KO mice, is characterized by increased mRNA expression of MGL2 and RETNLA which are major IL4 response genes[305], indicating that this cluster is composed of M2-like macrophages. This single cell RNA sequencing analysis indicates that **the absence of ADAMTS2 from the host causes a switch from pro-inflammatory to anti-inflammatory gene expression in macrophages in subcutaneous PyMT tumors.**

To confirm those observations, we performed FACS analysis. We first evaluated 14-days subcutaneous PyMT tumors as for sc-RNA sequencing. At this timing, we did not observe any extensive variations between immune cells from WT and TS2-KO mice, except for a trend towards an increase proportion of M2-like ($CD206^{high}$ $CD11c^{low}$) macrophages in tumors formed in TS2-KO mice. While being only a trend, this observation seemed to correlate with our sc-RNA sequencing data.

It is possible that the TME of 14-day subcutaneous PyMT tumors are too immunosuppressed to identify the effect of ADAMTS2 on the immune system. The innate immune system (macrophages, neutrophils, …) respond rapidly to tumor formation and may thus be affected faster by the immunosuppressive environment of the TME. To test this hypothesis, FACS analysis was performed on 7-days subcutaneous PyMT tumors. At this timing, we already observed the two-fold tumor growth increase in TS2-KO mice compared to in WT mice, which led to the conclusion that **ADAMTS2 impacts tumor growth early.**

FACS analysis on 7-day subcutaneous PyMT tumors from WT and TS2-KO mice revealed **a more immunosuppressive TME in TS2-KO mice**, as illustrated by increases in (i) M2-like macrophages, (ii) arginase-1 expression in macrophages, (iii) CD14 expression in M-MDSC and G-MDSC and (iv) IL-10 expressing T cells. Lower abundances of both dendritic cells and T cells were also observed in tumors from TS2-KO mice as compared to WT mice.

M2-like macrophages in our analysis are characterized by a high CD206/MRC1 expression. CD206 has been widely considered an immunosuppressive marker in macrophages and is linked to poorer overall survival and disease-free survival in patients with solid tumor[306]. ARG1 is an enzyme that uses L-arginine to produce L-ornithine and urea. Arginine is an amino acid at the basis of nitric oxide (NO) production by inducible nitric oxide synthase (INOS/nos2). The activity of ARG1 is thought to deplete the arginine pool, reducing its availability for NO production and T cell activation[307]. The expression of ARG1 by macrophages is a marker of immunosuppression and is linked to a reduced NO-mediated tumor cytotoxicity[308].

MDSCs are myeloid cells notorious for their immune suppressive function. There are subdivided into granulocyte- and monocyte-MDSC based on their cell of origin and their

expression of Ly6c and Ly6g. CD14 expression in MDSCs has been linked to an immunosuppressive TME[309].

IL-10 is a well-known immunosuppressive cytokine[310]. Dendritic cells and T cells are both major players in adaptive immunity. A reduction of their abundance may therefore relate to a lack of immunogenicity of the tumor in TS2-KO mice and subsequent reduction of infiltration.

Altogether, tumors formed in TS2-KO mice display a more immunosuppressive TME. This repressed immune system may reduce the cancer cell killing ability of the tumor-infiltration immune cells which could explain the faster tumor growth rate in TS2-KO mice.

The most straightforward strategy to verify *in vivo* the implication of the immune system is the use of immune-compromised mice. Using such a model for the study of the anti-tumor activity of ADAMTS2 is, however, hardened by the fact that generation of ADAMTS2 knockout immunocompromised mice represented a challenging process, certainly beyond the scope and timeframe of this work. Instead, we considered using an overexpression model into WT immunodeficient mice. On the other hand, we previously demonstrated that ADAMTS2 overexpression by cancer cells does not decrease tumor growth in WT mice.

However, a previous study of the laboratory[119] showed that "tumors" from HEK293 constitutively expressing ADAMTS2 barely developed in nude mice as compared to HEK293 control. This observation was intriguing, we therefore evaluated this discrepancy by investigating the effect of ADAMTS2 on tumor growth in immunocompromised mice. We aimed to progressively control for the limitations of the previous study by using (i) cancer cells instead of HEK293, using (ii) conditionally expressing cell lines instead of using two different ones and using (iii) different immunocompromised mice models.

In a first experimental model largely mimicking our previous study, we produced tumors in nude mice by subcutaneous injection of HEK293 conditionally expressing ADAMTS2. We could confirm that **ADAMTS2 expression by immortalized cells, indeed, reduces tumor growth in nude mice.** To ensure that this effect was not HEK293 cells dependent, we performed an equivalent experiment using our modified LLC cells that were subcutaneously injected in NOD-SCID mice. NOD-SCID mice, like nude mice, have no adaptive immunity due to a lack of T cells. In this model, the induction of ADAMTS2 expression by LLC significantly reduced tumor growth while induction of EGFP expression (used as control) had no significant effect. From this experiment, we concluded that **ADAMTS2 overexpression in immunocompromised mice expressing endogenous ADAMTS2 reduces tumor growth through a mechanism independent of adaptive immunity.**

We repeated this experiment in an even further immunocompromised mouse model. NSG for NOD-SCID gamma are NOD-SCID mice additionally knockout for IL2 receptor gamma, a receptor sub-unit involved in the formation of receptors for IL2, IL4, IL7, IL9 and IL15[311]. This alteration leads to additional defects in innate immunity like the absence of NK cells[312,313]. In NSG mice the induction of ADAMTS2 expression by LLC did not reduce tumor growth, indicating that

the anti-tumor effect of ADAMTS2 is mediated by the immune system, most likely the innate immunity.

Could CAFs drive the tumor suppressive role of ADAMTS2?

Our study using subcutaneous PyMT tumors highlights that ADAMTS2, expressed by host cells and not cancer cells, is responsible for its tumor suppressive function. This was intriguing given that PyMT cancer cells are widespread in the tumor and express about 20% of the intra-tumoral ADAMTS2 mRNA level which is enough to fully process type I collagen all around the tumor. This high, widespread and effective ADAMTS2 expression seems, nevertheless, to be insufficient to compensate for the absence of expression from host cells. From this observation, we can hypothesize that **ADAMTS2 impacts tumor growth through a cancer cell-independent mechanism.** This hypothesis is strengthened by the lack of observable role of ADAMTS2 on the migration, proliferation and transmigration of cancer cells (using either recombinant ADAMTS2, CAFs conditioned medium and cancer cells/CAFs co-cultures (data not shown)).

Through flow cytometry analysis, we determined that the relative cellular composition of subcutaneous PyMT tumors is 50% cancer cells, 25% TAMs, 15% stromal cells (endothelial cells, CAFs, …) and 10% other immune cells. While TAMs are more abundant than CAFs in this model, they express much less ADAMTS2. Based on our relative estimate of ADAMTS2 mRNA expression, stromal cells express 74% of the total ADAMTS2 in the tumor while cancer cells accounts for 20% and macrophages 6%. **CAFs thus express most of the ADAMTS2 found in the tumor.**

As previously stated, ADAMTS2 produced by CAFs does not seem to impact cancer cells directly. On the other hand, one or multiple intermediate players (co-factors, substrates derived from the ECM, endothelial cells or immune cells) could mediate an anti-proliferative signaling in cancer cells leading to reduced tumor growth observed in presence of ADAMTS2 produced by CAFs. To somewhat accurately create an *in vitro* model that could recapitulate the TME, a coculture of CAFs WT/TS2-KO with BMDMs WT/TS2-KO and PyMT cancer cells TS2-KO was evaluated but failed to provide relevant insight regarding into the involved mechanism.

With a very limited leeway using *in vitro* models, the use of various *in vivo* models helped us estimate the relative importance of the various components of the TME. Comparisons of non-desmoplastic (LLC-B16) and highly desmoplastic (subcutaneous PyMT) tumor models suggest that the ECM and matrices-producing stromal cells are unnecessary to mediate the ADAMTS2-mediated inhibition of tumor growth. The absence of striking difference in the delta of tumor growth rate between non-desmoplastic and highly desmoplastic tumor from WT and TS2-KO mice indicate that **matrice-producting CAFs and the ECM are dispensable for the tumor suppressive function of ADAMTS2 to occur.**

To exclude a potential role of CAFs, a conditional knockout leading to suppression of ADAMTS2 expression specifically in fibroblasts would be needed. This could be performed using transgenic mice generated using a Cre/lox system dependent on the COL1A1 promotor. To be efficient, this approach needs to lead to a specific and effective reduction of ADAMTS2 expression in CAFs. Indeed, ADAMTS2$^{+/-}$, mice while having 50% expression of ADAMTS2, show no

symptoms of dermatosparaxis and do not display increased tumor growth compared to WT mice (data not shown).

As a less expensive and time-consuming alternative than producing new transgenic mice, a transcriptomic analysis of CAFs from the TME (by RNA sequencing) could be performed using cell sorting or MACS isolation of fibroblasts (using anti-CD90.2 or anti-FAP antibodies). This experiment would, on the other hand, only provide an indication regarding the polarization and inflammation status of CAFs and would unlikely help to identify the root cause of the changes in the TME.

Could TAMs drive the tumor suppressive role of ADAMTS2?

Macrophages, while accounting for only 6% of the ADAMTS2 expression within the tumor, cannot be excluded as both mediators and ADAMTS2-producing cells driving tumor suppression. Macrophage/monocyte infiltration is widespread in solid tumors including LLC tumors[316] and MMTV-PyMT tumors[317], which may explain the persistent phenotype between our different *in vivo* models.

Moreover, the diversity of immune cell types that are affected by ADAMTS2 suggests that a general upstream mechanism is involved. Macrophages in tumors have pleiotropic roles ranging from antigen presentation, cytotoxicity, phagocytosis, stimulation and inhibition of other immune cells[318,319]. These pleiotropic roles allow macrophages to regulate most of the immune TME. If ADAMTS2 modifies macrophage differentiation and polarization, this modulation could trickle down to the rest of the tumor immune system and explain this widespread immunoregulation.

To evaluate the role of ADAMTS2 in macrophages, we first aimed to polarize WT and TS2-KO BMDMs into M1 and M2 macrophages. We assessed both the polarization status and the expression ADAMTS2 in these cells. ADAMTS2 expression was not induced by either M1 or M2 polarization, and the polarization status of WT and TS2-KO BMDMs was similar.

To induce ADAMTS2 expression by macrophages, glucocorticoid treatment is required[109,110]. Interestingly, glucocorticoid treatment leads to the polarization of macrophage into a subset called M2c. M2c macrophages produce TGFβ and IL10, and have a phagocytic function against apoptotic cells[320]. Glucocorticoids (methylprednisolone or dexamethasone), especially in combination with IL-4, induce a 6-fold increase of ADAMTS2 mRNA expression in THP1 (human monocytes), Raw264.7 (murine macrophages) and BMDMs (data not shown). The induction of ADAMTS2 expression in WT and TS2-KO BMDMs did not differentially affect the mRNA expression of key macrophages markers (data not shown).

BMDMs, while being more relevant than monocytes/macrophages cell lines, remain a poor model for the study of ADAMTS2 because (i) they can not be effectively used for 3D models, (ii) ADAMTS2 enzymatic activity is very low *in vitro* and (iii) we are unable to induce ADAMTS2 mRNA expression equivalent to levels found in TAMs. To evaluate the effect of enzymatically active ADAMTS2 on BMDMs polarization, we treated TS2-KO BMDMs (pre-incubated (M2c) or not (M0) with IL4 and glucocorticoids) with recombinant active ADAMTS2, and then assessed their polarization. But not impact of active ADAMTS2 on BMDMs polarization could be highlighted. Therefore, **ADAMTS2 does not seem to have any direct impact on BMDMs polarization.**

However, we cannot exclude the possibility that the inappropriate polarization status of BMDMs *in vitro* and the absence of cofactors which are otherwise present in the TME *in vivo*, prevent ADAMTS2 to affect macrophage polarization. To overcome these drawbacks, switching BMDMs to freshly isolated TAMs (by cell sorting or MACS isolation) could provide the missing parameters mediating ADAMTS2 regulation of macrophage polarization. TAMs from WT and

TS2-KO mice and comparing them by N-TAILS and RNA sequencing could reveal clues to the underlying mechanisms of tumor suppression driven by ADAMTS2.

With no relevant model, yet in place, to properly evaluate the function of ADAMTS2 secreted by macrophages, we can instead attempt to correlate the immunosuppressive phenotype found in absence of ADAMTS2 with the function of known (e.g. VEGFC, DKK3, TGFBRIII, LTBP1) and potential substrates of ADAMTS2 identified by N-TAILS on subcutaneous PyMT tumors (complement proteins and annexins).

VEGFC is abundantly produced by adipocytes and fibroblasts, and is the primary driver of lymphangiogenesis. Lymphangiogenesis is increased during wound healing[269] and triggered by pro-inflammatory factors like IL1β[321]. ADAMTS2 is involved in VEGFC maturation and may therefore participate in inflammatory response signaling. Macrophages express both VEGFC and its receptors VEGFR2 and VEGFR3[322], and can be located close to lymphatic vessels[323]. VEGFC expression by macrophages increases in response to inflammatory signals (TNFα, LPS and IL1β)[324]. In a cornea model, macrophage depletion reduces lymphangiogenesis and VEGFC expression following IL1β treatment[321]. Yet, VEGFC expression from myeloid cells seems to have inflammatory resolving function[325]. The role of VEGFC on TAMs polarization remain elusive[326] and its role on tumor development seems to indicate that VEGFC-VEGFR3 pathway activation promote tumor growth[327]. Based on our study, no relevant link could be identified between ADAMTS2-mediated VEGFC activation and tumor growth.

TGFβ is an immunosuppressive cytokine found within the ECM in a latent form requiring cleavage or biomechanical tension to be released. ADAMTS2 has been linked to TGFβ activation[120,293,328]. TGFβ is also found in its active form at the surface of immune cells such as Tregs complexed with GARP[329]. Macrophages can both produce and respond to TGFβ with implication in their differentiation, polarization or maintenance as in the case of alveolar macrophages[330]. Interestingly, macrophages seems be only responsive to TGFβ treatment upon Il4 and glucocorticoids (and not Il4 only) treatment which induces TGFβ receptor expression[331]. The combination of IL4 and glucocorticoids is the same treatment that induces the most ADAMTS2 mRNA expression in BMDMs *in vitro*. Co-expression of ADAMTS2 and TGFβ receptor may be a way to improve TGFβ signaling. Indeed, our lab showed that ADAMTS2 is able to cleave DKK3, LTBP1 and sTGFBRIII leading to increase TGFβ signaling[267]. ADAMTS2 would therefore induce immunosuppressive signaling by promoting the release and activation of TGFβ. However, the opposite phenotype has been highlighted in tumor using TS2-KO mice. A TGFβ mediated role for ADAMTS2 in tumor growth seems unlikely.

Dickkopf-related protein (DKK1, DKK2, DKK3 and DKK4) are inhibitory extracellular proteins of the Wnt signaling pathway. DKK are highly glycosylated protein produced mostly by mesenchymal, endothelial, neuronal, muscle and some glandular epithelial cells. DKK3 is the most widely expressed and has been identified as a substrate of ADAMTS2[267]. The ADAMTS2 cleavage site on DKK3 is not found in the other DKK-related proteins. The downstream effect of DKK3 cleavage by ADAMTS2 is unclear and could either increase or decrease DKK3 binding to its

receptor. DKK3 binds with high affinity to LRP5/6, preventing Wnt signaling and leading to β-catenin degradation. The effect of DKK3 on tumor development and the immune system is unclear. Some studies have described DKK3 as an immunosuppressive and pro-tumoral factor[332]. DKK3 has also been reported to be expressed and involved in maintaining tolerant CD8 T cells[333]. DKK3 has an immunosuppressive function on both CD4 and CD8 T cells[334] and prevent excessive inflammation[335]. On the other hand, other data indicate that DKK3 has tumor suppressive properties[336] and increase macrophage phagocytic activity against cancer cells[337]. However, the bulk of the literature indicates the immunosuppressive function of DKK3[338]. Therefore, for DDK3 to be involved in the tumor suppressive function of ADAMTS2, it must be assumed that cleavage of DKK3 would result in reduced binding to its receptor and thus reduced immunosuppression and, consequently, reduced tumor growth. This hypothesis could be tested by evaluating the impact of ADAMTS2 cleaved DKK3 on BMDMs polarization.

Glucocorticoids, annexin A1 and ADAMTS2

Given their special roles in both ADAMTS2 expression and immunosuppression, endogenous glucocorticoids, like cortisol, may play a role in the tumor suppressive role of ADAMTS2. Pathologies and treatments can modulate cortisol levels in patients. For example, schizophrenia treatment with haloperidol (D2 dopaminergic receptor blocker) reduces cortisol level in patient which correlates with treatment response[339]. Likewise, ADAMTS2 mRNA expression in PBMC is decreased with anti-psychotic drugs which correlates to response to treatment[106]. In breast cancer, cortisol levels correlate with relapse post-treatment[340]. Glucocorticoids may affect breast cancer proliferation by competitive binding with estrogen receptor, therefore reducing ER^+ breast cancer growth[341]. Moreover, glucocorticoids can be produced *in situ* by TAMs in the TME[342].

Glucocorticoid treatment induces annexin a1 expression in macrophages but not in blood leukocytes[325]. While annexin A1 is secreted rapidly upon glucocorticoids treatment, ADAMTS2 mRNA levels begin to rise slowly. ADAMTS2 may serve as a regulatory means to cleave and inactive annexin a1 to prevent excessive immunosuppression. Annexin knockout in myeloid cells inhibits tumor growth linked to the cGAS-STING pathway to induce type I IFN in tumors and M1 macrophages polarisation[343]. On the other hand, systemic knockout of Annexin A1 leads to reduced tumor growth and M1 macrophage polarization[344]. Annexin A1 may have a specific role to play on macrophages. While glucocorticoids treatment lead to T cell death[345], glucocorticoids have only an inflammation-resolving function on myeloid cells[346]. ADAMTS2 may be a resistance mechanism to annexin a1-mediated immune cell death in macrophages. Annexin A1 is a potent generalized immunosuppressive factor[296] that could explain the global immunosuppression found in tumors growing in TS2-KO mice. The absence of ADAMTS2 would drive an excessive and prolonged annexin a1 activity driving M2 macrophages polarization.

To investigate the role ADAMTS2 in the glucocorticoid response in the TME, we could repress the steroidogenesis in both WT and TS2-KO mice using pharmacological inhibitors such as metyrapone. If ADAMTS2 represses tumor growth by reducing the immunosuppressive potency

of glucocorticoids through annexin a1 cleavage, the inhibition of cortisol production could decrease tumor growth in TS2-KO mice back to WT mice level. Likewise, dexamethasone treatment could amplify the immunosuppression found in tumors from TS2-KO mice, and further increase tumor growth differences between WT and TS2-KO mice.

To validate the general implication of macrophages in the effect of ADAMTS2 expression on tumor growth, a mouse model could be generated in which ADAMTS2 expression would be specifically suppressed in myeloid cells (using LysMCre, lysozyme 2 promotor). Other methods could involve the depletion of macrophages using clodronate in liposome[347] or the expression and activation of human diphtheria toxin receptor in CD11b cells[348].

To confirm the general implication of the immune system, both WT and TS2-KO mice could be exposed to ionizing radiations to induce a generalized immunosuppression before using them for tumor growth models. We could also transplant a pool of immune cells from one genotype to the other in order to potentially reverse (WT in KO) or induce (KO in WT) the effect of ADAMTS2 on tumor growth.

How does ADAMTS2 impact the metastasis process?

The lymphangiogenesis hypothesis:

In this work, we have focused our study on the effect of ADAMTS2 on primary tumor growth. Elucidation of the effect of ADAMTS2 on metastatic dissemination has been, and continues to be, the subject of studies in our laboratory, but so far only hypotheses can be formulated. At present, our preferred working hypothesis is that the role of ADAMTS2 in lymphangiogenesis is probably responsible for the massive reduction in metastasis in TS2-KO mice as compared to WT mice. This hypothesis is supported by the observed reduction in tumor-draining lymph node hyperplasia in TS2-KO mice compared to WT mice, despite the tumors being twice as large. The absence of ADAMTS2 may prevent the formation of the pre-metastatic niche and/or the dissemination of cancer cells into lymph nodes.

Unfortunately, subcutaneous tumors do not produce observable metastases, preventing the use of this model to study the role of the lymphatic system in cancer cell dissemination. For this reason, we are currently developing an orthotopic tumor model formed by injecting MMTV-PyMT cancer cells injected into the mammary fat pad. Under conditions that more closely mimic those present during spontaneous mammary tumor formation in MMTV-PyMT mice, which produce lung metastases, we expect to improve the metastatic dissemination potential of PyMT cancer cells.

The epithelial to mesenchymal transition (EMT) hypothesis:

While the effect of ADAMTS2 on tumor growth is independent of ADAMTS2 expression by cancer cells, this may not be the case for metastatic dissemination. Indeed, the MMTV-PyMT model is the only tumor model used in our study that leads to lung metastasis. In this model, we can not dissociate the genotype of CAFs and macrophages with cancer cells. During EMT, cancer cells are likely to express ADAMTS2 as they change from an epithelial to a mesenchymal phenotype. We cannot exclude that ADAMTS2 expression by cancer cells is not involved in the EMT process (perhaps via TGFβ signaling) and, subsequently, in dissemination outside the primary tumor.

To test this hypothesis, the same orthotopic tumor model mentioned above could be used, with both PyMT WT and TS2-KO cancer cells transplanted into the fat pad of TS2-KO or WT mice. With this model, we may be able to determine if either the absence of ADAMTS2 expression by the host or by cancer cells is involved in its role on metastasis dissemination.

The lung vs bone marrow hypothesis:

While no differences were observed in the ECM of tumors from WT and TS2 KO mice, the lung ECM may be differentially affected by the absence of ADAMTS2. Alterations in ECM proteins, such as periostin or tenascin, have been linked to the pre-metastatic niche in the lung. We investigated the steady-state lung macrophage profile of WT and TS2 KO mice and identified

major changes in the abundance of macrophages and expression of functional markers (IL10 and ARG1) in lung macrophages in the absence of ADAMTS2.

These data may indicate that the absence of ADAMTS2 affects either the lung parenchyma or the whole body macrophage pool. Indeed, bone marrow ECM is involved in the differentiation of hematopoietic stem cells. Cleavage of collagen or other ECM proteins by ADAMTS2 could therefore affect the differentiation of myeloid progenitor cells.

FACS analysis of blood monocytes and resident macrophages from other tissues (e.g. Kupffer cells in the liver) could help determine whether the absence of ADAMTS2 affects monocytes/macrophages in a tissue-dependent manner or upstream in the genesis of myeloid cells.

How can ADAMTS2 repress tumor growth in immunocompromised WT mice but not immunocompetent WT mice?

Initially, the lack of effect on tumor growth of ADAMTS2 expression by cancer cells in WT mice was assumed to be related to the presence of ADAMTS2 from the host that "saturates" its effect. But if so, why would ADAMTS2 have an effect on tumor growth in *Adamts2*$^{+/+}$ immunodeficient mice?

On the basis of the elements mentioned above, we have formulated a hypothesis that might explain this opponent contradiction as well as the absence of anti-tumor effect of recombinant ADAMTS2 in NSG mice.

(i) Since the immune system appears to be responsible for the effect of ADAMTS2, we consider that the increase in tumor growth in TS2-KO mice relates to a decrease in cancer cell lysis.

(ii) Mediator of cancer cell lysis are CD8 T cells, NK cells and macrophages:
   a. In immunocompetent mice, both CD8 T cells and NK cells/macrophages are present and can all have a complementary role in cancer cell killing[349].
   b. In immunocompetent mice, increasing the amount of ADAMTS2 in the tumor has no added value on cancer cell lysis.
   c. In Nude and NOD-SCID mice, CD8 T cells are absent and cancer cells lysis is therefore only mediated by the innate immunity (NK cells/Macrophages).
   d. In NSG mice, both mediators of cancer cells lysis are absent.

Thus, **ADAMTS2 overexpression appears to decrease tumor growth when CD8 T cells are absent and when NK cells/macrophages are present.**

Based on these data, we hypothesized that:

(i) In immunocompetent WT mice, CD8 T cells drive most of the cancer cell killing masking the increased killing ability of innate immune cells by recombinant ADAMTS2.

(ii) In nude and NOD-SCID mice, the absence of CD8 T cells increases the importance of innate immune cells cytotoxic activity, allowing the effect of recombinant ADAMTS2 on these cells to be detected.

(iii) In NSG mice, innate immunity is shutdown, recombinant ADAMTS2 no longer has effectors to impact tumor growth and thus no reduction of tumor growth can be identified.

Summary

In this work, we describe for the first time the role of ADAMTS2 in tumor growth. We confirmed, through several *in vivo* models, that ADAMTS2 is a tumor suppressor. We provided the first data indicating that ADAMTS2 may play a key role in metastatic spread. By comparing of several *in vivo* models, we were able to show that ADAMTS2 affects tumor growth independently of its known functions in angiogenesis, collagen maturation, fibrosis and lymphangiogenesis. Instead, we highlighted that ADAMTS2 plays a key role early on in tumor development by stimulating the innate immunity within the tumor. We argue that ADAMTS2 expressed by the host, most likely by macrophages, is the key mediator of this suppressive effect on tumor growth.

This work paved the way for another study on ADAMTS2, this time focusing on understanding its role in metastatic spread.

ADAMTS2 is a protein that comes up frequently in –omics data and scientists are helpless to understand its role in their models. This work/publication will help others to see ADAMTS2 as not only as an ECM proteinase but also as an important player in the immune TME, potentially bringing forth new fields of study for this poorly understood enzyme.

References

1. Fallas, J. A., Gauba, V. & Hartgerink, J. D. Solution Structure of an ABC Collagen Heterotrimer Reveals a Single-register Helix Stabilized by Electrostatic Interactions. *J Biol Chem* **284**, 26851–26859 (2009).
2. Prockop, D. J. & Kivirikko, K. I. Collagens: molecular biology, diseases, and potentials for therapy. *Annu Rev Biochem* **64**, 403–434 (1995).
3. Humphries, S. M., Lu, Y., Canty, E. G. & Kadler, K. E. Active Negative Control of Collagen Fibrillogenesis *in Vivo*. *Journal of Biological Chemistry* **283**, 12129–12135 (2008).
4. Tanaka, T. *et al.* Visualized procollagen Iα1 demonstrates the intracellular processing of propeptides. *Life Science Alliance* **5**, (2022).
5. Gelse, K., Pöschl, E. & Aigner, T. Collagens--structure, function, and biosynthesis. *Adv Drug Deliv Rev* **55**, 1531–1546 (2003).
6. Myllyharju, J. & Kivirikko, K. I. Collagens, modifying enzymes and their mutations in humans, flies and worms. *Trends in Genetics* **20**, 33–43 (2004).
7. Gelse, K., Pöschl, E. & Aigner, T. Collagens—structure, function, and biosynthesis. *Advanced Drug Delivery Reviews* **55**, 1531–1546 (2003).
8. Fortunati, D., Chau, D. Y. S., Wang, Z., Collighan, R. J. & Griffin, M. Cross-linking of collagen I by tissue transglutaminase provides a promising biomaterial for promoting bone healing. *Amino Acids* **46**, 1751–1761 (2014).
9. Ellingson, A., Pancheri, N. & Schiele, N. Regulators of collagen crosslinking in developing and adult tendons. *eCM* **43**, 130–152 (2022).
10. Edwards, I. J. Proteoglycans in prostate cancer. *Nat Rev Urol* **9**, 196–206 (2012).
11. Campbell, I. D. & Humphries, M. J. Integrin Structure, Activation, and Interactions. *Cold Spring Harb Perspect Biol* **3**, a004994 (2011).
12. Fu, X. *et al.* Mesenchymal Stem Cell Migration and Tissue Repair. *Cells* **8**, (2019).

13. Watt, F. M. & Huck, W. T. S. Role of the extracellular matrix in regulating stem cell fate. *Nat Rev Mol Cell Biol* **14**, 467–473 (2013).

14. Hallmann, R. *et al.* The regulation of immune cell trafficking by the extracellular matrix. *Current Opinion in Cell Biology* **36**, 54–61 (2015).

15. Monteran, L. & Erez, N. The Dark Side of Fibroblasts: Cancer-Associated Fibroblasts as Mediators of Immunosuppression in the Tumor Microenvironment. *Frontiers in Immunology* **10**, (2019).

16. Huxley-Jones, J. *et al.* The evolution of the vertebrate metzincins; insights from Ciona intestinalis and Danio rerio. *BMC Evolutionary Biology* **7**, 63 (2007).

17. Wells, J. M., Gaggar, A. & Blalock, J. E. MMP generated matrikines. *Matrix Biology* **44–46**, 122–129 (2015).

18. Monboisse, J. C., Oudart, J. B., Ramont, L., Brassart-Pasco, S. & Maquart, F. X. Matrikines from basement membrane collagens: A new anti-cancer strategy. *Biochimica et Biophysica Acta (BBA) - General Subjects* **1840**, 2589–2598 (2014).

19. Ricard-Blum, S. & Salza, R. Matricryptins and matrikines: biologically active fragments of the extracellular matrix. *Experimental Dermatology* **23**, 457–463 (2014).

20. Lee, N. V. *et al.* ADAMTS1 mediates the release of antiangiogenic polypeptides from TSP1 and 2. *The EMBO Journal* **25**, 5270–5283 (2006).

21. Rosell-García, T. *et al.* Differential cleavage of lysyl oxidase by the metalloproteinases BMP1 and ADAMTS2/14 regulates collagen binding through a tyrosine sulfate domain. *J Biol Chem* **294**, 11087–11100 (2019).

22. Vadon-Le Goff, S., Hulmes, D. J. S. & Moali, C. BMP-1/tolloid-like proteinases synchronize matrix assembly with growth factor activation to promote morphogenesis and tissue remodeling. *Matrix Biology* **44–46**, 14–23 (2015).

23. Li, Y., Chen, Y., Wu, W., Li, N. & Hua, J. MMPs, ADAMs and ADAMTSs are associated with mammalian sperm fate. *Theriogenology* **200**, 147–154 (2023).

24. Dwivedi, S. D. *et al.* Mechanistic insight on the role of iRhom2-TNF-α-BAFF signaling pathway in various autoimmune disorders. *Adv Biol Regul* 101011 (2023) doi:10.1016/j.jbior.2023.101011.

25. Kuno, K., Iizasa, H., Ohno, S. & Matsushima, K. The exon/intron organization and chromosomal mapping of the mouse ADAMTS-1 gene encoding an ADAM family protein with TSP motifs. *Genomics* **46**, 466–471 (1997).

26. Colige, A. *et al.* cDNA cloning and expression of bovine procollagen I N-proteinase: a new member of the superfamily of zinc-metalloproteinases with binding sites for cells and other matrix components. *Proc Natl Acad Sci U S A* **94**, 2374–2379 (1997).

27. Takeda, S. ADAM and ADAMTS Family Proteins and Snake Venom Metalloproteinases: A Structural Overview. *Toxins (Basel)* **8**, 155 (2016).

28. Somerville, R. P. T. *et al.* ADAMTS7B, the full-length product of the ADAMTS7 gene, is a chondroitin sulfate proteoglycan containing a mucin domain. *J Biol Chem* **279**, 35159–35175 (2004).

29. Kelwick, R., Desanlis, I., Wheeler, G. N. & Edwards, D. R. The ADAMTS (A Disintegrin and Metalloproteinase with Thrombospondin motifs) family. *Genome Biol* **16**, 113 (2015).

30. Majerus, E. M., Zheng, X., Tuley, E. A. & Sadler, J. E. Cleavage of the ADAMTS13 propeptide is not required for protease activity. *J Biol Chem* **278**, 46643–46648 (2003).

31. Kramerova, I. A. *et al.* Papilin in development; a pericellular protein with a homology to the ADAMTS metalloproteinases. *Development* **127**, 5475–5485 (2000).

32. Taye, N., Redhead, C. & Hubmacher, D. Secreted ADAMTS-like proteins as regulators of connective tissue function. *American Journal of Physiology-Cell Physiology* (2024) doi:10.1152/ajpcell.00680.2023.

33. Kuno, K. *et al.* Molecular cloning of a gene encoding a new type of metalloproteinase-disintegrin family protein with thrombospondin motifs as an inflammation associated gene. *J Biol Chem* **272**, 556–562 (1997).

34. Thai, S. N.-M. & Iruela-Arispe, M. L. Expression of ADAMTS1 during murine development. *Mech Dev* **115**, 181–185 (2002).

35. Iruela-Arispe, M. L., Carpizo, D. & Luque, A. ADAMTS1: a matrix metalloprotease with angioinhibitory properties. *Ann N Y Acad Sci* **995**, 183–190 (2003).

36. Sun, Y., Huang, J. & Yang, Z. The roles of ADAMTS in angiogenesis and cancer. *Tumor Biol.* **36**, 4039–4051 (2015).

37. Rocks, N. *et al.* ADAMTS-1 metalloproteinase promotes tumor development through the induction of a stromal reaction in vivo. *Cancer Res* **68**, 9541–9550 (2008).

38. Ricciardelli, C. *et al.* The ADAMTS1 protease gene is required for mammary tumor growth and metastasis. *Am J Pathol* **179**, 3075–3085 (2011).

39. Inagaki, J. *et al.* ADAMTS1 inhibits lymphangiogenesis by attenuating phosphorylation of the lymphatic endothelial cell-specific VEGF receptor. *Exp Cell Res* **323**, 263–275 (2014).

40. Hulin, A. *et al.* Metallothionein-dependent up-regulation of TGF-β2 participates in the remodelling of the myxomatous mitral valve. *Cardiovasc Res* **93**, 480–489 (2012).

41. Kiani, C., Chen, L., Wu, Y. J., Yee, A. J. & Yang, B. B. Structure and function of aggrecan. *Cell Res* **12**, 19–32 (2002).

42. Verma, P. & Dalal, K. ADAMTS-4 and ADAMTS-5: Key enzymes in osteoarthritis. *Journal of Cellular Biochemistry* **112**, 3507–3514 (2011).

43. Liu, C.-J. *et al.* ADAMTS-7: a metalloproteinase that directly binds to and degrades cartilage oligomeric matrix protein. *FASEB J* **20**, 988–990 (2006).

44. Liu, C. *et al.* ADAMTS-12 associates with and degrades cartilage oligomeric matrix protein. *J Biol Chem* **281**, 15800–15808 (2006).

45. Dąbkowska, K. *et al.* GAAGs, COMP, and YKL-40 as Potential Markers of Cartilage Turnover in Blood of Children with Juvenile Idiopathic Arthritis Treated with Etanercept-Relationship with ADAMTS4, ADAMTS5, and PDGF-BB. *J Clin Med* **11**, 5069 (2022).

46. Pérez-García, S. *et al.* Wnt and RUNX2 mediate cartilage breakdown by osteoarthritis synovial fibroblast-derived ADAMTS-7 and -12. *J Cell Mol Med* **23**, 3974–3983 (2019).

47. Lai, Y. *et al.* ADAMTS-7 forms a positive feedback loop with TNF-α in the pathogenesis of osteoarthritis. *Annals of the Rheumatic Diseases* **73**, 1575–1584 (2014).

48. Wei, J.-L. *et al.* Role of ADAMTS-12 in Protecting Against Inflammatory Arthritis in Mice By Interacting With and Inactivating Proinflammatory Connective Tissue Growth Factor. *Arthritis Rheumatol* **70**, 1745–1756 (2018).

49. Bai, X. H., Wang, D. W., Luan, Y., Yu, X. P. & Liu, C. J. Regulation of chondrocyte differentiation by ADAMTS-12 metalloproteinase depends on its enzymatic activity. *Cell Mol Life Sci* **66**, 667–680 (2009).

50. Mizoguchi, T. *et al.* Coronary Disease Association With ADAMTS7 Is Due to Protease Activity. *Circ Res* **129**, 458–470 (2021).

51. Ma, Z. *et al.* Peptide Vaccine Against ADAMTS-7 Ameliorates Atherosclerosis and Postinjury Neointima Hyperplasia. *Circulation* **147**, 728–742 (2023).

52. Paulissen, G. *et al.* Control of allergen-induced inflammation and hyperresponsiveness by the metalloproteinase ADAMTS-12. *J Immunol* **189**, 4135–4143 (2012).

53. Moncada-Pazos, A. *et al.* ADAMTS-12 metalloprotease is necessary for normal inflammatory response. *J Biol Chem* **287**, 39554–39563 (2012).

54. Mead, T. J. *et al.* The metalloproteinase-proteoglycans ADAMTS7 and ADAMTS12 provide an innate, tendon-specific protective mechanism against heterotopic ossification. *JCI Insight* **3**, e92941.

55. Moncada-Pazos, A. *et al.* The ADAMTS12 metalloprotease gene is epigenetically silenced in tumor cells and transcriptionally activated in the stroma during progression of colon cancer. *J Cell Sci* **122**, 2906–2913 (2009).

56. Wang, D., Zhu, T., Zhang, F.-B. & He, C. Expression of ADAMTS12 in Colorectal Cancer-Associated Stroma Prevents Cancer Development and Is a Good Prognostic Indicator of Colorectal Cancer. *Dig Dis Sci* **56**, 3281–3287 (2011).

57. Li, C. *et al.* ADAMTS12 acts as a cancer promoter in colorectal cancer via activating the Wnt/β-catenin signaling pathway in vitro. *Ann Transl Med* **8**, 301 (2020).

58. Llamazares, M. *et al.* The ADAMTS12 metalloproteinase exhibits anti-tumorigenic properties through modulation of the Ras-dependent ERK signalling pathway. *J Cell Sci* **120**, 3544–3552 (2007).

59. El Hour, M. *et al.* Higher sensitivity of Adamts12-deficient mice to tumor growth and angiogenesis. *Oncogene* **29**, 3025–3032 (2010).

60. Fontanil, T. *et al.* Interaction between the ADAMTS-12 metalloprotease and fibulin-2 induces tumor-suppressive effects in breast cancer cells. *Oncotarget* **5**, 1253–1264 (2014).

61. Mohamedi, Y. *et al.* Lung Inflammatory Phenotype in Mice Deficient in Fibulin-2 and ADAMTS-12. *Int J Mol Sci* **25**, 2024 (2024).

62. Lapière, C. M., Lenaers, A. & Kohn, L. D. Procollagen peptidase: an enzyme excising the coordination peptides of procollagen. *Proc Natl Acad Sci U S A* **68**, 3054–3058 (1971).

63. Colige, A. *et al.* Characterization and partial amino acid sequencing of a 107-kDa procollagen I N-proteinase purified by affinity chromatography on immobilized type XIV collagen. *J Biol Chem* **270**, 16724–16730 (1995).

64. Nusgens, B. V. *et al.* Evidence for a relationship between Ehlers-Danlos type VII C in humans and bovine dermatosparaxis. *Nat Genet* **1**, 214–217 (1992).

65. Colige, A. *et al.* Human Ehlers-Danlos syndrome type VII C and bovine dermatosparaxis are caused by mutations in the procollagen I N-proteinase gene. *Am J Hum Genet* **65**, 308–317 (1999).

66. Wertelecki, W., Smith, L. T. & Byers, P. Initial observations of human dermatosparaxis: Ehlers-Danlos syndrome type VIIC. *J Pediatr* **121**, 558–564 (1992).

67. Bar-Yosef, O. *et al.* Multiple congenital skull fractures as a presentation of Ehlers-Danlos syndrome type VIIC. *Am J Med Genet A* **146A**, 3054–3057 (2008).

68. Malfait, F. *et al.* The natural history, including orofacial features of three patients with Ehlers-Danlos syndrome, dermatosparaxis type (EDS type VIIC). *Am J Med Genet A* **131**, 18–28 (2004).

69. Rincón-Sánchez, A. R. *et al.* Ehlers-Danlos Syndrome Type VIIC: A Mexican Case Report. *Case Rep Dermatol* **4**, 104–113 (2012).

70. Dubois, P. E., Veyckemans, F., Ledent, M. M., Michel, M. & de Clety, S. C. Anaesthetic management of a child with type VIIc Ehlers-Danlos syndrome. *Acta Anaesthesiol Belg* **52**, 21–24 (2001).

71. Fujimoto, A., Wilcox, W. R. & Cohn, D. H. Clinical, morphological, and biochemical phenotype of a new case of Ehlers-Danlos syndrome type VIIC. *Am J Med Genet* **68**, 25–28 (1997).

72. Pasch, M. C., Sillevis Smitt, J. H., Veenhuizen, L., Kuiters, G. R. & van Essen, A. J. [Boy with dermatosparaxis (Ehlers-Danlos type VIIC)]. *Ned Tijdschr Geneeskd* **144**, 2435–2436 (2000).

73. Van Damme, T. *et al.* Expanding the clinical and mutational spectrum of the Ehlers-Danlos syndrome, dermatosparaxis type. *Genet Med* **18**, 882–891 (2016).

74. Li, S. W. *et al.* Transgenic mice with inactive alleles for procollagen N-proteinase (ADAMTS-2) develop fragile skin and male sterility. *Biochem J* **355**, 271–278 (2001).

75. Le Goff, C. *et al.* Regulation of procollagen amino-propeptide processing during mouse embryogenesis by specialization of homologous ADAMTS proteases: insights on collagen biosynthesis and dermatosparaxis. *Development* **133**, 1587–1596 (2006).

76. Colige, A. *et al.* Domains and maturation processes that regulate the activity of ADAMTS-2, a metalloproteinase cleaving the aminopropeptide of fibrillar procollagens types I-III and V. *J Biol Chem* **280**, 34397–34408 (2005).

77. Colige, A. *et al.* Cloning and characterization of ADAMTS-14, a novel ADAMTS displaying high homology with ADAMTS-2 and ADAMTS-3. *J Biol Chem* **277**, 5756–5766 (2002).

78. Nagase, T. Prediction of the Coding Sequences of Unidentified Human Genes. VII. The Complete Sequences of 100 New cDNA Clones from Brain Which Can Code for Large Proteins in vitro. *DNA Research* **4**, 141–150 (1997).

79. Hurskainen, T. L., Hirohata, S., Seldin, M. F. & Apte, S. S. ADAM-TS5, ADAM-TS6, and ADAM-TS7, novel members of a new family of zinc metalloproteases. General features and genomic distribution of the ADAM-TS family. *J Biol Chem* **274**, 25555–25563 (1999).

80. Fernandes, R. J. *et al.* Procollagen II amino propeptide processing by ADAMTS-3. Insights on dermatosparaxis. *J Biol Chem* **276**, 31502–31509 (2001).

81. Janssen, L. *et al.* ADAMTS3 activity is mandatory for embryonic lymphangiogenesis and regulates placental angiogenesis. *Angiogenesis* **19**, 53–65 (2016).

82. Brouillard, P. *et al.* Loss of ADAMTS3 activity causes Hennekam lymphangiectasia-lymphedema syndrome 3. *Hum Mol Genet* **26**, 4095–4104 (2017).

83. Ogino, H. *et al.* Secreted Metalloproteinase ADAMTS-3 Inactivates Reelin. *J Neurosci* **37**, 3181–3191 (2017).

84. Yamakage, Y. *et al.* A disintegrin and metalloproteinase with thrombospondin motifs 2 cleaves and inactivates Reelin in the postnatal cerebral cortex and hippocampus, but not in the cerebellum. *Mol Cell Neurosci* **100**, 103401 (2019).

85. Bolz, H., Ramírez, A., von Brederlow, B. & Kubisch, C. Characterization of ADAMTS14, a novel member of the ADAMTS metalloproteinase family. *Biochim Biophys Acta* **1522**, 221–225 (2001).

86. Kentistou, K. A. *et al.* Large scale phenotype imputation and in vivo functional validation implicate ADAMTS14 as an adiposity gene. *Nat Commun* **14**, 307 (2023).

87. Dupont, L. *et al.* Spontaneous atopic dermatitis due to immune dysregulation in mice lacking Adamts2 and 14. *Matrix Biol* **70**, 140–157 (2018).

88. Wang, W.-M. *et al.* Transforming growth factor-beta induces secretion of activated ADAMTS-2. A procollagen III N-proteinase. *J Biol Chem* **278**, 19549–19557 (2003).

89. Zhou, S.-H. *et al.* Gene expression profiling of craniofacial fibrous dysplasia reveals ADAMTS2 overexpression as a potential marker. *Int J Clin Exp Pathol* **7**, 8532–8541 (2014).

90. Wang, X. *et al.* Critical Role of ADAMTS2 (A Disintegrin and Metalloproteinase With Thrombospondin Motifs 2) in Cardiac Hypertrophy Induced by Pressure Overload. *Hypertension* **69**, 1060–1069 (2017).

91. Kesteloot, F. *et al.* ADAM metallopeptidase with thrombospondin type 1 motif 2 inactivation reduces the extent and stability of carbon tetrachloride-induced hepatic fibrosis in mice. *Hepatology* **46**, 1620–1631 (2007).

92. Li, H., Dong, C., Cao, T. & Chang, S. [Expression of ADAMTS-2 and TGF-β1 in cirrhotic liver]. *Zhong Nan Da Xue Xue Bao Yi Xue Ban* **37**, 1026–1030 (2012).

93. Dong, C. *et al.* A Disintegrin and Metalloprotease with Thrombospondin Motif 2 May Contribute to Cirrhosis in Humans through the Transforming Growth Factor-β/SMAD Pathway. *Gut Liver* **7**, 213–220 (2013).

94. Stempfle, G., McGowen, M. R., Caravas, J. A. & Wildman, D. E. From PPROM to caul: The evolution of membrane rupture in mammals. *Appl Transl Genom* **2**, 70–77 (2013).

95. Flitcroft, D. I. *et al.* Novel Myopia Genes and Pathways Identified From Syndromic Forms of Myopia. *Invest Ophthalmol Vis Sci* **59**, 338–348 (2018).

96. Iglesias, A. I. *et al.* Cross-ancestry genome-wide association analysis of corneal thickness strengthens link between complex and Mendelian eye diseases. *Nat Commun* **9**, 1864 (2018).

97. Arning, A. *et al.* ADAMTS genes and the risk of cerebral aneurysm. *J Neurosurg* **125**, 269–274 (2016).

98. Arning, A. *et al.* A genome-wide association study identifies a gene network of ADAMTS genes in the predisposition to pediatric stroke. *Blood* **120**, 5231–5236 (2012).

99. McCorkindale, A. N., Patrick, E., Duce, J. A., Guennewig, B. & Sutherland, G. T. The Key Factors Predicting Dementia in Individuals With Alzheimer's Disease-Type Pathology. *Front Aging Neurosci* **14**, 831967 (2022).

100. Steiner, J. L., Pruznak, A. M., Navaratnarajah, M. & Lang, C. H. Alcohol Differentially Alters Extracellular Matrix and Adhesion Molecule Expression in Skeletal Muscle and Heart. *Alcohol Clin Exp Res* **39**, 1330–1340 (2015).

101. Vonk, L. A. *et al.* Endoplasmic reticulum stress inhibits collagen synthesis independent of collagen-modifying enzymes in different chondrocyte populations and dermal fibroblasts. *Biochem Cell Biol* **88**, 539–552 (2010).

102. Willis, E. L., Bridges, P. J. & Fortune, J. E. Progesterone receptor and prostaglandins mediate luteinizing hormone-induced changes in messenger RNAs for ADAMTS proteases in theca cells of bovine periovulatory follicles. *Mol Reprod Dev* **84**, 55–66 (2017).

103. Sadic, M. *et al.* Expression of ADAMTS2 and ADAMTS5 in the salivary gland of rats after radioiodine therapy. *Nucl Med Commun* **39**, 110–117 (2018).

104. Altuntaş, C., Alper, M., Keleş, Y., Sav, F. N. & Köçkar, F. Hypoxic regulation of ADAMTS-2 and -3 (a disintegrin and matrix metalloproteinase with thrombospondin motifs 2 and 3) procollagen N proteinases by HIF-1α in endothelial cells. *Mol Cell Biochem* (2022) doi:10.1007/s11010-022-04549-3.

105. Ruso-Julve, F. *et al.* Dopaminergic control of ADAMTS2 expression through cAMP/CREB and ERK: molecular effects of antipsychotics. *Transl Psychiatry* **9**, 306 (2019).

106. Crespo-Facorro, B., Prieto, C. & Sainz, J. Schizophrenia gene expression profile reverted to normal levels by antipsychotics. *Int J Neuropsychopharmacol* **18**, pyu066 (2014).

107. Hofer, T. P. J. *et al.* Tissue-specific induction of ADAMTS2 in monocytes and macrophages by glucocorticoids. *J Mol Med (Berl)* **86**, 323–332 (2008).

108. Chamoto, K. *et al.* Migration of CD11b+ accessory cells during murine lung regeneration. *Stem Cell Res* **10**, 267–277 (2013).

109. Jubb, A. W., Hofer, T. P., Hume, D. A. & Ziegler-Heitbrock, L. The preterm labor associated ADAMTS2 gene is induced by glucocorticoids. *Am J Obstet Gynecol* **219**, 122–123 (2018).

110. Estupiñán-Moreno, E. *et al.* Methylome and transcriptome profiling of giant cell arteritis monocytes reveals novel pathways involved in disease pathogenesis and molecular response to glucocorticoids. *Ann Rheum Dis* **81**, 1290–1300 (2022).

111. Paquette, A. G. *et al.* Comparative analysis of gene expression in maternal peripheral blood and monocytes during spontaneous preterm labor. *Am J Obstet Gynecol* **218**, 345.e1-345.e30 (2018).

112. Zhu, X. *et al.* Abnormal cortisol profile during psychosocial stress among patients with schizophrenia in a Chinese population. *Sci Rep* **12**, 18591 (2022).

113. Alper, M. & Kockar, F. IL-6 upregulates a disintegrin and metalloproteinase with thrombospondin motifs 2 (ADAMTS-2) in human osteosarcoma cells mediated by JNK pathway. *Mol Cell Biochem* **393**, 165–175 (2014).

114. Alper, M., Aydemir, A. T. & Köçkar, F. Induction of human ADAMTS-2 gene expression by IL-1α is mediated by a multiple crosstalk of MEK/JNK and PI3K pathways in osteoblast like cells. *Gene* **573**, 321–327 (2015).

115. D'Arienzo, R. *et al.* A deregulated immune response to gliadin causes a decreased villus height in DQ8 transgenic mice. *Eur J Immunol* **39**, 3552–3561 (2009).

116. Kevorkian, L. *et al.* Expression profiling of metalloproteinases and their inhibitors in cartilage. *Arthritis Rheum* **50**, 131–141 (2004).

117. Endo, J. *et al.* Comparative Analysis of Gene Expression between Cartilage and Menisci in Early-Phase Osteoarthritis of the Knee-An Animal Model Study. *J Knee Surg* **31**, 664–669 (2018).

118. Wang, L. *et al.* The alteration of A disintegrin and metalloproteinase with thrombospondin motifs (ADAMTS) in the knee joints of osteoarthritis mice. *J Histotechnol* **44**, 99–110 (2021).

119. Dubail, J. *et al.* ADAMTS-2 functions as anti-angiogenic and anti-tumoral molecule independently of its catalytic activity. *Cell Mol Life Sci* **67**, 4213–4232 (2010).

120. Bekhouche, M. *et al.* Determination of the substrate repertoire of ADAMTS2, 3, and 14 significantly broadens their functions and identifies extracellular matrix organization and TGF-β signaling as primary targets. *FASEB J* **30**, 1741–1756 (2016).

121. Multiplexed Protein Quantitation in Saccharomyces cerevisiae Using Amine-reactive Isobaric Tagging Reagents - ScienceDirect. https://www.sciencedirect.com/science/article/pii/S153594762032939X?via%3Dihub.

122. Kleifeld, O. *et al.* Identifying and quantifying proteolytic events and the natural N terminome by terminal amine isotopic labeling of substrates. *Nat Protoc* **6**, 1578–1611 (2011).

123. Kleifeld, O. *et al.* Isotopic labeling of terminal amines in complex samples identifies protein N-termini and protease cleavage products. *Nat Biotechnol* **28**, 281–288 (2010).

124. Prudova, A., auf dem Keller, U., Butler, G. S. & Overall, C. M. Multiplex N-terminome analysis of MMP-2 and MMP-9 substrate degradomes by iTRAQ-TAILS quantitative proteomics. *Mol Cell Proteomics* **9**, 894–911 (2010).

125. Schlage, P., Kockmann, T., Kizhakkedathu, J. N. & auf dem Keller, U. Monitoring matrix metalloproteinase activity at the epidermal-dermal interface by SILAC-iTRAQ-TAILS. *Proteomics* **15**, 2491–2502 (2015).

126. Prudova, A. *et al.* TAILS N-Terminomics and Proteomics Show Protein Degradation Dominates over Proteolytic Processing by Cathepsins in Pancreatic Tumors. *Cell Rep* **16**, 1762–1773 (2016).

127. Sabino, F. *et al.* In Vivo Assessment of Protease Dynamics in Cutaneous Wound Healing by Degradomics Analysis of Porcine Wound Exudates *[S]. *Molecular & Cellular Proteomics* **14**, 354–370 (2015).

128. Leduc, C. *et al.* In vivo N-Terminomics Highlights Novel Functions of ADAMTS2 and ADAMTS14 in Skin Collagen Matrix Building. *Front Mol Biosci* **8**, 643178 (2021).

129. Kolte, D., McClung, J. A. & Aronow, W. S. Chapter 6 - Vasculogenesis and Angiogenesis. in *Translational Research in Coronary Artery Disease* (eds. Aronow, W. S. & McClung, J. A.) 49–65 (Academic Press, Boston, 2016). doi:10.1016/B978-0-12-802385-3.00006-1.

130. Adams, R. H. & Alitalo, K. Molecular regulation of angiogenesis and lymphangiogenesis. *Nat Rev Mol Cell Biol* **8**, 464–478 (2007).

131. Cross, M. J. & Claesson-Welsh, L. FGF and VEGF function in angiogenesis: signalling pathways, biological responses and therapeutic inhibition. *Trends Pharmacol Sci* **22**, 201–207 (2001).

132. Kazerounian, S., Yee, K. O. & Lawler, J. Thrombospondins in cancer. *Cell Mol Life Sci* **65**, 700–712 (2008).

133. Maquart, F.-X., Pasco, S., Ramont, L., Hornebeck, W. & Monboisse, J.-C. An introduction to matrikines: extracellular matrix-derived peptides which regulate cell activity: Implication in tumor invasion. *Critical Reviews in Oncology/Hematology* **49**, 199–202 (2004).

134. Ribatti, D. Endogenous inhibitors of angiogenesis: A historical review. *Leukemia Research* **33**, 638–644 (2009).

135. METH-1, a human ortholog of ADAMTS-1, and METH-2 are members of a new family of proteins with angio-inhibitory activity - PubMed. https://pubmed.ncbi.nlm.nih.gov/10438512/.

136. Luque, A., Carpizo, D. R. & Iruela-Arispe, M. L. ADAMTS1/METH1 Inhibits Endothelial Cell Proliferation by Direct Binding and Sequestration of VEGF165*. *Journal of Biological Chemistry* **278**, 23656–23665 (2003).

137. Liu, Y.-J., Xu, Y. & Yu, Q. Full-length ADAMTS-1 and the ADAMTS-1 fragments display pro- and antimetastatic activity, respectively. *Oncogene* **25**, 2452–2467 (2006).

138. Su, S.-C., Mendoza, E. A., Kwak, H.-I. & Bayless, K. J. Molecular profile of endothelial invasion of three-dimensional collagen matrices: insights into angiogenic sprout induction in wound healing. *Am J Physiol Cell Physiol* **295**, C1215-1229 (2008).

139. Koo, B.-H. *et al.* ADAMTS9 Is a Cell-Autonomously Acting, Anti-Angiogenic Metalloprotease Expressed by Microvascular Endothelial Cells. *Am J Pathol* **176**, 1494–1504 (2010).

140. Uren, R. F. Lymphatic drainage of the skin. *Annals of Surgical Oncology* **11**, 179S-185S (2004).

141. Jones, D. & Min, W. An overview of lymphatic vessels and their emerging role in cardiovascular disease. *J Cardiovasc Dis Res* **2**, 141–152 (2011).

142. Maby-El Hajjami, H. & Petrova, T. V. Developmental and pathological lymphangiogenesis: from models to human disease. *Histochem Cell Biol* **130**, 1063–1078 (2008).

143. Karkkainen, M. J. *et al.* Vascular endothelial growth factor C is required for sprouting of the first lymphatic vessels from embryonic veins. *Nat Immunol* **5**, 74–80 (2004).

144. Jeltsch, M. *et al.* Hyperplasia of lymphatic vessels in VEGF-C transgenic mice. *Science* **276**, 1423–1425 (1997).

145. Lymboussaki, A., Olofsson, B., Eriksson, U. & Alitalo, K. Vascular Endothelial Growth Factor (VEGF) and VEGF-C Show Overlapping Binding Sites in Embryonic Endothelia and Distinct Sites in Differentiated Adult Endothelia. *Circulation Research* **85**, 992–999 (1999).

146. Rubbia-Brandt, L. *et al.* Lymphatic vessel density and vascular endothelial growth factor-C expression correlate with malignant behavior in human pancreatic endocrine tumors. *Clin Cancer Res* **10**, 6919–6928 (2004).

147. Joukov, V. *et al.* Proteolytic processing regulates receptor specificity and activity of VEGF-C. *EMBO J* **16**, 3898–3911 (1997).

148. Connell, F. *et al.* A new classification system for primary lymphatic dysplasias based on phenotype. *Clin Genet* **77**, 438–452 (2010).

149. Bos, F. L. *et al.* CCBE1 Is Essential for Mammalian Lymphatic Vascular Development and Enhances the Lymphangiogenic Effect of Vascular Endothelial Growth Factor-C In Vivo. *Circulation Research* **109**, 486–491 (2011).

150. Jeltsch, M. *et al.* CCBE1 enhances lymphangiogenesis via A disintegrin and metalloprotease with thrombospondin motifs-3-mediated vascular endothelial growth factor-C activation. *Circulation* **129**, 1962–1971 (2014).

151. McColl, B. K. *et al.* Plasmin Activates the Lymphangiogenic Growth Factors VEGF-C and VEGF-D. *J Exp Med* **198**, 863–868 (2003).

152. Lim, L. *et al.* Hemostasis stimulates lymphangiogenesis through release and activation of VEGFC. *Blood* **134**, 1764–1775 (2019).

153. Jha, S. K. *et al.* KLK3/PSA and cathepsin D activate VEGF-C and VEGF-D. *eLife* **8**, e44478 (2019).

154. Bui, H. M. *et al.* Proteolytic activation defines distinct lymphangiogenic mechanisms for VEGFC and VEGFD. *J Clin Invest* **126**, 2167–2180 (2016).

155. Scheuerle, A. E. *et al.* An additional case of Hennekam lymphangiectasia-lymphedema syndrome caused by loss-of-function mutation in ADAMTS3. *Am J Med Genet A* **176**, 2858–2861 (2018).

156. Benavente, S., Sánchez-García, A., Naches, S. & LLeonart, M. E. Therapy-Induced Modulation of the Tumor Microenvironment: New Opportunities for Cancer Therapies. *Front. Oncol.* **10**, (2020).

157. Peinado, H. *et al.* Pre-metastatic niches: organ-specific homes for metastases. *Nat Rev Cancer* **17**, 302–317 (2017).

158. Wechman, S. L., Emdad, L., Sarkar, D., Das, S. K. & Fisher, P. B. Vascular mimicry: Triggers, molecular interactions and in vivo models. *Adv Cancer Res* **148**, 27–67 (2020).

159. Costa, A. *et al.* Fibroblast Heterogeneity and Immunosuppressive Environment in Human Breast Cancer. *Cancer Cell* **33**, 463-479.e10 (2018).

160. Geng, X. *et al.* Cancer-Associated Fibroblast (CAF) Heterogeneity and Targeting Therapy of CAFs in Pancreatic Cancer. *Front. Cell Dev. Biol.* **9**, (2021).

161. Sahai, E. *et al.* A framework for advancing our understanding of cancer-associated fibroblasts. *Nat Rev Cancer* **20**, 174–186 (2020).

162. Öhlund, D. *et al.* Distinct populations of inflammatory fibroblasts and myofibroblasts in pancreatic cancer. *J Exp Med* **214**, 579–596 (2017).

163. Elyada, E. *et al.* Cross-Species Single-Cell Analysis of Pancreatic Ductal Adenocarcinoma Reveals Antigen-Presenting Cancer-Associated Fibroblasts. *Cancer Discov* **9**, 1102–1123 (2019).

164. Hennigs, A. *et al.* Prognosis of breast cancer molecular subtypes in routine clinical care: A large prospective cohort study. *BMC Cancer* **16**, 734 (2016).

165. Kai, F., Drain, A. P. & Weaver, V. M. The Extracellular Matrix Modulates the Metastatic Journey. *Developmental Cell* **49**, 332–346 (2019).

166. Provenzano, P. P. *et al.* Collagen density promotes mammary tumor initiation and progression. *BMC Medicine* **6**, 11 (2008).

167. Provenzano, P. P. *et al.* Collagen reorganization at the tumor-stromal interface facilitates local invasion. *BMC Medicine* **4**, 38 (2006).

168. Han, W. *et al.* Oriented collagen fibers direct tumor cell intravasation. *Proceedings of the National Academy of Sciences* **113**, 11208–11213 (2016).

169. Serres, E. *et al.* Fibronectin expression in glioblastomas promotes cell cohesion, collective invasion of basement membrane in vitro and orthotopic tumor growth in mice. *Oncogene* **33**, 3451–3462 (2014).

170. Van Obberghen-Schilling, E. *et al.* Fibronectin and tenascin-C: accomplices in vascular morphogenesis during development and tumor growth. *The International Journal of Developmental Biology* **55**, 511–525 (2011).

171. Spenlé, C. *et al.* Tenascin-C Orchestrates an Immune-Suppressive Tumor Microenvironment in Oral Squamous Cell Carcinoma. *Cancer Immunology Research* **8**, 1122–1138 (2020).

172. Postlethwaite, A. E. & Kang, A. H. Collagen-and collagen peptide-induced chemotaxis of human blood monocytes. *The Journal of experimental medicine* **143**, 1299–1307 (1976).

173. Weathington, N. M. *et al.* A novel peptide CXCR ligand derived from extracellular matrix degradation during airway inflammation. *Nat Med* **12**, 317–323 (2006).

174. Arnold, S. A. *et al.* Lack of host SPARC enhances vascular function and tumor spread in an orthotopic murine model of pancreatic carcinoma. *Disease Models & Mechanisms* **3**, 57–72 (2010).

175. Kaplan, G. In vitro differentiation of human monocytes. Monocytes cultured on glass are cytotoxic to tumor cells but monocytes cultured on collagen are not. *Journal of Experimental Medicine* **157**, 2061–2072 (1983).

176. Steitz, A. M. *et al.* Tumor-associated macrophages promote ovarian cancer cell migration by secreting transforming growth factor beta induced (TGFBI) and tenascin C. *Cell Death Dis* **11**, 1–15 (2020).

177. Egeblad, M., Rasch, M. G. & Weaver, V. M. Dynamic interplay between the collagen scaffold and tumor evolution. *Current Opinion in Cell Biology* **22**, 697–706 (2010).

178. Misiura, M. & Miltyk, W. Proline-containing peptides—New insight and implications: A Review. *BioFactors* **45**, 857–866 (2019).

179. Hui, Z. *et al.* Single-cell profiling of immune cells after neoadjuvant pembrolizumab and chemotherapy in IIIA non-small cell lung cancer (NSCLC). *Cell Death Dis* **13**, 1–18 (2022).

180. Quah, H. S. *et al.* Single cell analysis in head and neck cancer reveals potential immune evasion mechanisms during early metastasis. *Nat Commun* **14**, 1680 (2023).

181. Wang, C. *et al.* The heterogeneous immune landscape between lung adenocarcinoma and squamous carcinoma revealed by single-cell RNA sequencing. *Sig Transduct Target Ther* **7**, 1–17 (2022).

182. Van Wagoner, C. M. *et al.* Antibody-mediated phagocytosis in cancer immunotherapy. *Immunological Reviews* **319**, 128–141 (2023).

183. van der Horst, H. J. & Mutis, T. Enhancing Fc-mediated effector functions of monoclonal antibodies: The example of HexaBodies. *Immunological Reviews* **n/a**,.

184. Atkinson, J. P., Liszewski, M. K. & Yu, C. Y. Chapter 14 - Clinical aspects of the complement system in systemic lupus erythematosus. in *Systemic Lupus Erythematosus (Second Edition)* (ed. Tsokos, G. C.) 113–122 (Academic Press, 2021). doi:10.1016/B978-0-12-814551-7.00014-3.

185. Mamidi, S., Höne, S. & Kirschfink, M. The complement system in cancer: Ambivalence between tumour destruction and promotion. *Immunobiology* **222**, 45–54 (2017).

186. Bordron, A. *et al.* Complement System: a Neglected Pathway in Immunotherapy. *Clinic Rev Allerg Immunol* **58**, 155–171 (2020).

187. Dostert, C., Grusdat, M., Letellier, E. & Brenner, D. The TNF Family of Ligands and Receptors: Communication Modules in the Immune System and Beyond. *Physiol Rev* **99**, 115–160 (2019).

188. van Loo, G. & Bertrand, M. J. M. Death by TNF: a road to inflammation. *Nat Rev Immunol* **23**, 289–303 (2023).

189. Kruyt, F. A. E. TRAIL and cancer therapy. *Cancer Letters* **263**, 14–25 (2008).

190. LeBlanc, H. N. & Ashkenazi, A. Apo2L/TRAIL and its death and decoy receptors. *Cell Death Differ* **10**, 66–75 (2003).

191. Walczak, H. *et al.* Tumoricidal activity of tumor necrosis factor–related apoptosis–inducing ligand in vivo. *Nat Med* **5**, 157–163 (1999).

192. Gunalp, S. *et al.* TRAIL promotes the polarization of human macrophages toward a proinflammatory M1 phenotype and is associated with increased survival in cancer patients with high tumor macrophage content. *Front Immunol* **14**, 1209249 (2023).

193. Ciuleanu, T. *et al.* A randomized, double-blind, placebo-controlled phase II study to assess the efficacy and safety of mapatumumab with sorafenib in patients with advanced hepatocellular carcinoma. *Ann Oncol* **27**, 680–687 (2016).

194. von Pawel, J. *et al.* Phase II trial of mapatumumab, a fully human agonist monoclonal antibody to tumor necrosis factor-related apoptosis-inducing ligand receptor 1 (TRAIL-R1), in combination with paclitaxel and carboplatin in patients with advanced non-small-cell lung cancer. *Clin Lung Cancer* **15**, 188-196.e2 (2014).

195. Wang, H. *et al.* Activation of TIM1 induces colon cancer cell apoptosis via modulating Fas ligand expression. *Biochem Biophys Res Commun* **473**, 377–381 (2016).

196. Villa-Morales, M. & Fernández-Piqueras, J. Targeting the Fas/FasL signaling pathway in cancer therapy. *Expert Opinion on Therapeutic Targets* **16**, 85–101 (2012).

197. Mor, G. *et al.* Regulation of fas ligand expression in breast cancer cells by estrogen: functional differences between estradiol and tamoxifen. *J Steroid Biochem Mol Biol* **73**, 185–194 (2000).

198. Owen, J. L. *et al.* Expression of the inflammatory chemokines CCL2, CCL5 and CXCL2 and the receptors CCR1-3 and CXCR2 in T lymphocytes from mammary tumor-bearing mice. *Cell Immunol* **270**, 172–182 (2011).

199. Whiteside, T. L. Exosomes and tumor-mediated immune suppression. *J Clin Invest* **126**, 1216–1223 (2016).

200. Nooshabadi, V. T. & Arab, S. Targeting Tumor-derived Exosomes Expressing CD73: New Opportunities in the Pathogenesis and Treatment of Cancer. *Curr Mol Med* **21**, 476–483 (2021).

201. Filipazzi, P., Bürdek, M., Villa, A., Rivoltini, L. & Huber, V. Recent advances on the role of tumor exosomes in immunosuppression and disease progression. *Seminars in Cancer Biology* **22**, 342–349 (2012).

202. Naso, J. R. *et al.* Tumor infiltrating neutrophils and gland formation predict overall survival and molecular subgroups in pancreatic ductal adenocarcinoma. *Cancer Med* **10**, 1155–1165 (2020).

203. Liu, R. *et al.* Neutrophil infiltration associated genes on the prognosis and tumor immune microenvironment of lung adenocarcinoma. *Front. Immunol.* **14**, (2023).

204. Laumont, C. M., Banville, A. C., Gilardi, M., Hollern, D. P. & Nelson, B. H. Tumour-infiltrating B cells: immunological mechanisms, clinical impact and therapeutic opportunities. *Nat Rev Cancer* **22**, 414–430 (2022).

205. Zorko, N. A. *et al.* Natural Killer Cell Infiltration in Prostate Cancers Predict Improved Patient Outcomes. *Prostate Cancer Prostatic Dis* 1–9 (2024) doi:10.1038/s41391-024-00797-0.

206. Shimizu, S. *et al.* Tumor-infiltrating CD8+ T-cell density is an independent prognostic marker for oral squamous cell carcinoma. *Cancer Med* **8**, 80–93 (2019).

207. Larroquette, M. *et al.* Spatial transcriptomics of macrophage infiltration in non-small cell lung cancer reveals determinants of sensitivity and resistance to anti-PD1/PD-L1 antibodies. *J Immunother Cancer* **10**, e003890 (2022).

208. Fujiwara, T. *et al.* Macrophage Infiltration Predicts a Poor Prognosis for Human Ewing Sarcoma. *The American Journal of Pathology* **179**, 1157–1170 (2011).

209. Zhang, J. *et al.* High Infiltration of Tumor-Associated Macrophages Influences Poor Prognosis in Human Gastric Cancer Patients, Associates With the Phenomenon of EMT. *Medicine (Baltimore)* **95**, e2636 (2016).

210. Tomiyama, T. *et al.* Myeloid-derived suppressor cell infiltration is associated with a poor prognosis in patients with hepatocellular carcinoma. *Oncol Lett* **23**, 93 (2022).

211. Frontiers | Shaping Polarization Of Tumor-Associated Macrophages In Cancer Immunotherapy. https://www.frontiersin.org/journals/immunology/articles/10.3389/fimmu.2022.888713/full.

212. Kim, J. & Bae, J.-S. Tumor-Associated Macrophages and Neutrophils in Tumor Microenvironment. *Mediators of Inflammation* **2016**, e6058147 (2016).

213. Pan, Y., Yu, Y., Wang, X. & Zhang, T. Tumor-Associated Macrophages in Tumor Immunity. *Front Immunol* **11**, 583084 (2020).

214. Ostrand-Rosenberg, S. & Sinha, P. Myeloid-Derived Suppressor Cells: Linking Inflammation and Cancer 1. *The Journal of Immunology* **182**, 4499–4506 (2009).

215. Kusmartsev, S., Nefedova, Y., Yoder, D. & Gabrilovich, D. I. Antigen-specific inhibition of CD8+ T cell response by immature myeloid cells in cancer is mediated by reactive oxygen species. *J Immunol* **172**, 989–999 (2004).

216. Bronte, V. & Zanovello, P. Regulation of immune responses by L-arginine metabolism. *Nat Rev Immunol* **5**, 641–654 (2005).

217. Tumino, N. *et al.* Polymorphonuclear Myeloid-Derived Suppressor Cells Are Abundant in Peripheral Blood of Cancer Patients and Suppress Natural Killer Cell Anti-Tumor Activity. *Front. Immunol.* **12**, (2022).

218. Movahedi, K. *et al.* Identification of discrete tumor-induced myeloid-derived suppressor cell subpopulations with distinct T cell-suppressive activity. *Blood* **111**, 4233–4244 (2008).

219. Wolf, N. K., Kissiov, D. U. & Raulet, D. H. Roles of natural killer cells in immunity to cancer, and applications to immunotherapy. *Nat Rev Immunol* **23**, 90–105 (2023).

220. Salih, H. R., Rammensee, H.-G. & Steinle, A. Cutting Edge: Down-Regulation of MICA on Human Tumors by Proteolytic Shedding. *The Journal of Immunology* **169**, 4098–4102 (2002).

221. Fernández-Messina, L. *et al.* Differential Mechanisms of Shedding of the Glycosylphosphatidylinositol (GPI)-anchored NKG2D Ligands *. *Journal of Biological Chemistry* **285**, 8543–8551 (2010).

222. Waldhauer, I. *et al.* Tumor-Associated MICA Is Shed by ADAM Proteases. *Cancer Research* **68**, 6368–6376 (2008).

223. Boutet, P. *et al.* Cutting Edge: The Metalloproteinase ADAM17/TNF-α-Converting Enzyme Regulates Proteolytic Shedding of the MHC Class I-Related Chain B Protein1. *The Journal of Immunology* **182**, 49–53 (2009).

224. Kohga, K. *et al.* Sorafenib inhibits the shedding of major histocompatibility complex class I–related chain A on hepatocellular carcinoma cells by down-regulating a disintegrin and metalloproteinase 9. *Hepatology* **51**, 1264–1273 (2010).

225. Deng, W. *et al.* A shed NKG2D ligand that promotes natural killer cell activation and tumor rejection. *Science* **348**, 136–139 (2015).

226. Marin-Acevedo, J. A., Kimbrough, E. O. & Lou, Y. Next generation of immune checkpoint inhibitors and beyond. *Journal of Hematology & Oncology* **14**, 45 (2021).

227. Wherry, E. J. & Kurachi, M. Molecular and cellular insights into T cell exhaustion. *Nat Rev Immunol* **15**, 486–499 (2015).

228. Sakaguchi, S., Yamaguchi, T., Nomura, T. & Ono, M. Regulatory T Cells and Immune Tolerance. *Cell* **133**, 775–787 (2008).

229. Onizuka, S. *et al.* Tumor rejection by in vivo administration of anti-CD25 (interleukin-2 receptor alpha) monoclonal antibody. *Cancer Res* **59**, 3128–3133 (1999).

230. Shimizu, J., Yamazaki, S. & Sakaguchi, S. Induction of tumor immunity by removing CD25+CD4+ T cells: a common basis between tumor immunity and autoimmunity. *J Immunol* **163**, 5211–5218 (1999).

231. Sasada, T., Kimura, M., Yoshida, Y., Kanai, M. & Takabayashi, A. CD4+CD25+ regulatory T cells in patients with gastrointestinal malignancies: possible involvement of regulatory T cells in disease progression. *Cancer* **98**, 1089–1099 (2003).

232. Sato, E. *et al.* Intraepithelial CD8+ tumor-infiltrating lymphocytes and a high CD8+/regulatory T cell ratio are associated with favorable prognosis in ovarian cancer. *Proceedings of the National Academy of Sciences* **102**, 18538–18543 (2005).

233. Bates, G. J. *et al.* Quantification of Regulatory T Cells Enables the Identification of High-Risk Breast Cancer Patients and Those at Risk of Late Relapse. *JCO* **24**, 5373–5380 (2006).

234. Ghiringhelli, F., Ménard, C., Martin, F. & Zitvogel, L. The role of regulatory T cells in the control of natural killer cells: relevance during tumor progression. *Immunol Rev* **214**, 229–238 (2006).

235. Tanaka, A. & Sakaguchi, S. Regulatory T cells in cancer immunotherapy. *Cell Res* **27**, 109–118 (2017).

236. Pinzon-Charry, A., Maxwell, T. & López, J. A. Dendritic cell dysfunction in cancer: a mechanism for immunosuppression. *Immunol Cell Biol* **83**, 451–461 (2005).

237. Wculek, S. K. *et al.* Dendritic cells in cancer immunology and immunotherapy. *Nat Rev Immunol* **20**, 7–24 (2020).

238. Segura, E., Durand, M. & Amigorena, S. Similar antigen cross-presentation capacity and phagocytic functions in all freshly isolated human lymphoid organ–resident dendritic cells. *Journal of Experimental Medicine* **210**, 1035–1047 (2013).

239. Carlos, C. A. *et al.* Human Tumor Antigen MUC1 Is Chemotactic for Immature Dendritic Cells and Elicits Maturation but Does Not Promote Th1 Type Immunity 1. *The Journal of Immunology* **175**, 1628–1635 (2005).

240. Cal, S. & López-Otín, C. ADAMTS proteases and cancer. *Matrix Biology* **44–46**, 77–85 (2015).

241. Obika, M. *et al.* Tumor growth inhibitory effect of ADAMTS1 is accompanied by the inhibition of tumor angiogenesis. *Cancer Science* **103**, 1889–1897 (2012).

242. Dekky, B. *et al.* ADAMTS12 is a stromal modulator in chronic liver disease. *FASEB J* **37**, e23237 (2023).

243. Chen, R., Chen, J., Chen, M., Zhou, S. & Jiang, P. Metformin suppresses proliferation and glycolysis of gastric cancer by modulating ADAMTS12. *Genes Environ* **46**, 1 (2024).

244. Zou, R. *et al.* Effects of metalloprotease ADAMTS12 on cervical cancer cell phenotype and its potential mechanism. *Discov Oncol* **14**, 162 (2023).

245. Fontaine, J.-F. *et al.* Increasing the number of thyroid lesions classes in microarray analysis improves the relevance of diagnostic markers. *PLoS One* **4**, e7632 (2009).

246. Roemer, A. *et al.* The membrane proteases adams and hepsin are differentially expressed in renal cell carcinoma. Are they potential tumor markers? *J Urol* **172**, 2162–2166 (2004).

247. Carinci, F. *et al.* Potential markers of tongue tumor progression selected by cDNA microarray. *Int J Immunopathol Pharmacol* **18**, 513–524 (2005).

248. Kirana, C. *et al.* Combination of laser microdissection, 2D-DIGE and MALDI-TOF MS to identify protein biomarkers to predict colorectal cancer spread. *Clin Proteomics* **16**, 3 (2019).

249. Abbey, S. R. *et al.* The Human Odontoblast Cell Layer and Dental Pulp Proteomes and N-Terminomes. *J Dent Res* **97**, 338–346 (2018).

250. Becker-Pauly, C. *et al.* Proteomic analyses reveal an acidic prime side specificity for the astacin metalloprotease family reflected by physiological substrates. *Mol Cell Proteomics* **10**, M111.009233 (2011).

251. Jefferson, T. *et al.* The substrate degradome of meprin metalloproteases reveals an unexpected proteolytic link between meprin β and ADAM10. *Cell Mol Life Sci* **70**, 309–333 (2013).

252. Jefferson, T. *et al.* Metalloprotease meprin beta generates nontoxic N-terminal amyloid precursor protein fragments in vivo. *J Biol Chem* **286**, 27741–27750 (2011).

253. Schlage, P., Kockmann, T., Sabino, F., Kizhakkedathu, J. N. & Auf dem Keller, U. Matrix Metalloproteinase 10 Degradomics in Keratinocytes and Epidermal Tissue Identifies Bioactive Substrates With Pleiotropic Functions. *Mol Cell Proteomics* **14**, 3234–3246 (2015).

254. Schlage, P. *et al.* Time-resolved analysis of the matrix metalloproteinase 10 substrate degradome. *Mol Cell Proteomics* **13**, 580–593 (2014).

255. Starr, A. E., Bellac, C. L., Dufour, A., Goebeler, V. & Overall, C. M. Biochemical characterization and N-terminomics analysis of leukolysin, the membrane-type 6 matrix metalloprotease (MMP25): chemokine and vimentin cleavages enhance cell migration and macrophage phagocytic activities. *J Biol Chem* **287**, 13382–13395 (2012).

256. Tholen, S. *et al.* Double deficiency of cathepsins B and L results in massive secretome alterations and suggests a degradative cathepsin-MMP axis. *Cell Mol Life Sci* **71**, 899–916 (2014).

257. Tholen, S. *et al.* Contribution of cathepsin L to secretome composition and cleavage pattern of mouse embryonic fibroblasts. *Biol Chem* **392**, 961–971 (2011).

258. Zhang, H. E. *et al.* Identification of Novel Natural Substrates of Fibroblast Activation Protein-alpha by Differential Degradomics and Proteomics. *Mol Cell Proteomics* **18**, 65–85 (2019).

259. Jerke, U. *et al.* Neutrophil serine proteases exert proteolytic activity on endothelial cells. *Kidney Int* **88**, 764–775 (2015).

260. Prudova, A. *et al.* TAILS N-terminomics of human platelets reveals pervasive metalloproteinase-dependent proteolytic processing in storage. *Blood* **124**, e49–e60 (2014).

261. Eckhard, U. *et al.* The Human Dental Pulp Proteome and N-Terminome: Levering the Unexplored Potential of Semitryptic Peptides Enriched by TAILS to Identify Missing Proteins in the Human Proteome Project in Underexplored Tissues. *J Proteome Res* **14**, 3568–3582 (2015).

262. Eckhard, U., Marino, G., Abbey, S. R., Matthew, I. & Overall, C. M. TAILS N-terminomic and proteomic datasets of healthy human dental pulp. *Data Brief* **5**, 542–548 (2015).

263. Tholen, S. *et al.* Skin Barrier Defects Caused by Keratinocyte-Specific Deletion of ADAM17 or EGFR Are Based on Highly Similar Proteome and Degradome Alterations. *J Proteome Res* **15**, 1402–1417 (2016).

264. Mallia-Milanes, B. *et al.* TAILS proteomics reveals dynamic changes in airway proteolysis controlling protease activity and innate immunity during COPD exacerbations. *Am J Physiol Lung Cell Mol Physiol* **315**, L1003–L1014 (2018).

265. Gordon, M. H. *et al.* N-Terminomics/TAILS Profiling of Proteases and Their Substrates in Ulcerative Colitis. *ACS Chem Biol* **14**, 2471–2483 (2019).

266. Bell, P. A., Solis, N., Kizhakkedathu, J. N., Matthew, I. & Overall, C. M. Proteomic and N-Terminomic TAILS Analyses of Human Alveolar Bone Proteins: Improved Protein Extraction Methodology and

LysargiNase Digestion Strategies Increase Proteome Coverage and Missing Protein Identification. *J Proteome Res* **18**, 4167–4179 (2019).

267. Bekhouche, M. *et al.* Determination of the substrate repertoire of ADAMTS2, 3, and 14 significantly broadens their functions and identifies extracellular matrix organization and TGF-β signaling as primary targets. *FASEB J* **30**, 1741–1756 (2016).
268. Janssen, L. *et al.* ADAMTS3 activity is mandatory for embryonic lymphangiogenesis and regulates placental angiogenesis. *Angiogenesis* **19**, 53–65 (2016).
269. Dupont, L. *et al.* ADAMTS2 and ADAMTS14 can substitute for ADAMTS3 in adults for pro-VEGFC activation and lymphatic homeostasis. *JCI Insight* **7**, e151509 (2022).
270. Hofer, T. P. J. *et al.* Tissue-specific induction of ADAMTS2 in monocytes and macrophages by glucocorticoids. *J Mol Med (Berl)* **86**, 323–332 (2008).
271. Jubb, A. W., Hofer, T. P., Hume, D. A. & Ziegler-Heitbrock, L. The preterm labor associated ADAMTS2 gene is induced by glucocorticoids. *Am J Obstet Gynecol* **219**, 122–123 (2018).
272. Roemer, A. *et al.* Increased mRNA expression of ADAMs in renal cell carcinoma and their association with clinical outcome. *Oncol Rep* **11**, 529–536 (2004).
273. Li, S. W. *et al.* Transgenic mice with inactive alleles for procollagen N-proteinase (ADAMTS-2) develop fragile skin and male sterility. *Biochem J* **355**, 271–278 (2001).
274. Hubert, P. *et al.* Extracellular HMGB1 blockade inhibits tumor growth through profoundly remodeling immune microenvironment and enhances checkpoint inhibitor-based immunotherapy. *J Immunother Cancer* **9**, e001966 (2021).
275. Nagy, Á., Munkácsy, G. & Győrffy, B. Pancancer survival analysis of cancer hallmark genes. *Sci Rep* **11**, 6047 (2021).

276. Lin, E. Y. *et al.* Progression to Malignancy in the Polyoma Middle T Oncoprotein Mouse Breast Cancer Model Provides a Reliable Model for Human Diseases. *The American Journal of Pathology* **163**, 2113–2126 (2003).

277. Théret, N., Bouezzeddine, F., Azar, F., Diab-Assaf, M. & Legagneux, V. ADAM and ADAMTS Proteins, New Players in the Regulation of Hepatocellular Carcinoma Microenvironment. *Cancers* **13**, 1563 (2021).

278. Colige, A. *et al.* Characterization and partial amino acid sequencing of a 107-kDa procollagen I N-proteinase purified by affinity chromatography on immobilized type XIV collagen. *J Biol Chem* **270**, 16724–16730 (1995).

279. Bekhouche, M. *et al.* Determination of the substrate repertoire of ADAMTS2, 3, and 14 significantly broadens their functions and identifies extracellular matrix organization and TGF-β signaling as primary targets. *FASEB J* **30**, 1741–1756 (2016).

280. Attalla, S., Taifour, T., Bui, T. & Muller, W. Insights from transgenic mouse models of PyMT-induced breast cancer: recapitulating human breast cancer progression in vivo. *Oncogene* **40**, 475–491 (2021).

281. Lee, N. V. *et al.* Fibulin-1 acts as a cofactor for the matrix metalloprotease ADAMTS-1. *J Biol Chem* **280**, 34796–34804 (2005).

282. Chen, X. *et al.* COL5A1 promotes triple-negative breast cancer progression by activating tumor cell-macrophage crosstalk. *Oncogene* **43**, 1742–1756 (2024).

283. Zhu, L.-W. *et al.* Ficolin-A induces macrophage polarization to a novel pro-inflammatory phenotype distinct from classical M1. *Cell Commun Signal* **22**, 271 (2024).

284. Howard, M., Farrar, C. A. & Sacks, S. H. Structural and functional diversity of collectins and ficolins and their relationship to disease. *Semin Immunopathol* **40**, 75–85 (2018).

285. Martinez, V. G. *et al.* Fibroblastic Reticular Cells Control Conduit Matrix Deposition during Lymph Node Expansion. *Cell Rep* **29**, 2810-2822.e5 (2019).

286. Tacconi, C. *et al.* CD169+ lymph node macrophages have protective functions in mouse breast cancer metastasis. *Cell Rep* **35**, 108993 (2021).

287. Colige, A. C. Purification of Native or Recombinant ADAMTS2, and Procollagen I Cleavage Assay. *Methods Mol Biol* **2043**, 55–62 (2020).

288. Colige, A. C. Challenges and Solutions for Purification of ADAMTS Proteases: An Overview. *Methods Mol Biol* **2043**, 45–53 (2020).

289. Bornstein, P., Armstrong, L. C., Hankenson, K. D., Kyriakides, T. R. & Yang, Z. Thrombospondin 2, a matricellular protein with diverse functions. *Matrix Biology* **19**, 557–568 (2000).

290. Iruela-Arispe, M. L. Regulation of Thrombospondin1 by Extracellular Proteases. *Curr Drug Targets* **9**, 863–868 (2008).

291. Wang, Z. *et al.* The Basic Characteristics of the Pentraxin Family and Their Functions in Tumor Progression. *Front Immunol* **11**, 1757 (2020).

292. Rosell-García, T., Rivas-Muñoz, S., Colige, A. & Rodriguez-Pascual, F. Cleavage of LOXL1 by BMP1 and ADAMTS14 Proteases Suggests a Role for Proteolytic Processing in the Regulation of LOXL1 Function. *Int J Mol Sci* **23**, 3285 (2022).

293. Carter, E. P. *et al.* Opposing roles for ADAMTS2 and ADAMTS14 in myofibroblast differentiation and function. *J Pathol* (2023) doi:10.1002/path.6214.

294. Vandooren, J. & Itoh, Y. Alpha-2-Macroglobulin in Inflammation, Immunity and Infections. *Front. Immunol.* **12**, (2021).

295. Noris, M. & Remuzzi, G. Overview of Complement Activation and Regulation. *Semin Nephrol* **33**, 479–492 (2013).

296. Araújo, T. G. *et al.* Annexin A1 as a Regulator of Immune Response in Cancer. *Cells* **10**, 2245 (2021).

297. The Extracellular Actin-Scavenger System and Actin Toxicity | New England Journal of Medicine. https://www.nejm.org/doi/full/10.1056/NEJM199205143262006.

298. Kułakowska, A. *et al.* Hypogelsolinemia, a disorder of the extracellular actin scavenger system, in patients with multiple sclerosis. *BMC Neurology* **10**, 107 (2010).

299. van Beijnum, J. R. *et al.* Extracellular vimentin mimics VEGF and is a target for anti-angiogenic immunotherapy. *Nat Commun* **13**, 2842 (2022).

300. Wang, G. *et al.* Specific fibroblast subpopulations and neuronal structures provide local sources of Vegfc-processing components during zebrafish lymphangiogenesis. *Nat Commun* **11**, 2724 (2020).

301. Sleeman, J. P. The lymph node as a bridgehead in the metastatic dissemination of tumors. *Recent Results Cancer Res* **157**, 55–81 (2000).

302. Gillot, L., Baudin, L., Rouaud, L., Kridelka, F. & Noël, A. The pre-metastatic niche in lymph nodes: formation and characteristics. *Cell Mol Life Sci* **78**, 5987–6002 (2021).

303. Dong, C. *et al.* A Disintegrin and Metalloprotease with Thrombospondin Motif 2 May Contribute to Cirrhosis in Humans through the Transforming Growth Factor-β/SMAD Pathway. *Gut Liver* **7**, 213–220 (2013).

304. Koenitzer, J. R., Wu, H., Atkinson, J. J., Brody, S. L. & Humphreys, B. D. Single-Nucleus RNA-Sequencing Profiling of Mouse Lung. Reduced Dissociation Bias and Improved Rare Cell-Type Detection Compared with Single-Cell RNA Sequencing. *Am J Respir Cell Mol Biol* **63**, 739–747 (2020).

305. Jablonski, K. A. *et al.* Novel Markers to Delineate Murine M1 and M2 Macrophages. *PLoS One* **10**, e0145342 (2015).

306. Debacker, J. M., Gondry, O., Lahoutte, T., Keyaerts, M. & Huvenne, W. The Prognostic Value of CD206 in Solid Malignancies: A Systematic Review and Meta-Analysis. *Cancers* **13**, 3422 (2021).

307. Geiger, R. *et al.* L-Arginine Modulates T Cell Metabolism and Enhances Survival and Anti-tumor Activity. *Cell* **167**, 829-842.e13 (2016).

308. Chang, C.-I., Liao, J. C. & Kuo, L. Macrophage Arginase Promotes Tumor Cell Growth and Suppresses Nitric Oxide-mediated Tumor Cytotoxicity1. *Cancer Research* **61**, 1100–1106 (2001).

309. Veglia, F. *et al.* Analysis of classical neutrophils and polymorphonuclear myeloid-derived suppressor cells in cancer patients and tumor-bearing mice. *Journal of Experimental Medicine* **218**, e20201803 (2021).

310. Sun, Z. *et al.* IL10 and PD-1 Cooperate to Limit the Activity of Tumor-Specific CD8+ T Cells. *Cancer Research* **75**, 1635–1644 (2015).

311. Sugamura, K. *et al.* The interleukin-2 receptor gamma chain: its role in the multiple cytokine receptor complexes and T cell development in XSCID. *Annu Rev Immunol* **14**, 179–205 (1996).

312. Ishikawa, F. *et al.* Development of functional human blood and immune systems in NOD/SCID/IL2 receptor {gamma} chain(null) mice. *Blood* **106**, 1565–1573 (2005).

313. Shultz, L. D. *et al.* Human lymphoid and myeloid cell development in NOD/LtSz-scid IL2R gamma null mice engrafted with mobilized human hemopoietic stem cells. *J Immunol* **174**, 6477–6489 (2005).

314. Liu, T. *et al.* Cancer-associated fibroblasts: an emerging target of anti-cancer immunotherapy. *J Hematol Oncol* **12**, 86 (2019).

315. Alper, M. & Kockar, F. IL-6 upregulates a disintegrin and metalloproteinase with thrombospondin motifs 2 (ADAMTS-2) in human osteosarcoma cells mediated by JNK pathway. *Mol Cell Biochem* **393**, 165–175 (2014).

316. Liu, Y., Qi, X., Li, G. & Sowa, G. Caveolin-2 deficiency induces a rapid anti-tumor immune response prior to regression of implanted murine lung carcinoma tumors. *Sci Rep* **9**, 18970 (2019).

317. Owyong, M. *et al.* MMP9 modulates the metastatic cascade and immune landscape for breast cancer anti-metastatic therapy. *Life Science Alliance* **2**, (2019).

318. Christofides, A. *et al.* The complex role of tumor-infiltrating macrophages. *Nat Immunol* **23**, 1148–1156 (2022).

319. Mantovani, A., Allavena, P., Marchesi, F. & Garlanda, C. Macrophages as tools and targets in cancer therapy. *Nat Rev Drug Discov* **21**, 799–820 (2022).

320. Zizzo: Efficient clearance of early apoptotic cells... - Google Scholar. https://scholar.google.com/scholar_lookup?journal=J+Immunol.&title=Efficient+clearance+of+early+apoptotic+cells+by+human+macrophages+requires+M2c+polarization+and+MerTK+induction&author=G+Zizzo&author=BA+Hilliard&author=M+Monestier&author=PL+Cohen&volume=189&publication_year=2012&pages=3508-20&pmid=22942426&doi=10.4049/jimmunol.1200662&.

321. Watari, K. *et al.* Role of macrophages in inflammatory lymphangiogenesis: Enhanced production of vascular endothelial growth factor C and D through NF-κB activation. *Biochemical and Biophysical Research Communications* **377**, 826–831 (2008).

322. Stepanova, O. I., Krylov, A. V., Lioudyno, V. I. & Kisseleva, E. P. Gene expression for VEGF-A, VEGF-C, and their receptors in murine lymphocytes and macrophages. *Biochemistry Moscow* **72**, 1194–1198 (2007).

323. Schoppmann, S. F. *et al.* Tumor-Associated Macrophages Express Lymphatic Endothelial Growth Factors and Are Related to Peritumoral Lymphangiogenesis. *Am J Pathol* **161**, 947–956 (2002).

324. PEPPICELLI, S., BIANCHINI, F. & CALORINI, L. Inflammatory cytokines induce vascular endothelial growth factor-C expression in melanoma-associated macrophages and stimulate melanoma lymph node metastasis. *Oncol Lett* **8**, 1133–1138 (2014).

325. Glinton, K. E. *et al.* Macrophage-produced VEGFC is induced by efferocytosis to ameliorate cardiac injury and inflammation. *J Clin Invest* **132**, (2022).

326. Kannan, S. & Rutkowski, J. M. VEGFR-3 signaling in macrophages: friend or foe in disease? *Front Immunol* **15**, 1349500 (2024).

327. Tacconi, C. *et al.* Activation of the VEGFC/VEGFR3 Pathway Induces Tumor Immune Escape in Colorectal Cancer. *Cancer Research* **79**, 4196–4210 (2019).

328. Kaneko, N. *et al.* ADAMTS2 promotes radial migration by activating TGF-β signaling in the developing neocortex. *EMBO Rep* **25**, 3090–3115 (2024).

329. Wang, R. *et al.* GARP regulates the bioavailability and activation of TGFβ. *Mol Biol Cell* **23**, 1129–1139 (2012).

330. Yu, X. *et al.* The Cytokine TGF-β Promotes the Development and Homeostasis of Alveolar Macrophages. *Immunity* **47**, 903-912.e4 (2017).

331. Gratchev, A. *et al.* Activation of a TGF-β-Specific Multistep Gene Expression Program in Mature Macrophages Requires Glucocorticoid-Mediated Surface Expression of TGF-β Receptor II1. *The Journal of Immunology* **180**, 6553–6565 (2008).

332. Dickkopf-3 Contributes to the Regulation of Anti-Tumor Immune Responses by Mesenchymal Stem Cells - PubMed. https://pubmed.ncbi.nlm.nih.gov/26734010/.

333. Papatriantafyllou, M. *et al.* Dickkopf-3, an immune modulator in peripheral CD8 T-cell tolerance. *Proc Natl Acad Sci U S A* **109**, 1631–1636 (2012).

334. Meister, M. *et al.* Dickkopf-3, a tissue-derived modulator of local T-cell responses. *Front Immunol* **6**, 78 (2015).

335. Meister, M. *et al.* Self-Antigen Presentation by Keratinocytes in the Inflamed Adult Skin Modulates T-Cell Auto-Reactivity. *J Invest Dermatol* **135**, 1996–2004 (2015).

336. Kinoshita, R. *et al.* The cysteine-rich core domain of REIC/Dkk-3 is critical for its effect on monocyte differentiation and tumor regression. *Oncol Rep* **33**, 2908–2914 (2015).

337. Mourtada, J. *et al.* A novel ΔNp63-dependent immune mechanism improves prognosis of HPV-related head and neck cancer. *Front. Immunol.* **14**, (2023).

338. Mourtada, J., Thibaudeau, C., Wasylyk, B. & Jung, A. C. The Multifaceted Role of Human Dickkopf-3 (DKK-3) in Development, Immune Modulation and Cancer. *Cells* **13**, 75 (2024).

339. Woldesenbet, Y. M., Alenko, A., Bukata, I. T., Gedefaw, L. & Fikru, C. The status of serum cortisol before and after treatment of schizophrenia and its correlation to disease severity and improvement: A longitudinal study. *SAGE Open Med* **9**, 20503121211056216 (2021).

340. Wang, F. *et al.* Association of serum cortisol and cortisone levels and risk of recurrence after endocrine treatment in breast cancer. *Clin Exp Med* **23**, 3883–3893 (2023).

341. M, C. *et al.* Use of systemic glucocorticoids and risk of breast cancer in a prospective cohort of postmenopausal women. *BMC medicine* **19**, (2021).

342. Acharya, N. *et al.* Endogenous Glucocorticoid Signaling Regulates CD8+ T Cell Differentiation and Development of Dysfunction in the Tumor Microenvironment. *Immunity* **53**, 658-671.e6 (2020).

343. Hou, Z. *et al.* Loss of Annexin A1 in macrophages restrains efferocytosis and remodels immune microenvironment in pancreatic cancer by activating the cGAS/STING pathway. *J Immunother Cancer* **12**, e009318 (2024).

344. Moraes, L. A. *et al.* Annexin-A1 enhances breast cancer growth and migration by promoting alternative macrophage polarization in the tumour microenvironment. *Sci Rep* **7**, 17925 (2017).

345. Herold, M. J., McPherson, K. G. & Reichardt, H. M. Glucocorticoids in T cell apoptosis and function. *Cell Mol Life Sci* **63**, 60–72 (2005).

346. Quatrini, L. & Ugolini, S. New insights into the cell- and tissue-specificity of glucocorticoid actions. *Cell Mol Immunol* **18**, 269–278 (2021).

347. Kozicky, L. K. & Sly, L. M. Depletion and Reconstitution of Macrophages in Mice. *Methods Mol Biol* **1960**, 101–112 (2019).

348. Saito, M. *et al.* Diphtheria toxin receptor–mediated conditional and targeted cell ablation in transgenic mice. *Nat Biotechnol* **19**, 746–750 (2001).

349. Friedmann, K. S. *et al.* Interdependence of sequential cytotoxic T lymphocyte and natural killer cell cytotoxicity against melanoma cells. *The Journal of Physiology* **600**, 5027–5054 (2022).